MICRO- TO MACROSCALE MODELING OF DRINKING WATER TREATMENT AND DISTRIBUTION

by

Amy Louise Polaczyk

A dissertation submitted to the faculty of
The University of North Carolina at Charlotte
in partial fulfillment of the requirements
for the degree of Doctor of Philosophy
in Infrastructure and Environmental Systems

Charlotte

2010

Approved by:

Dr. James E. Amburgey

Dr. James B. Bowen

Dr. Valery Z. Grdzelishvili

Dr. Helene Hilger

Dr. Jordan C. Poler

ABSTRACT

AMY LOUISE POLACZYK. Micro- to macroscale modeling of drinking water treatment and distribution. (Under the direction of DR. JAMES E. AMBURGEY)

"*Everything should be made as simple as possible, but not simpler.*"
-attributed to Albert Einstein

This philosophy is often applied to studies involving numerical modeling. Models are valuable tools that can provide quantitative insight into a process or system, but must to be kept simple to remain meaningful. In this dissertation, three separate drinking water research projects were completed using numerical modeling as a tool to describe and understand systems. Each project aimed to best exploit models or the modeling process while keeping the modeled descriptions and interpretations as simple as possible. These projects illustrate that modeling is a useful technique for gaining understanding of system structure and process behaviors, may guide experiments to verify hypotheses, and provides valuable data for assisting decision making.

In the first project, five equations to calculate zeta potential for electrophoretic mobility measurements were compared to determine if complicated models return the same values determined by simple models. Results obtained by comparing models through analysis of electrophoretic mobility measurement uncertainty indicated that for 60% of the organisms studied, the Helmholtz-Smoluchowski or Henry equations produced zeta potential values that were not statistically different from equations which account for electrical double-layer distortion.

The goal of the second project was to determine the process variables that are considered most important to model the removal of *Cryptosporidium* oocysts through the

conventional drinking water treatment. Stepwise model analysis resulted in R^2 values of 0.47 to 0.89. Although the models did not have high predictive values, stepwise analysis indicated the variables with the highest potential to predict Log Cryptosporidium removals. Results showed that observational variables like the portion of filter run and optimality of coagulant dose were important variables in the removal of Cryptosporidium regardless of the coagulant dose. Cryptosporidium removal appeared to be related to metal ion concentration below 0.4 mg/L (as ion), while above this value, metal ion concentration was not as important because other factors appear to have a stronger affect on oocyst removal. This study suggested it may be possible for drinking water treatment facilities adding less than 0.4 mg/L metal ion (e.g., direct filtration plants) to observe higher Cryptosporidium removals by increasing the dose of coagulant applied.

In the third project, a distribution system model was developed to mimic the way it would be controlled by an operator. The model was then used to examine the causes of water aging in the system as well as operational scenarios that the utility could employ to improve the quality of water delivered to customers. This project provided an example of the techniques needed to use EPANET MSX for water age analysis and to examine the impact of individual tanks and their operation on system water age. Novel approaches to analyze data from hydraulic model simulations with respect to system water quality were used. For most of the water in the system, the age was dominantly controlled by the pipes (which contained 67% of total system volume) and only moderately influenced by the storage tanks (33% of total system volume). However, storage tank operation did show significant effects on the maximum water as well as the age of the water for the 3-5% of consumers receiving the oldest water.

DEDICATION

To my husband, Marco, for his unconditional love and extraordinary, unwavering support.

ACKNOWLEDGEMENTS

I would like to thank the faculty and staff of the Department of Civil and Environmental Engineering at UNCC for expanding my horizons in the civil engineering field. I express thanks to my advisor, Dr. James Amburgey for his guidance, support, and patience. Thank you to Dr. James Bowen, Mr. Ernesto Gianella, Dr. Valery Grdzelishvili, Dr. Helene Hilger, and Dr. Jordan Poler for serving on my committee and providing valuable assistance and feedback. Also to Dr. Jacek Dmochowski, Jonathan Halter and the UNCC URC and the COE MOSAIC computing team, especially Sumanth Venkatasubbaia, and Dr. Peter Cheung and Narumi Abe of UFMS, Brazil for their valuable assistance.

I am grateful for the financial support and research cooperation of the Gwinnett County Department of Public Utilities. Thank you to Neil Spivey, Reza Baniassad, Walker Hawes, John Kight, Younggyun Park, Halcrow, Inc., and Derceto in Atlanta for providing support and data for the third chapter of this work.

I am fortunate to be a part of the Polaczyk and Propato families, who fill my life with unconditional love and encouragement. Thank you, merci, grazie, and obrigada to all my friends near and far, especially Jayme. A special thanks to Sean, Laura, and Jackson for opening their home and hearts to me.

TABLE OF CONTENTS

LIST OF TABLES

LIST OF FIGURES

LIST OF ABBREVIATIONS

ε_0	Electric Permittivity of a Vacuum
η	Dynamic Viscosity
α	Particle Radius
ε_{rs}	Dielectric Constant (or relative permittivity)
ζ	Zeta Potential
κ^{-1}	Debye Length
e	Elementary Charge
u_e	Electrophoretic Mobility
I	Ionic Strength
k	Boltzmann's Constant
CDF	Cumulative Distribution Function
CDPs	Central Distribution Pressures
CI_m	Confidence Interval of the Mean
DBPs	Disinfection By-Products
DWDS	Drinking Water Distribution System
DWT	Drinking Water Treatment
EDL	Electrical Double Layer
EPM	Electrophoretic Mobility
EPS	Extended Period Simulation
GCWDS	Gwinnett County Water Distribution System
GUI	Graphical User Interface
HAAs	Haloacetic Acids
Hen	Henry Equation
HO	Hückel-Onsager Equation
HS	Helmholtz-Smoluchowski Equation
HSP	High Service Pump
IDSE	Individual Distribution System Evaluation
LT2ESWTR	US EPA's Long Term 2 Enhanced Surface Water Treatment Rule
MB	Modified Booth Equation
MCL	Maximum Contaminant Limit
MI	Metal Ion
MSX	Multi-species Extension (of EPAnet)
MW	Mangelsdorf-White Equation
NOM	Natural Organic Matter
OBH	O'Brien-Hunter Equation
PACl	Polyaluminum Chloride
PRV	Pressure Reducing Valve

QC	Quality Control
RMSE	Root Mean Square Error
RSS	Residual Sum of Square
SCADA	Supervisory Control and Data Acquisition
SS	Steady State
Stage 2 DBPR	Stage 2 Disinfectants and Disinfection By-Product Rule
TOC	Total Organic Carbon
TTHMs	Total Trihalomethanes
VSP	Variable Speed Pump

Chapter 3 Simulation Abbreviations

PRV-1	Increased central distribution pressures at night, decreased during the day
PRV-2	Increased central distribution pressures during periods of low demand and increased during high demand
30%-All	Decrease in volume of all tanks by 30%
30%-LRG	Decrease in volume of largest tanks by 30%
BO	Blow-off in Southern sector at 100 GPM for 3 hours
FT-LMN	Forced filling/draining of Lanier Mountain tanks
FT-GRAY	Forced filling/draining of Grayson tanks
FT-RQ	Forced filling/draining of Rock Quarry tank
1GRAY-C	One of the two 10 MG Grayson Tanks closed
1LMN-C	One of the two 5 MG Lanier Mountain Tanks closed
MB&GS-C	Medlock Bridge and Goshen Springs Tanks closed
NTA-All	No aging/reaction in all tanks
NTA-LMN	No aging/reaction in all Lanier Mountain tanks
NDEA	No aging/reaction in pipes leading to dead end nodes

CHAPTER 1: COMPARISON OF MODELS TO CALCULATE THE ZETA POTENTIALS OF MICROBES IN DRINKING WATER

The stability of microorganisms in water is related to their surface charge, which is commonly approximated using the zeta potential. Zeta potential cannot be measured directly and so is calculated from measurements of electrophoretic mobility (EPM). In this project, five equations were used to convert experimentally determined EPM's of microorganisms to zeta potentials. The Helmholtz-Smoluchowski (HS), Henry, Hückel-Onsager, modified Booth, and O'Brien and Hunter equations were compared for their ranges of applicability when used to calculate zeta potential values from EPM measurements of various microbes in 1 mM KCl, a solution intended to simulate the conductivity of natural or treated drinking water. For the majority of microbes, results showed the computationally demanding modified Booth and O'Brien and Hunter equations produced zeta potentials that were not significantly different from those predicted by the HS and Henry equations. The more computationally intensive equations produced zeta potentials that were significantly different from the simpler equations at low ratios of particle radius to electrical double-layer thickness (i.e. low $\kappa\alpha$ values) with moderate to high values of EPM. The easily-employed equations of HS and Henry were sufficient to calculate zeta potentials for 60% microbes studied in 1 mM KCl, while 40% required the application of an equation to account for relaxation of the electrical double layer of the microbe.

1.1 Introduction

Electrostatic interactions between environmental microbes and surfaces play a significant role in determining the behavior of microorganisms in natural and engineered systems. These interactions can be evaluated in part by determining an organism's zeta potential (ζ). The zeta potential approximates the electrical potential of the inner portion of the layer of ions that adsorb to a particle when it is placed in a liquid medium. Based on the zeta potential, it is theoretically possible to determine the likelihood that a microorganism will attach to other particles and surfaces under a given set of conditions. Understanding zeta potential and microbial interactions can allow for better control of systems where microbial attachment to surfaces is either desirable or undesirable.

The zeta potential cannot be measured directly but must be calculated from electrokinetic measurements, such as the electrophoretic mobility (EPM). Calculation of the zeta potential takes into account the particle size and characteristics of the suspending matrix, making the zeta potentials of different sized particles or particles in different suspensions comparable where comparison of the EPM values may be misleading. For example, a virus, bacterium, and parasite may all have the same zeta potential but different EPM values due to their different sizes. By comparing the EPM measurements one may conclude they organisms have very different electrostatic surface characteristics when they do not.

Several equations of varying computational intensity are available to calculate zeta potential. In order to avoid introducing error into the zeta potential calculation of a particle beyond the uncertainty associated with the EPM measurement the correct equation should be applied. The consequences of an incorrectly calculated zeta depend

on the application for which the zeta potential is being determined. If comparing the calculated zeta potential to those determined through other means of measuring electrokinetic phenomena (e.g., comparing the zeta potential of a filter media measured by sedimentation potential to that of a microbe measured by electrophoresis for the purposes of optimizing attachment) it may be important to calculate the 'true' zeta potential. Delgado and coworkers recently published a thorough review of measurement and interpretation of electrokinetic phenomena (EKP) that provided practical guidelines for calculating zeta potential (2007).

In this study, the guidelines of Delgado and coworkers were applied to electrophoretic mobilities of various microbes in a 1 mM KCl solution. This matrix represents an ionic strength typical of potable water in the United States. The main objective of this study was to compare different methods of calculating zeta potential using a real-world data set and to report the zeta potentials of multiple classes of microbes under the stated conditions. The organisms examined included bacteriophages (MS2 and phi X174), human viruses (Hepatitis A HM-175, Echovirus, and Adenovirus), vegetative bacteria (F. tularensis, Y. pestis, E. faecalis, S. enterica, and E. coli), bacterial endospores of (B. atrophaeus subsp. globigii and B. anthracis Sterne-strain), and protozoan parasites (Cryptosporidium parvum oocysts and Giardia intestinalis cysts). By calculating the most accurate zeta potential possible from electrophoretic mobility measurements, the electrical surface charge characteristics of pathogenic organisms and their commonly used surrogates could then compared to determine their similarity or difference as well as provide information for engineering systems where electrostatic interactions are relied upon to remove microbes from tap water matrices.

1.1.1 Zeta Potential Theory

Particles in liquid matrices are surrounded by an electrical double layer (EDL), which is often depicted using the Stern model as shown in Figure 1.1. The thickness of the EDL is represented by the Debye length (κ^{-1}) and is determined by the composition, concentration, and temperature of the electrolyte solution in which the particle is suspended (Delgado et al., 2007). The Debye length equation is:

$$\kappa^{-1} = \left(\frac{\varepsilon_{rs}\varepsilon_0 kT}{2N_A e^2 I} \right)^{0.5} \tag{1.1}$$

Where ε_{rs} is the dielectric constant (or relative permittivity) of the electrolyte solution, ε_0 the electric permittivity of a vacuum, k the Boltzmann constant, T temperature in Kelvin, N_A the Avogadro constant, e the elementary charge, and I the ionic strength of the electrolyte in mole/m^3. The values of these constants can be found in Table 1.3 on page 24.

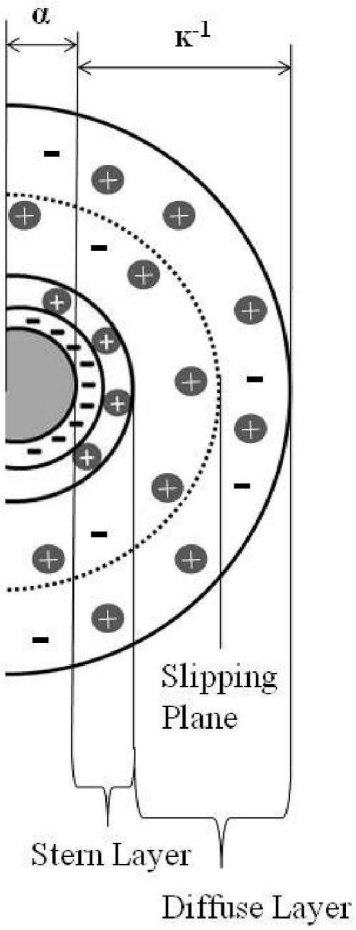

Figure 1.1: Schematic of charge layers at a particle surface.

Microbes tend to have a negative surface charge (or Nernst Potential) at pH values near neutral due to functional groups on their surfaces and/or the adsorption of ions or molecules from the suspending solution (Keck, 2006). The layer of ions closest to the particle surface is called the Inner Helmholtz Layer (IHL). Tightly bound to the IHL is a layer of ions called the Outer Helmholtz Layer (OHL). The IHL and OHL together form the Stern layer (Delgado et al., 2007). Within this layer, ions are strongly

attracted and therefore may be considered fixed to the particle surface. The Stern layer moves with the particle when it is in motion.

Adjacent to the Stern layer is the diffuse layer. In this layer the ions are less attracted to the particle than the ions in the Stern layer, but are still influenced by it. Within the diffuse layer lies the hydrodynamic plane of shear, or slipping plane. When the particle moves, the ions inside the slipping plane move with it. The zeta potential is defined as the electrical potential at the slipping plane and approximates the electrical potential of the inner portion of the diffuse layer (Wilson et al., 2001).

Zeta potential cannot be measured directly; therefore it is calculated from measurements of electrokinetic phenomena (EKP). Commonly the electrophoretic mobility, or terminal velocity of a particle when it is subjected to an electrical field, is measured and used to calculate the zeta potential. Several other methods exist to measure EKP. These include electro-osmosis, streaming potential, streaming current, sedimentation potential, and colloid vibration potential (Delgado et al., 2007). A key parameter for calculating the correct zeta potential using data collected from any measurement of EKP is $\kappa\alpha$, the ratio of the particle radius (α) to the Debye length (κ^{-1}).

The Helmholtz-Smoluchowski (HS) equation is the common 'default' equation used by many instruments and researchers alike for converting EPM to zeta potential:

$$\zeta = \frac{u_e \eta}{\varepsilon_{rs} \varepsilon_0} \tag{1.2}$$

where u_e is the electrophoretic mobility, η is the dynamic viscosity of the liquid, ε_{rs} is the dielectric constant (or relative permittivity) of the electrolyte solution, and ε_0 the electric permittivity of a vacuum. It is a straightforward equation, but is only considered accurate for relatively large particles in solutions of moderately high ionic strength. In this

instance the EDL may be considered 'thin' in comparison to the size of the particle ($\kappa\alpha >> 1$).

Particles that are very small, suspended in low ionic strength, or organic solutions may have 'thick' EDL's ($\kappa\alpha << 1$). To calculate the zeta potential of these particles the Hückel-Onsager (HO) equation is suggested:

$$\zeta = \frac{3u_e\eta}{2\varepsilon_{rs}\varepsilon_0} \tag{1.3}$$

The HO equation results in a zeta potential that is 1.5 times larger than that of Helmholtz-Smoluchowski for the same conditions; therefore, the choice of the incorrect equation can result in the calculation of a zeta potential value that is in error by 50%. In the 1930's, Henry developed an equation to relate the Helmholtz-Smoluchowski and Hückel-Onsager equations by introducing the function f(κa):

$$\zeta = \frac{3u_e\eta}{2\varepsilon_{rs}\varepsilon_0 f(\kappa\alpha)} \tag{1.4}$$

f(κa) is a sigmoid curve that varies from 1 to 1.5 with the extremes equivalent to the HO and HS approximations, respectively (Henry, 1931). Henry proposed two expansions of this function, which were subsequently simplified and combined by Ohshima (1994):

$$f(\kappa\alpha) = 1 + \frac{1}{2}\left[1 + \left(\frac{2.5}{\kappa\alpha\left[1 + 2\exp(-\kappa\alpha)\right]}\right)\right]^{-3} \tag{1.5}$$

A graphical representation of this relationship is presented in Figure 1.2. Using the HS, Henry and HO equations is the easiest way to convert EPM measurements to zeta potential; however, this approach may not always provide the most accurate results (Delgado et al., 2007).

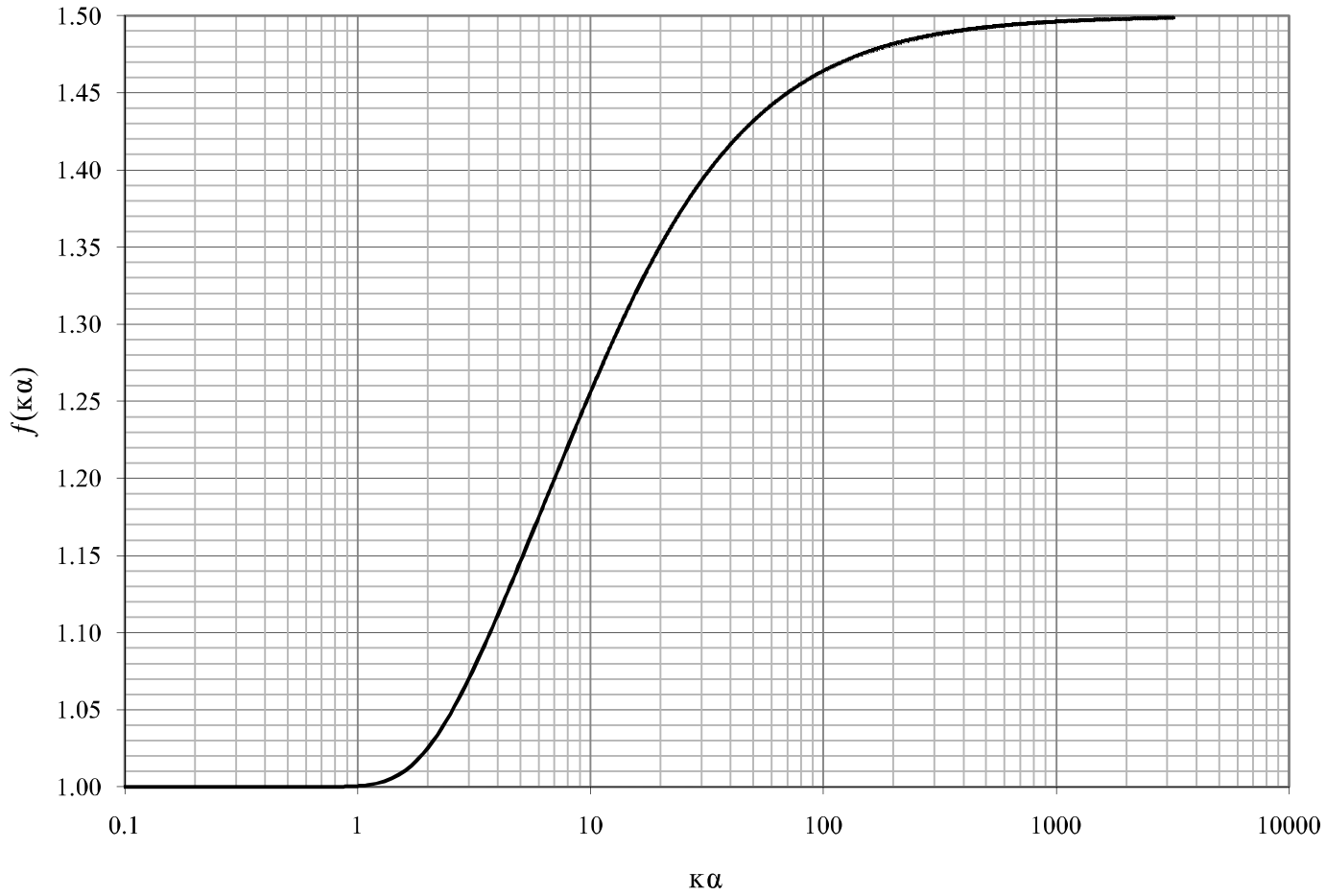

Figure 1.2: $f(\kappa\alpha)$ vs. $\kappa\alpha$ as calculated by the equation of Ohshima.

As a particle moves through an electrolyte solution during electrophoresis, the EDL may distort and reduce the measured electrophoretic mobility. The zeta potential will be miscalculated if these distortions are not accounted for. Distortion occurs in three main forms: retardation, concentration polarization, and surface conductance. Figure 1.3 illustrates the effect of retardation and concentration polarization distortions on the EDL. The term surface conductance appears in the literature to describe two different phenomena: 1) conduction inside the slipping plane and 2) additional electrical conduction that occurs in the aqueous phase due to the presence of electrical double layers (Lyklema and Minor, 1998). Both may affect zeta potential calculations (Einolf and Carstensen, 1967; Zukoski and Saville, 1986; Van Loosdrecht et al., 1987; Mangelsdorf and White, 1990; van der Wal et al., 1997; Lyklema and Minor, 1998; Delgado et al., 2007; Lopez-Garcia et al., 2009). To clearly distinguish between the two ideas, in this work the term surface conductance will only be used to refer to the additional electrical conduction occurring due to the presence of electrical double layers.

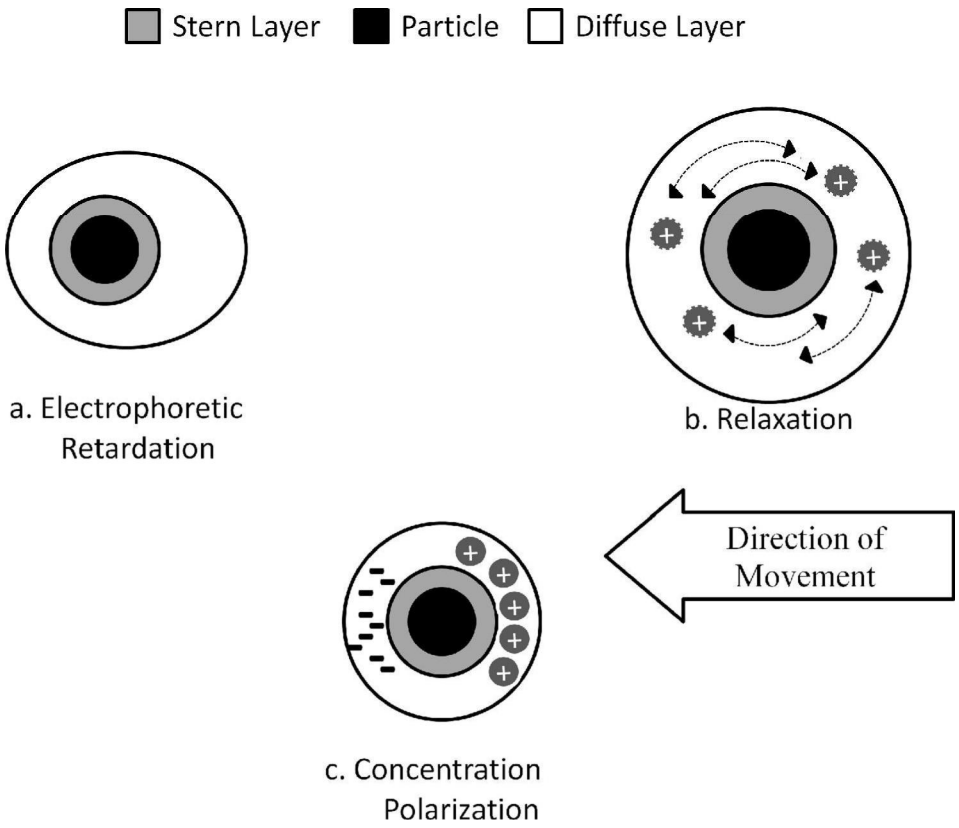

Figure 1.3: Distortion of the electrical double layer.

Retardation of the double layer can occur either through electrophoretic retardation or relaxation effects. In electrophoretic retardation, the electrical field exerts a force on the liquid suspension that is passed to the electrolyte molecules. The resulting flow causes a retarding force on the EDL of the particle, as shown in Figure 1.3a (Moncho et al., 2001). EDL relaxation arises from the motion of the ions in the mobile portion of the diffuse layer (i.e. those outside the slipping plane). These ions are constantly rearranging themselves in an attempt to coincide with the particle's center of negative charge, as depicted in Figure 1.3b (Deshiikan and Papadopoulos, 1998). Concentration polarization of the EDL occurs when there is an accumulation of charge on one side of the particle and depletion on the other, as shown in Figure 1.3c. This usually happens when the particle zeta potential is high (> 50mV) (Delgado et al., 2007).

The Helmholtz-Smoluchowski, Henry, and Hückel-Onsager equations account for electrophoretic retardation, but not relaxation, surface conduction, or conduction inside the slipping plane. The modified Booth equation (MB) corrects for retardation, relaxation, and surface conduction effects (Deshiikan and Papadopoulos, 1998; Lyklema and Minor, 1998). The O'Brien and Hunter (OBH) theory accounts for retardation, relaxation, surface conduction and concentration polarization, but is complicated by its prediction of an EPM maximum. Mangelsdorf and White's (MW) theory, among others, may be used to account for ion motion in the Stern layer (Mangelsdorf and White, 1998; Lopez-Garcia et al., 2007). Table 1.1 presents these equations and the distortions they account for.

Table 1.1: Zeta potential theories and the electrical double-layer distortions they consider.

Equation	Electro-phoretic Retardation	Relaxation	Surface Conduction	Concentration Polarization	Conduction Inside Slipping Plane
Hückel-Onsager /Henry/ Helmholtz-Smoluchowski	X				
Modified Booth	X	X	X		
O'Brien-Hunter	X	X	X	X	
Mangelsdorf-White	X	X	X	X	X

Booth was one of the first researchers to incorporate relaxation of the EDL into zeta potential theory (1950). Recently Deshiikan and Papadopoulos (1998) have presented the modified Booth equation, a programmable version of Booth's original graphical theory, making it much simpler to apply. The main benefit of using this theory is avoiding the mobility maximum predicted by the O'Brien and Hunter theory (1978).

The O'Brien and Hunter (OBH) equation is a simplified derivation of a theory proposed by Dukhin and collaborators used to predict the EPM from a zeta potential value (O'Brien and Hunter, 1981). The OBH equation also provides a "practical alternative" to the well-known theory of O'Brien and White that has been used by colloid scientists for several decades (O'Brien and Hunter, 1981). The OBH equation is applicable to symmetrical electrolytes (the cation and anion have the same valence, e.g., KCl). The OBH equation is simpler to employ than the original O'Brien and White theory, but produces zeta potentials that are in agreement with those resulting from the full O'Brien and White calculations, especially at high κα values (O'Brien and Hunter, 1981). A drawback of this equation is its prediction of an EPM maximum. This leads to complications using the OBH theory to calculate zeta potential from EPM measurements. Figure 1.4 shows the EPM vs. OBH zeta potential for the κa values of the organisms used in this study and illustrates the mobility maximum predicted, leading more than one possible zeta potential for a given EPM value. The EPM maximum is especially important at low κα values and precludes the use of this equation for particles with κα below ~ 20. Figure 1.4 also shows the OBH theory tends to the HS equation for $\kappa\alpha >> 1$. The OBH theory accounts for surface conduction but, like the other equations employed in this study, this theory will underestimate the zeta potential when conduction inside the slipping plane is present (Moncho et al., 2001).

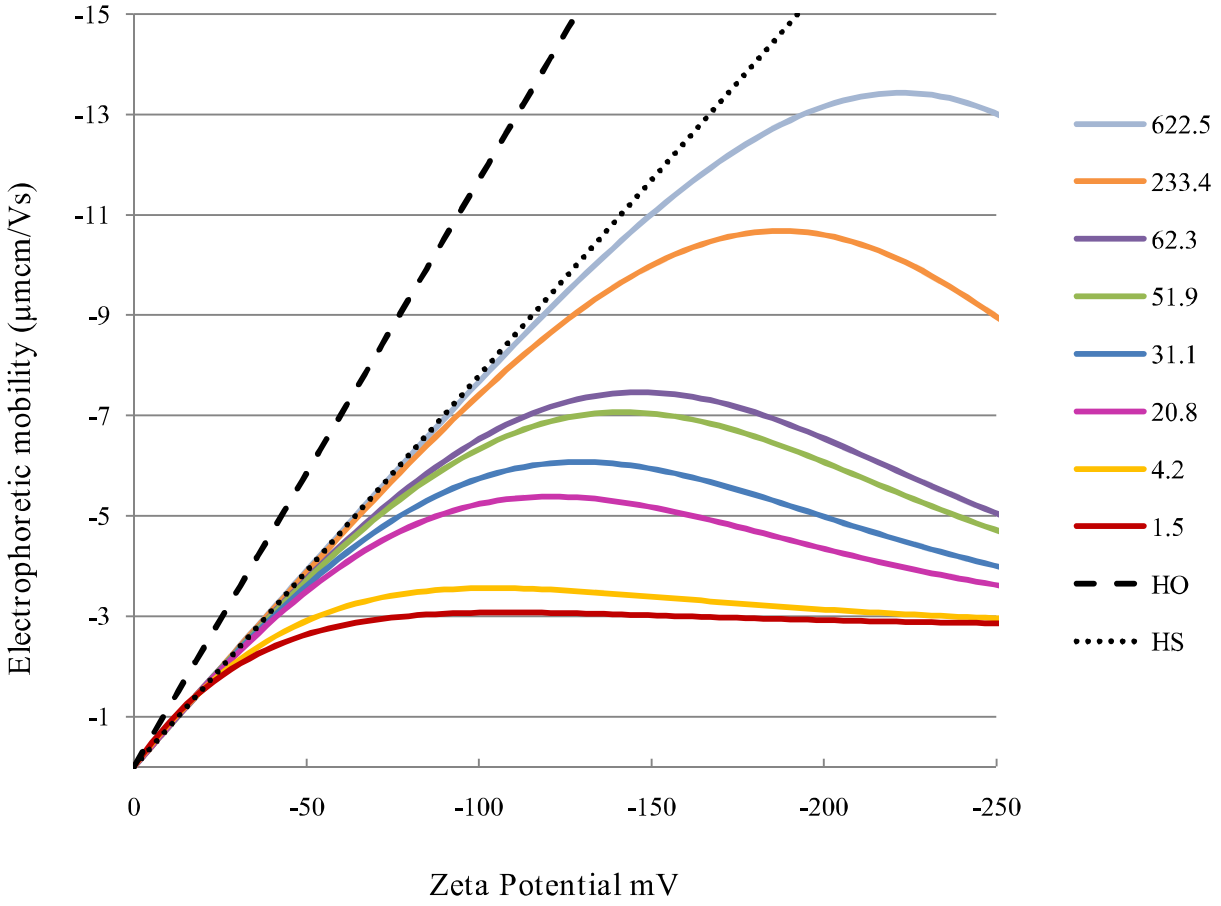

Figure 1.4: Electrophoretic mobility vs. zeta potential for κα values representative of study organisms according to O'Brien and Hunter.

Conduction of ions inside the slipping plane may be referred to in the literature as anomalous surface conduction, Stern layer, stagnant layer, or inner layer conductivity (Mangelsdorf and White, 1998; Delgado et al., 2007). In order to account for conduction inside the slipping plane the zeta potential must be calculated using a more computationally intensive theory. Such treatments have been put forth in the literature by Mangelsdorf and White (1990, 1998) and López-García, Grosse, and Horno (2007), among others. To employ these theories, additional information must be known about the particle surface, including: the affinity of the solution ions to the surface of the particle, the ratio of ionic mobility in the Stern layer to that in the solution, and the maximum number of free sites on the particle surface available for ionic species to attach (Malvern Instruments, 2007). These values of these parameters could be assumed for microorganisms. For example, Cryptosporidium is covered with carboxylate groups (Ranucci et al., 1993; Dai and Holzalski, 2003) and bacteria with phosphoric, carboxylic, hydroxyl, and amine groups (Hong and Brown, 2008). Ion affinity could be deduced based on the chemistry of these functional groups. However, these assumptions would introduce further uncertainty into the zeta potential calculation. Therefore models accounting for conduction inside the slipping plane were not pursued further in this study.

1.1.2 Microbes

The Poisson-Boltzmann equation characterizes the charge density around a particle in solution and is a fundamental link between the measured electrophoretic mobility and zeta potential. The five equations considered in this study make assumptions about the particle in order to solve the Poisson-Boltzmann equation: they assume ideal systems where the particle is rigid and spherical and moves in the laminar

flow regime, its surface is nonconducting, the Stern layer is at rest and does not move independently of the particle or conduct due to the field applied during electrophoresis, and the dielectric constant, viscosity, and ionic mobilities are uniform throughout mobile part of the double layer (Sennett and Oliver, 1965; van der Wal et al., 1997).

Bacteria, viruses, and parasites are non-ideal. Many are not rigid or spherical, but flexible and vary in shape. Microbes do not tend to have smooth surfaces and may possess external structures (e.g., cilia and flagella). Because of surface projections and functional groups, the boundaries between the Stern and diffuse layers may not be clearly defined. Cilia and flagella may themselves be charged and affect the electrophoretic mobility (Shi et al., 1996). Consequently, the location of the slipping plane may be highly variable in time and space. This variability may lead to conduction within the slipping plane, which would then violate the assumptions made by the models considered herein and result in the calculation of a zeta potential that is smaller in magnitude (Zukoski and Saville, 1986). The need to incorporate surface conduction or particle conductivity into the zeta potential calculation of bacterial cells is documented (van der Wal et al., 1997) and typical for bacteria in low ionic-strength environments (Einolf and Carstensen, 1967).

Several equations to calculate the zeta potential of conducting or "soft" particles possessing protruding functional groups have been proposed (Ohshima, 2000a; Ohshima, 2000b; Ohshima, 2001; Lopez-Garcia et al., 2007). Like the MW equation, detailed information about the particle surface (e.g., surface conductivity) is required to apply these theories and the EPM/zeta potential ceases to be the main parameter needed for characterization of the EDL (Ohshima, 2006; Delgado et al., 2007). Yunus and

coworkers (2002) published a simple method for determining bacterial particle conductivities, and rigorous determinations of the zeta potential of microorganisms should include both EPM and particle conductivity measurements.

1.1.3 Application of Equations

The measurement of EPM is always associated with a certain level of error. However, once the EPM measurement is obtained, the error of the zeta potential calculation can be controlled by choosing the most appropriate equation. The choice of equation ultimately depends on the accuracy of the EPM measurement and the amount of error the researcher is willing to accept. By determining the most accurate zeta potential possible with the available input data, the calculated zeta potential values can be compared to those determined by other means and/or for other interfaces with more confidence. Delgado and coworkers (2007) have provided an excellent review and detailed guidance for converting EPM measurements to zeta potential values. Their guidelines, along with the suggestions of equation limitations of Deshiikan and Papadopoulos (1998) and O'Brien and Hunter (1981), are presented graphically in Figure 1.5. This figure, called the equation zone chart, shows the boundaries of the equation application zones according to $\kappa\alpha$ and presumed zeta potential values as calculated by the Helmholtz-Smoluchowski equation. The boundaries of these zones are not sharp and it should be assumed that there is overlap between zones. The most clearly defined zones are those at the extremes of $\kappa\alpha$. For example, zones A4, B4 and C4 represent where $\kappa\alpha$ is < 1 and the HO and MW equations are most applicable for zeta potentials lower than $|50|$ mV and higher than $|50|$ mV, respectively. If $\kappa\alpha$ is large ($>> 1$) and the zeta potential is $\leq |25|$ mV (Figure 1.5 zones A1, A2, and A3) the choice of equation may also be

straightforward, since in these zones the HS or Henry equations are applicable (Delgado et al., 2007).

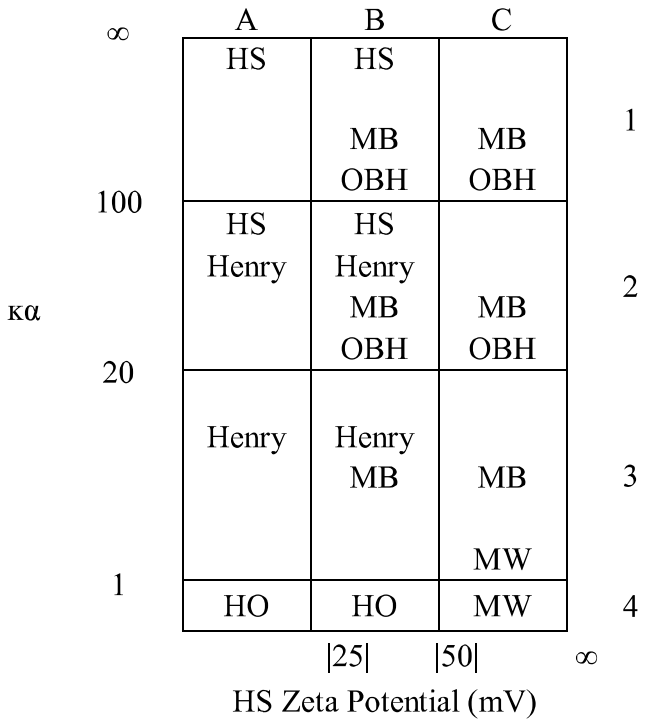

Figure 1.5: Equation zone chart. HS – Helmholtz-Smoluchowski, HO – Hückel-Onsager, MB – Modified Booth Equation, OBH – O'Brien-Hunter, MW – Mangelsdorf-White

The first complication in choosing an equation comes from deciding what a "large κα" value is. Delgado and coworkers suggest that κα > 20 is sufficient to consider the particle to be in the 'large κα regime' (2007). As shown by the representation of the Henry equation in Figure 1.2, a more appropriate guideline may be κα > 100 or even 1000, since $f(\kappa\alpha)$ does not reach 1.5 until κα is much greater than 20, suggesting that the Henry equation may be a more appropriate choice than the default HS equation for a large proportion of zeta potential calculations of environmental microbes. The second complication arises from the possibility of conduction inside the slipping plane, which would reduce the EPM and lead to smaller zeta potential values. "If the EPM of the

particle decreases with increasing electrolyte concentration, conduction inside the slipping plane can be considered negligible and the results of the HS equation trusted. If not, conduction inside the slipping plane may be significant" (Delgado et al., 2007). In this work, it was assumed that conduction inside the slipping plane (and Stern layer) was not significant, although studies have shown this is not always true for microorganisms (van der Wal et al., 1997).

At intermediate κα values, the particle and its double layer are of comparable size, which may lead to significant lowering of the EPM due to relaxation and retardation effects (Moncho et al., 2001), possibly requiring correction. In these zones (A2, A3, B2 and B3) where κα is between 20 and 100 and the HS zeta potential is ≤ |50| mV, the Henry equation is applicable (Delgado et al., 2007). In fact, the Henry equation may also be used over the range of κα values (as long as the HS zeta potential is low) since at extremes of κα the Henry equation defaults to the HS or HO equation. However, at HS zeta potentials above |50| mV (Figure 1.5, zones C1-3) the HS/Henry/HO equations may not be appropriate because of the occurrence of surface conductance (Delgado et al., 2007). The OBH and MB equations, which account for this phenomenon, may be required in these zones. The OBH and MB equations are suggested in zones B1 and B2, where HS zeta potential is intermediate (|25| to |50| mV), in order to account for possible EDL relaxation effects occurring at lower zeta potentials. O'Brien and Hunter have reported that their equation can be used for most values of zeta potential at κα values as low as 30 (1981). Therefore the OBH equation is not included in zone B3, where the κα is less than 20.

1.1.4 Project Goal

This work compared five methods of calculating zeta potential using an experimentally collected data set of electrophoretic mobilities to determine if the resulting zeta potentials were significantly different, and if complicated theories such as the OBH and MB were warranted when applying these theories to EPM's of microorganisms in low ionic strength water. Zeta potentials for various microbes in a 1 mM KCl solution, which represents the ionic strength normally found in potable water, were reported using each equation.

1.2 Materials and Methods

1.2.1 Organisms

A list of the microorganisms examined in this study is shown in Table 1.2. Bacteria and bacteriophage stocks were grown in batch culture and preserved according to the American Type Culture Collection methods (ATCC; Manassas, VA). Bacterial endospores were prepared according to a USEPA protocol. In this procedure, bacterial cells were grown in sterile Generic Spore Media (8g Nutrient Broth, 40mg $MnCl_2$, and 100mg $CaCl_2$ in 1-L deionized water) at 37 ^{o}C on a rotary shaker. After five days of incubation, the culture was evenly dispensed into 15mL conical tubes and placed in a 70 ^{o}C water bath for 20 minutes, then centrifuged at 4000xg for 20 minutes. The resulting supernatant was discarded and the pellets washed with 10ml of cold, sterile deionized water, vortexed for one minute, and centrifuged again at 4000xg for 20 minutes. The washing step was done twice. Following the second wash and centrifugation the resulting endospores were suspended in 40% ethanol for preservation. Bacteria and bacteriophage samples were thawed from frozen stocks for EPM measurements.

Human viruses studied were Hepatitis A virus (HAV) HM-175 clone 24A, Echovirus VR-1038, and two Adenovirus strains: AdV2 and AdV40 (Dugan strain). All virus stocks were prepared according to Cromeans and coworkers (Cromeans et al., 1989; Cromeans et al., 2008). Cryptosporidium parvum oocysts were obtained from the laboratory of Dr. Michael Arrowood of the Centers for Disease Control and Prevention, where they were purified using the method of Arrowood and Donaldson (1996). Giardia intestinalis cysts were purchased from Waterborne, Inc. (New Orleans, LA). Polystyrene microspheres (Carboxylate 4.5µm Fluoresbrite™ YG, Polysciences, Inc) were purchased from Polysciences, Inc. (Warrington, PA).

Table 1.2: Study organisms.

Microbe class	Organism Name	ATCC # or designation	Particle diameter (nm)	κα in 1mM KCl	Average Particle Concentration (pfu, cfu, or (oo)cysts/mL)
Bacteriophage	MS-2	15597-B1	23	1.2	3.0E+09
	Phi X-174	13706-B1	26	1.3	2.4E+08
Human Virus	Hepatitis A (HAV) HM-175	clone 24A	27	1.4	
	Echovirus	VR-1038	29	1.5	1.0E+06
	Adenovirus V40 (AdV40)	Dugan strain	80	4.2	
	Adenovirus V2 (AdV2)		80	4.2	
Vegetative Bacteria	F. tularensis	LVS	400	20.8	1.0E+07
	Y. pestis	A1122	600	31.1	1.0E+07
	E. faecalis	19433	700	36.3	1.0E+07
	S. enterica	14028	1000	51.9	1.1E+07
	E. coli	11775	1000	51.9	1.0E+07
Bacterial endospores	B. atrophaeus	subsp. globigii	1000	51.9	1.0E+07
	B. anthracis	Sterne strain	1200	62.3	1.0E+07
Parasites	Microspheres	Fluoresbrite™ YG	4500	233.4	1.0E+06
	C. parvum	Iowa 29IA8	5000	259.4	1.0E+06
	G. intestinalis	Human Isolate H-3	12000	622.5	5.0E+05

All organism samples were rinsed 3 to 5 times in 1 mM KCl (a 1:1 electrolyte solution) prior to analysis. In the US, conductivity of potable water varies from 50 to 1500 μS/cm (American Public Health Association et al., 1998). This range corresponds to KCl concentrations of roughly 0.1 to 10 mM (15 to 1,412 μS/cm). A midrange value of 1 mM KCl (conductivity approximately 146.9 μS/cm) was chosen to represent typical tap water. Atmospheric interactions (e.g., carbon dioxide partitioning) with samples were considered and all solutions were allowed to reach equilibrium with the atmosphere prior to analysis, resulting in a pH ~ 5.7 at the time of EPM measurement.

Electrophoretic mobilities of heat-inactivated C. parvum and Quality Control (QC) samples of three different organisms were also measured. The EPM of C. parvum was collected after heat-inactivation at 55 ^{o}C for 30 minutes and 80 ^{o}C for one hour. Inactivated oocysts were prepared and measured the same day as the original oocyst stock. Quality Control samples of S. enterica, B. atrophaeus subsp. globigii endospores, and C. parvum oocysts were also measured. Thirty-one days elapsed between the initial and QC-1 measurements of S. enterica and B. atrophaeus endospores. Two QC measurements were taken of the C. parvum stock. The first (QC-1) was taken 43 days after and the second (QC-2) 63 days after the initial EPM measurement.

1.2.2 Electrophoretic Mobility

The electrophoretic mobilities of study microbes were measured using a Zetasizer Nano ZS® (Malvern Instruments Inc., Westborough, MA). This instrument relies on a variation of laser Doppler velocimetry (LDV) to determine EPM. LDV uses an electrophoresis cell with an applied electrical potential and measures the particle mobility generated by assessing the frequency shift of light caused by particles moving in

the cell (Malvern Instruments Ltd., 2008). In addition, mixed mode measurement and phase analysis light scattering are employed to avoid electroosmotic effects (Malvern Instruments Ltd., 2007). To obtain electrophoretic mobility measurements, new capillary cells were rinsed with 10 mL of ultrapure water by attaching two 10mL syringes of ultrapure water to the cell and cycling the water back and forth 10 times. Samples were vortexed for 15 seconds, loaded into a sterile 3 mL syringe then added to the folded capillary cell taking care to avoid air bubbles. An additional 1-2 mL of sample was passed through the cell to ensure complete cell loading. Thermal contact plates were placed on each side of the capillary cell and the cell was promptly inserted into the instrument. A standard operating procedure (SOP) stored in the instrument's software was used to collect measurements. The stored SOP prompted for the sample name, measurement temperature (25 ^{o}C), temperature equilibration time to avoid thermal currents during measurements (~ 3 minutes), the number of readings to be used to produce one zeta potential value (typically 20 to 30, but was automatically determined by the instrument during measurement), and the number of replicate measurement to be performed on a single sample (set to 3). Separate samples from the same organism preparation were analyzed in duplicate or triplicate.

The double layer thickness of all microbes (κ^{-1}) in 1mM KCl was calculated to be 9.6 nm using equation 1.1. The size and shape of each microbe was determined by literature review and median values were used when a range of sizes was found. For non-spherical particles, the volumes of the microbes were calculated based on their sizes and shapes, and the resulting volumes were converted into equivalent diameters of

spheres with the same volume. Size information for each microbe is presented in Table 1.2.

1.2.3 Calculation of Zeta Potentials from Electrophoretic Mobilities

Due to the wide range of particle sizes used in this study and the desire to use a single electrolyte concentration typical of natural water samples, it was not possible have a single set of conditions that always satisfied the conditions of the Helmholtz-Smoluchowski or Hückel-Onsager models. Electrophoretic mobilities were used to calculate zeta potential using the Helmholtz-Smoluchowski/Henry/Hückel-Onsager system, modified Booth, and O'Brien and Hunter equations. All calculations used the constants presented in Table 1.3 as required.

Electrophoretic mobility measurements were taken well prior to initiation of zeta potential calculation and the guidelines provided by Delgado and coworkers were followed as closely as possible. However, it was not possible to determine if EPM decreased with increasing electrolyte concentration in order to rule out conduction inside the slipping plane. Organism conductivity measurements were not completed at the time of EPM measurement. To calculate the zeta potentials using the Helmhotz-Smoulchowski, Hückel-Onsager, and Henry functions (equations 1.2 through 1.4) along with Ohshima's expression for $\kappa\alpha$ (equation 1.5) were programmed in Microsoft Excel 2007. The MB equation as presented by Deshiikan and Papadopoulos (1998) was employed by programming the published code into MATLAB® (Version R2008b, The MathWorks, Natick, MA). The O'Brien and Hunter simplification was used to represent the O'Brien and White theory (O'Brien and Hunter, 1981). This equation was applied by

programming equation 24 from Delgado and coworkers (2007) into MATLAB and solving via the FZERO function with original guesses of 2 and 10.

Table 1.3: Constants used for zeta potential calculations.

Relative permittivity of KCl	$\varepsilon_{rs} = 78.5$
Dynamic viscosity of KCl	$\eta = 0.89 \times 10^{-3}$ N·s·m^{-2}
Temperature	T = 298.15 K
Limiting conductance of K^+	73.5 (x 10^{-4} m^2·s·equiv^{-1})
Limiting conductance of Cl^-	76.3 (x 10^{-4} m^2·s·equiv^{-1})
Dimensionless ion mobility	m = 0.15
Boltzmann constant	k = 1.38 x 10^{-23} m^2·kg·s^{-2}·K^{-1}
Avogadro constant	N_A = 6.02 x 10^{23} mol^{-1}
Elementary charge	e = 1.60 x 10^{-19} C

In order to compare the five zeta potential models, the best estimate of electrophoretic mobility for each organism was determined. The EPM of each study organism was measured three times and in duplicate or triplicate by the Zetasizer. This resulted in six to nine EPM measurements for each organism (i = 6 or 9). However, each EPM measurement output by the instrument was the average of several (M ≈ 30) measurements. For each EPM output i of a total of M measurements, the instrument provided the best estimate of the mean mobility and standard deviation of the population of mobility measurements, represented by $\hat{x}_i$ and σ_i. If x_{ij} is the jth mobility measurement of n_i measurements in sample i, then the overall best estimate of the mean mobility, $\bar{x}$,and the standard deviation of the mean, σ, were given by:

$$\bar{x} = \sum_{i=1}^{M} \sum_{j=1}^{n_i} x_{ij} \Big/ \sum_{i=1}^{M} n_i \qquad (1.6)$$

and

$$\sigma = \left[\sum_{i=1}^{M} \sum_{j=1}^{n_i} (x_{ij} - \bar{x})^2 \Big/ \left(\sum_{i=1}^{M} n_i - 1 \right) \Big/ \sum_{i=1}^{M} n_i \right]^{1/2} \tag{1.7}$$

Since the individual measurements x_{ij} were not available, in order to get the overall best estimate the output data were combined to calculate the mean and standard deviation of the mean as:

$$\bar{x} = \sum_{i=1}^{M} n_i \hat{x}_i \Big/ \sum_{i=1}^{M} n_i \tag{1.8}$$

and

$$\sigma = \left[\sum_{i=1}^{M} \left[(n_i - 1)\sigma_i^2 + n_i (\hat{x}_i - \bar{x})^2 \right] \Big/ \left(\sum_{i=1}^{M} n_i - 1 \right) \Big/ \sum_{i=1}^{M} n_i \right]^{1/2} \tag{1.9}$$

The best estimate of the zeta potential was assessed the using the different models. For each model the zeta potential was calculated using the best estimate of the mean mobility, $\bar{x}$. The standard deviation of each mean zeta potential was approximated using the formula:

$$\sigma_Z = \left| \frac{\partial f}{\partial u_e} \right| \sigma \tag{1.10}$$

Where $\frac{\partial f}{\partial u_e}$ was the first-order derivative of the zeta potential calculation with respect to the EPM. First-order derivatives with respect to EPM for each of the models studied are presented in APPENDIX A.

In order to compare the zeta potential values output by the different models, an ANOVA was performed for each organism, followed by Tukey's Honestly Significant Difference (HSD) post-hoc test to make pair-wise comparisons. The individual organism

results were grouped by the zones presented in the equation zone chart (Figure 1.5) and examined to determine if simplifications of the equation zone chart were possible.

1.3 Results

Electrophoretic mobility measurements were obtained for 22 microbe samples suspended in 1mM KCl (conductivity ~ 147 μS/cm, pH ~ 5.7). EPM measurements are reported in the units of μm•cm/V•s, a convention used to simplify numerical and graphical representation. Average EPM measurements and 95% confidence intervals of the mean (CI_m) for study organisms are presented in Figure 1.6. The majority of organism EPMs had narrow 95% CI_m's. However, Echovirus showed a very high variation in its EPM measurements and subsequently a very wide 95% confidence interval. The average EPM measurements of all the organisms examined were in the range of 0 to -7 μm•cm/V•s.

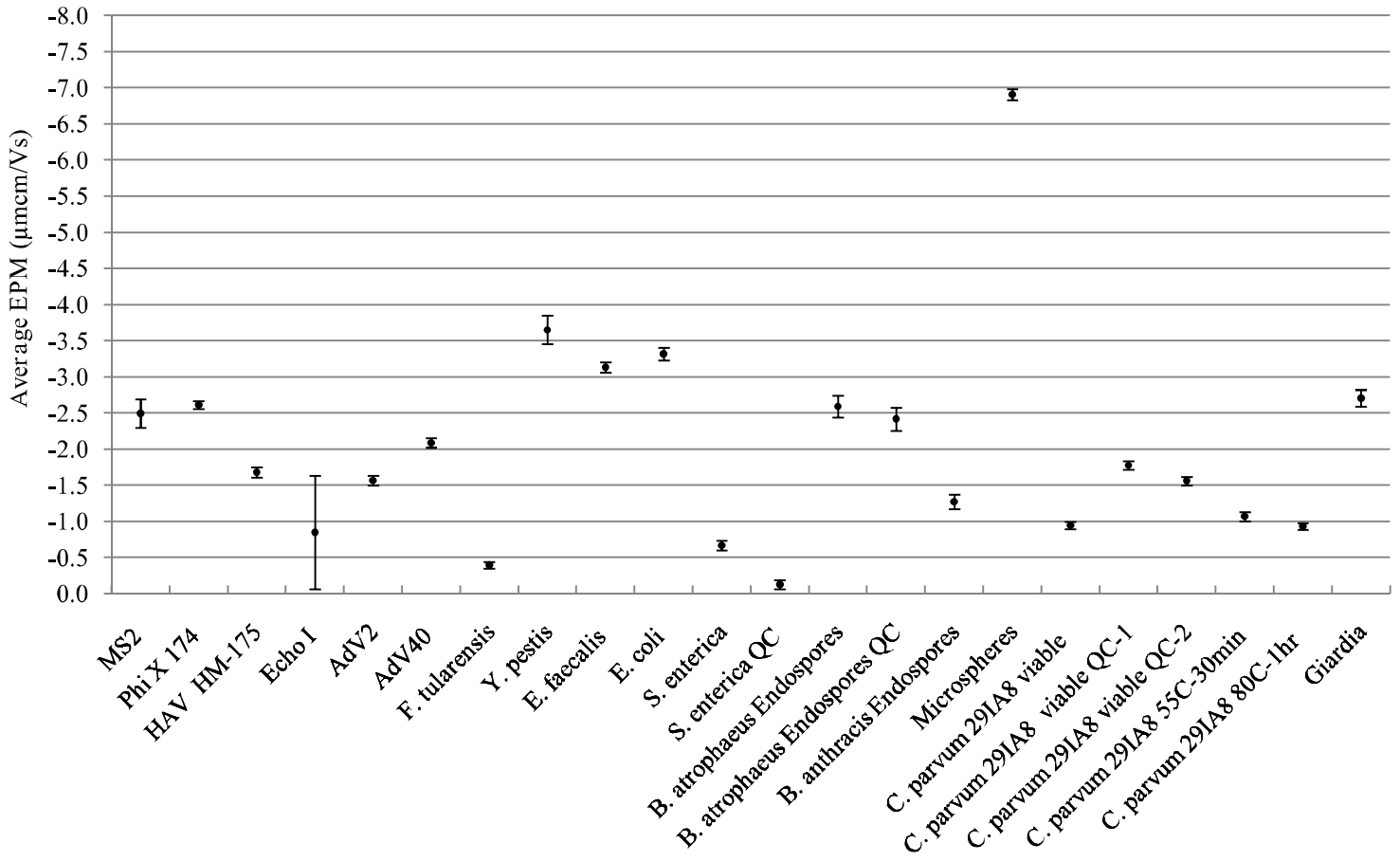

Figure 1.6: Average electrophoretic mobilities of study organisms with 95% CI_m

The Hückel-Onsager, Henry, Helmholtz-Smoluchowski, modified Booth, and O'Brien-Hunter equations were used to convert the EPM for each microbe sample to zeta potential. Programming the zeta potential equations was straightforward with the exception of a typographical error found in the Deshiikan and Papadopoulos paper and the theoretical mobility maximum predicted by the O'Brien and Hunter equation. While reproducing the graphs of Deshiikan and Papadopoulos, a sign error was found in the code provided in the article. It should be noted that when programming the Function Z^*_3, for $1.52 < x \leq 3.40$, the code should read $Z^*_3 = -0.02096594772 + 0.0256531567x - 0.007420778x^2 + 0.0007183267x^3$, rather than the relationship provided in Deshiikan and Papadopoulos, 1998, Table 1. Employing the OBH model was complicated by the theoretical mobility maximum predicted, which is illustrated in Figure 1.4. Table 1.4 shows that this equation led to two zeta potential solutions for the same electrophoretic mobility, which O'Brien and Hunter avoided in some part by employing Zeta bar (= $e\zeta/kT$). Generally the first result returned a low zeta potential, while the second returned a very high zeta potential that, under most circumstances would be theoretically improbable. According to O'Brien and White, if the absolute value of the true zeta potential was greater than 250 mV, this would violate the Poison-Boltzmann equation on which the equation is based (1978). Therefore the first solution obtained from the OBH equation (MATLAB starting guess = 2) was used in model comparisons, while the second solution was retained only for reference.

Table 1.4: Comparison of results for κα = 50 to those of O'Brien and Hunter (1981). Predicted mobility maximum occurs between -6.83 and -6.91 μm•cm/V•s.

O'Brien and Hunter (1981)			MATLAB OUTPUT			
Mobility (μm•cm/V•s)	Zeta bar (=eζ/kT)	Zeta (mV)	Zeta 1 (mV)	% error	Zeta 2 (mV)	% error
-4.45	9.99	-256.99	-61.73	76	-259.11	-1
-6.49	6.89	-177.06	-106.09	40	-180.11	-2
-6.91	5.68	-145.95	-126.64	13	-155.78	-7
-6.83	4.90	-125.83	-120.91	4	-162.18	-29
-6.55	4.31	-110.69	-108.11	2	-177.53	-60
-6.18	3.83	-98.40	-96.63	2	-192.85	-96
-5.76	3.42	-87.96	-86.59	2	-207.96	-136
-5.34	3.07	-78.78	-77.68	1	-223.34	-183
-4.91	2.76	-70.55	-69.63	1	-239.61	-240
-4.48	2.45	-63.02	-62.24	1	-257.70	-309

Table 1.5 presents the average EPM, its standard deviation of the mean, zeta potentials determined by the 5 models, and zone placement for each organism. Figure 1.7 displays the location of each organism with respect to the zones and shows that the majority fell in zones A1 through B3 (κα greater than 1, zeta potential less than |50| mV), and several organisms were classed into intermediate areas where the choice of equation is not easily made. In 1 mM KCl, viruses were placed in zones A3 and B3 due to their low κα values. Bacteria (both vegetative and endospores) were placed in zones A2 and B2, while parasites fell within zones A1 and B1. Only microspheres had a HS zeta potential greater than |50| mV, placing them in zone C1.

Table 1.5: Zeta potential results of all 5 models.

Sample Name	κα	Zone	$f(\kappa\alpha)$	n Total EPM meas.	Avg. EPM μm•cm /V•s	EPM Std Dev of the mean μm•cm/ V•s	HS	Hen	HO	MB	OBH sln 1
MS2	1.2	B3	1.04	141	-2.49	0.10	-31.8	-45.8	-47.7	-50.1	-45.5
Phi X 174	1.3	B3	1.04	207	-2.61	0.03	-33.3	-47.9	-50.0	-52.9	-50.3
HAV HM-175	1.4	A3	1.05	228	-1.68	0.04	-21.4	-30.7	-32.2	-32.2	-22.9
Echo I	1.5	A3	1.05	165	-0.85	0.40	-10.8	-15.4	-16.2	-15.8	-9.7
AdV2	4.2	A3	1.13	199	-1.57	0.03	-20.0	-26.6	-30.0	-27.5	-20.5
AdV40	4.2	B3	1.13	204	-2.09	0.03	-26.6	-35.4	-39.9	-37.6	-29.6
F. tularensis	20.8	A2	1.36	227	-0.39	0.02	-5.0	-5.6	-7.5	-5.7	-4.8
Y. pestis	31.1	B2	1.40	201	-3.65	0.10	-46.6	-50.0	-69.9	-54.4	-50.8
E. faecalis	36.3	B2	1.41	198	-3.13	0.04	-40.0	-42.5	-59.9	-44.9	-42.1
B .atrophaeus endospores	51.9	B2	1.43	236	-2.59	0.08	-33.1	-34.6	-49.6	-35.7	-33.8
B. atrophaeus endospores QC day 31	51.9	B2	1.43	243	-2.42	0.08	-30.8	-32.3	-46.3	-33.2	-31.5
E. coli	51.9	B2	1.43	198	-3.32	0.04	-42.3	-44.3	-63.5	-46.3	-44.2
S. enterica	51.9	A2	1.43	249	-0.66	0.03	-8.5	-8.9	-12.7	-9.0	-8.4
S. enterica QC day 31	51.9	A2	1.43	257	-0.12	0.03	-1.6	-1.6	-2.4	-1.7	-1.5
B. anthracis	62.3	A2	1.44	245	-1.27	0.05	-16.2	-16.8	-24.3	-17.1	-16.2
Microspheres	233.4	C1	1.48	198	-6.91	0.04	-88.2	-89.1	-132.2	-93.3	-92.4
C. parvum 29IA8 viable	259.4	A1	1.49	218	-0.94	0.03	-12.0	-12.1	-18.0	-12.3	-12.0
C. parvum 29IA8 viable QC-1 day 43	259.4	A1	1.49	213	-1.78	0.03	-22.7	-22.9	-34.0	-23.2	-22.7
C. parvum 29IA8 viable QC-2 day 63	259.4	A1	1.49	226	-1.56	0.03	-19.9	-20.1	-29.8	-20.3	-19.9
C. parvum 29IA8 55 ^{o}C-30min	259.4	A1	1.49	220	-1.07	0.03	-13.6	-13.8	-20.4	-13.9	-13.6
C. parvum 29IA8 80 ^{o}C-1hr	259.4	A1	1.49	214	-0.93	0.02	-11.9	-12.0	-17.8	-12.1	-11.8
Giardia intestinalis	622.5	B1	1.49	215	-2.70	0.06	-34.5	-34.6	-51.8	-35.0	-34.5

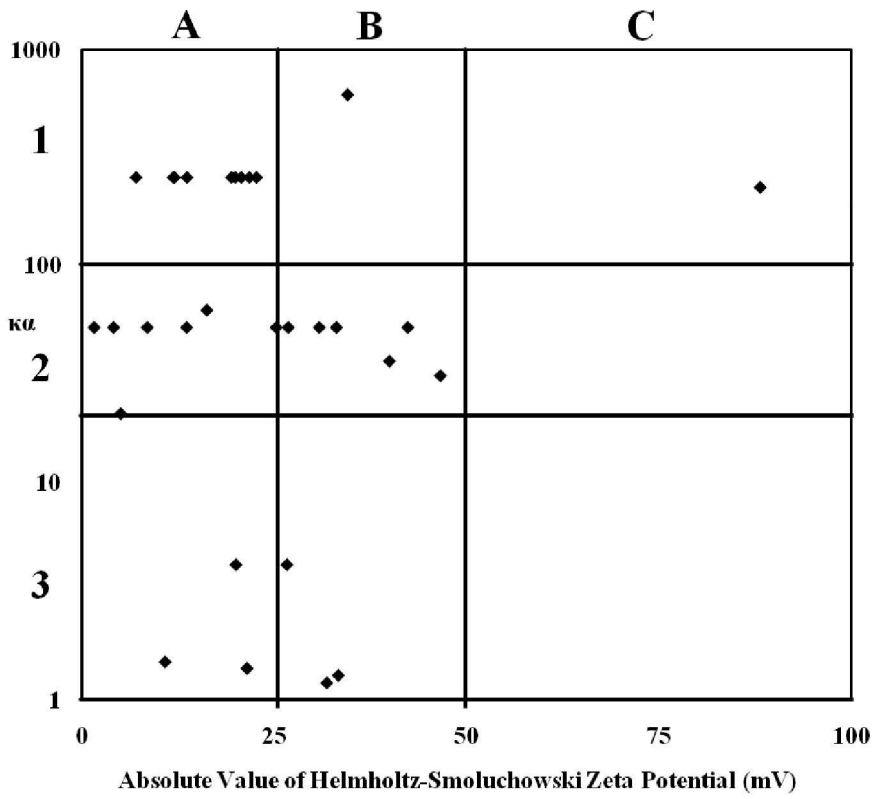

Figure 1.7: Zone chart with average Helmholtz-Smoluchowski zeta potentials of study organisms.

An ANOVA performed on individual study organisms found the 5 models under consideration produced significantly similar zeta potentials at the 95% confidence level. Echovirus and QC S. enterica had mobility deviations greater than their EPM's, leading to rejection of the null hypothesis due to high within-group variability. Results of Tukey's HSD post-hoc test were grouped by zones, as presented in Figure 1.5 and Figure 1.7, with the goal of simplifying the graphical guidelines. Table 1.6 presents the results of Tukey's HSD analysis within the zones and suggests the choice of equation may be simplified in several zones. In Table 1.6 zeros indicate that 0% of the organisms were found to have significantly different zeta potentials using the equations in question, while a value of 100 indicates 100% of the organisms in that zone had significantly different

zeta potentials. In zones A1 and A2 all of the equations resulted in zeta potential values that were not significantly different. In zone B2, an important percentage of the organisms had significantly different zeta potentials when calculated using different equations. For example, in zone B2 the HS equation resulted in significantly different zeta potentials than were predicted by the MB equation in 43% of the examined cases. Only one organism (Giardia intestinalis) fell within zone B1, therefore the results in this zone must be interpreted with caution. In zone A3, only the Henry equation is suggested for use and statistical analysis showed that equations resulted in significantly different zeta potential values in all cases except H-MB and HS-OBH.

Table 1.6: Percent of organisms with significant difference between zeta potentials as determined by Tukey's Honestly Significant Difference test. 0 = no organisms in group were significantly different, 100 = 100% organisms in group were significantly different.

Zone	n	HS-H	HS-MB	HS-OBH	H-MB	H-OBH	MB-OBH	HS-HO	H-HO	HO-MB	HO-OBH
A1	9	0	0	0	0	0	0	100	100	100	100
A2[a]	4	0	0	0	0	0	0	100	100	100	100
A3[b]	2	100	100	0	0	100	100	100	50	50	100
B1	1	0	0	0	0	0	0	100	100	100	100
B2	7	14	43	14	14	0	14	100	100	100	100
B3	3	100	100	100	67	67	67	100	67	67	33
C1	1	0	100	100	100	100	0	100	100	100	100

[a] Two Salmonella observations were removed due to high standard deviation

[b] Echo virus data removed due to high standard deviation

The results presented in Table 1.6 highlight the continuum that exists in the HS/Henry/HO equations. The HS and HO equations resulted in different zeta potentials in 100% of the cases examined, as would be expected as HO = 1.5HS. As all organisms in this study had $\kappa\alpha$ values greater than 1 in 1mM KCL, the HO calculation is shown for comparative purposes only. The Henry equation was only different from the HS in zones A3 and B3, when the $\kappa\alpha$ value approached 1 and so the results of the Henry equation

approximated the results of the HO equation. Similarly, the Henry equation began to show a reduced percentage of significant differences from the HO equation in zones A3 and B3, indicating that in these zones the Henry equation was necessary and the HS and HO equations may not have been suitable.

Results in the intermediate zones of B2 and B3 were not completely clear from the comparison presented in Table 1.6. In these zones graphical representations of the 95% CI_m's made differences between organisms and equations more apparent. Figure 1.8, which shows the zeta potentials of organisms in zone B2, revealed that all the equations except HO tended to produce similar zeta potentials as the $\kappa\alpha$ values increased and EPM values decreased in this zone. More importantly, since their 95% CI_m's overlapped, Figure 1.8 shows that the zeta potentials determined by the Henry and O'Brien and Hunter equations were the same. This was confirmed by Tukey's HSD results. As shown in Table 1.6, the HS and MB equations produced significantly different zeta potentials in 43% of the organisms in zone B2, which precluded the simplification of equation choice in this zone. However, for the purposes of this study, the HS equation was selected for application to organisms in this zone. This choice led to a difference in zeta potential estimations of 14% for Y. pestis and 11% for E. faecalis. Although there were few observations in zone B3, results suggested that none of the equations resulted in similar zeta potentials. The small number of instances where less than 100% of the organisms in B3 were significantly different (H-MB, H-OBH, MB-OBH) were caused by MS2 indicating no difference between equations due to its relatively high standard deviation.

Only polystyrene microspheres had a $\kappa\alpha$ and EPM high enough to fall within zone C1. Results for this organism indicated the O'Brien and Hunter and modified Booth equations were significantly different from the Henry and Helmholtz-Smoluchowski equations while the MB and OBH equations were not significantly different from each other.

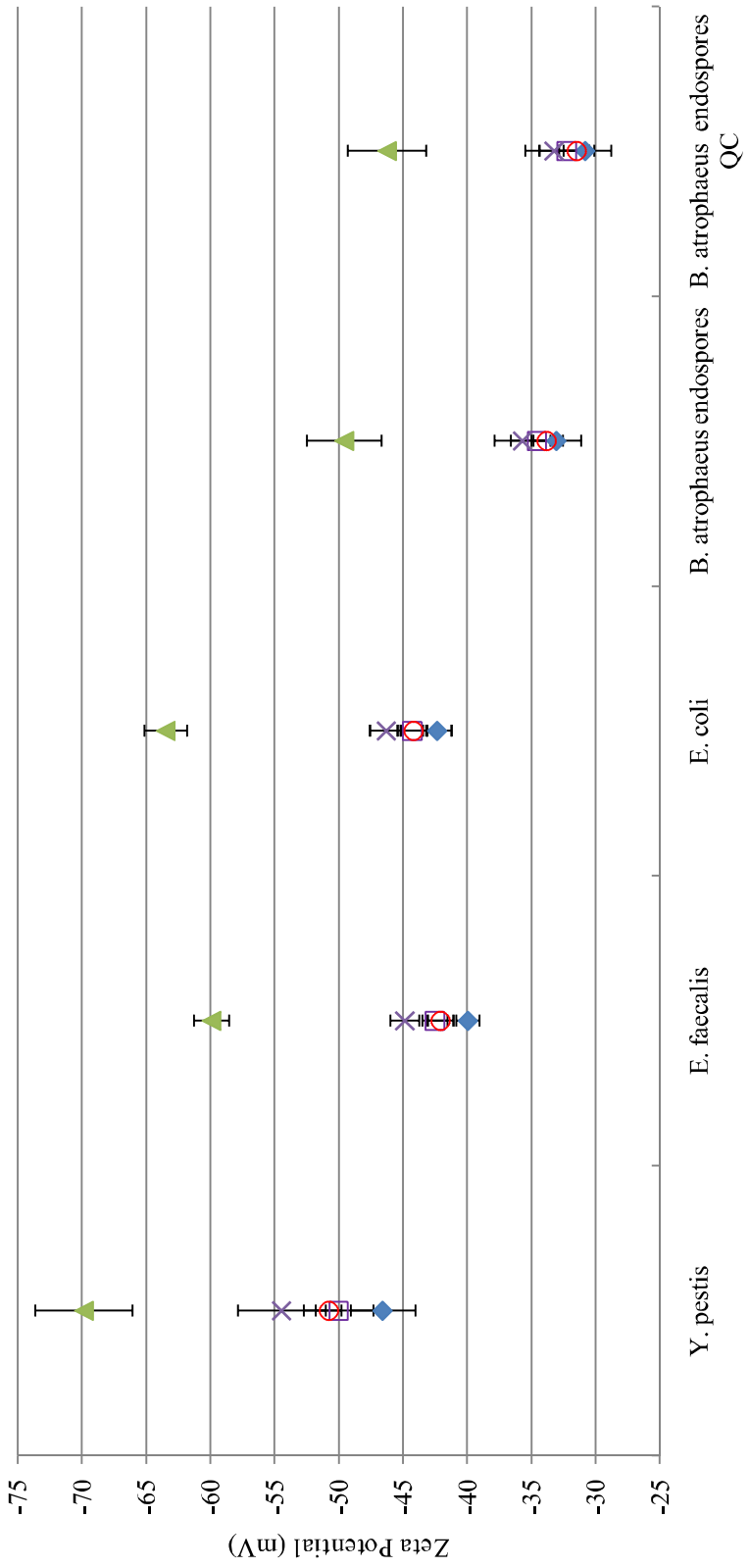

Figure 1.8: Comparison of model results in zone B2.

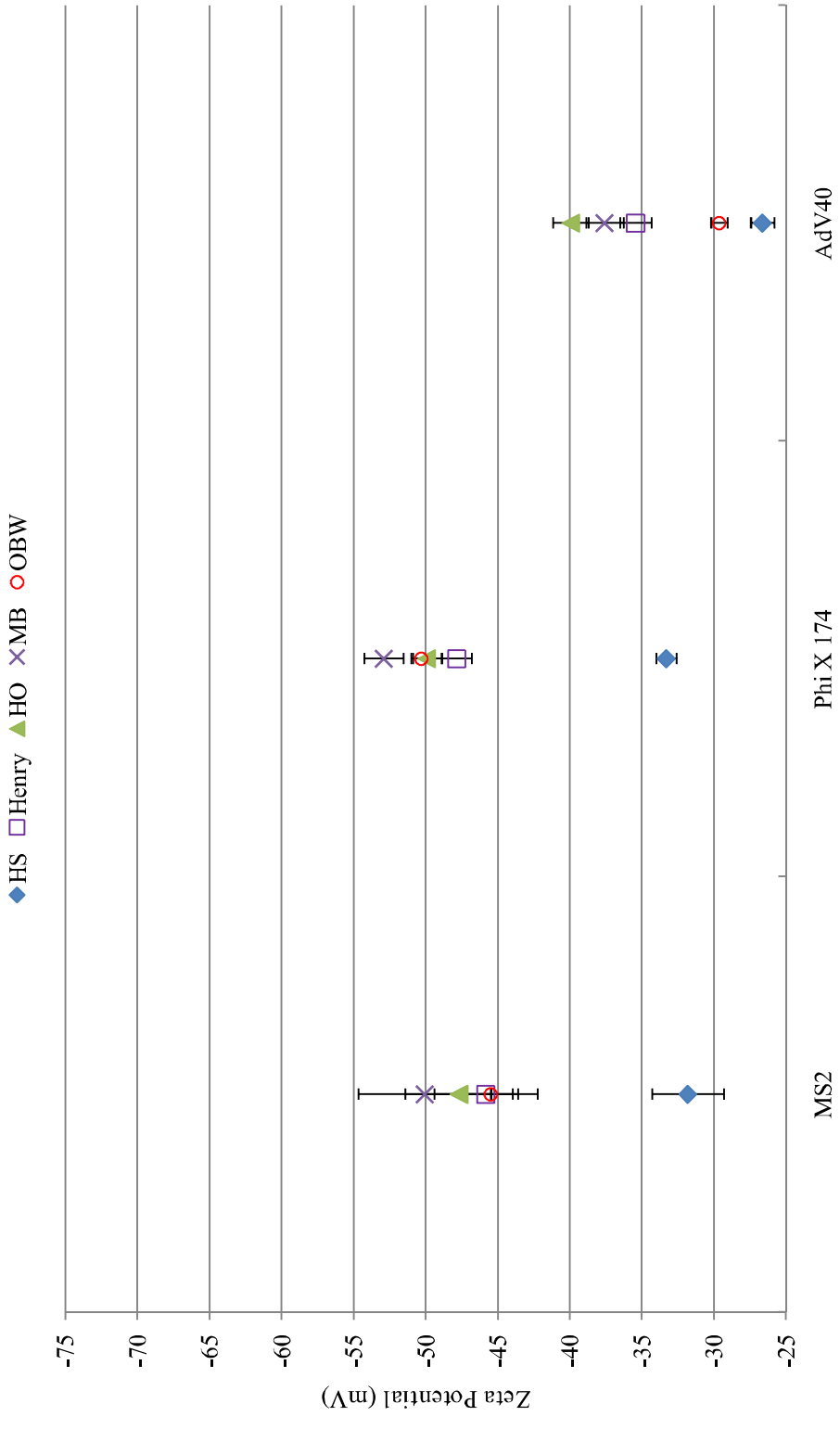

Figure 1.9: Comparison of model results in zone B3.

Uncertainty of Zeta Potential Calculation due to Independent Variables

By conducting a first-order sensitivity analysis, the uncertainties of zeta potential calculations due to EPM (u_e) measurements and temperature were assessed. The error due to the EPM was assumed to be equal to the standard deviation of the EPM measurement determined via equations 1.9 and 1.10. The relative errors due to u_e measurement are presented in Table 1.7. These values ranged from 0.6% for Microspheres to 47% for Echovirus, but were generally less than 5%.

Table 1.7: Relative error of zeta potential measurements due to uncertainty of the electrophoretic mobility.

Sample Name	Equation	Mean Zeta (mV)	Zeta SD (mV)	u_e Error %
MS2	MB	-50.1	2.35	4.7
phi X 174	MB	-52.9	0.69	1.3
HAV HM-175	Hen	-30.7	0.66	2.2
Echovirus	Hen	-15.4	7.29	47.3
AdV2	Hen	-26.6	0.57	2.1
AdV40	MB	-37.6	0.66	1.8
F. tularensis	HS	-5.01	0.29	5.8
Y. pestis	HS	-46.6	1.29	2.8
E. faecalis	HS	-40	0.47	1.2
B .atrophaeus endospores	HS	-33.1	0.99	3.0
B. atrophaeus endospores QC day 31	HS	-30.8	1.04	3.4
E. coli	HS	-42.3	0.57	1.3
S. enterica	HS	-8.48	0.42	5.0
S. enterica QC day 31	HS	-1.57	0.40	25.3
B. anthracis	HS	-16.2	0.65	4.0
Microspheres	OBH	-92.4	0.54	0.6
C. parvum 29IA8 viable	HS	-12	0.34	2.8
C. parvum 29IA8 viable QC-1 day 43	HS	-22.7	0.38	1.7
C. parvum 29IA8 viable QC-2 day 63	HS	-19.9	0.38	1.9
C. parvum 29IA8 55 ^{o}C-30min	HS	-13.6	0.41	3.0
C. parvum 29IA8 80 ^{o}C-1hr	HS	-11.9	0.31	2.6
Giardia intestinalis	HS	-34.5	0.76	2.2

The uncertainty of zeta potential calculations due to temperature was determined for the HS, Henry, and HO equations. The Malvern Zetasizer Nano ZS has a precision of 0.1 ^{o}C (Malvern Instruments Ltd, 2010), leading to an uncertainty of 0.2% for the HS and HO equations. Since the uncertainty of the zeta potential due to temperature is based on the uncertainty of the $\kappa\alpha$ value, the relative error of the zeta potential due to temperature for the Henry equation also affects the $f(\kappa\alpha)$. For a $\kappa\alpha = 60$ (e.g., in the linear portion of Figure 1.2) the uncertainty due to temperature was 0.1%. Therefore, for the majority of study organisms, the uncertainty due to temperature effects was one order of magnitude lower than the uncertainty due to the EPM measurement.

1.4 Discussion

1.4.1 Electrophoretic Mobility vs. Zeta Potential

EPM measurements of microorganisms in 1mM KCl were found to be similar. Figure 1.6 showed that all organisms studied had mean EPM's values between zero and -7 μm•cm/V•s. Human virus AdV2 and Cryptosporidium QC-2 oocysts both had average EPM values of -1.57 μm•cm/V•s. However, when the equation guidelines were applied, the AdV2 zeta potential was calculated using the Henry equation, and resulted in a zeta potential of -26.6 mV, while the zeta potential of the Cryptosporidium QC-2 oocysts was calculated with the HS equation to be -19.9 mV. This 25% difference in zeta values highlights the importance of calculating the zeta potential rather than comparing the electrophoretic mobilities of organisms directly, since samples may have similar EPM values but different zeta potential values due to different organism sizes (Delgado et al., 2007). In general, EPM values that were collected under different conditions cannot be

readily compared. However, the calculation of zeta potential takes into account factors such as the size of the organism and the thickness of the electrical double layer, facilitating comparison between types of particles (or organisms) and measurements taken in different experiments.

1.4.2 Equations

Five equations to calculate zeta potential from EPM measurements were applied to the experimentally acquired data set. The calculated zeta potentials were compared via ANOVA using the variance imparted to the zeta potential value by the uncertainty of the EPM measurement. As all comparisons between zeta potentials were made using a single data set, the conclusions made here may apply only to this study.

As shown in Figure 1.7, the majority of zeta potentials determined using the HS equation were less than |50| mV. According to Delgado and coworkers, this ruled out the need to account for concentration polarization (2007). When concentration polarization was taken into account for HS zeta potentials greater than |25| mV by using the MB or OBH equations, the differences between the resulting zeta potentials were not significantly different from the HS output except in zones B2, B3 and C1. Using a more computationally intensive theory in zones A1, A2, and B1 was unnecessary, and the simplest equation (e.g., HS) could be applied. However, in zone A3 the Henry equation should be used because of low $\kappa\alpha$ values.

In zones B2 and B3, the HS-calculated zeta potential had moderate to high values where concentration polarization and surface conduction may have needed to be accounted for. At $\kappa\alpha$ values from 20 to 100 (zone B2), the OBH and MB equations tended to result in zeta potentials that were not significantly different from the Henry

equation. Only one organism of the 7 in this zone, E. faecalis, suggested significant differences between all the models. Since only 43% of the study organisms in zone B2 had HS zeta potentials that were significantly different than the MB equation, a simplification could not be made to this zone. This may also suggest that zone B2 should be divided into sub-zones or the zone approach is not appropriate for this section of the chart. Although a simplification to zone B2 could not be made, the HS equation was applied to organisms in this zone for reference purposes.

In zone B3, where $\kappa\alpha$ was less than 20 and HS-calculated zeta potential was moderate to high, the MB and OBH equations resulted in significantly different zeta potentials than the HS and Henry equations. Only one organism did not support this result, bacteriophage MS2, which had a high standard deviation of the EPM. O'Brien and Hunter state that using the OBH equation "at a $\kappa\alpha$ value of approximately 30, the error is tolerable and can be allowed for most values of zeta potential" (1981). This, along with the findings presented here, suggests that in the case of organisms with $\kappa\alpha$ in the range of 1 to 20, the full O'Brien and White theory may be required and the O'Brien and Hunter approximation is not sufficient. The MB equations produces higher zeta potentials in this range because of the relaxation correction, which begins affect zeta potential calculations when the HS-predicted zeta potential is greater than |25|mV. However, the correction for relaxation is not considered significant until an HS zeta potential ~ |50|mV (Deshiikan and Papadopoulos, 1998). Yet results showed that in zone B3 the MB equation predicted significantly higher zeta potentials than both the Henry and OBH equations. At low values of $\kappa\alpha$ the EDL is considered 'thick' and because the EDL large in comparison to the size of the particle the effect of relaxation could be

significant and require correction in this zone (Moncho et al., 2001). The Booth correction functions have their highest values in the region of κα 1 to 40, with a maximum near κα = 10. Overall, results suggested the MB equation should be applied to organisms in zone B3 in order to fully correct for relaxation effects.

The only particle that clearly required the use of the MB or OBH equations was the Carboxylate-modified 4.5μm Fluoresbrite™ YG microspheres. This Cryptosporidium surrogate was the only organism placed in zone C1, where κα and EPM are high, suggesting concentration polarization and surface conductance were occurring and needed to be accounted for. For this organism the MB and OBH equations resulted in the same zeta potentials. With only one observation in this zone, conclusions in this region could not be made.

Comparison of the five zeta potential theories suggested the guidelines presented by Delgado and coworkers (2007) are applicable to environmental microbes in 1mM KCl. This assessment also showed the MB equation should be used at low κα and moderate HS-calculated zeta potentials. Figure 1.10 presents simplified guidelines determined from this study.

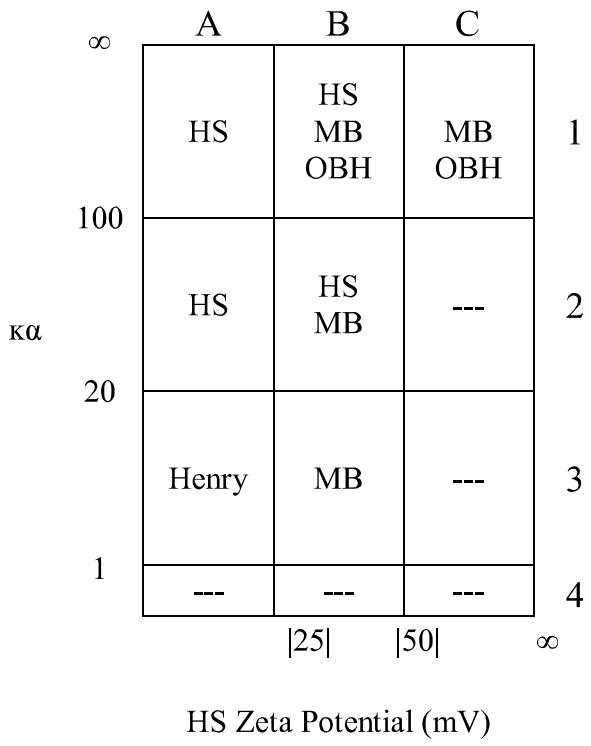

Figure 1.10: Simplified guidelines based on zones in Figure 1.5 for zeta potential calculation.

Because of significant differences between the results of the Hückel-Onsager and Helmholtz-Smoluchowski equations, the choice of equation must be examined when calculating the zeta potentials of organisms in environmental matrices. By assuming one equation over another, a significantly different zeta potential will be calculated. This is particularly of importance when relying on instrument defaults for calculating the zeta potential directly from EPM measurements. The HO and HS equations are usually available, but the Henry, MB and OBH equations are typically not built-in to software packages. The results of this study indicated the Henry and MB equations are needed to accurately determine the zeta potential when κα values are between 1 and 20. For environmental microbes in low ionic strength matrices, κα values were frequently found to be in this range. By reporting only the EPM, this problem may be avoided; however

the EPM doesn't account for the organism size. In addition, EPM should be interpreted based on the properties of the electrolyte matrix, which are incorporated into zeta potential calculations. An accurate knowledge of the zeta potential (and thus the electrostatic properties) of microorganisms in water matrices provides important information for understanding and predicting their stability and adhesion characteristics.

1.4.3 Microbes

Based on the guidelines established in this study, the best estimate of zeta potentials of the environmental microbes studied are presented in Table 1.8. Table 1.8 also includes the 95% CI_m of the best zeta potential calculated using equation 1.10 (the first-order derivative of the zeta potential with respect to the mobility, as shown in APPENDIX A, multiplied by the standard deviation of the mean EPM) multiplied by 1.96. Generally the Helmholtz-Smoluchowski equation was used for bacteria and parasites and the Henry or MB equations for viruses. The O'Brien and Hunter equation was selected for conversion of the EPM of carboxylated microspheres. Results showed the majority of organisms had zeta potentials higher than |40|mV. Comparisons between groups of organisms showed differences existed between microbes of public health concern and their commonly used surrogates, as well as originally measured microbe stocks and their QC samples.

Table 1.8: Best zeta potentials with 95% CI_m.

Sample Name	κα	Zone	Equation	Mean Zeta (mV)	Zeta 95% CI_m (mV)
MS2	1.2	B3	MB	-50.08	4.60
phi X 174	1.3	B3	MB	-52.91	1.36
HAV HM-175	1.4	A3	Hen	-30.71	1.30
Echovirus	1.5	A3	Hen	-15.42	14.29
AdV2	4.2	A3	Hen	-26.61	1.11
AdV40	4.2	B3	MB	-37.58	1.30
F. tularensis	20.8	A2	HS	-5.01	0.57
Y. pestis	31.1	B2	HS	-46.57	2.52
E. faecalis	36.3	B2	HS	-39.95	0.92
B .atrophaeus endospores	51.9	B2	HS	-33.06	1.94
B. atrophaeus endospores QC day 31	51.9	B2	HS	-30.83	2.04
E. coli	51.9	B2	HS	-42.33	1.11
S. enterica	51.9	A2	HS	-8.48	0.83
S. enterica QC day 31	51.9	A2	HS	-1.57	0.78
B. anthracis	62.3	A2	HS	-16.21	1.28
Microspheres	233.4	C1	OBH	-92.4	1.06
C. parvum 29IA8 viable	259.4	A1	HS	-12.01	0.66
C. parvum 29IA8 viable QC-1 day 43	259.4	A1	HS	-22.68	0.75
C. parvum 29IA8 viable QC-2 day 63	259.4	A1	HS	-19.9	0.74
C. parvum 29IA8 55 ^{o}C-30min	259.4	A1	HS	-13.63	0.81
C. parvum 29IA8 80 ^{o}C-1hr	259.4	A1	HS	-11.86	0.60
Giardia intestinalis	622.5	B1	HS	-34.51	1.49

The "best" mean zeta potential estimates are presented in Table 1.8. These zeta potentials were compared to the results of the 4 alternative equations studied via percent difference, the results of which are shown in Table 1.9. For the Giardia cysts and Cryptosporidium oocysts all equations (except HO) returned zeta potentials within 1-2% of the zeta calculated according to the suggested HS equation. The OBH equation was selected the best theory to apply to calculate the zeta potential of microspheres. However, Table 1.9 shows the Henry equation produced a zeta estimate that is only 5% less than that predicted by the OBH theory.

The viruses studied fell into two groups, requiring the use of either the Henry equation (zone A3) or MB equation (zone B3). These two equations provided similar results in zone A3, with the MB giving a zeta potential result that was within 5% of the

Henry equation. In zone B3 the differences between the Henry and MB equations ranged from 6 to 11%. This may be attributed to the influence of the Booth correction functions, which have their maximum values in this zone.

Although a definitive simplification could not b made between the MB and HS equations in zone B2, the zeta potentials of all bacteria were calculated via the HS equation for comparison. On average, the zeta potential values predicted by the HS were 9% different from those of the MB, 5% different from the Henry equation and only 2% different from the OBH theory. Table 1.9 shows the differences were most pronounced at lower $\kappa\alpha$ values.

Table 1.9: Comparison of best zeta potential equation to others via percent difference. Grey shaded cells indicate the "best "equation as defined herein.

Sample Name	κα	Zone	Equation	% difference from zeta predicted by:				
				HS	Hen	HO	MB	OBH sln 1
AdV2	4.2	A3	Hen	-33	0	11	3	-30
Echovirus	1.5	A3	Hen	-43	0	5	2	-59
HAV HM-175	1.4	A3	Hen	-43	0	5	5	-34
B .atrophaeus endospores	51.9	B2	HS	0	4	33	7	2
B. anthracis	62.3	A2	HS	0	4	33	5	0
B. atrophaeus endospores QC	51.9	B2	HS	0	4	33	7	2
C. parvum 29IA8 viable	259.4	A1	HS	0	1	33	2	0
C. parvum 29IA8 viable QC-1	259.4	A1	HS	0	1	33	2	0
C. parvum 29IA8 viable QC-2	259.4	A1	HS	0	1	33	2	0
C. parvum 29IA8 55 ^{o}C-30min	259.4	A1	HS	0	1	33	2	0
C. parvum 29IA8 80 ^{o}C-1hr	259.4	A1	HS	0	1	33	2	0
E. coli	51.9	B2	HS	0	4	33	9	4
E. faecalis	36.3	B2	HS	0	6	33	11	5
F. tularensis	20.8	A2	HS	0	10	33	11	-4
Giardia intestinalis	622.5	B1	HS	0	0	33	1	0
S. enterica	51.9	A2	HS	0	4	33	6	-1
S. enterica QC	51.9	A2	HS	0	4	33	6	-2
Y. pestis	31.1	B2	HS	0	7	33	14	8
AdV40	4.2	B3	MB	-41	-6	6	0	-27
MS2	1.2	B3	MB	-57	-9	-5	0	-10
phi X 174	1.3	B3	MB	-59	-11	-6	0	-5
Microspheres	233.4	C1	OBH	-5	-4	30	1	0

Under study conditions, bacteriophages (i.e., MS2 and phi X174) appeared to have significantly higher zeta potentials than human viruses. MS2 and phi X174 are commonly used as surrogates for human viruses due to their non-pathogenicity to humans and rapid, inexpensive detection methods. In 1 mM KCl, bacteriophages appeared to have zeta potentials that were significantly greater in magnitude than the human viruses. Figure 1.11 shows the difference between bacteriophage and human virus zeta potentials is significant at the 95% confidence limit.

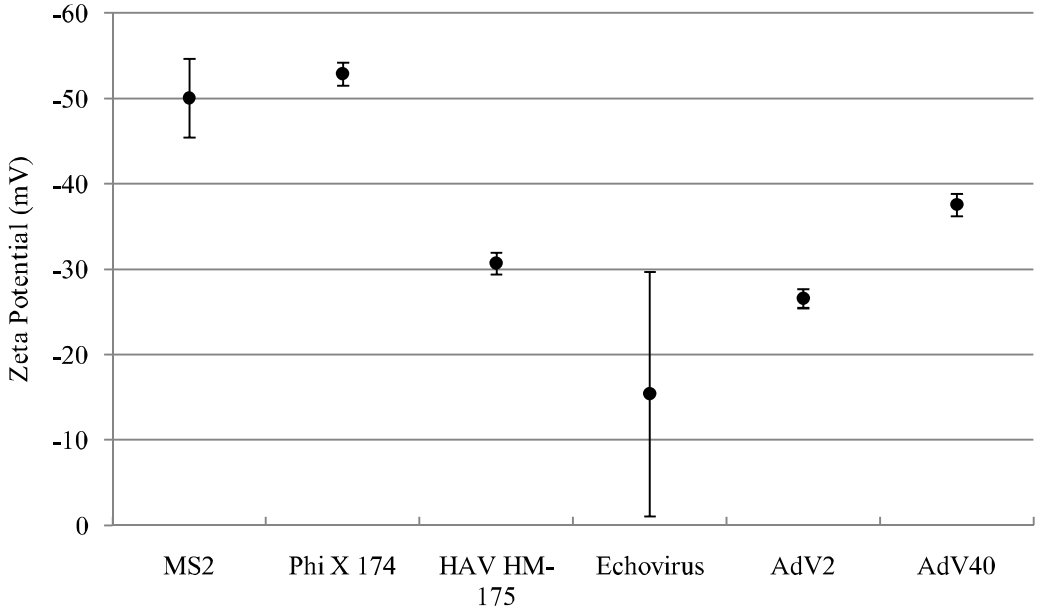

Figure 1.11: Average zeta potentials of bacteriophages and viruses. Error bars represent the 95% CI_m.

Endospores of B. atrophaeus subsp. globigii are often used as surrogates for B. anthracis when testing water security and concentration methods. Data collected here suggested B. atrophaeus endospores had a zeta potential that is twice that of the vaccine strain of B. anthracis in 1 mM KCl. Quality control measurements of the EPM of B.

atrophaeus suggested that over a one-month period, the EPM and zeta potentials of the endospores did not change.

The EPM of the same viable C. parvum oocyst stock was tested on three different occasions for quality control. The mean EPMs of each C. parvum QC sample were significantly different at the 95% confidence level (Figure 1.6). Brush and coworkers found a different result and noted the EPM of Cryptosporidium oocysts remained unchanged for 121 days following collection (1998). As seen in Figure 1.12, the zeta potentials of each stock were also significantly different. This indicated the zeta potential of Cryptosporidium oocysts may vary over time. Heat inactivation at 55^{o}C for 30 minutes did not appear to change the zeta potential from viable oocysts, while treatment at 80^{o}C for 1 hour had a small yet significant effect on the zeta potential. High-heat treatment may have significantly changed the zeta potential of C. parvum oocysts, but the inactivated oocysts still had a zeta potential within the range of viable QC oocysts studied.

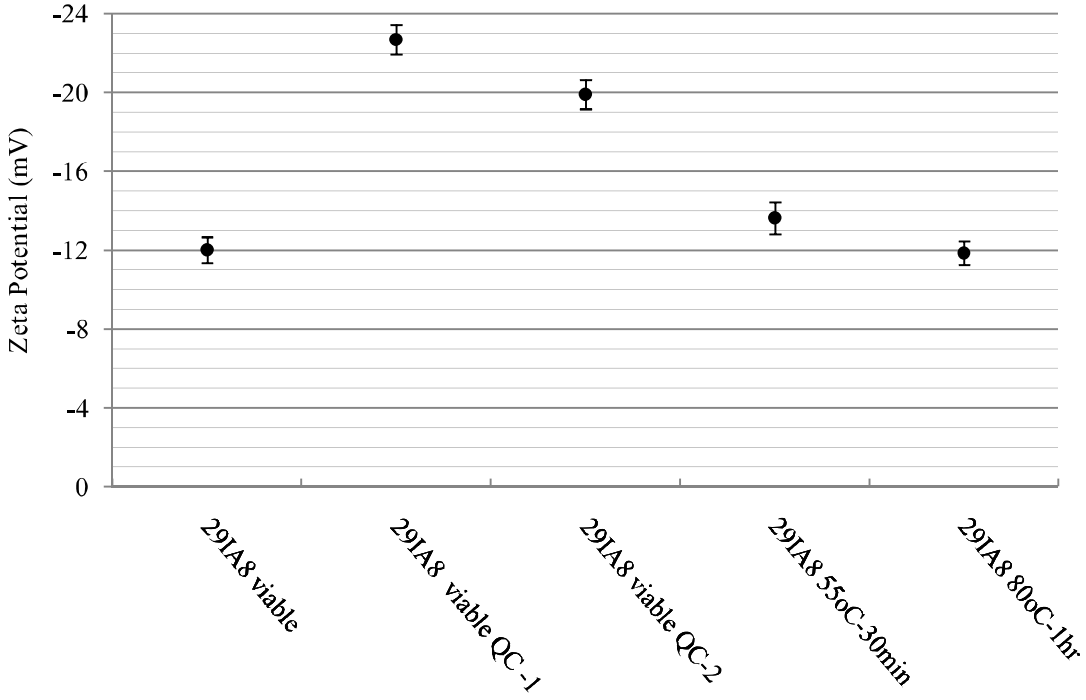

Figure 1.12: Mean zeta potentials of C. parvum oocysts. Error bars represent the 95% CI_m.

The electrokinetic properties of microbes have been studied extensively. The electrophoretic mobilities and zeta potentials of several organisms are reported in peer-reviewed literature. Van Loosdrecht and coworkers chose to report electrophoretic mobility values for bacterial cells rather than calculating zeta potentials, citing that the conductivities within the slipping plane of different bacteria are likely to be very similar (1987). Van der Wal and coworkers compared zeta potential values obtained using a modified version of Fixman's theory (which made assumptions about bacterial wall conductivity in order to account for ion conduction inside the slipping plane) to those output by the Helmholtz-Smoluchowski equation (1997). Their results showed the HS equation generally underestimated the zeta potential of the bacterial species studied (van

der Wal et al., 1997). Lytle and coworkers measured the EPMs of several environmentally relevant organisms in phosphate buffers to investigate the effect of pH, ionic strength, cation type, and ion concentration (2002). This group reported EPMs and zeta potentials calculated using the Helmholtz-Smoluchowski equation. Their study found that increasing the pH increased the magnitude of organism EPM. They also found that increasing the ionic strength of the solution generally decreased the magnitude of wild-type E. coli EPM and a mobility maximum was not noted (Lytle et al., 2002). This may suggest surface conduction was absent and the Henry or HS equation could be employed for E. coli cells.

1.5 Summary

The conversion of EPM measurements of microbial particles to zeta potentials is complicated by their non-ideal nature. This work used a real-world data set to demonstrate the choice of equation for calculating zeta potential for EPM measurements can be simplified. While the choice of equation will always be dictated by the level of accuracy required for a particular application, the Henry and Helmholtz-Smoluchowski equations can, in most cases, provide zeta potentials that are not significantly different from those derived from the more computationally complicated O'Brien and Hunter and modified Booth equations.

In this work, the HS equation could be applied for most particles with $\kappa\alpha > 20$, regardless of presumed zeta potential. As the Henry equation will default to the HS equation, it was suggested for particles in this range. The HS equation might be simpler to employ as it is commonly available in commercial software programs and does not require the calculation of $f(\kappa\alpha)$.

Based on the results of this study, equations more computationally complex than the HS (or Henry) equation were often necessary. This occurred when concentration polarization was suspected (i.e., $\kappa\alpha$ less than 100 and the HS zeta between |25| and |50| mV (zones B2 and B3)). In zone B2 a simplification could not be made since the difference between the MB and HS predicted zeta potentials was significant in nearly 50% of the organisms examined. However, this was not the case in zone B3 where the MB equation was preferred in order to correct for relaxation effects.

For 60% of the organisms studied, the HS or Henry equations produced zeta potential values that were not statistically different from those predicted by the OBH and MB equations. The OBH and MB equations include correction factors that account for relaxation, concentration polarization, and surface conduction of the electrical double layer. However, in this study it was observed that the differences imparted to zeta potentials by double layer distortion corrections were often smaller than the uncertainty of the EPM measurement from which the zeta potential value was calculated.

1.6 Conclusions

The results of this research led to two important conclusions. First, choosing the incorrect equation to convert electrophoretic mobility measurements to zeta potential can result in a miscalculation of up to 59% difference. Moreover, based on the analyzed dataset, the choice of the "best" equation for calculating the zeta potentials of viruses and parasites was more obvious than for bacteria. The zeta potentials of viruses could be calculated with the Henry or modified Booth equations and parasites with the Helmholtz-Smoluchowski equation. For bacteria, the application of the Helmholtz-Smoluchowski equation appeared sufficient when the organisms were classified in zone A2; however,

the majority of bacterial samples were placed in zone B2, where corrections for EDL distortions resulted in significantly different zeta potential values for 43% of the organisms. Second, while applying the correct model is imperative, the differences between the predictions of different zeta potential equations may be exceeded by the error associated with electrophoretic mobility measurements. This should be considered when using computationally intensive methods for calculating zeta potential.

1.7 Perspectives and Suggestions for Future Research

In this study, the EPM of several microorganisms and a surrogate (microspheres) were measured in simulated tap water, a matrix used with the intention of providing determining the zeta potentials of microorganisms in treated water. This matrix is simpler than an actual water sample. Tap and natural water samples usually contain natural organic matter (NOM) that may attach to organism surfaces. NOM is highly negative at the pH range of natural waters and NOM adsorbed to particles has been found to dominate the surface forces and therefore their stability (Mosley et al., 2003)

Apart from accounting for the effects of adsorbed species, the surface conductivity should be measured alongside the electrophoretic mobility in order to calculate the most accurate zeta potentials possible for microorganisms. Yunus and coworkers have suggested a simple method for measuring surface conductivity (2002). This information must then be employed in the correct theory, whether it is the Mangelsdorf-White, Lopez-Garcia-Grosse-Horno, or Ohshima's soft particle theory. As particle diameter may change with pH, this possibility should also be considered and incorporated into zeta potential investigations. In order to extend the utility of the simplified zone chart suggested in this study, a data set that allows for the comparison of

equations that account for conductivity in the Stern layer should be applied to the proposed scheme and the results compared.

CHAPTER 2: MODELING CRYPTOSPORIDIUM REMOVAL THROUGH DRINKING WATER TREATMENT TO IDENTIFY IMPORTANT PROCESS PARAMETERS

Despite years of focused research, the drinking water treatment community lacks quantitative knowledge of the relationship between physical and chemical drinking water treatment process parameters and Cryptosporidium oocyst removal efficiency. In this study, a meta-analysis of existing Cryptosporidium removal data was completed in order to gain insight into the oocyst removal process. The formulation of multi-parameter models was used to investigate the relationship between physical/chemical parameters and Cryptosporidium removal. Models developed using stepwise regression showed that the portion of the filter run and optimality of coagulant dose were important parameters regardless of the coagulant dose. Cryptosporidium removal appeared to be related to metal ion concentration below 0.4 mg/L (as ion), while above this value, metal ion concentration was not as important. Above metal ion concentrations of 0.4 mg/L other factors, such as effluent turbidity, appeared to have a stronger relationship to oocyst removal.

2.1 Introduction

The USEPA's Long Term 2 Enhanced Surface Water Treatment Rule (LT2ESWTR) assigns presumptive organism removal credits to drinking water utilities based on the treatment processes they use. Credits were developed by a review of numerous studies and assigned utilities base Cryptosporidium removal credits of 0.5 to 3 Log (corresponding to 68.4-99.9% oocyst removal) (USEPA 2005). The Log removal assigned to a utility is based on source water quality as well as the treatment processes selected from the EPA's "microbial toolbox" used to meet oocyst removal requirements. Drinking Water Treatment Plants (DWTPs) frequently achieve higher removals than prescribed under the LT2ESWTR, yet may be required to invest large sums of money in implementing treatment methods listed in the microbial toolbox to reach the required removal credits (Brown and Cornwell, 2007).

Efforts to identify surrogate measurements for oocyst removals have generally been unsuccessful (LeChevallier et al., 1991; Nieminski and Ongerth, 1995; Mazounie et al., 2000). However, a meta-analysis of these studies may provide new quantitative insight into oocyst removal through the drinking water treatment process. Meta-analysis is a statistical analysis approach that uses the results of several independent studies considered to be 'combinable' (Huque, 1988). In this study, a meta-analysis approach was used to elucidate the process variables that best explain oocyst removal.

2.2 Background

2.2.1 Cryptosporidium

Cryptosporidium is a coccidian parasite that infects humans and a wide range of animals. It is passed via the fecal-oral route through ingestion (and possibly inhalation)

of contaminated water or food. Cryptosporidium has a complex lifecycle but almost always exists in the environment as an oocyst. Cryptosporidium oocysts are spherical, 4.2 to 5.4 μm in diameter, and have a thick outer wall (Centers for Disease Control DPDx, 2008). This protective outer wall renders oocysts relatively insensitive to disinfection by chlorine. The zeta potential of Cryptosporidium in tap water is not well defined but could vary between -12 and -23 mV depending on oocyst age (see Figure 1.12 on page 50). During water treatment the zeta potential of Cryptosporidium parvum is affected by water quality, coagulant type and dosage, and pH, in addition to chemical inactivation prior to treatment (Emelko, 2003).

Removal of Cryptosporidium is commonly quantified using a Log scale. This convention expresses levels of decreased Cryptosporidium in water by factors of 10, and can be related to percent removal using the formula:

$$\% \text{ removal} = 100 - 10^{(2-R)}$$

where R is the Log removal. For example, 1 Log removal equates to removal of 90% of the influent organisms.

2.2.2 Drinking Water Treatment

Drinking water treatment (DWT) is based on a multiple barrier approach, relying on several interdependent steps to remove particles and contaminants. Many processes are used in practice, with the core 'conventional' treatment process is typically carried out in four steps:

1. Coagulation: addition of a chemical with rapid mixing to promote the aggregation of small particles into larger particles or flocs.

2. Flocculation: slow mixing to encourage the growth of flocs.
3. Sedimentation: separation of flocs from liquid by gravity
4. Rapid Filtration: removal of flocs and particles by attachment, and/or straining during passage through a granular media filter.

Coagulation is a complex process comprised of three main steps: coagulant formation, particle destabilization, and interparticle collisions. Coagulant formation is the hydrolysis of the added chemical, and it is these hydrolysis products that facilitate coagulation (Letterman et al., 1999). Coagulant formation happens very quickly (<10 s) and is completed during rapid mixing (detention time ~1 min). Interparticle collisions begin during coagulation, but occur predominantly in the flocculation process (Letterman et al., 1999).

During flocculation, water passes through several flocculators (low-speed mixing basins) typically over a time of 20 minutes to 1 hour. Destabilization, which occurs during this period, reduces particle repulsion and leads to successful interparticle collisions. Effective coagulation and flocculation are imperative to the success of sedimentation and granular filtration. As the pores in granular media filters can be several orders of magnitude larger than the particles to be removed (i.e. viruses and bacteria), incorporation of microbes into flocs is important in the removal process.

Sedimentation is a time-intensive step that relies of gravity and effective particle destabilization to remove flocs. The 'Ten States Standards' (used by 10 US states and the Canadian province of Ontario) requires a minimum 4 hr detention time in the sedimentation basin (Water Supply Committee of the Great Lakes--Upper Mississippi River Board of State and Provincial Public Health and Environmental Managers, 2007).

Because of their small size and low density, oocysts have low settling velocities and are not readily removed in settling tanks. However, if they are incorporated into flocs of 100μm or larger, they may be removed by sedimentation (Edzwald et al., 2000).

Rapid sand filtration may also be referred to as depth or granular media filtration. Filters are commonly comprised of a several feet of sand, anthracite coal, granular activated carbon, or combinations of these materials (Cleasby and Logsdon, 1999). Filtration relies on the collision of particles with media grains (collectors) and their subsequent attachment for removal. Removal of particles through straining also occurs to a lesser extent. Under optimal conditions a combination of coagulation, flocculation, sedimentation and granular media filtration have been found to result in protozoan pathogen removals in excess of 4 Log (LeChevallier and Au, 2004).

Direct/Inline/Conventional Treatment

The treatment approach employed at a DWTP largely depends on the quality of the source water. Conventional treatment is typically used to treat source waters with high turbidity and color. This approach includes coagulation, flocculation, sedimentation, and filtration. Direct filtration omits the sedimentation step and relies on coagulation, flocculation, and depth filtration for particle removal. Inline filtration is comprised of coagulation and very limited flocculation before depth filtration, permitting the particle destabilization necessary for effective removal by filtration. Inline treatment does not incorporate a sedimentation step to remove microbes (LeChevallier and Au, 2004). Figure 2.1 presents a schematic representation of the three treatment trains in order to highlight the similarities and differences between them. Inline and direct filtration can be difficult to distinguish from one another but are similar in that they

require lower coagulant doses than conventional filtration to avoid rapid filter clogging (Cleasby and Logsdon, 1999). Both Patania and coworkers (1995) and Hendricks and coworkers (2005) found that conventional filtration generally resulted in higher Log removals of Cryptosporidium oocysts (but not higher removals of turbidity) than direct or inline filtration.

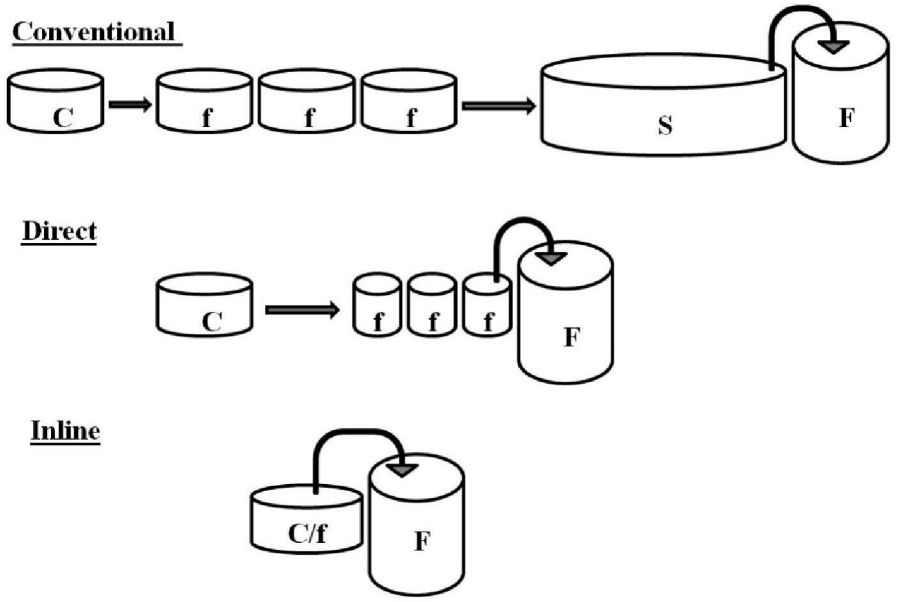

Figure 2.1: Schematic representation of three common drinking water treatment trains.

Pilot and bench-scale filtration experiments are widely used for designing treatment and to aid in operation (Hendricks, 2006) due to their smaller footprint, ease of operation, and cost-effectiveness. However, it is difficult to exactly replicate the treatment process at the bench or pilot scale. A large factor is the inability to accurately scale-down the sedimentation process. In addition, the coagulation and flocculation scheme may also be dictated by the amount of coagulant added rather than the physical

configuration of the pretreatment processes. Lower levels of coagulant typically correspond to direct or inline filtration and higher levels to conventional treatment.

2.2.3 Coagulation Theory

Coagulation is the general process of "inducing contacts between chemical and colloidal particles to effect a reaction" between the two, forming "micro-flocs" (Hendricks, 2006). Micro-flocs then combine to form flocs during flocculation. Effective engineering of the coagulation/flocculation process depends on selecting the proper chemicals, adding them at the proper dose and pH, and facilitating collisions between the coagulant and particles (Hendricks, 2006). Coagulation is characterized as having two main mechanisms, charge neutralization, which typically occurs at a pH less than 6, and sweep floc formation, which takes place at pH greater than 6, depending on the coagulant type and dose (Hendricks, 2006). Improper coagulation has given rise to a large portion of the problems experienced with rapid filtration (Hendricks, 2006).

2.2.4 Filtration Theory

The main goal of rapid sand filtration theory is to account for the concentration of solids suspended in the influent water, the amount of solids deposited on the media, and the headloss in a filter over space and time (Hendricks, 2006). Both physical and chemical variables affect particle removal during filtration and are included in filtration models. Physical variables include the filtration rate, water temperature, size and shape of the media particles, filter bed porosity, and the size and density of particles (Yao et al., 1971; Hendricks, 2006). Chemical factors are focused on the surface characteristics of suspended particles and filter media, including their zeta-potentials (O'Melia and Stumm, 1967). Specific variables that may influence chemical processes include pH, ionic

strength, and ion content of the water (O'Melia and Stumm, 1967). Haas and coworkers (2001) summarized both sets of variables and how they relate to coagulation and filtration, asserting that the effectiveness of coagulation, flocculation and sedimentation depends on coagulant dose, pH, turbidity, color, particle zeta potential, temperature, mixer type, mixing rate, tank shape, detention time and overflow rate while filtration processes depend on water quality parameters (turbidity, natural organic matter (NOM) type and concentration, color, pH, and temperature), as well as chemical types and concentrations added, the type, size and depth of the media, water flow rate and portion of the filter cycle (2001).

As not all of these parameters are measured during experimentation or reported in the literature, only a subset of available variables were available for inclusion in the meta-analysis of Cryptosporidium removal conducted herein. Parameters available for model formulation included pOH, polymer dose, filter influent and effluent turbidity, filter media depth and effective size, and the portion of filter run during which the data were collected and are discussed here in further detail.

Coagulant Dose

Coagulation is considered to be the "critical phase" of water filtration and dosage is the factor that determines the effectiveness of filtration (Hendricks, 2006). The most commonly used coagulants are the trivalent metal salts Alum ($Al_2(SO_4)_3$) and Ferric Chloride ($FeCl_3$). According to Hendricks, "Aluminum and ferric iron may be substituted one for the other in most of the hydrolysis reactions" (2006). Prehydrolyzed metal salts such as polyaluminum chloride (PACl) and other polymers may also be used as primary coagulants to a lesser extent. The reactions of these metal ions with water

during the coagulation depend of pH, coagulant dosage, ionic strength, and alkalinity (i.e., hardness) among other factors (Hendricks, 2006). The work of States and coworkers (2002) suggested the effectiveness of Cryptosporidium oocyst removal appeared to be similar for alum, ferric chloride, and PACl in a conventional treatment train. Dugan and coworkers (2001) tested this theory by loading filters in a conventional treatment train with water of equivalent particulate concentrations coagulated with alum, ferric chloride, or PACl and found no significant differences in Cryptosporidium removal with respect to coagulant type.

Optimum coagulant dosing is designed to produce the lowest turbidity filter effluent possible and maximize particle removal. However, optimization of particle removal does not assure that the coagulant dose is optimized with respect to removal of biological particles, including Cryptosporidium (Hendricks, 2006). It has been suggested that Cryptosporidium removals are more sensitive to coagulant conditions than turbidity (Huck et al., 2002), making optimum coagulant dosing even more critical to achieve high Log removals. Huck and coworkers found sub-optimal coagulation to substantially reduce oocyst removals through the conventional treatment train (2002). Hendricks and coworkers found that alum dosages less than the optimal resulted in proportionately lower Cryptosporidium Log removals and noted a linear relationship between alum dose and oocyst Log removal through inline and conventional treatment trains (2005). Dugan and coworkers also found suboptimal coagulation had a dramatic impact on oocyst removal resulting in Log removals at or below 1.5 Log, while in optimized runs Cryptosporidium removal averaged >3.7 Log through a conventional treatment train (2001).

It is not clear how much, if any, removal of Cryptosporidium is achieved through filtration when no coagulant is added. Huck and coworkers found "essentially zero removal" of Cryptosporidium under the no-coagulant condition and confirmed that seeded organisms were not being lost in the pilot plant (2002). However, Hendricks and colleagues found removals through media without coagulation to be 1 Log due to straining and possible attachment of oocysts to filter media (2005). Both findings demonstrate the crucial importance of coagulation.

pOH

pH is known to be important for successful particle removal via coagulation (Amirtharajah and Mills, 1982, Van Benschoten and Edzwald, 1990). While the coagulation pH may not be directly related to oocyst removal, it bears heavily on the effectiveness/optimality of coagulation. Figure 2.2 and Figure 2.3 illustrate the effect that pH and coagulant dose can have on coagulation for both Aluminum and Iron salts. Edzwald and Tobiason (1999) stated that optimum coagulation pH conditions should be in the low 6's for warm waters and nearer to 7 in cold water for low alkalinity (e.g., soft), low to moderate humic acid level waters. Based on Figure 2.2 and Figure 2.3, optimal sweep coagulation using both Alum and Ferric Chloride coagulants occurs is in the region of pH 6 to 8 (Amirtharajah and Mills, 1982; Johnson and Amirtharajah, 1983).

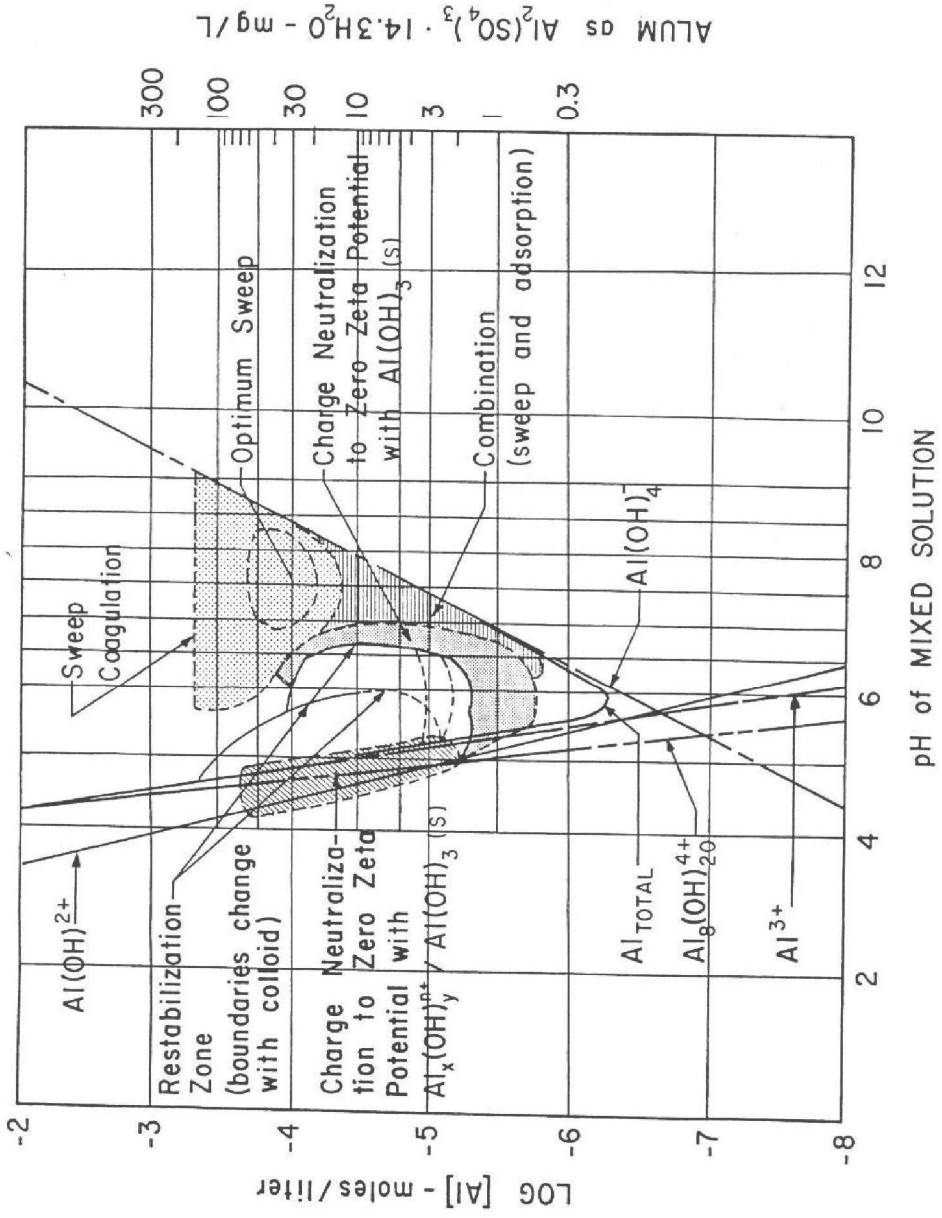

Figure 2.2: pC-pH diagram for Alum (Amirtharajah and Mills, 1982).

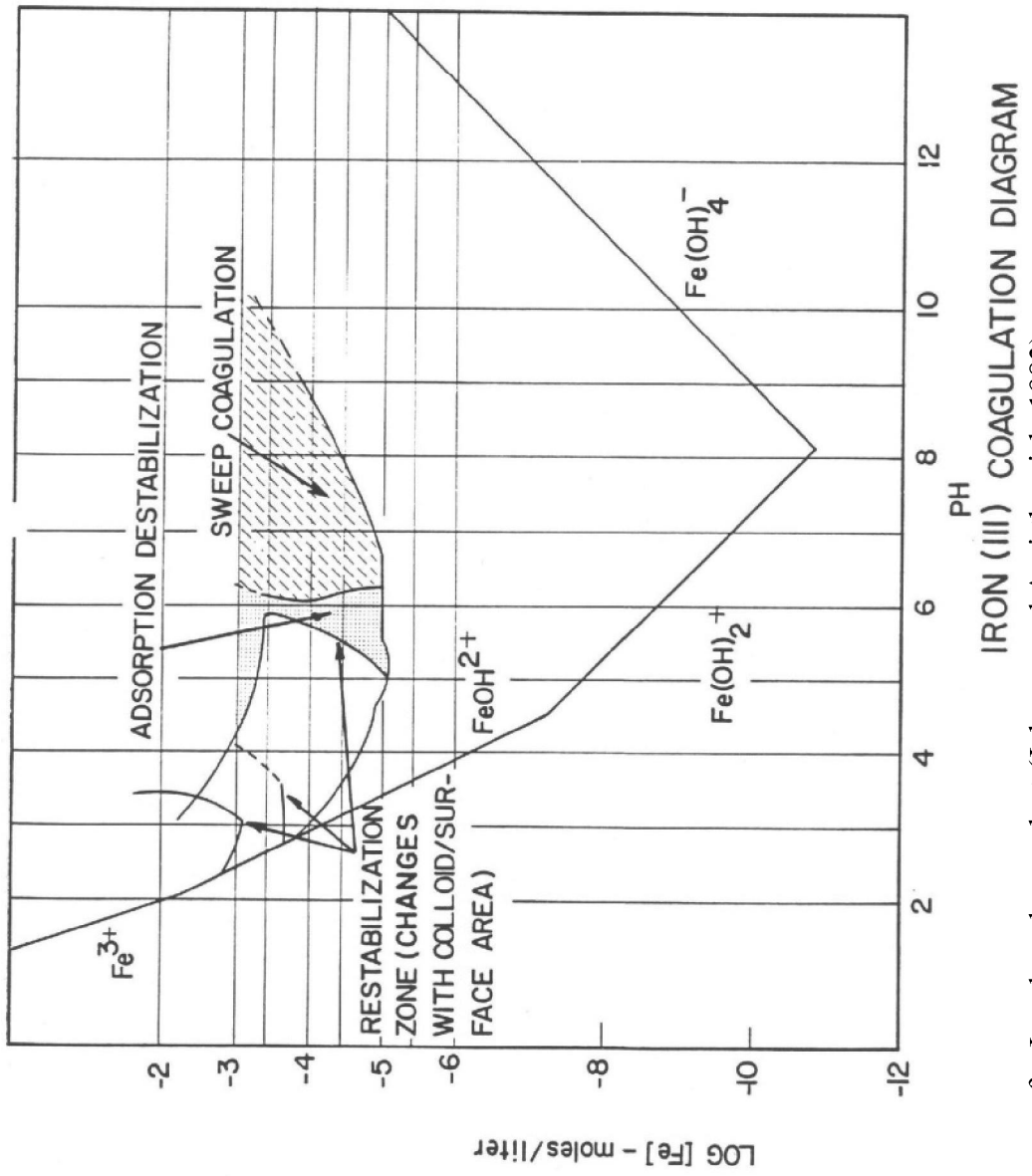

Figure 2.3: pC-pH diagram for Iron-based coagulant (Johnson and Amirtharajah, 1983).

OH^- has been shown to be a more important complexing ligand than H^+ in Al hydrolysis reactions (Van Benschoten and Edzwald, 1990). As suggested by Edzwald and Tobiason's findings stated above, the interaction of temperature and pH has an important effect on the success of coagulation reactions. Van Benschoten and Edzwald also determined the "effects of low temperature on alum … to be a result of changes in OH^- caused, in part, by the temperature dependence of the ion product of water" (1990). This issue may be both kinetic and stoichiometric. Table 2.1 presents the ionization constants of water at different temperatures. Based on the relationship in Table 2.1 it is evident that low temperatures lead to reduced OH^- concentrations for a given pH, creating a kinetic (temperature-based) limitation. The resulting reduction in available OH^- ions to complex with Aluminum ions then creates a stoichiometric limitation of the formation of coagulation species. Therefore the use of pOH may be a more appropriate explanatory variable of Cryptosporidium removal as it combines pH and temperature data and directly represents the key hydrolysis products participating in coagulation processes.

Table 2.1: Equilibrium constants of water (Stumm and Morgan, 1996).

Temperature (^oC)	pKw	Kw	$[OH]^-$ at pH =7
0	14.93	$10^{-14.93}$	$10^{-7.93}$
5	14.73	$10^{-14.73}$	$10^{-7.73}$
10	14.53	$10^{-14.53}$	$10^{-7.53}$
15	14.35	$10^{-14.35}$	$10^{-7.35}$
20	14.17	$10^{-14.17}$	$10^{-7.17}$
25	14	$10^{-14.0}$	$10^{-7.0}$
30	13.83	$10^{-13.83}$	$10^{-6.83}$
50	13.26	$10^{-13.26}$	$10^{-6.26}$

Polymer

Polymers are commonly added during or after coagulant addition to "influence the characteristics of the floc" and improve coagulation and filtration (Hendricks, 2006). Polymers can be cationic, anionic, or nonionic. Cationic polymers can be used as primary coagulants and replace metal salts; however this is usually cost-prohibitive in practice. When added in along with metal salts to improve floc formation, polymers are often called coagulant aids or flocculants (Hendricks, 2006). Anionic polymers, also referred to as filter-aids, appear to be the most commonly used in research studies, perhaps because they are added before filtration and the amount used is usually 10 to 100 times lower than the cationic polymer concentration required. Polymers also have the benefit of not being pH or temperature dependent, which allows for an improvement in coagulation efficiency without the need to optimize process parameters. In practice cationic polymers are generally added when coagulant concentrations are low, leading to an inherent relationship between the amount of polymer and metal ion concentration.

Influent Water Turbidity

According to filtration theory, particle removal depends on the number of successful collisions between particles and filter media. Experimental observations have indicated the number of successful collisions increase with an increasing particle concentration (Yao et al., 1971; Prasanthi et al., 1997). Therefore, increasing influent particle concentration may increase the Log removal of Cryptosporidium (Assavasilavasukul et al., 2008). Pilot-scale studies have also confirmed this, with Dugan and coworkers finding that higher influent water turbidities led to higher oocyst removals (2001) and Nieminski and Ongerth observing that raw water quality (turbidity and algal

content) controlled the removal of seeded Giardia cysts and Cryptosporidium oocysts more than the mode of treatment (1995).

Effluent Water Turbidity

Effluent water turbidity is a logical surrogate for predicting oocyst removal through the treatment process. While several studies have confirmed that the removal of turbidity is correlated to oocyst removal, the correlation has not been found to be strong enough to rely on filter effluent turbidity alone as a surrogate. Mazounie and coworkers found removal of particles, algae, and aerobic spores consistently underestimated Cryptosporidium removal in a full-scale treatment plant (2000). In a survey of 66 plants treating surface water, LeChevallier and colleagues found oocyst and turbidity removal to be positively correlated at a level of $r = 0.41$ ($R^2 = 0.19$, $p<0.01$) (1991), while Nieminski & Ongerth reported a correlation of $r = 0.74$ ($R^2 = 0.55$, $p<0.1$) between oocyst removal and turbidity removal for conventional and inline treatment (1995). Dugan and Williams also noted high Cryptosporidium removals to be associated with low filter effluent turbidities (2004). Xagoraraki and coworkers found a moderate correlation ($r = -0.65$) between effluent oocyst concentration and turbidity for conventional treatment and reported oocyst removal was best when effluent turbidities were greater less than 0.2 NTU and worst when greater than 0.7 NTU (2004). The USEPA asserts that, under appropriate coagulant conditions, when a drinking water treatment plant achieves a finished turbidity less than 0.3 Nephelometric Turbidity Units (NTU), the Cryptosporidium removal should be at least 2 Log and suggests the highest Log removals occur when finished water turbidity is less than 0.1 NTU. The USEPA also cautions that

"although turbidity is an indicator of filtration performance, it is not a direct indicator of pathogen removal" (2005).

Media Depth and Size

Drinking water filters are typically composed of multiple layers of media. Filtration research tends to be completed with mono or dual media filters. The size, shape, and depth of the media are considered important parameters to model physical processes of particle removal in filters (O'Melia and Stumm, 1967; Hendricks, 2006). The zeta potentials of the oocyst (Emelko et al., 2003) and the filter media (O'Melia and Stumm, 1967) are also important criteria since they dictate the microscale electrostatic interactions occurring at the media surface; however, these values are not commonly quantified in Cryptosporidium removal studies. One of the basic dependent functions in filtration theory states that particle concentration decreases with distance from the top of the filter (Hendricks, 2006). Yet monomedia and dual media filters have been found to result in no significant difference in oocyst removal (Patania et al., 1995; Hendricks et al., 2005). Other investigations of media type and design demonstrated that these parameters have a small effect on oocyst removal by filters (Swertfeger et al., 1999; Dugan et al., 2001; Emelko et al., 2005).

Portion of Filter Run

A normal filter run is composed of 4 phases based on the time elapsed and turbidity removal observed: filter ripening, steady state operation, early breakthrough, and breakthrough (Hendricks, 2006). Figure 2.4 shows an example breakthrough curve with the four phases of a typical filter run. During filtration, a zone of solids deposit saturation, or wave front, develops and moves down through the filter (Hendricks, 2006).

A filtration run is thought to start with filter ripening, during which the flocs in the influent water begin to coat the media, establish the zone of deposit saturation, and serve as additional collectors (O'Melia and Stumm, 1967). After ripening, the steady state removal period occurs and is the longest portion of the filter run. During the steady state period the zone of deposit saturation is moving downwards through the media and the observed effluent turbidity remains approximately constant. Early breakthrough begins when the filter begins to reach a maximum amount of collectors and the saturated zone of deposit is approaching the bottom of the filter media (Hendricks, 2006). Breakthrough occurs when the filter effluent turbidity begins to increase, indicating the wave front has 'broken through" the functional depth of the filter. Breakthrough signals the end of the filter run and most drinking water treatment plants stop their filter runs before early-breakthrough occurs.

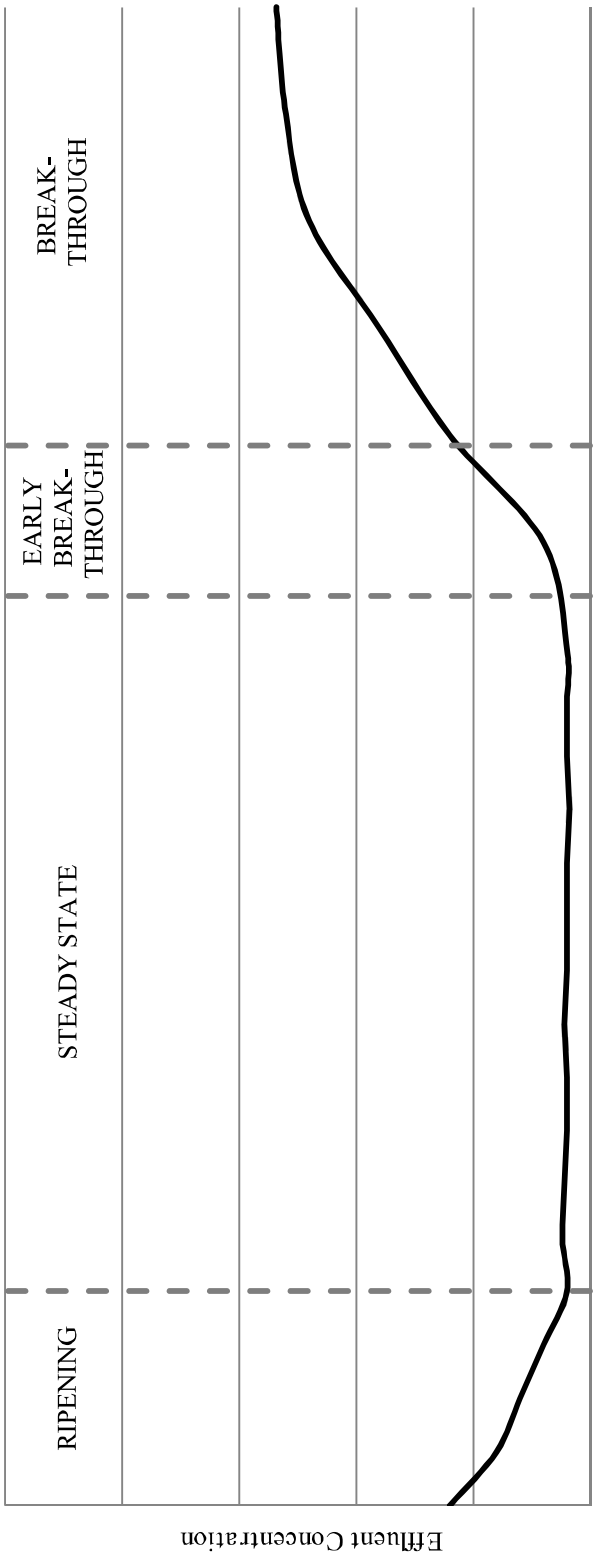

Figure 2.4: Example breakthrough curve with phases of filtration (Lawler and Benjamin, 2003).

2.2.5 Previous Modeling Efforts

A meta-analysis of Cryptosporidium removal was conducted by Haas and coworkers (2001). Among their goals were to conduct a critical review of existing data on the removal and inactivation of Cryptosporidium by different water treatment processes, determine correlations between process variables and oocyst removals, and formulate models to predict oocyst removal. The group used data collected through literature review as well as from unpublished studies to develop regression models to predict Cryptosporidium removal through individual processes in drinking water treatment. Each data point included in their study was given a quality rating depending on the available information on the study scale, details of the treatment processes, and oocyst enumeration methods used. Only data points receiving the highest quality assessment were incorporated into model formulations, resulting in regression models that relied on a limited number of observations. Their model for coagulation-flocculation-sedimentation (cfs) model relied on data points from 4 studies and included 31 observations. The cfs model produced was dependent on coagulant concentration, process influent pH, and polymer concentration with an adjusted R^2= 0.94 and root mean square error (RMSE) of 0.24. This group discovered the way coagulant dose was considered in the model was very important, and that when included as milligrams per liter of metal ion (MI) a better fit was achieved. Models were also formulated for direct and rapid gravity filtration. The model for direct filtration was based on only one study with 4 observations and one dependent variable, influent turbidity. The model determined for rapid gravity filtration was based on 24 observations, included pH, effluent turbidity, filter depth, and flow rate and had an adjusted R^2 value of 0.78, RMSE

of 0.34, with n=24 (Haas et al., 2001). Haas and coworkers cautioned the interpretation of the rapid gravity model determined, since collinearity was observed between the flow rate, depth, and pH variables (2001).

2.2.6 Model Formulation

The approach used in the model building process depends largely on the understanding of the system being modeled. Filtration theory is necessary to consider in the process of creating descriptive models. Statistical approaches may be employed to determine the "best" subset of available variables to include in the model formulation. In this project, linear models were developed using stepwise statistical methods to determine the best subset of variables to include in model formulations. Model formulations were then examined for their implications on what parameters appear to influence the removal of Cryptosporidium oocysts in experimental trials.

2.2.7 Variable Selection via Stepwise Regression

Statistical procedures like stepwise regression can guide the investigator to find a suitable subset of variables to include in a model. Stepwise regression is a popular variable selection approach and three variations can be used: forward, backward, and stepwise selection. Each relies on significance testing of parameter estimates of prospective variables to determine if a variable enters or remains in the model. In forward selection, the model is built by starting with the predictor variable that has the highest level of correlation with the output variable. Potential variables are then added one at a time and may stay in the model based on a significance level of the parameter estimate to stay (Rawlings et al., 1998). In the SAS software system used in this study, variables are added based on the significance of the F-statistic of the variable. The F-

statistic tests the null hypothesis that the parameter estimate is 0 and the p-value is the probability associated with the determined F-statistic. Model selection is complete when none of the variables have a p-value of the F statistic that satisfies the significance to enter criteria (The SAS Institiute Inc., 2007). The backward selection process begins with the full model that includes all possible regressors and removes them one at a time beginning with the highest p-value of the F-statistic of the parameter estimates until the model includes only variables with parameter estimates below p-level of significance level to stay. The forward and backwards selection processes do not "account for the effects that addition or deletion of a variable can have on the contributions of other variables to the model" (Rawlings et al., 1998). The full stepwise procedure is a forward selection procedure that rechecks the importance of all previously included variables at each step (Rawlings et al., 1998). In the SAS system, the stepwise process stops when none of the variables outside the model has an F-statistic significant at the entry level and every variable in the model is significant at the significance to stay level, or when the variable to be added to the model is the one just deleted from it (The SAS Institiute Inc., 2007).

Stepwise procedures can be very useful for determining a suitable subset of variables to include in a model but there are drawbacks associated with the stepwise approach. Forward, backward, and stepwise regression for variable selection may all result in different subsets of variables, so it cannot be asserted that stepwise procedures will identify the 'best' subset, but rather a set of possible models. The models may then be compared by the adjusted R^2 values and RMSE to assess their descriptive and predictive value.

2.2.8 Variables Not Considered: Scale and Spike Concentration

Low oocyst concentration and its high method detection limit make it difficult to quantify Cryptosporidium removal at the full-scale drinking water treatment plants. The current study combines data from pilot and bench-scale testing with the goal of applying the findings to full-scale DWTPs, which may add to the overall uncertainty of the model. Major differences were not noted by Hendricks and coworkers when comparing removal data for organism removals between a pilot and full scale plant (2005) while Nieminski and Ongerth found parasite removals were on the order of 0.5 Log less for full-scale than pilot scale tests (1995).

It has been suggested that the concentration of Cryptosporidium oocysts may influence the removal rates observed (Harrington et al., 2007). Assavasilavasukul and coworkers found oocyst removal through conventional treatment to be dependent on the initial pathogen concentrations (2008). This research group and observed low Log removals when low pathogen seed concentrations were used and suggested that the initial oocyst concentration can explain 44% of the variance in Log removal data (Assavasilavasukul et al., 2008). Other investigators have not noticed a relationship between the influent oocyst concentration and Log removal values (Hendricks et al., 2005). APPENDIX B presents the relationship between oocyst seed concentration and Log removal for the observations used in the present study and does not show a clear relationship between Log removal and the influent oocyst concentration. The influence of spike concentration on Log removal is a matter for debate and research.

Variability is expected in all meta-analyses. Despite standardization of detection methods, differences in analytical reliability, processed sample volume, method detection

limits, and influent microorganism concentrations can all contribute to the reported differences in the Cryptosporidium removal of filters (Huck et al., 2002). The current study approaches the project goal with this inherent variability in mind.

2.2.9 Project Goal

This meta-analysis of Cryptosporidium removal data aimed to produce a model that related commonly measured parameters to the removal of Cryptosporidium through the 'standard' drinking water treatment process. The focus was not to create a model with strong predictive power, as it is known that a model determined to predict the performance of any drinking water treatment plant under any conditions is bound to fail (O'Melia and Stumm, 1967). Rather, the goal was to use the model building process and resulting models for data exploration purposes and to determine what data in the literature show to be the most important variables affecting Cryptosporidium oocyst removal.

2.3 Materials and Methods

2.3.1 Data collection and Classification

Multiple literature reviews were conducted to find existing data on Cryptosporidium removal in a manner similar to that used by Haas and coworkers (2001). References were included into the database if the study was focused on drinking water filtration, quantified Cryptosporidium oocyst removal and not that of a surrogate, and used accepted methods of filtration and organism detection. To find as many applicable studies as possible, articles included in the study subjected to a cited reference search to find any new papers that referenced studies included in the database. The number of observations for model formulation was increased by using individual experiments rather

than summarized results, which led to the use of several data points from the same authors (as shown in APPENDIX C).

Roughly 45% of the data used for this study were presented as a range of Log removals. Additionally, approximately 25% of the removal data in the original data set were right censored (Log removals listed as greater than the detection limit due to non-detection of organisms). In the model formulations presented, the average of ranges were taken as actual removals, while right censored values were removed from the data set as they may result from analytical problems and cannot be analyzed using standard regression (Haas et al., 2001). Bayesian meta-analysis can overcome the need to delete censored values and avoid the resulting loss of information or accuracy (Qian et al., 2004). However, since Bayesian analysis relies on prior knowledge of model parameter estimates this approach was not employed.

Data were classified by treatment train type and analytical methods used. Categorical variables were created to represent data collected during the ripening, steady state, early-breakthrough, and breakthrough periods of filter runs, the type of filtration used, and to indicate when sub-optimal coagulation was used. Continuous variables included MI concentration calculated from the coagulant dose (alum, PACl or ferric chloride), cationic polymer dose, coagulation pOH, raw water turbidity, filtered water turbidity, media depth, media effective size, filtration rate, and influent water TOC. The media depth and effective size were subdivided into media depth/effective size 1 and 2, where media 1 was the top (sand) layer of the filter and media 2 the lower (anthracite) layer. The final data set was composed of 115 total observations from 15 different studies and is presented in APPENDIX C. Where data were missing, study authors were

contacted to obtain unpublished values. Several observations were missing data for influent TOC, pH and temperature. The latter missing values resulted in fewer observations having sufficient data to calculate pOH, reducing leading to a reduction in the data set when pOH is included in model formulation.

2.3.2 Calculated Variables

Metal Ion Concentration

Coagulant doses were converted to total metal ion (MI) concentration. It was assumed that all the alum used was $Al_2(SO_4)_3 \cdot 14.3\ H_2O$, ferric coagulant was $FeCl_3$, and polyaluminum chloride (PACl) was $Al_2Cl(OH)_5$. The chemical formula for PACl was not explicitly stated by the researchers (Nieminski and Ongerth, 1995 and States et al., 2002) who included it in their filtration studies. The formula of $Al_2Cl(OH)_5$ was selected in order to represent a polyaluminum chloride with basicity of 83% (Van Benschoten et al., 1992). MI concentrations were calculated by multiplying the coagulant dose by the percentage of the coagulant that is metal ion: 0.09 for Alum, 0.21 for Ferric coagulant, and 0.31 for PACl. For example, the molecular weight of alum is 600 per mole and 54 of that is metal ion, 54/600 = 0.09, so 9% of alum is metal ion.

pOH

pOH was calculated using temperature (T) in degrees Celsius and coagulation pH data. The temperature dependent pKw was determined from the linear relationship:

$$pKw = -0.037*T + 14.919 \quad (2.1)$$

derived from the data provided in the CRC Handbook of Chemistry and Physics (Lide, 2004). The pH value was then subtracted from pK_w to obtain pOH.

2.3.3 Categorical Variables

Several nominal variables were associated with each observation. These included the portion of filter run, whether coagulation was optimized or sub-optimal, and the type of treatment train. The type of treatment train was assigned based on the coagulant dose used rather than the configuration asserted by the study authors. Observations where less than 0.4 mg/L of total MI was applied were considered direct/inline filtration, while those greater than 0.4 were considered conventional treatment. This generally corresponded to the treatment train configuration described by study authors, although there were 35 observations where inline treatment was specified that were classified as conventional due to high concentration of metal ion added. Because only two levels were associated with this variable, it was represented with either a zero (< 0.4 mg/L MI) or 1 (> 0.4 mg/L MI). Whether coagulant was dosed in an optimal or sub-optimal concentration according to the study authors was also represented in this way, with a 1 representing suboptimal coagulation and zero representing optimized coagulant doses. The portion of filter run variable had three levels: steady state, early breakthrough, or breakthrough. The majority of data used were collected during steady state operation. A qualitative variable with a levels is usually represented with a-1 variables, with each assigned a value of either 0 or 1 (Montgomery and Peck, 1982). In this case X_{pfr1} and X_{pfr2} represented the variables and were assigned values as presented in Table 2.2.

Table 2.2: Values for variables representing the portion of filter run.

Portion of Filter Run	Value X_{pfr1}	Value X_{pfr2}
Steady State	0	0
Early Breakthrough	0	1
Breakthrough	1	0

2.3.4 Descriptive Statistics and Correlation Analysis

Initial data exploration was conducted using Microsoft Excel. MATLAB® (R2007b, The MathWorks, Natick, MA) was used to assess data normality and determine correlation coefficients. Normality testing was completed by using the Jarque-Bera test, which is a two-sided goodness of fit test that uses the number of observations, skewness and kurtosis to determine if a sample comes from a normal distribution. This test accepts the null hypothesis at the $\alpha = 0.05$ level if the sample is normally distributed and rejects if it is not. As the majority of the data were found not to be normally-distributed, non-parametric correlation analyses were carried out. Spearman's Rho (P) and its corresponding probability value were calculated in order to determine correlations between parameters. Because of the large amount of missing data, Spearman's P was calculated using a pairwise option which allowed for the maximum amount of data to be used in correlation analysis. In this test, pairwise means P(i,j) is calculated between two variables (i and j) using rows with no missing values in column i or j, while other columns were ignored (The MathWorks, Natick, MA). Analyses were carried out on the entire data set, as well as subsets of the data based on the MI concentration.

2.3.5 Stepwise Regression

SAS® version 9.2 (SAS Institute, Cary, NC) was used to conduct forward, backward, and stepwise regression analyses. These procedures resulted in linear model formulations of the "best" subsets. SAS stepwise regression procedures require all observations to have values for each parameter, so any observations that were incomplete were excluded in the stepwise model formulation. The model selection approach was designed to maximize the amount of data available for stepwise selection methods. First,

the TOC variable was removed from the set of potential regressors, increasing the number of observations available for use in model selection. Second, models were selected using a repeated stepwise selection procedure. In this approach, the variables determined in the first application of stepwise selection procedures were used as the starting set of variables for a second round of stepwise selection. This approach was repeated until all the variables in the starting set were included in the final model formulation, allowing for a maximum amount of observations to be included in model formulations since the amount of data available increased with the removal of potential regressors.

The MODEL statement in the REG procedure was run in the SAS environment. Log Cryptosporidium removal (henceforth referred to as removal) was specified as the dependent variable and MI concentration, polymer dose, pOH, media depth 1 and 2, effective size 1 and 2, effluent turbidity, influent turbidity, portion of filter run, optimality of coagulation as the regressors. Analysis of the full data set was run twice, once with the inclusion of a treatment train variable and once without. Variables that had two levels or were related to each other were grouped together to require that they enter and exit model formulations together (i.e. portion of filter run 1 was grouped with portion of filter run 2). Software default values were used for the partial F statistic p-value criteria for entry, exit, and to remain in the model for forward, backward, and stepwise selection, respectively. These values are listed in Table 2.3.

Table 2.3: Stepwise p-value Criteria.

Selection Procedure	p-value of F statistic Criterion
Forward	0.5 to Enter
Backward	0.1 to Stay
Stepwise	0.15 to Enter and to stay

Models were compared using the Adjusted R^2 values as well as Root Mean Squared Error (RMSE). Adjusted R^2 is used in order to avoid the phenomenon of increasing R^2 values as additional regressors are added to the model. Adjusted R^2 was calculated according to:

$$\overline{R}_p^2 = 1 - \left(\frac{n-1}{n-p}\right)\left(1 - R_p^2\right) \tag{2.2}$$

Where n is the number of observations used, p is the number of variables included in the model, and R_p^2 is the R^2 value of the model with p variables (Montgomery and Peck, 1982).

The possibility of model over fitting was avoided as much as possible. "The process of searching through a large number of potential subset models for the one that best fits the data capitalizes on the random variation in the sample to "overfit" the data"(Rawlings et al., 1998). For example, a model with 10 variables would be expected to fit a data set with 10-observation better than a single variable model would. When each variable in the model has to explain only one observation, the variables may begin to describe the natural variability in the original data set and might not have meaning in the real-world.

2.4 Results

2.4.1 Descriptive Statistics

Analysis of the full data set was completed to determine important characteristics or trends. The average values for continuous variables are presented in Table 2.4. Through examination of the maximum and minimum values in the full data set, it is apparent that some data points were collected from filters that contained no media and filtration trials where no coagulant was used. These observations were reported by Hendricks and co-workers in order to assess the amount of removal through their pilot-plant (2005). The majority of the continuous variables were found to be non-normally distributed via the Jarque-Bera test, as shown in Table 2.5. Because of the non-Gaussian distribution of the majority of variables, correlation coefficients were determined using Spearman's P.

Table 2.4: Descriptive statistics for continuous variables. sd = standard deviation of the sample

Process Parameter	All Data					MI > 0.4 mg/L			MI < 0.4 mg/L		
	n	min	max	avg	sd	n	avg	sd	n	avg	sd
Metal Ion (mg/L)	115.0	0.0	8.5	2.1	1.9	97.0	2.5	1.8	18.0	0.1	0.1
Polymer (mg/L)	115.0	0.0	3.0	0.4	0.7	97.0	0.3	0.6	18.0	0.9	0.8
pH	87.0	5.0	8.3	6.7	0.8	73.0	6.6	0.8	14.0	6.9	0.5
Temperature (^{o}C)	102.0	2.2	25.0	12.7	6.7	84.0	12.4	6.6	18.0	14.0	7.1
pOH	79.0	5.9	9.8	7.9	0.9	65.0	7.9	1.0	14.0	7.5	0.5
Media depth (cm)	108.0	0.0	940.0	270.9	364.0	90.0	283.1	378.9	18.0	209.7	278.4
Media depth 2 (cm)	107.0	0.0	330.0	27.9	53.5	89.0	26.2	48.6	18.0	36.7	74.3
Effective Size 1 (mm)	106.0	0.0	1.8	1.0	0.3	88.0	1.0	0.2	18.0	1.0	0.5
Effective Size 2 (mm)	105.0	0.0	0.6	0.3	0.2	87.0	0.3	0.2	18.0	0.4	0.3
Effluent Turbidity (NTU)	100.0	0.2	103.0	6.2	15.2	88.0	0.1	0.2	18.0	2.2	0.9
Influent Turbidity (NTU)	103.0	0.0	3.2	0.2	0.6	82.0	7.0	16.7	15.0	0.8	1.2
Filtration rate (m/h)	115.0	2.4	19.6	9.5	4.0	97.0	9.2	4.0	18.0	10.9	4.1
Inf. Total Organic Carbon (mg/L)	39.0	1.5	5.0	2.6	1.0	28.0	2.8	1.1	11.0	2.0	0.3
Log Cryptosporidium Removal	115.0	0.0	6.1	3.3	1.6	97.0	3.7	1.5	18.0	1.4	1.0

Table 2.5: Results of Jarque-Bera analysis for normality. When h=0, sample is normally distributed, if h=1, non-Gaussian distribution.

Process Parameter	All Data		MI > 0.4 mg/L		MI <0.4 mg/L	
	h	p	h	p	h	p
Metal Ion (mg/L)	1	0.001	1	0.001	0	0.327
Polymer (mg/L)	1	0.001	1	0.001	0	0.219
pH	0	0.500	0	0.440	1	0.004
Temp (^{o}C)	1	0.024	1	0.027	0	0.225
pOH	0	0.211	0	0.134	0	0.434
Media depth 1 (cm)	1	0.001	1	0.006	1	0.002
Media depth 2 (cm)	1	0.001	1	0.001	1	0.001
Effective Size 1 (mm)	1	0.001	1	0.001	1	0.034
Effective Size 2 (mm)	1	0.006	1	0.013	0	0.056
Effluent Turbidity (NTU)	1	0.001	1	0.001	0	0.183
Influent Turbidity (NTU)	1	0.001	1	0.001	1	0.036
Filtration rate (m/h)	0	0.184	1	0.027	0	0.120
TOC (mg/L)	1	0.007	1	0.039	1	0.003
Log Cryptosporidium Removal	0	0.059	0	0.126	0	0.500

Coagulant doses and coagulation pHs of observations included in the data set were compared to the pC-pH diagrams published by Amirtharajah and Mills (1982) and Johnson and Amirtharajah (1983) as shown in Figure 2.5 and Figure 2.6, respectively. Figure 2.5 shows both optimal and sub-optimal Alum doses fell within the restabilization zone, indicating the importance of coagulant stoichiometry in this portion of the coagulation diagram. Some data points (circled in Figure 2.5) were located in the zone of insolubility of aluminum. In these observations, polymers were used to ensure effective coagulation. Data points in Figure 2.6 show that some of the observations made when ferric coagulant dose was considered optimal were not located in the "optimal" sweep coagulation zone. Data were regarded as optimal or sub-optimal as reported by the original study authors for the purpose of model formulations presented herein.

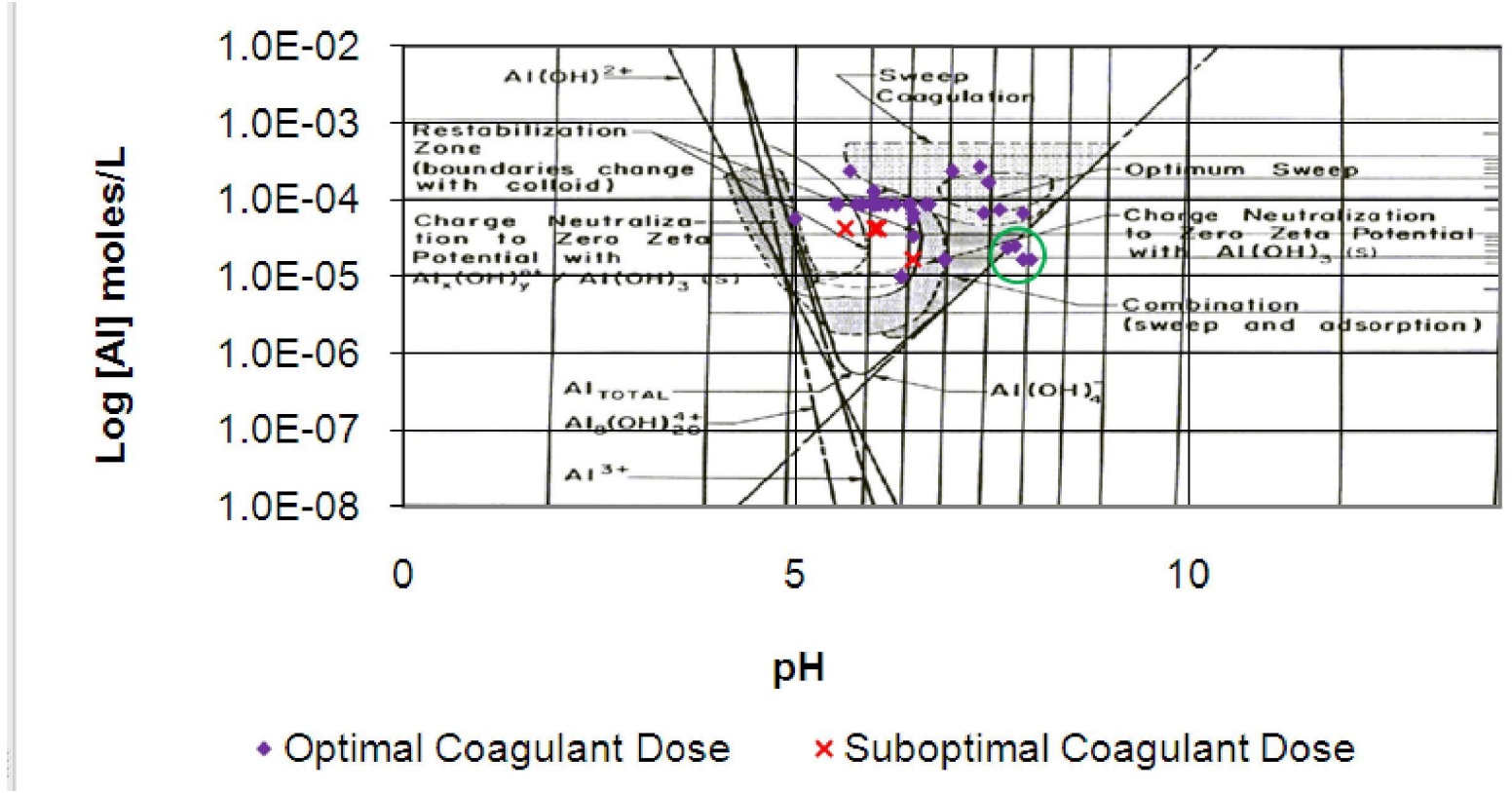

Figure 2.5: Alum coagulation diagram of Amirtharajah and Mills (1982) with meta-analysis data. Circled points were trials where polymer was used.

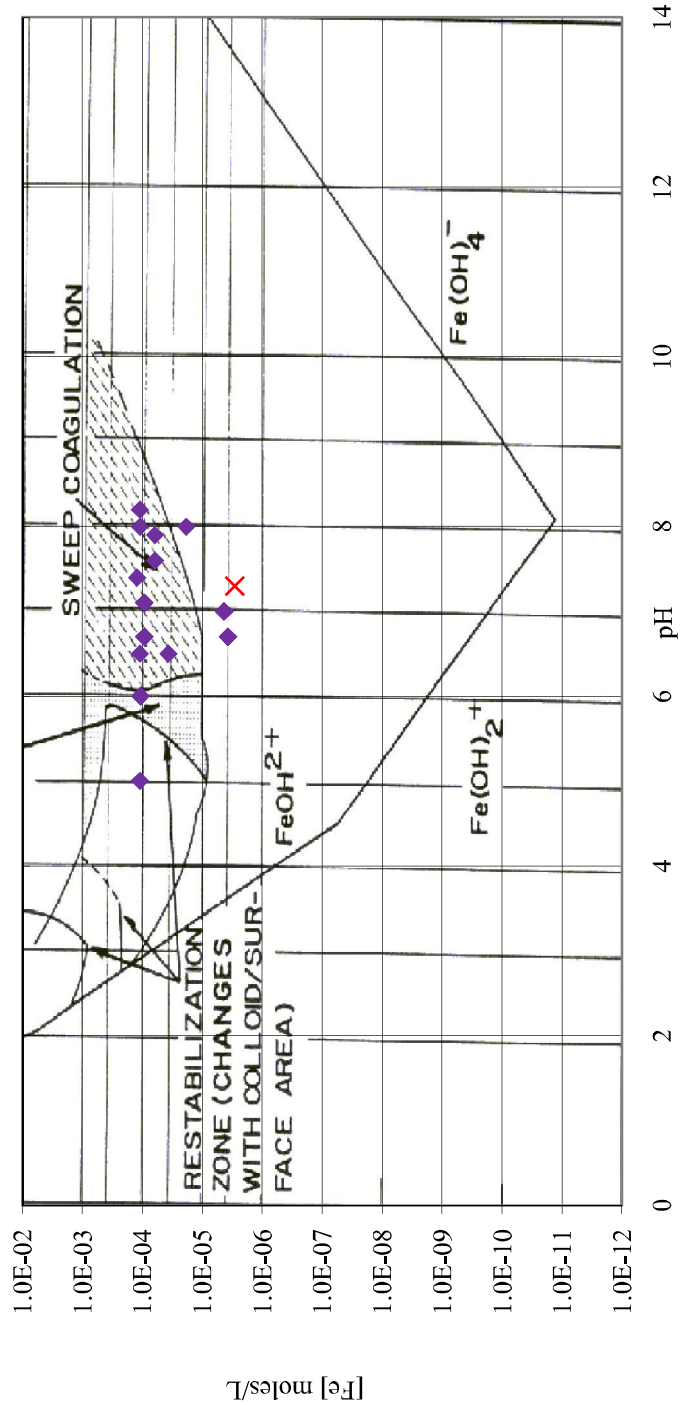

Figure 2.6: Iron coagulation diagram of Johnson and Amirtharajah (1983) with meta-analysis data.

2.4.2 Correlation Analyses and Scatter Plots

2.4.2.1 Full Data Set

Correlation analysis of continuous variables in the full data set using Spearman's P is presented in Table 2.6. This table shows MI concentration and effluent turbidity were the two variables with the highest correlation to removal. MI concentration was weakly positively correlated with the removal with a P value of 0.41, while effluent turbidity was moderately negatively correlated to the Log Cryptosporidium removal with a P value of -0.67. Both of these correlations were found to be significant with $p < 0.001$. Collinearity (near-linear dependence between potential explanatory variables) was noted (Rawlings et al., 1998). Table 2.6 shows moderately strong linear relationships (those greater than |0.50|) occurred among the depth, effective size, and filtration rate variables.

Table 2.6: Spearman's Rho values based on full data set (includes breakthrough and sub-optimal coagulation).

Process Parameter	MI (mg/L)	Poly. (mg/L)	pH	Temp (°C)	pOH	Media depth 1 (cm)	Media depth 2 (cm)	Eftive Size 1 (mm)	Eftive Size 2 (mm)	Inf. Turb. (NTU)	Eff. Turb. (NTU)	Filt. rate (m/h)	TOC (mg/L)
Poly.	-0.35												
pH	-0.16	0.33											
Temp	0.06	0.39	0.5										
pOH	0.08	-0.38	-0.97	-0.65									
Media depth 1	-0.13	0.07	-0.42	-0.45	0.48								
Media depth 2	0.04	0.02	0.17	0.32	-0.23	-0.44							
Eftive. Size 1	0.01	0.49	0.14	0.49	-0.23	-0.23	0.57						
Eftive. Size 2	0.07	0.32	0.17	0.38	-0.19	-0.37	0.73	0.76					
Inf. Turb.	0.2	-0.02	-0.05	0.34	0.05	-0.16	0.16	-0.05	0.02				
Eff. Turb.	-0.14	-0.14	0.0	-0.19	-0.01	0.03	0.13	-0.11	-0.12	-0.11			
Filt. rate	-0.09	0.21	-0.13	-0.34	0.22	0.57	-0.29	-0.26	-0.28	-0.12	0.09		
TOC	0.3	-0.04	-0.17	0.12	0.18	-0.67	-0.08	0.11	-0.15	0.22	0.01	-0.3	
Log Removal	0.41	0.0	-0.08	0.07	0.13	0.0	-0.03	0.11	0.16	0.03	-0.67	-0.11	0.19

When the independent variables were plotted against Log Cryptosporidium removal with the data collected during the breakthrough phase of filtration with sub-optimal coagulant doses separated, as presented in Figure 2.7 and Figure 2.8, important trends were noted. Figure 2.7 shows data points collected during suboptimal coagulation and the breakthrough portion of the filter run appeared to change the slope of the plot of removal vs. effluent turbidity from that occurring during steady state. In Figure 2.8 the plot of removal vs. MI concentration shows suboptimal coagulation and breakthrough (including early breakthrough) operation adds more variation to the relationship between removal and MI concentration. There were no data points collected during the breakthrough phase that resulted from suboptimal coagulant dose.

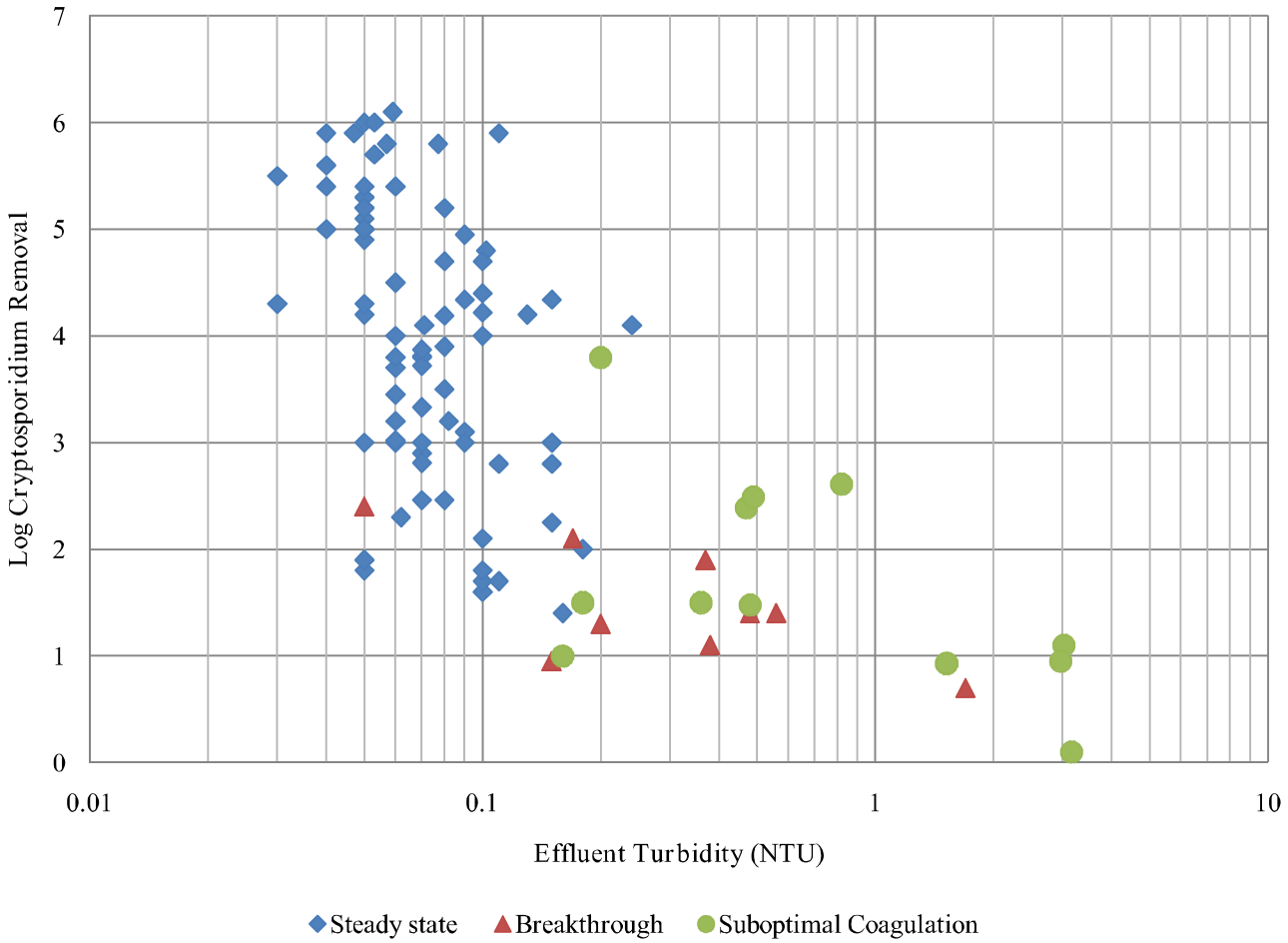

Figure 2.7: Log Cryptosporidium removal vs. effluent turbidity for full data set, n=115.

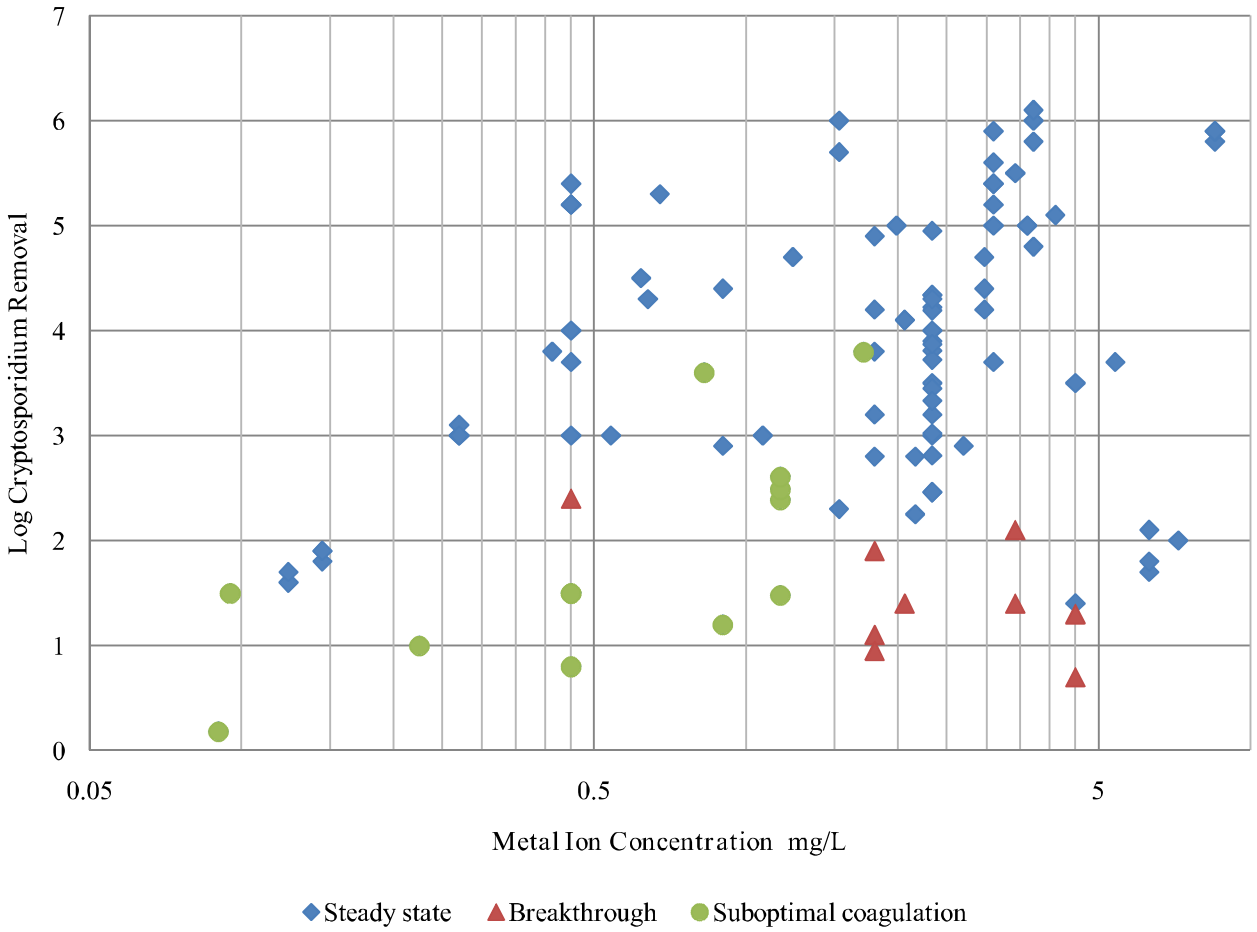

Figure 2.8: Log Cryptosporidium removal vs. Metal ion concentration for full data set, n=115.

2.4.2.2 Conventional Filtration (Metal Ion > 0.4 mg/L)

Conventional filtration was defined as any study that used a MI concentration greater than 0.4 mg/L. Spearman's P's returned from this analysis are shown in Table 2.7. In this data subset (n=97) the correlation between the effluent turbidity and removal (P=-0.69, $p<0.001$) was similar to that observed in the full data set; however, the correlation between the removal and MI concentration (P=0.16, p=0.13) was less than half of that observed for the full data set. Collinearity was also noted in this data subset among the effective size and depth variables.

Table 2.7: Spearman's Rho for conventional treatment (Metal ion concentration > 0.4 mg/L).

Process Parameter	MI (mg/L)	Poly. (mg/L)	pH	Temp (°C)	pOH	Media depth 1 (cm)	Media depth 2 (cm)	Eftive Size 1 (mm)	Eftive Size 2 (mm)	Inf. Turb. (NTU)	Eff. Turb. (NTU)	Filt. Rate (m/h)	TOC (mg/L)
Poly.	-0.23												
pH	-0.1	0.45											
Temp	0.16	0.37	0.58										
pOH	-0.08	-0.43	-0.98	-0.7									
Media depth 1	-0.13	-0.05	-0.42	-0.52	0.5								
Media depth 2	0.09	-0.15	0.19	0.24	-0.22	-0.6							
Eftive. Size 1	0.15	0.25	0.17	0.44	-0.21	-0.45	0.55						
Eftive. Size 2	0.24	0.08	0.24	0.32	-0.2	-0.56	0.72	0.72					
Inf. Turb.	0.28	0.09	-0.12	0.45	0.09	-0.08	0.2	0.06	0.12				
Eff. Turb.	-0.02	-0.16	-0.06	-0.29	0.09	0.03	0.19	-0.04	-0.07	-0.14			
Filt. Rate	-0.03	0.26	-0.11	-0.35	0.21	0.65	-0.29	-0.26	-0.32	-0.13	0.02		
TOC	0.12	0.19	-0.57	0.22	0.51	-0.49	0.11	0.61	0.47	0.14	-0.04	-0.19	
Log Removal	0.16	0.13	0.05	0.15	-0.01	-0.02	-0.03	0.19	0.23	0.07	-0.69	-0.12	0.13

2.4.2.3 Inline/Direct Filtration (Metal Ion <0.4 mg/L)

Inline/direct filtration was defined as any study that used a MI concentration less than 0.4 mg/L as ion. Spearman's P values for analysis of this subset are shown in Table 2.8. In this data subset, much higher correlations between independent variables and removal were noted, in part due to the small number of data points in this subset (n=18). Collinearity between independent variables was also observed. Strong correlations existed between metal ion and polymer concentration (P =0.93), effective size of the top media layer (media layer 1) (P =0.60), effective size of the lower media layer (media layer 2) (P =0.76), influent turbidity (P = -0.74) and effluent turbidity (P = -0.78). The effective size variables were also found to have a moderate correlation with depth of media layer 2.

Table 2.8: Spearman's Rho for direct/inline filtration (Metal ion concentration < 0.4 mg/L).

Process Parameter	MI (mg/L)	Poly. (mg/L)	pH	Temp (°C)	pOH	Media depth 1 (cm)	Media depth 2 (cm)	Eftive Size 1 (mm)	Eftive Size 2 (mm)	Inf. Turb. (NTU)	Eff. Turb. (NTU)	Filt. Rate (m/h)	TOC (mg/L)
Poly.	0.93												
pH	-0.52	-0.52											
Temp	0.34	0.28	-0.18										
pOH	0.46	0.46	-0.63	-0.38									
Media depth 1	0.18	0.28	-0.16	-0.19	0.33								
Media depth 2	0.34	0.45	0.12	0.55	-0.29	0.2							
Eftive. Size 1	0.60	0.68	0.07	0.66	-0.44	0.13	0.77						
Eftive. Size 2	0.76	0.85	-0.38	0.44	0.14	0.27	0.70	0.83					
Inf. Turb.	-0.74	-0.66	0.43	-0.33	-0.06	-0.47	-0.15	-0.44	-0.57				
Eff. Turb.	-0.78	-0.89	0.12	-0.13	-0.17	0.12	-0.34	-0.68	-0.71	0.31			
Filt. Rate	-0.04	0.00	-0.3	-0.42	0.54	0.34	-0.46	-0.56	-0.19	-0.19	0.38		
TOC	-0.57	-0.88	0.83	0.37	-0.82	-1.00	0.31	0.42	-0.56	0.57	0.34	-0.63	
Log Removal	0.87	0.96	-0.53	0.27	0.48	0.49	0.55	0.69	0.87	-0.66	-0.86	0.02	-0.86

When removal was plotted against metal ion concentration, each subset showed a different relationship between the two variables, as shown in Figure 2.9. Where MI was less than 0.4 mg/L, the relationship between coagulant added and removal was relatively strong with an R^2 value of 0.60. Where MI was greater than 0.4 mg/L coagulant dose, the relationship was very weak, with an R^2 value of only 0.01. The entire data set had an R^2 value of 0.13. This result suggested that below a MI dose of 0.4 mg/L, the coagulant dose could explain the Log Cryptosporidium removal. However, above 0.4 mg/L MI did not appear to be an important parameter to predict removal and other factors appeared to dominantly affect the oocyst removal.

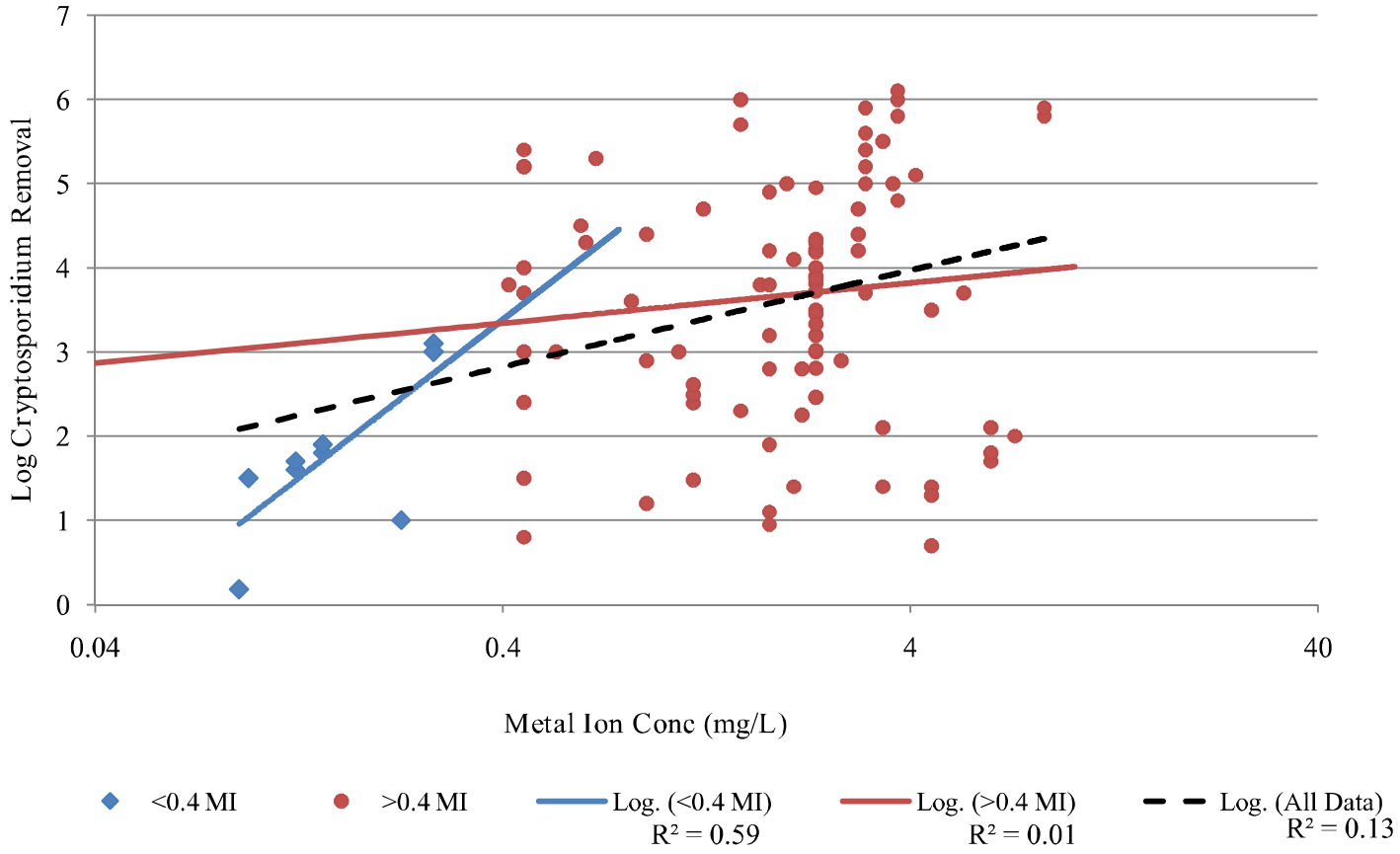

Figure 2.9: Metal ion as a potential predictor of Log Cryptosporidium removal.

2.4.3 Stepwise Regression

2.4.3.1 Full Data Set

Stepwise regression analysis of the full model without TOC included in the selection was conducted in two ways. In one model formulation, a variable to differentiate between treatment train variables was included, in the other formulation it was not. Of the 115 possible observations, 60 were used to formulate both models in the first round of variable selection.

When the variable to differentiate between treatment trains was included in the model formulation, the stepwise selection procedure resulted in the best preliminary model. A description of the results of the backward elimination and forward variable selection procedures is presented in APPENDIX D The model created in the first round of stepwise variable selection included the polymer dose, portion of filter run, coagulant optimality, and treatment train variables plus an intercept term. The second round of stepwise variable selection resulted in a model in which only the categorical variables of portion of filter run, coagulant dose optimality, treatment train, and intercept were included. The final model used all 115 available observations and had an R^2 value of 0.56. Parameter estimates for this model are presented in Table 2.9 (an ANOVA table is available in APPENDIX E). The most striking characteristic of this model was that it included no continuous independent variables. Figure 2.10 presents a scatter plot of predicted vs. actual removal values for this model, which highlights that the model formulation can only result in one of 5 values, depending on the combination of the categorical variables represented.

Table 2.9: Parameter estimates for full data set with treatment train variable obtained using repeated stepwise selection. Adjusted R^2 = 0.56, RMSE = 1.07, n = 115

Variable	Parameter Estimate	Standard Error	t value	p
Portion of filter run 1	-2.37	0.49	-4.79	<.0001
Portion of filter run 2	-2.95	0.55	-5.37	<.0001
Coagulant Dose Optimality	-1.83	0.29	-6.22	<.0001
Treatment Train	1.77	0.30	5.90	<.0001
Intercept	2.33	0.29	7.96	<.0001

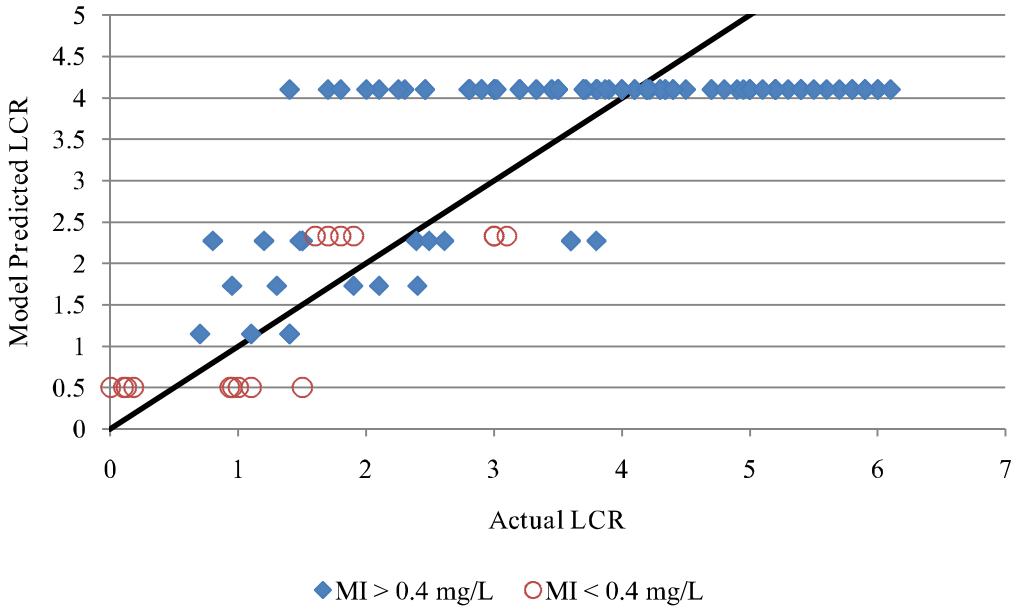

Figure 2.10: Predicted vs. actual Log Cryptosporidium removal for all data with treatment train variable model.

When the full data set model was formulated without a variable to differentiate between treatment trains, the series of models produced had lower adjusted R^2 values than the models that included the treatment train variable (discussed in further detail in APPENDIX F). The results of models with and without the treatment train variable clearly demonstrate that to best model Log Cryptosporidium removal, the data set should be divided based on the treatment train. In this study, the treatment train variable was

defined by the amount of coagulant used, thus dividing the data set into two subsets: one with coagulant dose greater than 0.4 mg/L MI and one with less than 0.4 mg/L MI. Stepwise analyses were also conducted on these subsets.

2.4.3.2 Conventional Filtration (Metal Ion > 0.4 mg/L)

The data subset composed of observations with MI concentration greater than 0.4 mg/L represented the conventional filtration treatment train. This subset had 97 total observations with 49 of these missing data, resulting in a data set of 46 observations which were used in the first stepwise regression procedures. The backward elimination approach was found to produce the best model formulation (results of the forward and stepwise approaches are presented in APPENDIX D for comparison). The first backward selection model resulted in a model that included 10 variables plus the intercept: MI, pOH, media depth 1 and 2, effective media size 1 and 2, portion of filter run 1 and 2, coagulant dose optimality, and filtration rate. The second backward elimination procedure resulted in a model containing the portion of filter run 1 and 2, coagulant dose optimality, and filtration rate variables, as well as an intercept term. This model was formulated based on all 97 available observations and had an adjusted R^2 value of 0.43 and an RMSE of 1.09. Parameter estimates for this model are presented in Table 2.10 and Figure 2.11 presents a plot of the values predicted by the repeated backward selection model against the observed removal values (an ANVOA table is presented in APPENDIX E). This figure highlights the lack of fit of this model to the data. The majority of the predicted values were in the 3 to 5 Log removal range, but their actual removals varied from 1.4 to 6 Log. Although this was the “best” model obtained through

stepwise variable selection procedures, it was not able to account for the majority of the variability in this data subset.

Table 2.10: Parameter estimates for MI > 0.4 mg/L model obtained using repeated backward elimination selection. Adjusted R^2 = 0.43, RMSE = 1.09, n = 97

Variable	Parameter Estimate	Standard Error	t value	p
Portion of Filter Run 1	-2.48	0.51	-4.89	<.0001
Portion of Filter Run 2	-2.99	0.56	-5.32	<.0001
Coagulant Dose Optimality	-2.03	0.37	-5.50	<.0001
Filtration Rate	-0.08	0.03	-2.81	0.006
Intercept	4.86	0.29	16.61	<.0001

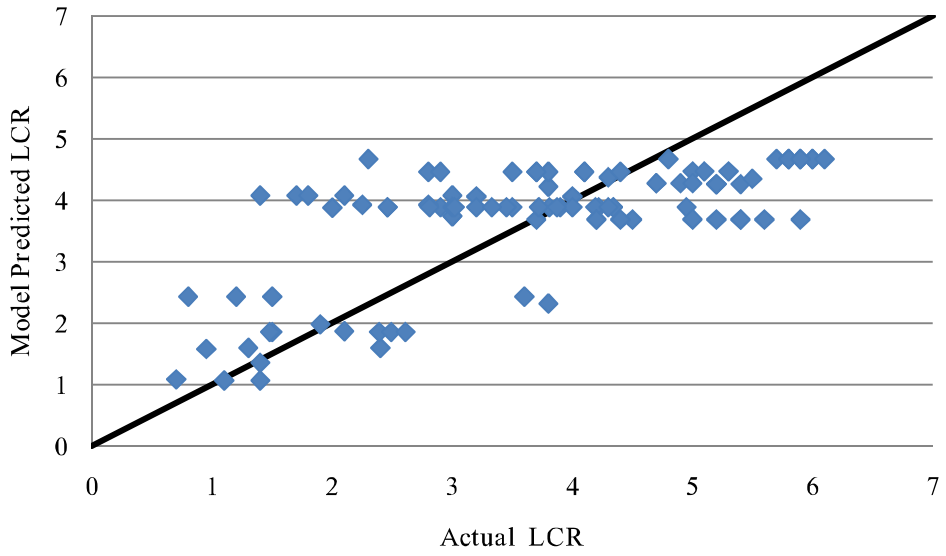

Figure 2.11: Predicted vs. actual Log Cryptosporidium removal for MI > 0.4 mg/l model

2.4.3.3 Inline/Direct Filtration (Metal Ion <0.4 mg/L)

The data subset comprised of observations where the MI concentration was less than 0.4 mg/L had 18 total observations which included 6 observations from Hendricks and coworkers taken when no metal ion was added (2005). Because collinearity between the polymer and MI concentrations was observed, polymer dose was not included in set

of possible explanatory variables. In general, when a low dose of coagulant (MI) is used, polymer is added to improve the filtration process, which may have contributed to the observed collinearity. Repeated stepwise selection produced a model that had an adjusted R^2 value of 0.89, an RMSE of 0.31, and contained 4 regressors: metal ion concentration, media depth 1 and 2, coagulant dose optimality, and an intercept term. Parameter estimates and model statistics for this model are shown in Table 2.11 (an ANVOA table is presented in APPENDIX E). A notable feature of Table 2.11 is the low parameter estimates associated with the media depth variables. Because the values of media depth were up to three orders of magnitude greater than the metal ion dose, these low parameter estimates occurred because the data were not standardized, not because of the "unimportance" of the variable. Figure 2.12 presents a plot of the values predicted by this model against the observed removal values, and illustrates the ability of this model to return removal values very similar to those observed.

Table 2.11: Parameter estimates for MI < 0.4 mg/L model obtained using repeated stepwise selection. Adjusted $R^2 = 0.89$ RMSE = 0.32, n = 18

Variable	Parameter Estimate	Standard Error	t value	p
Metal Ion	6.49	1.11	5.86	<0.0001
Depth of Media 1	0.0011	0.00029	3.8	0.0022
Depth of Media 2	0.0023	0.00105	2.21	0.0452
Coagulant Dose Optimality	-0.83	0.21	-3.96	0.0016
Intercept	0.78	0.24	3.24	0.0065

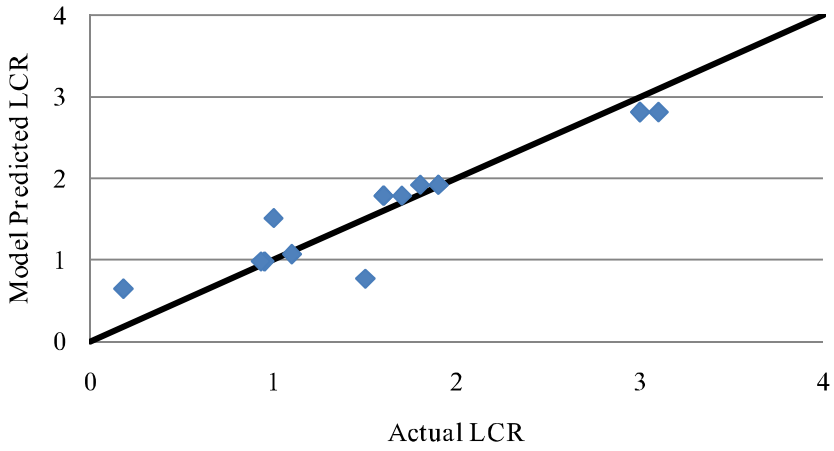

Figure 2.12: Predicted vs. actual Log Cryptosporidium removal for MI < 0.4 mg/L model.

Of the three models produced for the MI < 0.4 mg/L subset, the results of the repeated stepwise procedure had the least number of regressors and was the only one where the MI parameter estimate was significantly different from zero at the $p<0.001$ level. The models that resulted from repeated forward and backwards selection procedures had lower RMSE and higher adjusted R^2 values, but contained seven parameters in addition to the intercept term. This was considered an excessive number of parameters considering this data subset was comprised of only 18 observations and the models were deemed 'overfit'. Results of the repeated forward and backwards selection procedures are presented in APPENDIX D.

Summary

The four best models obtained using repeated stepwise variable selection techniques are presented in Table 2.12. ANOVA tables for each of these models are located in APPENDIX E. The optimality of coagulant dose variable appeared in all four models, which suggested this to be an important variable for Cryptosporidium removal. An analysis of parameter estimates for this variable, which had values of .20 to -2, was

facilitated by the fact that was a categorical and only took values of 0 or 1. Therefore, the non-optimality of the coagulant dose appeared to reduce the predicted removal by up to 2 Log. The results also showed the importance of separating the models based on coagulant dose (MI concentration), as the variables found to be most related to Log Cryptosporidium removal in the MI<0.4 mg/L subset were different from those in the MI >0.4 mg/L model.

Table 2.12: Best stepwise selection models.

Data Set	Adj. R^2	n	Explanatory Variables (+ Intercept)
Full (with Treatment Train)	0.56	115	Portion of Filter Run, Coagulant Dose Optimality, Treatment Train
Full (without Treatment Train)	0.28	115	Effective Size, Effluent Turbidity, Coagulant Dose Optimality, Filtration Rate
> 0.4 mg/L MI	0.47	97	Portion of Filter Run, Coagulant Dose Optimality, Filtration Rate
< 0.4 mg/L MI	0.89	18	Metal Ion Concentration, Filter Media Depth, Coagulant Dose Optimality

2.4.3.4 Steady-State Filter Operation/Optimal Coagulant Dose Data Only

Further examination of the data collected during steady-state operation and using optimal coagulation was completed based on several factors. First, drinking water treatment facilities generally optimize their coagulant dose. Second, only water produced during the steady state portion of the filter run is sent to the distribution system for consumption. Finally, model formulations included the portion of filter run and coagulant dose optimality categorical variables in each model where they were applicable, suggesting further analysis should focus on specific categories of these variables. Analysis of the steady-state operation/optimal coagulation data was completed

without including observations made when polyaluminum chloride was used as a coagulant due to uncertainty in the content of metal ion in PACl (see APPENDIX G).

Spearman's P correlation coefficients for continuous explanatory variables taken during steady state filter operation and optimal coagulant dose (without PACl) and Log Cryptosporidium removal are shown in Table 2.13. According to these results, effluent turbidity had the highest capability to predict Cryptosporidium removal in the all data and conventional treatment data sets, with P values of -0.49 (n=82) and -0.56 (n=73), respectively. When direct/inline treatment was considered, the metal ion and polymer dose were the strongest predictors of Cryptosporidium removal, both with a P value of 0.96 (n=9). Correlation results indicated the same patterns of collinearity were present in the steady state/ optimal coagulant dose data set as noted in full data set for all the data and MI > 0.4 mg/L (conventional) data subset. However, since there were 50% less observations, a higher degree of collinearity was noted in the MI < 0.4 mg/L steady state/optimal coagulant dose data set than its full data counterpart.

Table 2.13: Correlation analysis for steady state optimal coagulant dose data without PACl data.

Continuous Explanatory Variable	Spearman's Rho with Log Cryptosporidium Removal		
	All Data (n=82)	Conventional MI > 0.4 mg/L (n=73)	Direct/Inline MI < 0.4 mg/L (n=9)
MI (mg/L)	0.23	-0.01	0.96
Poly. (mg/L)	-0.16	0.12	0.96
pH	0.01	0.07	-0.48
Temp (°C)	0.02	0.16	-0.59
pOH	0.07	-0.04	0.93
Media depth 1 (cm)	-0.16	-0.12	0.83
Media depth 2 (cm)	-0.13	0.04	-0.83
Eftive Size 1 (mm)	-0.07	0.26	-0.8
Eftive Size 2 (mm)	0.04	0.32	0.35
Inf. Turb. (NTU)	0.01	-0.07	-0.48
Eff. Turb. (NTU)	-0.49	-0.56	-0.46
Filt. Rate (m/h)	-0.09	-0.14	0.83
TOC (mg/L)	0.35	0.13	-0.83

Correlations between removal and effluent turbidity and removal and metal ion concentration were higher when all the data was included than when only the steady state/optimal coagulant dose data were considered. The most important observation in the relationship between MI and removal with the restricted data set was the change in sign of the slope for the MI > 0.4 subset. Figure 2.13 shows the relationships between the MI dose and removal for the three data sets using only optimized coagulant dose and the steady state portion of the filter run observations. This figure shows when the metal ion dose was greater than 0.4 mg/L, metal ion dose and Cryptosporidium removal were inversely related - the less MI added, the more removal occurred. Although the correlation coefficient was not strong ($R^2 = 0.02$), this could still suggest a very different relationship between MI and removal when MI is above a threshold value. In the current

study, 0.4 mg/L was selected as the threshold value; however, this boundary may be specific to this data set and could change with the incorporation of additional observations.

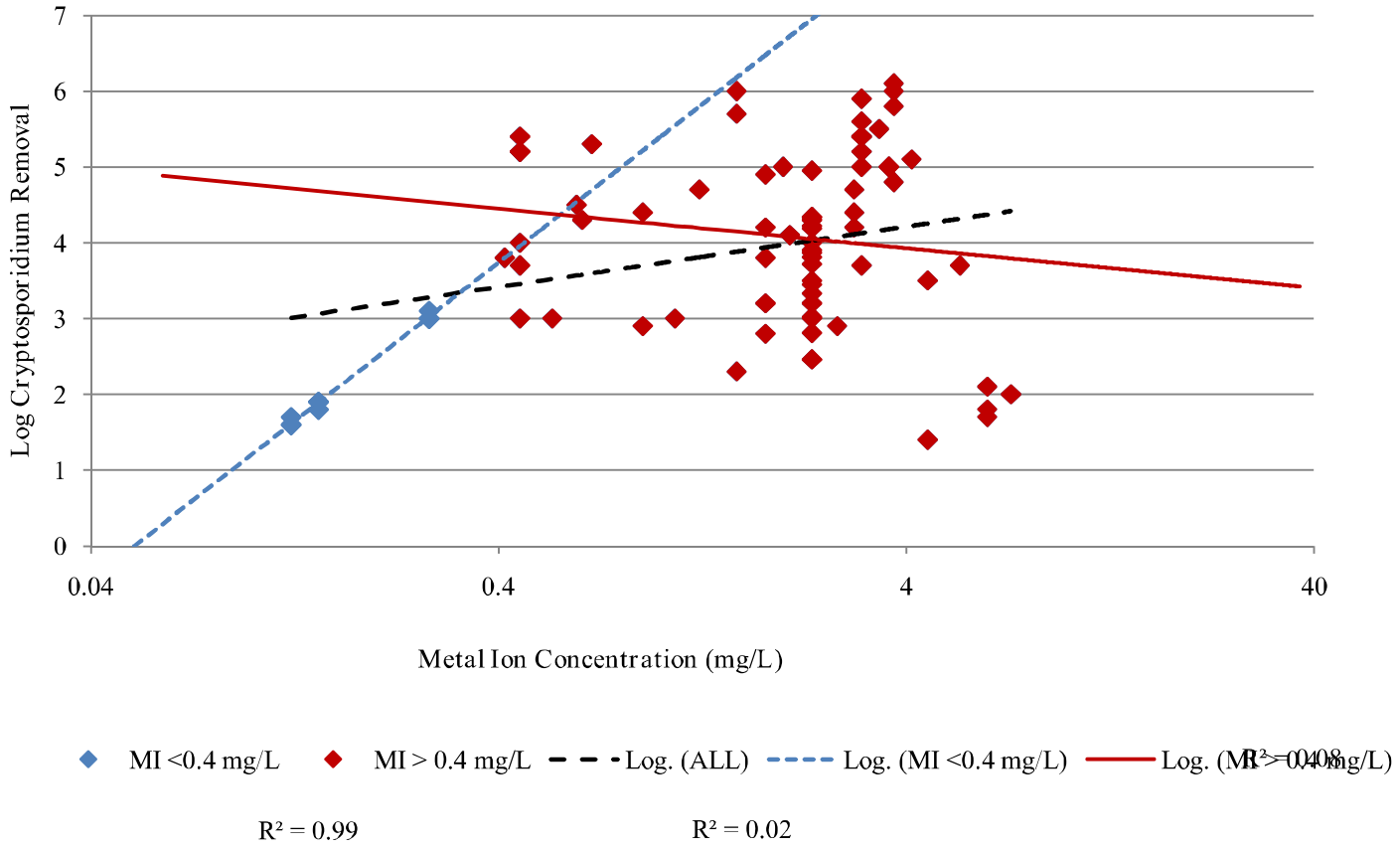

Figure 2.13: Metal ion as a potential predictor of Log Cryptosporidium removal with optimum coagulant dosing and during the steady state portion of the filter run.

Repeated stepwise regression was conducted using the 82 observations taken during steady state filter operation and optimal coagulant dose with PACl data removed. Possible explanatory variables were: metal ion concentration, polymer concentration, pOH, media depth (1 & 2), media effective size (1 & 2), effluent and influent turbidity, filtrate rate, and treatment train. Stepwise selection results of the data set that excluded suboptimal coagulation, breakthrough filtration, and PACl (n=82) were generally the same as when the full data set (n=115) was analyzed. Like the results of the full data set, in the analysis of the data set of optimal coagulant dose and steady-state filtration operation, the treatment train variable was selected in all three variable selection procedures, suggesting a division of the data into two subsets (greater than and less than 0.4 mg/L metal ion).

When the optimal coagulant dose and steady state filtration data was divided into subsets based on metal ion concentration, the stepwise selection results were similar to those of the data set where the portion of filter run and coagulant dose optimality variables were included. In the subset where MI dose was above 0.4 mg/L (n=73), the effluent turbidity was selected by stepwise selection as the best single predictor of Log Cryptosporidium removal, with an adjusted R^2 value of 0.19. This adjusted R^2 was 50% lower than the adjusted R^2 of 0.43 noted for the previously determined backward selection model that included the portion of filter run, coagulant dose optimality, and filtration rate variables (shown in Table 2.10 on page 103). In observations where MI dose was below 0.4 mg/L, stepwise variable selection procedures indicated MI could predict removal with an adjusted R^2 value of 0.99, although this data set was small (n=9).

2.5 Discussion

The goal of this project was to produce a model (or series of models) that could relate coagulant dose and/or other easily quantified drinking water treatment parameters to the removal of Cryptosporidium through the coagulation/flocculation/sedimentation/filtration process. The focus was not to create a predictive model but rather to use the models for data exploration purposes and determine what data in the literature show to be the most important variables affecting Cryptosporidium oocyst removal. These results are based only on a sample of the data available in the literature and any conclusions drawn may apply only to this particular data set.

This meta-analysis indicated important points regarding the relationship of coagulant dose to removal. Below a threshold level of coagulant dose (0.4 mg/L metal ion) the relationship between the coagulant dose and removal is linear and strong, while above this threshold other parameters influence Log Cryptosporidium oocyst removal and coagulant dose does not appear to be as important. Therefore more than one linear model was needed to best describe the relationship between Cryptosporidium removal and coagulant dose added.

The data subset where metal ion concentration was less than 0.4 mg/L only contained 18 data points, limiting the power of statistical analysis. Even so, the Log Cryptosporidium values in this subset exhibited a strong correlation to the metal ion concentration. Hendricks and coworkers also found that alum dosages less than the optimal resulted in proportionately lower Cryptosporidium Log removals and noted a linear relationship between alum dose and oocyst Log removal through inline and

conventional treatment trains (2005), which supports the results of the current study. Data from the study of Hendricks and coworkers were included model formulations presented herein but were not expected to greatly influence the MI<0.4 data subset because only their zero coagulant dose observations were included. In addition, the definitions of inline and conventional treatment were different for the two studies. While the Hendricks study classified treatment train based on whether or not flocculation and sedimentation basins were used, herein it was defined on the basis on coagulant dose added. Yet in both studies a similar result was observed.

Collinearity issues were noted in the full data set and subsets. Media depth, effective size, and filtration rate were noted to be correlated in each data set. Correlation between these independent variables may have been due to the small amount of studies used and the common approach used by researchers to pilot-scale testing. Haas and coworkers also noted collinearity between filtration rate and filter depth in their rapid filtration model and suggested that experiments should be conducted in which these variables are varied in a more independent fashion (2001). The highest degree of collinearity appeared in the MI < 0.4 mg/L data set between the MI and polymer doses. Because polymer is usually added when coagulant (hence MI) doses are low, the collinearity between these variable was a logical occurrence.

By comparing the two full data set models, results suggested Cryptosporidium removal efficiency achieved through different treatment trains have different dependencies on process parameters. This idea was supported by the, the better model fit (as determined by the adjusted R^2 value) for the model that included a treatment train

variable as compared to the model where the distinction between the treatment trains was not made.

Stepwise procedures indicated that the optimality of coagulant dose and portion of filter run were important variables. Optimality of coagulant dose appeared in all four model formulations, while portion of filter run was included in both the full data set with treatment train and the greater than 0.4 mg/L MI models. The portion of filter run variable did not appear in the MI < 0.4 mg/L subset because all of the data in that subset was taken during steady state filtration conditions.

In the MI > 0.4 mg/L MI subset, the MI variable did not appear in any of the stepwise-selected models, which suggested that coagulant dose was not an important factor in conventional treatment. Throughout model development, filtrate rate appeared in models for this data set which suggested filtrate rate may be, along with the categorical variables of portion of filter run and coagulant dose optimality, an indicator of removal, with a high filtrate rate leading to a lower removal. Based on the Spearman's P of -0.69 in Table 2.7 (which corresponds to an R^2 value of 0.36), effluent turbidity may be the best single surrogate for predicting removal at coagulant doses above 0.4 mg/L as metal ion.

Analysis using only observations collected during steady state filter operation and optimal coagulant dose (with PACl data removed) did not significantly change the selected variables in each data set. Analysis of the full range of metal ion concentrations showed the treatment train categorical variable was required and the metal ion dose was still the best predictor of removal below MI of 0.4 mg/L. In the data subset where the metal ion concentration was greater than 0.4, effluent turbidity was determined to be the

best single variable for predicting Log Cryptosporidium removal during optimal coagulant dosing and steady state filter operation. This result was similar to that noted by LeChevallier and coworkers (1991). Although the correlation coefficient was not significant, the inversion of the relationship between MI concentration and removal above the metal ion concentration of 0.4 mg/L (shown in Figure 2.13) was an interesting observation and should be investigated further when more data are available.

The explanatory variable of pOH was included in model formulations rather than pH as it may more directly represent the relationship between metal ion and pH by including temperature, as suggested by Edzwald and Van Benschoten (1990). However, results indicated pOH was not necessarily found to be a better explanatory variable than pH for predicting Cryptosporidium removal. A higher correlation coefficient was found between pOH and removal in the full data set used in this study. However, the Spearman's P value between removal and pOH was lower than that of removal and pH in the MI > 0.4 and MI < 0.4 mg/l subsets. Temperature, pH, and pOH were not included in any of the model formulations.

The results of stepwise regression models had interesting implications relative to the US EPA's "microbial toolbox" which assigns removal Cryptosporidium removal credits based on the treatment processes used. The portion of filter run and optimality of coagulant dose were found to be important categorical variables. However, these are not quantitative measurements, but qualitative descriptions that may vary from one observer to the next. The US EPA does not explicitly specify that utilities must only deliver water that was produced during the steady state portion of the filter run; instead the toolbox requires utilities to achieve an effluent turbidity $\leq$ 0.15 NTU in 95% of the combined

filter effluent samples taken each month (USEPA, 2007a). Likewise optimal coagulant dose is not explicitly required, only that a coagulant must be added continuously when a pre-sedimentation basin is used (USEPA, 2007a). The pre-sedimentation removal credit also depends on turbidity removal. From this perspective, the findings which suggested effluent turbidity is an important indicator of Cryptosporidium removal support the basis of the US EPA's microbial toolbox crediting. However, the inclusion of categorical variables in model formulations indicate Cryptosporidium removal depends on factors beyond turbidity removal which may not be easily quantifiable.

2.6 Summary

This study found that below a threshold coagulant dose (herein determined as 0.4 mg/L MI) Log Cryptosporidium removal appeared have a strong linear relationship to metal ion concentration, and hence coagulant dose. However, above the 0.4 mg/l metal ion threshold coagulant dose, effluent turbidity was found to have the best correlation to Log Cryptosporidium removal, which supports its use as a surrogate indicator. Among the potential explanatory variables considered, portion of filter run and optimality of coagulant dose were statistically shown to influence Log Cryptosporidium removal. However, these variables tend to be qualitative in nature and difficult to define. Several of the models developed herein supported current understanding of the relationships between coagulation and filtration variables and oocyst removal, while others suggested novel relationships between variables that may warrant further investigation.

2.7 Conclusions

The results of this Meta-analysis led to two major conclusions. First, the type of filtration or treatment train used is an important variable for forecasting the Log

Cryptosporidium removal achieved through treatment. This lends support to the USEPA's microbial toolbox, which assigns direct filtration a removal credit 0.5 Log lower than conventional filtration. Second, when the metal ion concentration was less than 0.4 mg/L, a linear relationship between metal ion and Log Cryptosporidium removal was observed. Therefore it may be possible for drinking water treatment facilities operating in this range (e.g., direct filtration plants) to observe higher Cryptosporidium removals simply by increasing the dose of coagulant applied.

2.8 Perspectives/Suggestions for Future Research

The models developed in this study used all the available data to build the models, without reserving any part of the data to test the final models. Therefore these models should be tested with the results of studies not included here. In addition, pilot or full scale oocyst-removal trials could be designed specifically to test the validity of the developed models. Data collected through such an endeavor would allow for more confidence in the models presented here. Furthermore, the results of stepwise regression analyses may depend on the order in which variables are added to the model, especially in forward and stepwise variable selection. In this study, the consequences of changing the order of variable addition during stepwise analyses were not examined.

In collecting data to conduct this meta-analysis, it was noted that some authors reported many more details about filtration conditions than others. It is understood that the goals of different studies precluded researchers from collecting all of the data required for the model formulations used herein. However, future meta-analyses would be easier to conduct and may have more statistical power if researchers included just a

few simple values and clarifying points, such as coagulation pH, water temperature, and the chemical formula of the coagulant used or the MI concentration used in coagulation.

CHAPTER 3: DEVELOPMENT AND USE OF A NETWORK MODEL TO QUANTIFY WATER AGE REDUCTION IN A DRINKING WATER DISTRIBUTION SYSTEM

Drinking water, like food, is best when consumed fresh. In this study, a real-world drinking water distribution system was examined to quantify the effect of specific operational changes that may be employed by a utility to reduce water age and improve the quality of water delivered to customers. A skeletonized, time-controlled hydraulic model was calibrated and used to create logic-controlled pump and valve operations that mimicked the heuristics used by the system operators. This logic-controlled model was then employed to assess the effects of alternative tank and distribution pressure scenarios on water age throughout the system. Three novel approaches for simulating and analyzing drinking water distribution systems were applied. First, a more rigorous water-quality definition of storage tank turnover rate was defined and employed. Second, the EPANET Multispecies Extension (MSX) was used to simulate water age in the system, including scenarios where water did not age in individual system tanks or at dead-end nodes, allowing for the determination of the effect of specific physical features of the system on water age. Finally, scenarios were quantitatively compared using the cumulative distribution function of water age at demand nodes. The cost of each operational scenario was estimated and water quality modeling of disinfection byproducts and chlorine residual carried out. Results suggested aging of water in the system was due predominantly to the pipe layout and demand while tanks affected the age of only the

oldest 12% of delivered water. Five of the scenarios examined reduced the variability of the age of delivered water by more than 8 hours: Closing one of the Grayson tanks, closing the Medlock Bridge and Goshen Springs tanks, increasing the central pressures at night and decreasing them during the day, reducing the volume of all tanks by 30%, and reducing the volume of the three largest tanks by 30%.

3.1 Introduction

Drinking water treatment plants use multiple technologies to ensure safe tap water is delivered to consumers. Raw water is typically treated using physical, chemical, and, in some cases, biological processes before entering the drinking water distribution system (DWDS). A disinfectant, most commonly chlorine, is added during or after treatment. Current U.S. drinking water regulations require a detectable disinfectant residual at any point of water consumption in the DWDS. A disinfectant residual can control regrowth of microorganisms remaining after primary disinfection and minimize the formation of biofilms within pipes. This residual is also assumed to inactivate pathogens that might enter a DWDS after primary disinfection, thereby preventing consumer exposure to viable microbes. However, residual chlorine reacts with natural organic matter (NOM) present in treated water to form disinfection byproducts (DBPs). The potential adverse health effects of DBPs are well documented, and exposure to DBPs in excess of the USEPA's prescribed maximum contaminant level over many years may lead to liver, kidney, or central nervous system problems and increased cancer risk (USEPA, 2007b). Regulatory limits on DBP concentrations at points of consumption are becoming more stringent. Therefore, water utilities are in the difficult position of maintaining a

disinfectant dosage that provides effective for pathogen control while limiting excessive DBP formation in the DWDS.

To balance the risk posed by microbial and chemical contaminants in drinking water, it is critical to identify system operation strategies that may improve consumer protection within the current regulatory framework. A surrogate quantity often used to evaluate water quality is its age. Water should be treated like food (Martell et al., 2002), which is considered healthiest when consumed fresh. If water has a long retention time in the DWDS, there is an increased likelihood that its quality will deteriorate. If a contamination event occurs, the probability of it affecting a large volume of water increases with the time the contaminated water in retained in the system. Regrowth and spread of a biological contaminant are higher if the water has a low disinfectant residual due to the significant decay caused by a long residence time. Although water age is not a regulated parameter, it may be a useful indicator of both DBP formation and disinfectant residual. In general, more DBPs are formed due to the longer contact time between the disinfectant and NOM and there is an increased probability of biofilm-related problems with increased retention time in the distribution system (Clark et al., 1993).

The primary goal of this project was to quantify the effect of specific operational changes that may be employed by a drinking water utility located near Atlanta, Georgia to reduce water age in the distribution system. To achieve this goal, multiple management control scenarios were simulated using a skeletonized hydraulic model of the distribution system. In addition, water quality modeling for two major classes of DBPs as well as energy consumption analyses were carried out.

3.2 Background

3.2.1 Regulatory Framework

Over 200 million people in the U.S. are served by public water systems that apply a disinfectant, leading to a large population potentially exposed to DBPs through drinking water (USEPA, 1998). Literature on the adverse health effects of DBPs has accumulated in the last decades (Bull and Kopfler, 1991; Singer, 1994; Waller et al., 1998; Bielmeier et al., 2001) and routes of exposure include both drinking and bathing in chlorinated drinking water. The Safe Drinking Water Act of 1974 (Section 1442, 42 U.S.C. 300j-1) and its subsequent amendments were promulgated by the USEPA in order to safeguard public health and ensure the quality of drinking water from source to tap. A key section of the Safe Drinking Water Act is the Stage 2 Disinfectants and Disinfection Byproducts Rule (Stage 2 DBPR), which protects public health by limiting exposure to DBPs, specifically trihalomethanes (THMs) and haloacetic acids (HAAs) (USEPA, 2006). As part of compliance with the Stage 2 DBPR, the USEPA has required that utilities complete an Individual Distribution System Evaluations (IDSE). These are one-time studies conducted to identify locations in the distribution system with high concentrations of THMs and HAAs. It is intended that water systems will use the results from the IDSE, in conjunction with monitoring data, to select compliance monitoring locations for the Stage 2 DBPR (USEPA, 2007c). Large distribution systems must meet the IDSE requirements by conducting significantly increased monitoring or by hydraulic modeling of the distribution system.

3.2.2 Water Age

Water age is primarily a function of water demand, system operation, and DWDS design (USEPA, 2002a). Water distribution systems function to deliver and store water for high demand periods, fire fighting, and in case of power outages. A major challenge comes from balancing the need to have an ample supply of water available with providing high quality (e.g., low age) water. Modifying hydraulics through system management or physical improvements can reduce water age. Improved management includes better operation of storage tanks (i.e. by decreasing the average storage time), re-routing water by changing valve settings, and implementing a flushing plan. Physical system improvements involve looping dead ends, installing blow-offs, and replacing oversized pipes (USEPA, 2007c). In the United States, the average distribution system retention time is 1.3 days and the average maximum is 3 days, based on a survey of 800 medium and large water utilities (AWWA &AWWARF, 1992).

In terms of changing operation to reduce water age, it helps to consider the short-term water balance of a distribution system. A schematic of this idea is shown in Figure 3.1.

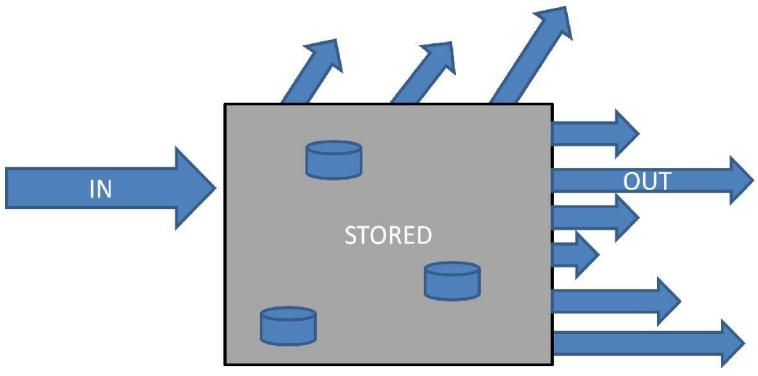

Figure 3.1: Simplified schematic of short-term distribution system water balance.

The water balance (ignoring leakage) can be thought of as:

INPUT - OUTPUT=REQUIRED STORAGE + OPERATIONAL BUFFER (3.1)

Where the INPUT water is coming from the treatment plant, OUTPUT is the demand, and REQUIRED STORAGE is the amount of water always kept in tanks (i.e. total volume of all the tanks at minimum level, for fire fighting, pressure maintenance, or emergency supply). Any difference between these can be simplified to the represent the OPERATIONAL BUFFER within the distribution system. This buffer represents water that passes through the system over a certain time period that can be adjusted spatially or temporally order to improve water age. The OUTPUT is difficult to control and the REQUIRED STORAGE may be dictated by public ordinance or requirements for pressure maintenance, leaving the INPUT portion of the water balance to be controlled in order to create a larger window of operational flexibility.

3.2.3 Dead Ends

Nearly every distribution system contains dead-end pipes (Hanson et al., 2007). Often their inclusion is the consequence of a trade-off between loops (for reliability and redundancy), and branches that cause dead-ends for cost savings during the construction of the system (Walski et al., 2003). There are no federal regulations in the U.S. dealing directly with dead-end pipes, but they can lead to long residence times due to stagnation (Hanson et al., 2007).

The best practice for dealing with dead end mains is to discourage their inclusion during construction. When dead-ends are unavoidable, regulatory guidance dictates ensuring capability to flush dead-end pipes by fitting the pipe with flushing appurtenances (i.e., a hydrant or blow-off) (Hanson et al., 2007). Pipe looping may lead

to reduced stagnation but may have a much lower potential to reduce water age than improved storage tank management (Walski, 2007).

3.2.4 Storage Tanks

Direct pumping of water from the treatment plant to the tap maximizes the quality of water delivered to consumers by reducing water age but is rarely done. The use of storage equalizes demands on supply sources, stabilizes system flows and pressures, allows for better service, and provides reserve supplies (Grayman and Clark, 1993). However, storage tanks are widely acknowledged to have negative effects on water quality that were first quantified in 1985 (Burlingame and Brock, 1985; Grayman et al., 1996; Martell et al., 2002; USEPA, 2002b; Edwards and Maher, 2008). Prior to the late 1980's, storage tank designs were based on functional and aesthetic requirements, while sizing and location were based on considerations such as meeting adequate fire demand requirements, drinking water demand, and minimum pressures (Kennedy et al., 1993) as opposed to water quality. Because tanks have not historically been designed to maximize water quality, insufficient mixing and 'short-circuiting' of water often occurs, leading to high water age. Kennedy and coworkers (1993) observed the degree of mixing within a tank was a function of tank operation and inlet and outlet locations rather than the shape of the tank and established that tank filling and draining schedules have profound effects on water quality.

Several operational changes can be employed to reduce the negative impacts of storage tanks on water age. Tank level variations can be increased to 'turn over' the tank, pumps can be programmed to be governed by tank level, and bypassing tanks when not

needed can also improve the quality of water delivered to customers (Grayman and Clark, 1993; Kennedy et al., 1993).

Tank turnover refers to the time required to completely replace the water in a tank. Several guidelines have been published suggesting turnover times or the percent of tank volume replaced in a day. The most important of these is by the AWWA, which recommends a 2.5 day turnover rate for tanks, or 40% turnover per day (Kirmeyer et al., 2000). The state of Ohio suggests that 20% of the volume change daily (5 day turnover rate) (U.S. Army Center for Health Promotion and Preventative Medicine, 1997). German regulations suggest a 5 to 7 day maximum retention time in reservoirs with cement-based internal surface, while Swiss guidelines advise a 1 to 3 day maximum retention time due to lower chlorine residuals carried there (Martell et al., 2002). Because storage tanks have different hydraulic and physical characteristics due to structure age, design, and location in the distribution system, each will have different turnover needs to in order to maximize water quality.

3.2.4.1 Calculation of Tank Turnover

The turnover rate, or amount of time needed to replace all the water in a storage tank, is simple to understand but not as easy to quantify. If the inflow/outflow of a tank were both constant and mixing conditions were ideal, the calculation of turnover time would simplify to:

$$T = V_{total} / q_{in} \tag{3.2}$$

Where T is the turnover time, V_{total} is the maximum observed tank volume (or a chosen reference volume) and q_{in} is the observed flow rate into the tank. Since in practice the flow into tanks tends to be variable, this calculation will result in a different T for

each new flow observation. This complication is overcome by determining the 'average' turnover rate over a determined time period.

The definition of turnover stated above is strictly hydraulic, it considers all the water to be of equal quality and does not account for dilution of old water in a tank by fresh water that enters. This was recently pointed out by Edwards and Maher, who found a tank to have a 2.5 day turnover rate by simple calculation (40% turnover), but model simulations indicated only 10% of the water in the tank had been replaced by new water from the distribution system in 2.5 days (2008). Because the turnover time of a tank is a metric intended to improve water quality, it should not be strictly hydraulic in definition.

3.2.4.2 Examples of Storage Tank Management to Improve Water Age

A case study conducted by Clark and Grayman demonstrated the effect of tank filling and draining on water age near a tank. When the level of water in a tank varied by 9 feet, the water age in the system near the tank was equal to 7 days, but when the level varied only by 1 foot, the water age at the same sampling points was roughly 20 days. This illustrates that decreasing the water level variation increases the age of the water in and near the tank but ultimately leads to a decrease in older water throughout the system. As a consequence, a decision must be made to either minimize the age of the water in the vicinity of the tank or minimize the spread of old water through the distribution system (Clark et al., 1993). Clark and Grayman summarize this finding succinctly, stating "different operational decisions could lead to different areas being adversely affected by the tank to differing degrees. For example, one policy could lead to a small area being adversely affected to a large degree, whereas another policy could result in a larger area being less severely affected" (1993). A perfect scenario may not exist (as trade-offs must

always be made), but proper management can lead to a distribution of lower water ages within the system, lower water age variability, and a more uniform distribution of water quality.

Gauthier and coworkers (2000) also studied the interaction between pump and tank management and provide an instance of using hydraulic models to test engineering judgment. This research team examined one area of a large North American distribution system with a hydraulic configuration that led to high tank residence times and found that by setting pumps to be governed by tank level in conjunction with decreasing tank capacity, the age of water leaving the tanks could be reduced by up to 7 days. The utility they studied chose to maintain the tank capacity but changed pump operation, which resulted in a reduction of the maximum age of water leaving the tank from 7.9 to 3.4 days (Gauthier et al., 2000).

Edwards and Maher quantified how water quality is affected by various tank operational parameters, as well as type and location, by conducting water age and source trace analysis (2008). Their results showed that a 20 ft level variation in a tank once a day resulted in a 20% water age reduction over a 15 ft level variation twice a day. They also noted the negative impact of a "sloshing" effect, or water being repeatedly cycled into and out of a reservoir during filling and draining, on the age of a tank.

Another way to avoid the negative effects tanks can have on water age is to bypass them. Kennedy and coworkers suggested "if possible, consideration should be given to taking excess storage facilities offline during periods of low flow in order to improve the turnover rate in remaining online reservoirs" (1993). This practice results in less storage and may approach direct pumping, but it may not provide sufficient supply

for fire fighting and raises the question of how to handle the older water in the bypassed tanks.

3.2.5 Flushing/Blow-offs

System flushing uses high velocity flows to remove stagnant water and sediment from distribution mains, temporarily improving water quality in specific areas of the DWDS. Flushing programs are common in the U.S., with 54% of utilities participating in a survey responding that they have a regularly scheduled flushing program in place, and 56% had a dead-end flushing program (Chadderton et al., 1992). Flushing allows for removal of sediment, reduction in bacterial counts, and increased chlorine concentrations (Chadderton et al., 1993; Federation of Canadian Municipalities, 2003).

Flow rates used to remove high-age water can be much lower than required by flushing and blow-off valves can be used instead of fire hydrants (Laptos, 2009). Blow-off valves are often located near dead-ends in a DWDS (Committee on Public Water Supply Distribution Systems, 2006) and can be automated and controlled remotely or manually. However, using water blow-offs to control system water age has drawbacks that make them a less attractive option than improving tank and pump operations. First, blow-offs are a temporary solution and focus only on isolated sections of the distribution system. Second, using blow-offs to reduce water age may result in the loss of significant amounts of water, which may be difficult to justify during periods of water conservation.

3.2.6 Operational Cost

A consideration in any distribution management study is energy expenditure and cost. Energy costs are the largest expense for nearly all water utilities worldwide and can use up to 65% of a utility's annual budget (Boulos et al., 2001). Moreover, water and

wastewater systems are among the United States largest energy consumers accounting for 3% of annual U.S. electricity consumption (Bunn, 2006). Any management strategies proposed to improve water quality must be balanced with their associated energy requirements, which is important for both cost and environmental sustainability. Commercial software packages to achieve both cost-reduction and water quality maintenance are available. For example, Aquadapt™ (Derceto, San Francisco, CA) is a fully automatic real-time pump scheduling system designed to minimize energy cost while maintaining water quality (Bunn, 2006).

3.2.7 Hydraulic Models

Hydraulic models have been used to predict water age in distribution systems for more than 20 years (Grayman, 2006). Modeling can be conducted through either steady state or extended period (or time-varying) simulation. Steady state simulations represent a simplified version the distribution system where the hydraulics are constant in time and do not account for changes in pump or valve status. Steady state models therefore serve as an approximation of network conditions. Extended period simulation (EPS) is a series of steady state simulations that are run one after the other at specified time intervals an can incorporate pump and valve operations. This approach allows for the simulation of the way a system changes in response to varying demands and operational conditions (AWWA, 2005). Similarly, models can be calibrated in either steady state or extended period modes. Steady state calibration adjusts the model to fit a "snap-shot" view whereas an extended period calibration fine tunes the model to fit time-varying data (Bundy, 2001). Models may represent all the pipes present in a DWDS (full pipe) or just the most hydraulically relevant pipes (skeletonized). Skeletonized models generally

represent all pipes with a certain diameter and larger (e.g., 8 inches and up). Water quality studies are ideal when conducted on full-scale models but skeletonized models have much faster simulation times. Hydraulic modeling software can also simulate different types of mixing regimes in tanks. A modeler can specify tanks to be instantaneously and completely mixed (most common default assumption), to have a plug-flow/first in-first out (FIFO) or last in-first out (LIFO) mixing regime, or to have some other, more tank-specific mixing characteristics. The choice of mixing regime may have a significant effect on the age of delivered water.

A calibrated, EPS model of a distribution system is a useful tool to evaluate system management scenarios and determine those that are most effective for reducing the age of water delivered to consumers. According to an AWWA survey of 174 U.S. utilities, 14% of those with a calibrated hydraulic model already use it to reduce water age, and in the future 40% expect to use their model for this purpose (AWWA, 2005). The application of hydraulic modeling to meet the IDSE requirements also presented utilities with the possibility to use their system model to identify water quality improvements through decreasing water age. Thus, it behooves the research community to provide guidance so utilities may effectively use their hydraulic models to improve operations.

Despite the increase in use of hydraulic models for determining ways to reduce water age, few peer-reviewed articles have been published that quantified the effect of operational changes on water age throughout the distribution system. Speight and DiGiano (2003) used a water quality model to analyze a small drinking water distribution system, and found tank sizing and operation significantly affect water quality. They

suggested alternate water storage configurations and a flushing program to improve water age. Other studies have proposed more complicated means such as flow rerouting (Prasad and Walters, 2006), dynamic programming of pumps (Nitivattananon et al., 1996) and genetic algorithms for pump scheduling (Murphy et al., 1994) to improve water quality and reduce operating costs.

3.2.8 Gwinnett County System

The real-world water distribution system examined in this project was the Gwinnett County Water Distribution System (GCWDS) located near Atlanta in northern Georgia. At the time of the study the system was the largest municipal water distribution system in Georgia (Pennington and Jakubowski, 2007). At the time of this study the utility served 750,000 residents and the pipe network included more than 3,600 miles of pipe with sizes ranging from 108 to 2 inches in diameter. The network included 66 pumps, 16 tanks, 122,288 pipes, and 119,681 pipe junctions. The total pipe volume was approximately 123 million gallons (MG), while the maximum capacity of system storage tanks was 59 MG, suggesting that 68% or more of the system volume was located in the pipes and 32% or less in the tanks. Daily demands on the system fluctuated depending on the season: in 2007, the lowest monthly average demand reported was 73 million gallons per day (MGD) in January and the highest at 124 MGD in August. Based on these demands and the maximum system volume, the average system retention time (or water age) was 2.5 days in January and 0.7 days (16 hours) in August of 2007.

The two treatment plants in the Gwinnett County system draw raw water from Lake Sidney Lanier. At the time of this study, both plants used pre-ozonation, ferric chloride coagulation, and granular filtration for treatment. Free chlorine, fluoride, and a

phosphate blend were added prior to distribution. The Lanier Filter Plant is the older of the two plants and has the capacity to produce 150 MGD. The Shoal Creek Filter Plant had a capacity of 75 MGD and delivered its effluent water to the Lanier Filter Plant. The effluent from the two plants was mixed and stored in clearwells (total capacity of 45 MG) before being sent into the distribution system. This simplified system modeling as there was only one water source. However, it may also have contributed to higher water age.

At the time of this study the GCWDS was controlled manually. Operators monitored the system pressures, flows, and tank level and decided which pumps should be turned on or off based on system pressures at key nodes along with tank levels. Pressure and level guidelines were in place; however, each operator had a different approach to maintaining the recommended values. Manual operation allowed for good control of the network but had significant room for improvement with regard to water quality.

Two previous studies of the Gwinnett County DWDS were conducted, with one revealing some areas of the network had water ages of up to 12 days (Kim et al., 2006). Both studies conducted field testing and batch kinetic studies to test the total Trihalomethane (TTHM) and Haloacetic Acid (HAA) formation in the DWDS and used a hydraulic model to determine the areas of the network where water quality was the poorest. Bundy's sampling results showed that the location with the longest residence time consistently corresponded to the highest chlorine decay and DBP formation (2001). Average TTHM and HAA9 (The sum of 9 different HAA's) concentrations were 33.8 μg/L and 10.3 μg/L, respectively, which were much less than the Maximum Contaminant Levels (MCLs) required by the EPA 80 μg/L of TTHMs and 60 μg/L for

HAAs (Bundy, 2001; USEPA, 2006). Results of the batch kinetic studies are shown in Table 3.1.

Table 3.1: Rate coefficients and constants from previous studies of the Gwinnett County drinking water distribution system (25 ^{o}C)

Study	Species	$C_{DBP,L}$	$C_{DBP,O}$	k (per day)
Bundy 2001	Cl^-	0	2.0 mg/L	-0.125
	TTHM	40.0 µg/l	0	0.43
	HAA9	24.0 µg/l	0	0.45
Kim and coworkers 2006	Cl^-	0	2.0 mg/L	-0.1039
	TTHM	58.5 µg/l	0	0.325
	HAA5	49.3 µg/l	0	0.143

At the time of Bundy's study, a completed distribution system model of the Gwinnett County network was unavailable. The network model used for simulation was a skeletonized model of the DWDS containing pipes ~8 inches and larger. The model included 2 reservoirs, 12 pump stations, 12 tanks, and approximately 1,850 pipes and 1,290 junctions. Calibration was carried out in steady state mode and simulations were run in EPS mode, with time-based determined from daily pumping reports of the day being modeled to turn pumps and valves on and off. Negative pressures were found at two of the pump stations during the extended period simulation, but were not expected to affect the water quality results (Bundy, 2001).

In the study conducted by Kim and coworkers (2006), a batch kinetic study was completed and used to model DBP formation in a full-pipe hydraulic model of the system developed by Envirosoft Engineering of Marietta, Georgia (Kim et al., 2006; Arniella, 2007). Model predictions were then compared to real-world conditions using tracer studies. The rates determined by Kim and coworkers for TTHM and HAA5 (the sum of 5 different HAA's) formation and chlorine decay, are compared to those of Bundy in

Table 3.1. These rates were slower than those of Bundy but resulted in higher DBP formation potentials; although the maximum attainable concentrations were still lower than the USEPA MCLs.

Kim and coworkers conducted two tracer experiments, one in October and the other in December of 2004. The October tracer study determined an average water age of 1.8 days with the majority of samples having water ages less than 3 days. The December tracer test, suggested an average water age of roughly 4 days. Tracer studies revealed sampling locations further away from the treatment plant generally had longer water retention times and lower residual chlorine levels. The south and eastern peripheral regions of the distribution system were identified as problematic. The authors asserted the results in the second tracer test might have been less accurate, because the retention time was greater (i.e. as demand was lower and more sampling locations were further away from the treatment plant).

Kim and coworkers used WaterGEMS (Haestad Methods, Watertown, CT) to run hydraulic and water quality models. Their simulations were run in a 'modified steady state' mode with fixed water demand, constant tank levels, and unchanged pump status over time for 13 days with a 1 hour hydraulic time-step. The October simulation was given a daily demand of 66.1 MGD, and for the December simulation the daily demand was 55.2 MGD. By not including pump and storage tank operations, the predictive value of this model was limited. However, linear regression analysis of tracer test and model predictions suggested the model was reasonably accurate and resulted in R^2 values for the October and December tracer tests of 0.80 and 0.70, respectively. While these studies provided useful predictions of where the DBPs in the Gwinnett County DWDS were the

highest, they did not provide insight as to why these areas experience high DBP concentrations or what could be done to reduce them.

3.2.9 Project Goal

The goal of this study was to quantify the water quality improvements that could be achieved by changing operations of the Gwinnett County, Georgia distribution system. In order to test new management scenarios, the research consisted of three phases: 1) creation of a logic-controlled model of the distribution system, 2) hydraulic simulations to determine the physical features of the network most responsible for elevated water age, 3) quantitative assessment of the effects of operational scenarios on water age and DBP concentrations.

In the first phase of research, controls that turned pumps on or off depending on specific activation pressures were programmed into a calibrated EPANET model of the network. This was intended to produce a logically-controlled, reactive model in which tanks are drained to maintain required system pressures. The logic-controlled model allowed for changes in operation of individual tanks (with the unchanged tanks responding to new system hydraulics accordingly).

Phase two developed new methodologies to simulate and analyze system water quality. The EPANET-MSX system was adapted to solve for water age alongside HAA5, TTHM, and free chlorine residual simulations. The flexibility of the MSX system was also exploited to quantitatively determine the effect of tanks and dead ends on the age of delivered water. These results provided information on which physical features of the distribution system had the highest impact on water age and where efforts to ameliorate high water ages should be focused.

Phase three aimed to determine the operational scenarios with the highest ability to improve delivered water age. Once the most effective scenarios for reducing the age of delivered water were determined, a simulation that combined several of the most successful alternative operational scenarios was examined Data collected during the operational scenario simulations were also used to determine if decreased tank turnover times significantly reduced the age of delivered water. In addition, two classes of DBPs and Cl^- were modeled. Through incorporating known kinetic values for this system, the baseline model and most effective management scenarios were used to determine their effect on the sampling locations used by the utility to fulfill the IDSE sampling requirements.

3.3 Methods

3.3.1 Hydraulic Model

A skeletonized hydraulic model of the system was obtained from Halcrow, Inc. (Atlanta, (Atlanta, GA). The skeletonized model included 3,830 pipes, 3,445 pipe junctions, 77 valves, 53 pumps, 15 storage tanks, and 2 raw water reservoirs. Detailed information about the pipe materials are shown in

Table 3.2. Figure 3.2 presents the junction elevations and pipe diameters of the skeletonized model. Figure 3.3 shows the locations of the storage tanks within the Gwinnett County DWDS. The skeletonized model represented approximately 31% of the pipe length and 65% of the pipe volume of the full system; therefore, it fell short of conforming to the USEPA IDSE skeletonization criteria requiring 50% of pipe length and 75% of pipe volume (USEPA, 2007d). In the skeletonized model the pipe volume was 80 MG and operational tank volume was 40 MG, suggesting that 67% or more of the

system volume was located in the pipes and 33% or less was in the tanks (a proportion similar to that of the full pipe model).

Table 3.2: Pipe lengths and volumes for full pipe and skeletonized models.

Pipe Diameter (in)	Full Pipe Model			Skeletonized Model		
	Total Length (ft)	Total Length (%)	Total Volume (MG)	Total Length (ft)	Total Length (%)	Total Volume (MG)
≤ 6	3193108	16.76%	3.5	127181	0.67%	0.2
8	11186669	58.71%	29.2	1414779	7.43%	3.7
10	660726	3.47%	2.7	568566	2.98%	2.3
12	2123095	11.14%	12.5	1993926	10.46%	11.7
16	967781	5.08%	10.1	1003826	5.27%	10.5
20	18496	0.10%	0.3	19220	0.10%	0.3
24	295365	1.55%	6.9	306493	1.61%	7.2
30	99710	0.52%	3.7	103299	0.54%	3.8
36	55438	0.29%	2.9	54585	0.29%	2.9
≥ 48	453265	2.38%	51.4	398183	2.09%	37.8
Total	19,053,985		123.2	5,990,058		80.4
Total (mi)	3,609			1,134		

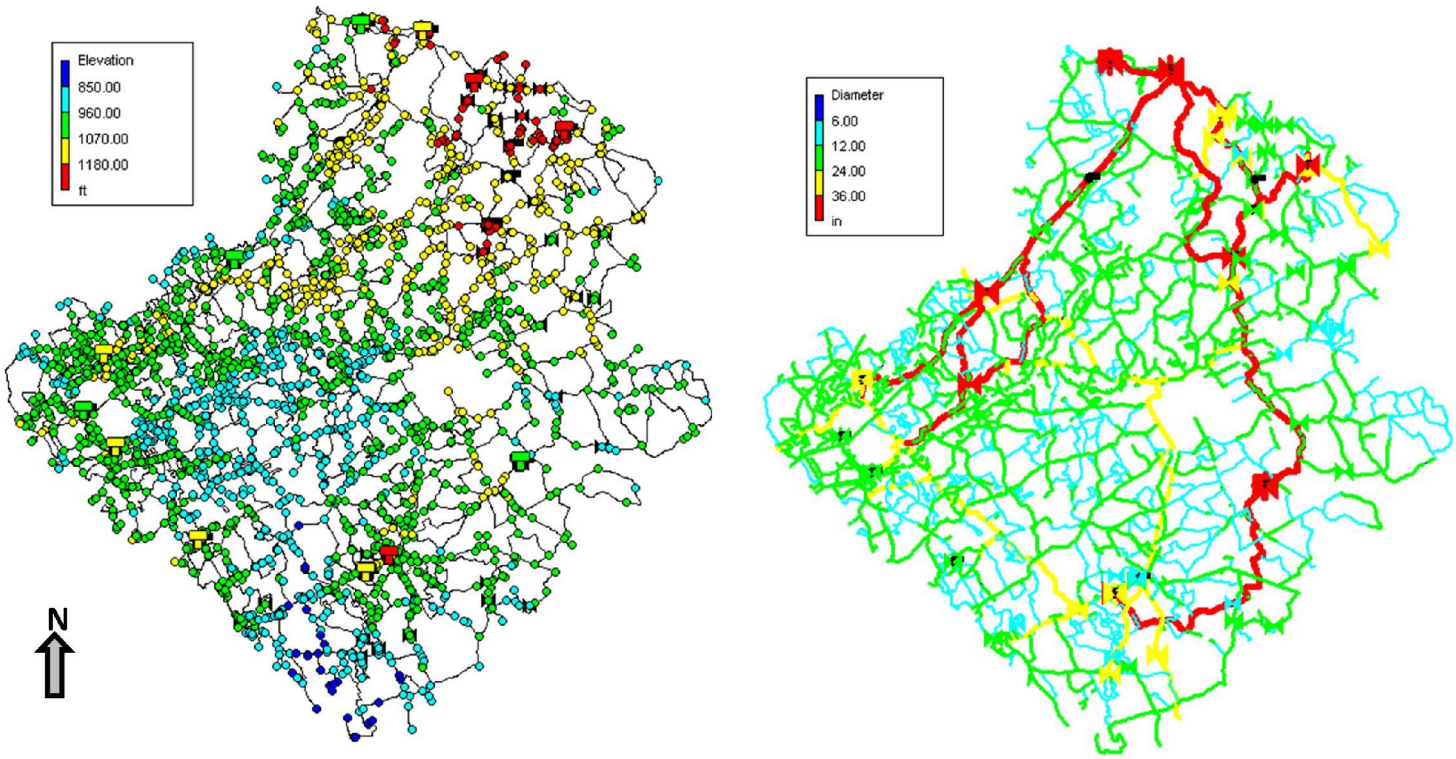

Figure 3.2: Gwinnett County skeletonized distribution system with junction elevations and pipe diameters.

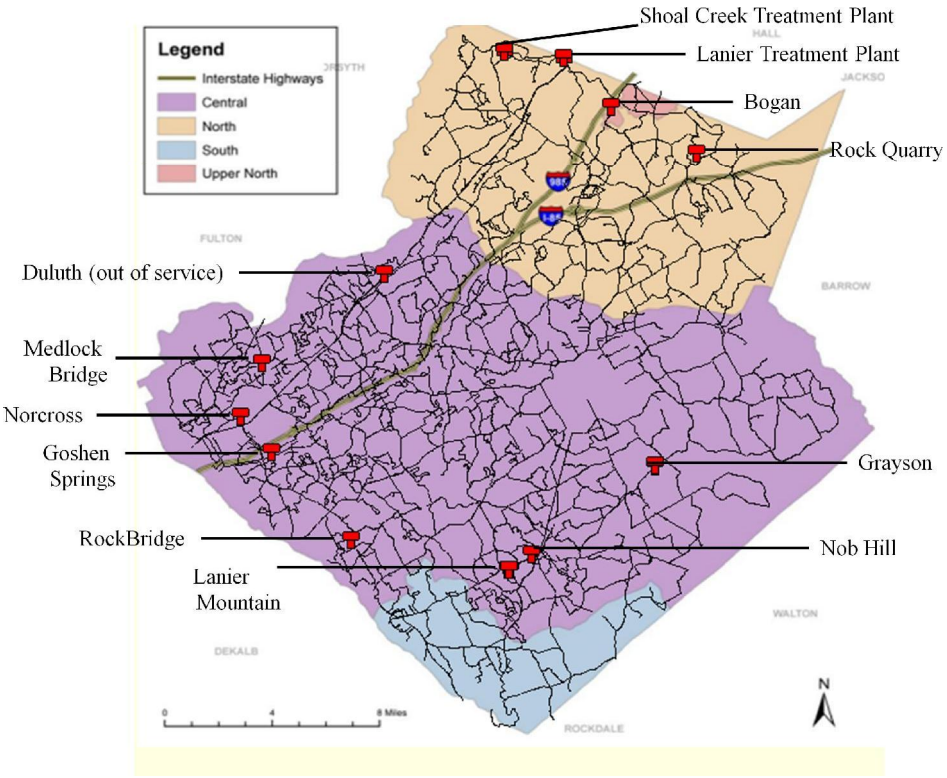

Figure 3.3: Pressure zones and storage tank locations in the Gwinnett County drinking water distribution system.

The GCWDS was divided into 4 pressure zones as shown in Figure 3.3. Each zone was supplied by the Lanier filter plant located in the northern part of the network. Water entered the system through two transmission mains: the Central main, a 6.5 ft diameter pipe serving the central/south pressure zone and the North main 4 ft in diameter serving the north, upper north and part of the central zones. A detailed view of the pipe layout following the Lanier filter plant is shown in Figure 3.4. In the actual distribution system, the high service pumps providing water to the system were variable speed pumps (VSPs). The VSPs were set to constantly deliver a specified pressure and had drives that adjusted to changes in demand to make sure that pressure is achieved. EPANET does not yet have the capability to model VSPs. Therefore, the high service VSPs were represented in the hydraulic model by using pumps that were continuously operated

followed by a pressure reducing valve (PRV) that was set to deliver the desired pump output pressure. The PRVs on the Central and North transmission mains are circled in Figure 3.4.

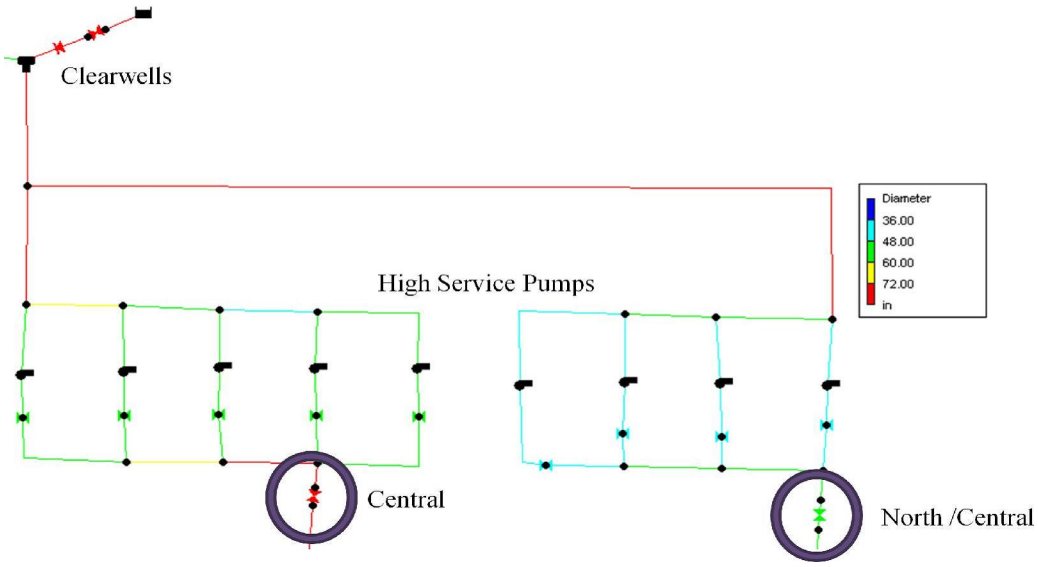

Figure 3.4: Pressure reducing valves (circled) on the transmission mains following high service pumps at the Lanier Treatment Plant.

The skeletonized model obtained from Halcrow, Inc. relied on time-based controls to operate pumps and valves, and had been calibrated via WaterGEMS Darwin Calibrator (Bentley, Exton, PA) to the period of August 6 through 10, 2007 using EPS conditions. While the time-controlled model physically represented the system, it did not replicate the actions of the system operators. At the time of this study, the majority of system storage tanks were operated manually, with operators turning on pumps or opening valves to stay within prescribed pressure ranges at certain network nodes. Because a time-controlled system model does not respond to changes in input or demand flows the way the operators would, a new logic-controlled baseline model was desired to run operations. The logic-based model allowed for changes in central pressures or pump

operations to be simulated and showed the effects these changes would have under current operational guidelines. In order to create the most accurate logic-controlled model possible, a new time-controlled model was calibrated to a one day period in August 2007 to serve as the basis for creating the logic-based controls. All model development and hydraulic simulations were accomplished using EPANET.

3.3.2 EPANET 2.0 and Multispecies Extension

EPANET 2.0 Graphical User Interface (EPANET-GUI), Programmer's Toolkit (EPANET-PT), and the multispecies extension (MSX) to the Programmer's Toolkit were used to conduct hydraulic and water quality simulations. EPANET is public domain software intended for use to conduct extended-period simulations of hydraulic and water quality behavior in DWDSs and is available for free download from the USEPA (Rossman, 2000).

The EPANET-GUI was used to develop logic-based controls and operational scenarios while the EPANET-PT and its MSX extension were used to perform simulations of system hydraulics and water quality. EPANET-PT is library of functions, available for Windows and LINUX operating systems, that simulates the hydraulic behavior in a pipe network. An analyst can specify time, quality, energy, and hydraulic parameters built-in to EPANET, including the tank mixing regime. Both the EPANET-GUI and PT can model storage tanks as completely mixed, FIFO, LIFO, or 2-compartment. EPANET-MSX "provides a collection of functions that allow programmers to utilize EPANET's hydraulic and water quality solution engine within their own custom applications" (Shang et al., 2008b). In the MSX system a text file (*.msx file) describing the reaction rates of the modeled chemicals in the system is

supplied by the user. One short-coming of the EPANET-PT /MSX system is the inability for the user to retrieve hydraulic data (e.g., nodal pressures and tank heads) from a simulation run using this combination of libraries. Consequently, two simulations were run for each scenario tested in this study: one simulation run using only the EPANET-PT to obtain pressure, tank head, and energy data output and one simulation run using the MSX system to collect water age, TTHM, HAA5, and free Cl^- concentrations at demand nodes.

Using the EPANET MSX extension to model water age is a novel application. Until now the MSX extension has been used to model chemical species, but not directly water age. While it is possible to simulate age using the MSX system, preliminary simulations showed that the use of a simple zero order reaction rate in an *.msx file resulted in different calculated water ages between the EPANET GUI and EPANET dll/MSX output. The problem arose from a lack of definition of the 'source' of water in the system in the MSX system and was rectified by simulating age from a 'starting point' in the network onwards (specified as a node located directly before the Lanier filter plant clearwells) using a two species model. With this reactive model:

$$\begin{cases} \dfrac{dB}{dt} = 0 \\ \dfrac{dA}{dt} = B \end{cases} \tag{3.3}$$

where A is the age concentration and B is a dummy non-reactive concentration, water age could be simulated starting from any point of the network and onward by placing a continuous flow-paced source of B=1 mg/l of the dummy species at that point. From equation 3.3, one can see that $A=A_0$ if B=0 while $A=A_0+t$ if B=1. Therefore, if initially $A_0=0$ everywhere, the value of A at any node of the network is the accumulated age from

the time the water passes the node considered (source of B). The MSX system also provides the researcher the flexibility to specify the reaction rate in individual tanks and pipes in the [PARAMETERS] section of the *.msx file. This flexibility allowed for simulation of scenarios where water did not age in tanks or pipes leading to dead-end nodes at the periphery of the system.

3.3.3 Time-Controlled Model Development

From the previous skeletonized hydraulic model, a new baseline model was developed to simulate a 24-hr period. Hourly data from August 22, 2007 was obtained from the utility's Supervisory Control and Data Acquisition (SCADA) system. This day represented a yearly peak usage day. It did not rain for several days prior, SCADA records were complete (no reporting faults), and the water balance over the 24-hour period resulted in no net storage (-0.09 MG/24 hours). Since no net storage and very little net consumption occurred over the 24-hour period, it could be repeated for many days without net gains or losses. The graphical representation of the water balance for August 22, 2007 is shown in Figure 3.5. The inflow represents the output from the treatment plant during a one hour period, the delta storage represents the amount of water stored, and inflow-delta storage is equal to the system demand.

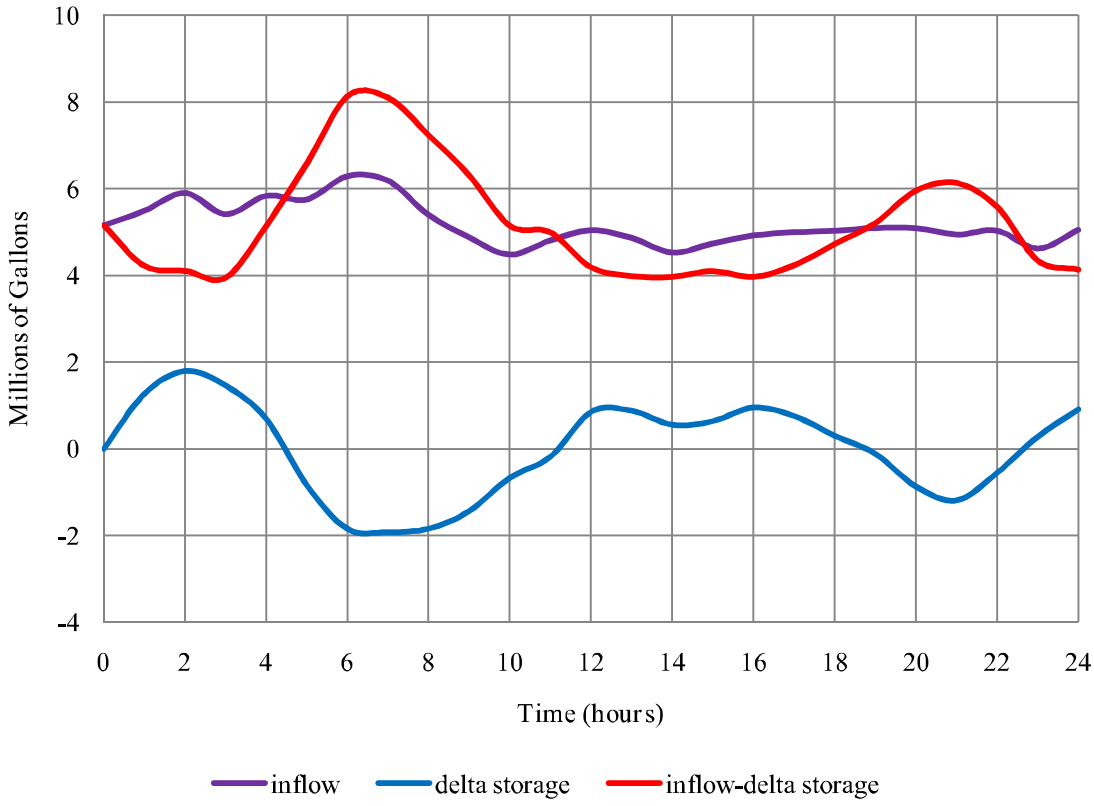

Figure 3.5: August 22, 2007 Water Balance

For calibration, tank and pump operations were entered into EPANET as time-based controls. Demands were adjusted based on the water balance of the system flows on August 22, 2007, which had a total daily demand of 125 MG. As Gwinnett County was predominantly residential, a diurnal residential demand pattern was used for nearly all nodes with time-variable demand. Leakage was not considered. Data for pressure and flow at calibration nodes were used as calibration points. When necessary, flow data were calculated from changes in tank head. Calibration was conducted using EPANET CALIBRATOR, a software extension developed by the RESAN group at the University of Mato Gross do Sul, MS, Brazil (Cheung, 2006). The calibration was conducted via Genetic Algorithm by adjusting the Hazen-Williams roughness coefficients (C values) to match observed flow data.

3.3.4 Logic-Controlled Model Development

The logic-controlled model was developed to create a reactive system with which to test alternative operation scenarios. Controls based on system pressures were assigned to pumps and valves using SCADA data for the modeled day and the guidelines followed by operators. A tabular representation of these guidelines is shown in Table 3.3. In addition to using pressures at key nodes, some flow-based controls were also employed. Time-based controls were used to ensure tanks were filled during the night. Logical controls were created and fine-tuned by trial and error and their success judged quantitatively by minimizing the sum of squared residuals between the tank head and pressures at key nodes of the logical-control model to those of the SCADA data for the modeled day. Logical controls are presented in APPENDIX F. Pressure "transients", or ephemeral spikes in pressure, at control set points led to erratic pump opening and closure that was not representative of actual system operation. To avoid the effects of pressure transients on controls, a one minute hydraulic time step was implemented.

Table 3.3: Tank information and pressure set points used by Gwinnett County system operators (effective date 2/14/2007).

Location	Optimum Pressure (PSI)	Pressure Range (PSI)	Level Range (ft)	Total Volume (MG)	Number of Tanks
Bogan	80-90	70-100	25-45	5	1
Central High Service	50	40-65	NA	NA	NA
Goshen Springs	75-80	60-96	50-110	2	2
Grayson	100-110	95-130	20-46	20	2
Nob Hill	NA	NA	25-30	0.4	1
Lanier Clearwell	NA	NA	12-19	45	5
Lanier Mountain	30-33	20-40	20-35	15	3
Medlock Bridge	90-80	70-113	20-35	2	1
Norcross	90-80	85-110	10-35	5	1
North High Service	90	90-100	NA	NA	NA
Rock Bridge	56-65	55-80	20-37	5	1
Rock Quarry	80	71-89	NA	10	1

3.3.5 Scenario Simulations

The main goal of this project was to create a list of operational scenarios that may be employed by the Gwinnett County utility to reduce water age. To accomplish this task, three types of simulations were run. Base simulations were used to characterize the system as it was operated on August 22, 2007. System characterization simulations were developed and run to quantify the effects of tanks and dead end nodes on the age of delivered water. Operational scenario simulations were run to assess the ability of different management practices to reduce the age of delivered water.

To ensure that steady state water quality was achieved, the Base model was run for 432 hours (18 days) to obtain initial quality for water age, DBP, and Cl^- concentrations. Unless otherwise noted, the values for age, TTHM, HAA5, and Cl^- at

432 hours were the initial conditions used included in the *.msx file and used for each scenario simulation. Model simulations were then run for 120 hours (5 days). All simulations were run with 1-minute hydraulic and water quality time steps with the mixing regime in tanks specified as completely mixed.

An inconsistency was noted between the user's manual and performance of the MSX system when attempting to input the initial quality. In EPANET-MSX "the initial concentration of a bulk species within a pipe is assumed equal to the initial concentration at the downstream node of the pipe" (Shang et al., 2008a). However, including only the initial quality for nodes in the *.msx file caused errors. This issue was overcome once initial quality values for both nodes and pipes were included. Data were reported during the last 24 hours of the 5 day simulation, except for the blow-off scenario where only the first 24 hours of the simulation were considered. Information collected from the EPANET-PT simulations included:

1. Average tank turnover times
2. Tank water levels (collected each 30 minutes)
3. Pressures (for any nodes below 20 PSI)
4. Energy consumed by each pump
5. Daily and annual cost of pump operations

The MSX extension was used to collect data for water age, and TTHM, HAA5, and Cl^- concentrations. A standard Euler integrator was used to solve water quality equations, with the relative and absolute concentration tolerance set to 0.001 and a water quality time step of 1 minute. Data was recorded every 10 minutes. Information

collected for each water quality parameter during the last 24 hours of simulation using the MSX system included:

1. Concentration at each node and tank

2. Average, standard deviation, maximum, and minimum concentrations at each node and tank

3. Cumulative distribution function

Data were compared using the methods described later in this section to quantify the effect of each scenario on water quality in the DWDS.

3.3.6 Base Simulations

The logic-controlled model of GCWDS operations on August 22, 2007 was the 'Base' operational model. Data from the 120 hour simulation of this model were used as the reference point to determine the expected water quality under 'current' operations. This model also served as the quantitative baseline for determining the success of operational scenarios at improving tank turnover times, reducing water age, and improving water quality.

3.3.7 System Characterization

In order to understand the sources of high water age in the DWDS, scenarios where water aging did not occur in system tanks or dead end nodes were compared to the Base scenario. The main system characterization simulations examined are presented in Table 3.4. Unless otherwise noted, these simulations were run using the hydraulics of the Base scenario but with an adapted EPANET MSX text file. An example *.msx file is shown in Figure 3.6. The adapted *.msx file specified that the reaction rates and initial conditions for each water quality parameter in the tank(s) or pipes leading to the dead end nodes were zero. These simulations indicated which of the tanks had the largest effect on

water age and quality, and indicated the maximum water age reductions attainable under the tested hydraulic scenario through improving tank operations.

Table 3.4: System characterization simulations.

Scenario Name	Description
NTA-All	No aging/reaction in all tanks
NTA-LMN	No aging/reaction in all Lanier Mountain tanks
NTA-GRAY	No aging/reaction in all Grayson tanks
NTA-RQ	No aging/reaction in Rock Quarry tank
NTA-NCRS	No aging/reaction in Norcross tank
NTA-MB	No aging/reaction in Medlock Bridge tank
NTA-GS	No aging/reaction in Goshen Springs tank
NTA-BGN	No aging/reaction in Bogan tank
NDEA	No aging/reaction in pipes leading to dead end nodes

```
[TITLE]
  CDF - AGE, TTHM, HAA, Cl

[OPTIONS]
  AREA_UNITS FT2                    ;Surface concentration (mass/FT2)
  RATE_UNITS DAY                    ;Reaction rates (concentration/day)
  SOLVER     EUL                    ;Standard Euler integrator
  TIMESTEP   60                     ;60 sec solution time step
  RTOL       0.001                  ;Relative concentration tolerance
  ATOL       0.001                  ;Absolute concentration tolerance

[SPECIES]
  BULK AGE   MG                     ;Age, where MG = Time
  BULK TTHM  UG                     ;TTHM
  BULK HAA   UG                     ;HAA5
  BULK CL    MG                     ;Chlorine
  BULK B     MG                     ;dummy tracer 1
  BULK C     UG                     ;dummy tracer 2

[COEFFICIENTS]
  CONSTANT  Kp       1              ;Age rxn MG/L/day
  CONSTANT  Kb       0              ;Dummy tracer
  CONSTANT  Kt       0.325          ;TTHM bulk: at 25C
  CONSTANT  TTHMl    58.5           ;TTHM formation potential ug/L
  CONSTANT  Kh       0.143          ;HAA5 bulk: at 25C
  CONSTANT  HAAl     49.3           ;HAA formation potential ug/L
  CONSTANT  Kz       0.1039         ;CL bulk: rate coefficient estimated from curve fitting
  CONSTANT  Cmax     2.0            ;Cmax = source conc of Cl

[PIPES]
  RATE  AGE      Kp*B               ;Age
  RATE  TTHM    -Kt*(TTHM-TTHMl)*C  ;Rate for TTHM formation
  RATE  HAA     -Kh*(HAA-HAAl)*C    ;Rate for HAA formation
  RATE  CL      -Kz*CL              ;Bulk free Cl decay
  RATE  B        Kb*B               ;Zero rate
  RATE  C        Kb*C               ;Zero Rate

[PARAMETERS]
    TANK   3421    Kp    0         ; Grayson 1
    TANK   3421    Kt    0         ; Grayson 1
    TANK   3421    Kh    0         ; Grayson 1
    TANK   3421    Kz    0         ; Grayson 1

    TANK   3422    Kp    0         ; Grayson 2
    TANK   3422    Kt    0         ; Grayson 2
    TANK   3422    Kh    0         ; Grayson 2
    TANK   3422    Kz    0         ; Grayson 2


[SOURCES]
SETPOINT 9     AGE   0.00001
SETPOINT 9     B     1.0
SETPOINT 3429  CL    2.0           ;2.0 mg/L Cl at source
SETPOINT 3429  C     1.0

[QUALITY]
```

Figure 3.6: Sample *.msx file representing no aging or reaction in Grayson tanks without initial quality included.

3.3.8 Operational Scenarios

To address the main project goal of identifying scenarios that could be employed by the GCWDS to reduce water age, eleven operational scenarios were examined. These scenarios are described in Table 3.5.

Table 3.5: Operational scenario simulations.

Scenario Name	Description
PRV-1	Increased central distribution pressures (CDPs) at night, decreased during the day
PRV-2	Increased CDPs during periods on low demand and increased during periods of high demand
30%-All	Decrease in volume of all tanks by 30%
30%-LRG	Decrease in volume of largest tanks (Grayson, Lanier Mountain, and Rock Quarry) by 30%
BO	Blow-off in Southern sector at 100 GPM for 3 hours
FT-LMN	Forced filling/draining of Lanier Mountain tanks
FT-GRAY	Forced filling/draining of Grayson tanks
FT-RQ	Forced filling/draining of Rock Quarry tank
1GRAY-C	One of the two 10 MG Grayson Tanks closed
1LMN-C	One of the two 5 MG Lanier Mountain Tanks closed
MB&GS-C	Medlock Bridge and Goshen Springs Tanks closed

3.3.8.1 Changing Central Distribution Pressures

In the GCWDS, pressurized water enters the system via two transmission mains (Central and North) as shown in Figure 3.4 (page 141). Variable speed pumps (VSPs) are used by the utility to supply this water. In the hydraulic model, these VSPs are represented by constant speed pumps followed by pressure reducing valves (PRVs) on the North and Central transmission mains since EPANET does not currently have the capabilities to model VSPs. The central distribution pressures, the pressures at which water entered the distribution system through the central and north transmission mains, were changed by adjusting the settings of the PRVs in the hydraulic model (whereas in

the actual system this would be accomplished by adjusting the settings of the VSPs). Modifying the central distribution pressures (CDPs) changed the IN portion of the water balance (Figure 3.1, page 123) not by affecting the amount of water entering the distribution system, but by changing the pressure at which it was added. Since operations were dictated by system pressures, these changes provided an operational buffer with regards to the pressure, tanks to drain or fill while respecting system pressure set points. For example, when central distribution pressures were low, storage tanks could be drained to maintain system pressure and when central distribution pressures were high, tanks could be filled faster leading to reduced water age. Two scenarios where the CDPs were changed were assessed for their capability to reduce the age of delivered water.

In the Base model, the North PRV was set to 90 PSI at all times while the Central PRV was maintained at 63 PSI during the day and increased to 70 PSI during the night. In scenario PRV-1, two changes were made: the North PRV was operated in a manner similar to that of the Central valve, with increased pressure at night and decreased during the day, and the pressure settings of the PRV valves were made to be more extreme than those of the Base operational scenario. In the PRV-2 scenario pressure changes were made twice per day to coincide with the peaks in the daily diurnal demand curve (represented by the inflow-delta storage line in Figure 3.5, page 145). In PRV-2, higher pressures were introduced during periods of low demand and lower pressures during periods of high demand. This strategy was designed to encourage faster filling of storage tanks during low-demand periods and to provide more customer demand for water in storage tanks during periods of high demand. PRV settings and the times they were applied are shown in Table 3.6. Graphical representations of the PRV settings for the

Central and North transmission lines are presented in Figure 3.7 and Figure 3.8, respectively.

Table 3.6: Pressure Reducing Valve settings (PSI) for changed central distribution pressures scenarios.

Scenario	Base		PRV-1		PRV-2			
Time	2:00A	10:00A	12:00A	8:00A	3:00A	10:00A	6:00P	10:00P
Central	70	63	80	55	55	80	60	80
North	90	90	100	80	80	100	80	100

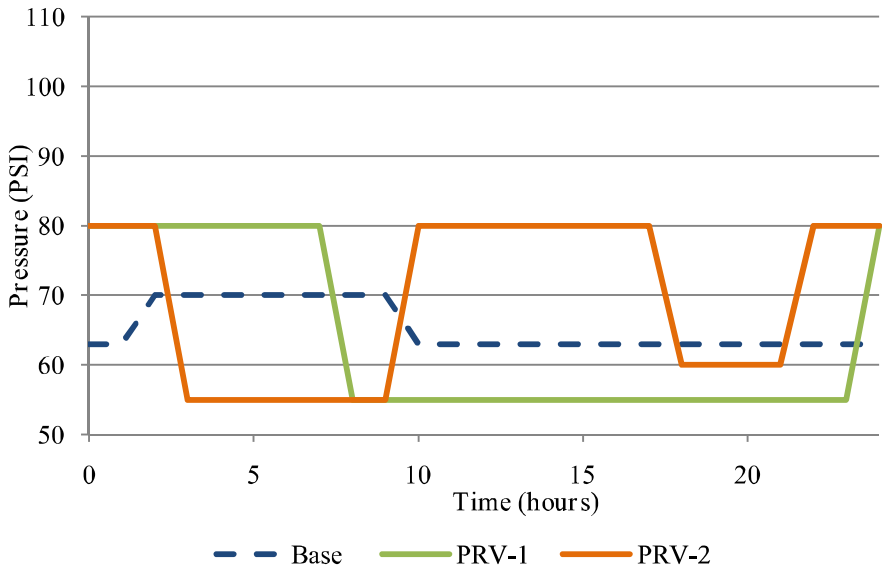

Figure 3.7: Central distribution pressures at Central transmission line.

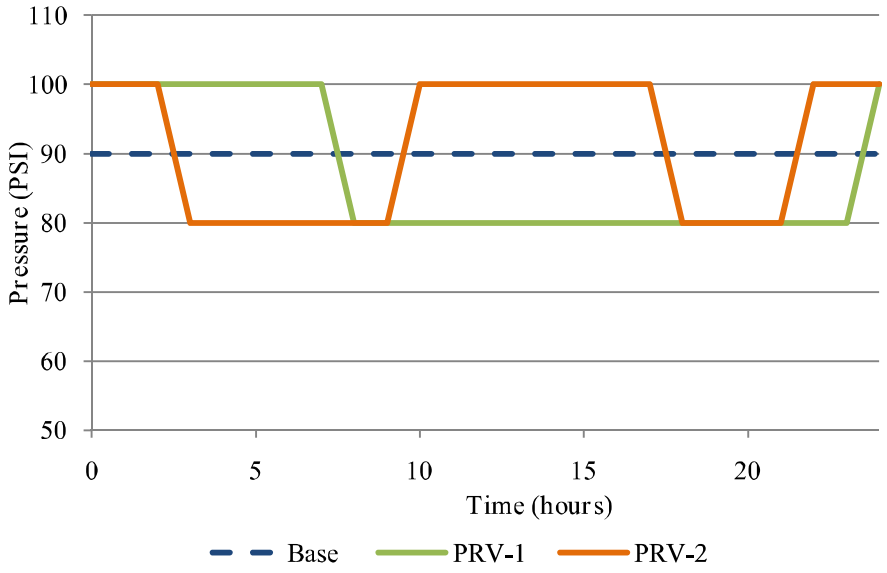

Figure 3.8: Central distribution pressures at North transmission line.

3.3.8.2 Decrease in Volume of All Tanks

Because retention time is directly related to storage volume, reducing the volume of storage with the distribution system can achieve significant reductions in retention time (Brandt, 2007). One of the simplest ways to reduce the operational volume of a tank is to reduce the operational top water level (Brandt, 2007). This approach was applied to decrease the effective volume of each storage tank by 30%, represented by the 30%-All simulation. The maximum water height was reduced for each tank as shown in Table 3.7. In applying the new maximum levels, there were instances where it was also necessary to reduce the initial level of the tank. When the volume reduction scenario maximum tank water level was less than the initial water level, a new initial level was specified. The new initial level was determined by subtracting the difference between the maximum and initial levels in the Base scenario from the new maximum level specified in the reduced volume scenario.

Table 3.7: Tank level settings for reduced volume simulations.

Tank	Base Max Level (ft)	Base Initial Level (ft)	30% -All Initial Level (ft)	30% -All Max Level (ft)
Bogan	34.7	32.0	33.9	33.9
Goshen Springs	120.0	64.6	28.6	84.0
Grayson 1	43.2	35.5	35.0	40.7
Grayson 2	42.0	34.8	31.2	38.4
Nob Hill	37.0	30.1	26.2	33.1
Lanier 1	40.0	34.7	22.7	28.0
Lanier 2	40.0	34.7	22.7	28.0
Lanier 3	40.0	34.7	22.7	28.0
Medlock Bridge	40.0	36.9	24.9	28.0
Norcross	38.0	32.4	21.0	26.6
Rock Bridge	40.0	8.5	0.0	28.0
Rock Quarry	44.0	40.2	27.0	30.8

3.3.8.3 Decrease in Volume of Largest Tanks

The 30%-LRG scenario was run to quantify the effect of only decreasing the effective storage volumes of the three largest system tanks. These tanks/groups of tanks were located at Lanier Mountain, Grayson, and Rock Quarry. The Lanier Mountain site is comprised of three tanks each with a maximum volume of 5 MG. On the base modeled day, the Lanier Mountain tanks provided approximately 1 MG of water or 0.8% of the total demand for the day. In comparison the two 10 MG Grayson tanks provided 6.4 MG or 5% of the daily demand and the 10 MG Rock Quarry tank provided 2.3 MG or 2% of the daily demand.

3.3.8.4 Forced Filling and Draining Of Large Tanks

The ability to fill or drain a tank is based on the interaction of several network parameters, including flow, pressure, and demand. Three scenarios to quantify the effects

of forced tank filling and draining to improve water turnover were examined. In scenario FT-LMN, the Lanier Mountain tanks were drained and filled using time-based controls as presented in Table 3.8. Tank levels could not be used to control the Lanier Mountain tanks because of the high degree of interaction of the individual tanks at this location. The FT-GRAY scenario relied on controls based on the water level in the tanks. In this scenario, the pumps that drain the tanks were programmed to turn on when the water level in both tanks was 42 feet and turn off when the tanks reached a level of 36 feet. The valves that filled the tanks were then opened until the water levels reached 42 feet and the pumps came on, at which time the fill valves were closed. Tank water level was also used to control the pump and valve operation in the FT-RQ scenario. In this scenario the pumps that drain the tank were programmed to turn on when the tank water level reached 44 feet and turn off when the tanks reached a level of 37 feet. The valves that filled the tanks were then opened until the water level reached 44 feet when the pumps came on and the fill valves were closed.

Table 3.8: Controls for forced turnover of Lanier Mountain tanks.

Time (hours)	Tank Status
0	draining
3	filling
8	draining
11	filling
15	draining
18	filling

3.3.8.5 Tank Closures

Closing tanks to eliminate extraneous system storage volume was examined in scenarios 1GRAY-C, 1LMN-C, and MB&GS-C. In the 1GRAY-C scenario, one of the two 10 MG Grayson tanks was ‘closed’ by closing the valves before and after Grayson

tank #1, requiring the total amount of water usually supplied by and stored in this tank to be provided by and stored in the tank that remained open. Similar control was imposed at the Lanier Mountain location in the 1LMN-C scenario. In this scenario, Lanier Mountain tank #1 was 'closed'. In the MB&GS-C scenario, both the Medlock Bridge and Goshen Springs tanks (2 MG each) were closed. This scenario was motivated by changes to the network planned by the utility (Toader, 2009).

3.3.8.6 Blow-off

Several variables can be varied within a blow-off scenario, including the location, flow rate/velocity, length of flushing time, and the time of day the flushing occurs. Therefore, the combination of variables creates a large set of potential simulations for each blow-off location considered. Preliminary examination of the system water age at 23 days of simulation showed several potential locations for blow-off testing. However, tank trace examination using the EPANET-GUI showed that these areas also received a significant amount of water from nearby storage tanks. Rather than focusing on the optimization of several blow-off scenarios, effort was placed on improving the age of the water leaving the tanks.

To quantify the potential improvement a blow-off of high water age could provide, a blow-off scenario (BO) was examined. Due to the temporary effect of blow-offs, only the first 24 hours of the BO simulation were examined as opposed to the 5 day simulations examined for other operational scenarios. In this scenario, an additional demand of 100 GPM was placed at node 726, a dead end in the vicinity of the Lanier Mountain tanks where average water age was noted be particularly high in the Base simulation. The 100 GPM demand was applied from clock time 12 hours to 15 hours on

the first day of the 5 day simulation. This resulted in flushing 18,000 gallons over 3 hours, which would fill two large tanker trucks and could then be used for irrigation or grey water purposes.

3.3.9 Methods for Scenario Comparison

3.3.9.1 Hydraulic Requirements

The alternative operational scenarios aimed to maintain pressure set-points as closely as possible while ensuring system pressures remained higher than 20 PSI (the minimum suggested for fire flow). In order to assess the ability of each scenario to maintain the required pressure throughout the simulation while avoiding the generation of massive data output files, pressure information was collected for a node only when it experienced pressure lower than 20 PSI. Nodes connected to pumps where pressures could be negative or lower than 20 PSI due to the opening or closing of pumps or valves were not considered. These 339 nodes were removed from the pressure data using a post-data processing procedure run in MATLAB® (R2007b, The MathWorks, Natick, MA).

EPANET 2 reports information each time there is a change in pressure at a node rather than at specified time intervals. Therefore, in order to further reduce the amount of pressure data reported to a manageable set, a second post-processing step was run in MATLAB, with subsequent data analysis completed in Microsoft Excel. In the second post-processing procedure, the pressure data was analyzed to determine the time and duration of each low pressure event. Low pressure events less than 5 minutes in length were removed and data was examined using histograms that showed the duration and clock time of the low pressure events.

3.3.9.2 Tank Turnover Calculation

The water quality definition of tank turnover used in this study is defined as the time it takes to replace 90% of the water in the storage tank with dilution effects considered. To determine turnover rate, water in the tank was treated as if initially there is a tracer present in the tank at a given concentration, c_0, and the time required to reduce its value to a reference level is calculated. This time is the "water quality turnover time". The general mass conservation equation of a tracer in a completely mixed tank is:

$$\frac{dc(t)}{dt} = \frac{q_{in}}{V(t)}(c_{in}(t) - c(t)) \tag{3.4}$$

where c(t) is the concentration in the tank, $c_{in}(t)$ is the concentration of the tracer entering the tank, q_{in} is the flow of water entering the tank, and V(t) is the total volume of water in the tank. If it is assumed that $c_{in}=0$, then the turnover time is the time T when

$$\frac{c(T)}{c_0} = \exp(-\int_0^T \frac{q_{in}}{V} dt) = r \tag{3.5}$$

where r is the required turnover. In this study, when using this water quality definition, a tank is considered 'turned over' at the time where r =0.1 (when the initial concentration of the tracer has been reduced by 90%). The average turnover time was calculated for each tank based on the data collected in the 5th day of the 5 day simulation, (except for the BO scenario). When a tank had a turnover time greater than 1 day, data from the 5th day of simulation was repeated until T was achieved.

3.3.9.3 Quantitative Scenario Comparison

To compare the overall impact of each scenario on water age, the spatial/temporal distribution of delivered water volume as function of water age for each scenario was

studied. Several metrics were used to compare simulation scenarios, many of them determined from the empirical cumulative distribution function (CDF) of the age of delivered water. To limit the effects of initial conditions, the CDF of the age of delivered water was calculated during the last 24 hours of each simulation. The age of delivered water CDF presents the percentage of delivered water on the Y axis with an age lower than the corresponding values on the X axis, as shown in Figure 3.9. The ideal delivered water age CDF of could be represented by a vertical line, which would suggest all the delivered water has the same age. However, due to the system size and layout this is not generally possible and the CDF of the Base scenario shows that there are significant percentages of delivered water with ages that are less than and much greater than this value. Comparing the CDF curves of different scenarios, the effect of different operational scenarios on water age could be interpreted and multiple scenarios compared simultaneously.

The CDF analysis approach is explained using Figure 3.9 and Table 3.9 as examples. Figure 3.9 shows the results of the Base model with logic-based controls compared to vertical line meant to represent the idealized scenario where every consumer receives water with an age equal to the median age. This graph shows the percent of delivered water (on the Y axis) with an age equal to or less than a specified water age value (on the X axis). Table 3.9 compares the values of the CDFs in Figure 3.9 at different points along the curves. The median water age is located at the point where the Base curve crosses 50% on the Y-axis. For the Base scenario the median age of delivered water was equal to 1.1 days. Examination of the median age is useful, but it does not account for the deviations from the median value and the 'tails' of the curve,

which represent the delivered water with the highest and lowest age. The tail at the top of the graph, which represents the highest age, is of the most concern. A successful scenario should reduce the length of this tail, indicating the customers receiving the highest age water get water of a lower age under the new scenario than they would under the Base scenario. This could also be judged by examination of the maximum age of delivered water, which occurs at the 100% point of the cumulative distribution, as well as other points (75, 90, and 95% of water delivered) along the top tail.

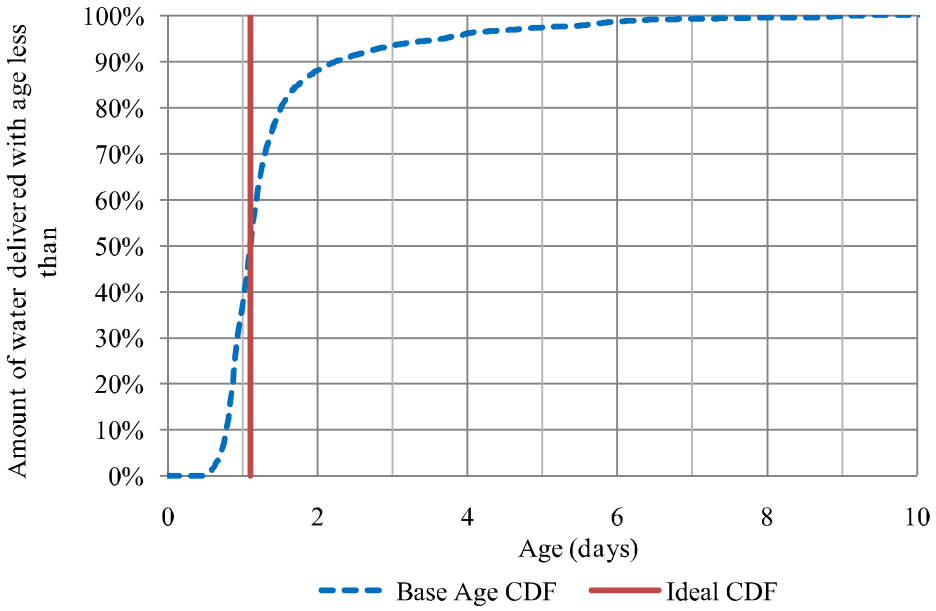

Figure 3.9: Cumulative distribution of the age of delivered water for the Base model.

Table 3.9: Comparison of ages at different points of the Base scenario and ideal cumulative distribution function curves.

	Base CDF	Ideal CDF	difference
5%	0.69	1.10	-0.41
50%	1.08	1.10	-0.02
90%	2.22	1.10	1.12
95%	3.66	1.10	2.56
100%	9.15	1.10	8.05
95%-5%	2.97	0.00	2.97

Several manipulations of the CDF curve were used for scenario assessment. By subtracting the age of the bottom 5% of the water from the age of 95% of delivered water, the variability of 90% of the delivered water age was calculated. A narrower range of water ages ensures the quality of delivered water is less variable, as illustrated in Table 3.9. Additionally, the difference in average water age for the final 24 hours of simulation was viewed in the EPANET GUI by entering this value in the [QUALITY] section of the *.inp file. This allowed for a review of the spatial effect of operational changes on the average water age.

3.3.10 Water Quality Modeling

The EPANET MSX extension was used to simultaneously model water age and Cl^-, TTHM and HAA5 concentrations throughout the system using previously determined kinetics for the Gwinnett County system. DBP formation rates were determined from batch kinetic studies by Kim and coworkers (2006) to fit the model:

$$C_{DBP} = C_{DBP,L}-(C_{DBP,L}-C_{DBP,O})*\exp(-kt) \quad (3.6)$$

Where C_{DBP} is the DBP concentration at time t, $C_{DBP,L}$ is the DBP formation potential (= the concentration after 7 day batch reaction), $C_{DBP,O}$ is the initial DBP concentration, k is the first-order rate constant, and t is time (Rossman, 2000). Chlorine decay was calculated by curve fitting to a first-order equation. Rates determined by Bundy and Kim and coworkers are presented in Table 3.1 (page 134). It is important to note that the formation potential values for TTHMs and HAAs were not contingent on chlorine concentrations and were less than the MCLs of these chemicals required by the USEPA. By employing the rate data of Kim and coworkers, TTHM concentrations predicted by

the model could reach a maximum concentration of 58.5 μg/L, while the MCL for TTHMs is 80 μg/L (2006). Similarly, in the model HAAs were limited to a maximum concentration of 49.3 μg/L while they have a MCL of 60 μg/L (USEPA, 2006). The maximum TTHM concentration attainable through the kinetics applied to the model (58.5 μg/L) was lower than the maximum observed in field measurements conducted by the utility (75.2 μg/L). Conversely, the maximum obtainable HAA concentration according to applied kinetics was higher than observed during the field measurements (49.3 μg/L and 41.9 μg/L, respectively).

Analysis of the DBP and chlorine concentrations focused on IDSE sampling locations. These twelve locations were determined by the utility as the places with the poorest water quality. Half of the exact locations indicated by the utility were not available on the skeletonized model due to removal of the small pipes where these sampling points were located. In these cases, the closest available node on the skeletonized model was designated to represent that site. Eleven nodes were determined to coincide with the twelve IDSE sampling locations.

3.3.11 Energy Consumption Analysis

EPANET 2.0 was used to compute pumping energy and cost provided for each simulation by providing data available on pump efficiency and energy cost. Energy use information was then associated with proposed operational scenarios and used to determine the feasibility of implementing each scenario. This information along with water age results provided a simple cost/benefit analysis to determine the most practical scenarios for the utility to implement.

Average pump efficiencies and energy cost information was obtained from Derceto (Toader, 2009) and included in each scenario. When no pump information was available, an average efficiency of 75% was applied. When necessary, cost was calculated from energy bills based on the kilowatt hours (kWh) used and total cost. Approximately eight months of cost per kWh were calculated and an average was determined. Table 3.10 presents the efficiency and cost information for each pump station considered in the cost calculation. The pumps at the North and Central High Service locations (which maintain the central distribution pressures) and the Grayson tanks were subject to day ahead (DA) energy tariffs that in changed hourly, as shown in Figure 3.10.

Table 3.10: Average Efficiency and Cost for each pump location considered. DA = day ahead pricing shown in Figure 3.10.

Pump Location	Average% Efficiency	Average Cost ($/kWh)
Bogan	75	0.065
Central High Service	77	DA
Goshen Springs	75	0.124
Grayson	39	DA
Nob Hill	75	0.107
Lanier Mountain	41	0.099
Medlock Bridge	75	0.127
Norcross	64	0.088
North High Service	77	DA
Rock Bridge	37	0.096
Rock Quarry	40	0.138

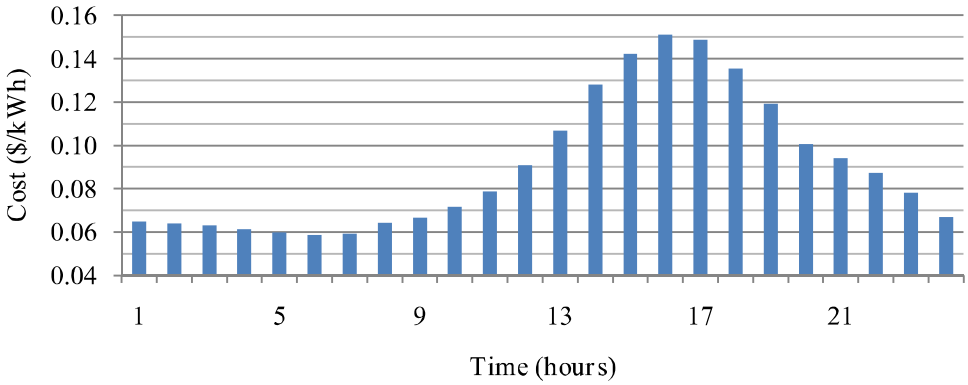

Figure 3.10. Day ahead pricing used for high service and Grayson pumps.

3.4 Results

3.4.1 Model Calibration

Calibration was completed using the EPANET CALIBRATOR (Cheung, 2006). Calibration improved the capability of the model to replicate tank levels but slightly reduced the capability of the model to reproduce the pressures observed at the calibration nodes. The residual sum of squares (RSS) for tank levels was 270 for the calibrated model and 432 for the uncalibrated model, indicating the output of the calibrated model matched the observed SCADA data more closely than the uncalibrated. However, the uncalibrated model to reproduced the pressures observed in the SCADA data more accurately than the calibrated model (RSS = 3413 and 3776, respectively).

3.4.2 Logic-Driven Controls

Logic-driven model controls for the Base scenario model are presented in APPENDIX F. The calibrated time-controlled model was adjusted to better match tank heads and central distribution pressures, and it was used along with the SCADA data to determine the success of the logic-controlled model to reproduce conditions observed on the modeled day. RSS comparison showed the logic-controlled model was able to match

the SCADA tank level data as well as the time-driven controls (RSS = 77.1 and 77.7, respectively), while logical controls were less successful at reproducing system pressures than the time-controlled model (RSS =5997.7 and 5280.3, respectively). Graphs comparing tank water level and pressures at key nodes for the time-based model, logic-based model, and SCADA data are located in APPENDIX I.

The benefit of the logic-based model was its ability to react to changes in system operation. This allowed for changes in operations to be simulated while pressure set points were maintained. The majority of scenarios did not have drastic effects on system pressure, and the timing of tank filling and draining tanks was rarely changed. Logic-based controls used for the Rock Quarry tank were based on flows that did not vary at all when operations were changed and were functioned identically to time-based controls (see APPENDIX J). Changes in tank operations observed under alternative operation scenarios were often due to the rate of filling or draining of tanks rather than modified filling and draining times.

These findings supported the need of a well-constructed logic-based control system to allow for the 'response' of system features to operational changes. When implementing a logically-controlled system, the focus should be placed on maintaining system pressures rather than reproducing water levels in tanks. In this regard, a modeler should strive for a model that represents a general condition, not a particular 24-hour period.

3.4.3 Base Simulation

Simple age calculations based on system volume and demand, and average velocity and furthest distance from the treatment plant were used to collect general

information about the system water age. By calculating system retention time from the total system volume in the skeletonized model (120 MG) and base demand (125 MG), an average water age of 0.96 days was determined. Based on the average velocity of 0.61 mph (or 0.89 ft/s) and a straight-line distance of 27 miles, the water age at the furthest node from the point of distribution (i.e., the Lanier Filter Plant) would be 1.85 days. Results below suggested the average retention time determined from system volume and demand was very similar to modeling results; however, the average water age at the point furthest from the treatment plant had a water age of 2.9 days. This discrepancy could be attributed to the effects of storage tanks, the tortuosity of flow, and variations in velocity throughout the DWDS.

Results of the 5-day simulation of the Base model scenario provided a baseline to which other model scenarios could be compared. Figure 3.11 presents the average water age observed at each node during the final day of this simulation. Areas on the edges of the network and furthest from the Lanier Filter Plant (located at the Northern tip of the network) tended to have the highest water age. These results agreed with previous water age modeling efforts of the GCWDS (Kim et al., 2006).

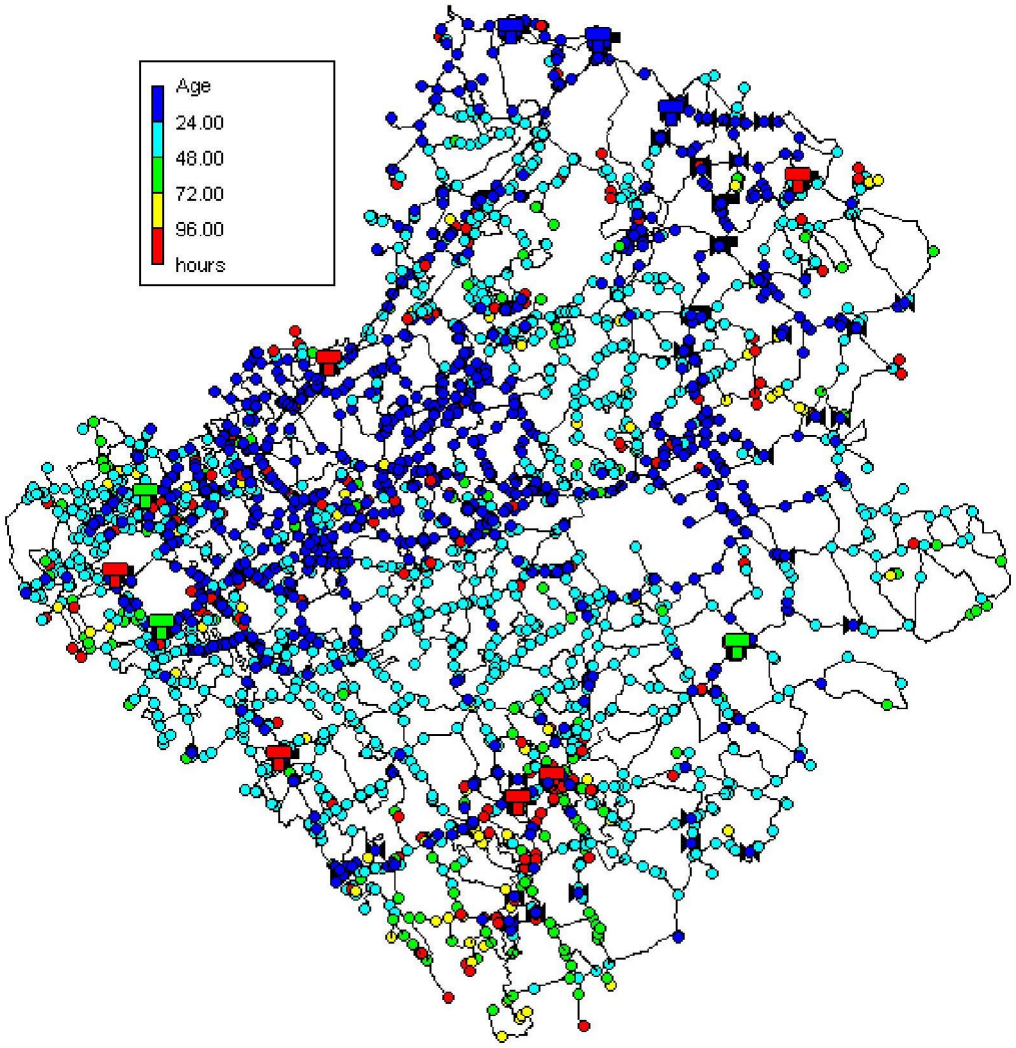

Figure 3.11: Average water age after 23 days of simulation.

The Base model simulation also supplied the cumulative distribution functions and tank turnover times used to assess the effect of system characterization and operational scenario simulations on delivered water age. Table 3.11 presents the water ages observed in the Base scenario at points along the CDF curve. The median age of delivered water in the Base scenario was 1.1 days and the maximum age was 9.2 days. The median water age was only 3 hours more than the average retention time calculated from the skeletonized model system volume and base demand. The CDF of this scenario had a long tail at the top of (noted in the large difference in water age at the 95% and

100% points). Ninety percent of demand was supplied by water with an age less than or equal to 2.2 days and five percent of the demand was supplied with water with an age greater than 3.7 days.

Table 3.11: Water age at specified points on the Base scenario cumulative distribution function curve.

Demand Delivered	Age (hours)
0%	0.5
5%	0.7
10%	0.8
25%	0.9
50%	1.1
75%	1.4
90%	2.2
95%	3.7
100%	9.2

Table 3.12 presents the hydraulic and water quality turnover times as well as the average age observed (during the final 24 hours of simulation) for each storage tank in the Base network model. The hydraulic turnover times represented the amount of time needed to replace all the water in the tank and were calculated using equation 3.2. The water quality turnover times were determined using equation 3.5 and represented how much time was required to replace 90% of the water in the tank considering dilution effects. These results confirmed the water quality definition of tank turnover provided a more conservative estimate of this metric as compared to the standard hydraulic definition. The average water age is the average age over the last 24 hours of simulation of water in each tank. Average water age results showed that there was a large disparity in age occurred between the two Grayson tanks. Grayson tank 1 had an average age that

was more than two days older than tank 2. Closer examination suggested this occurred because of a pipe layout that led to water sloshing, and the recirculation of stored water only affected tank 1. A similar situation occurred at the Lanier Mountain tanks. It was not known if this was an artifact of the hydraulic model or was actually occurring in the distribution system.

The choice of mixing regime in the storage tanks may influence system water age. In this study water in a tank was assumed to be completely and instantaneously mixed. In most storage tanks this ideal situation is not achieved and tank mixing may be short circuited, which may lead to serious differences in delivered water age. For example, if tanks were not completely mixed but instead were subjected to a LIFO (Last-In, First-Out) regime, the age of delivered water may be lower than observed when complete mixing is assumed; however, the average age of water in tanks could be much higher. Conversely, if the FIFO (First-In, First-Out or plug-flow) regime was assumed, the age of delivered water may be higher, but the average age of water in the tanks could be lower than that of the completely mixed tanks. This topic is discussed further in APPENDIX K.

Table 3.12: Average water quality and hydraulic tank turnover times and average water age observed in the Base model.

Tank	Water Quality Turnover (days)	Hydraulic Turnover (days)	Average Age (days)
Bogan	1.0	0.4	1.0
Goshen Springs	2.7	1.2	2.2
Grayson 1	3.5	1.3	5.1
Grayson 2	3.8	1.5	2.9
Nob Hill	2.8	1.1	6.5
Lanier Mountain 1	24.5	9.3	14.4
Lanier Mountain 2	18.4	6.8	11.1
Lanier Mountain 3	27.6	10.4	14.7
Medlock Bridge	3.8	1.4	2.7
Norcross	5.7	2.3	4.2
Rock Bridge	365.0	319.4	26.7
Rock Quarry	8.5	3.2	5.3

Although efforts were made to avoid them, transient pressures below 20 PSI occurred sporadically throughout the system. Investigation into the cause suggested momentary shut-offs of the high service pumps (HSPs) that supplied the North transmission main were the source of the majority of low pressure events. These momentary lapses in pressure may have been due to local flow instabilities caused the way variable speed pumps (VSPs) were handled in the model (see APPENDIX L for a full discussion). Figure 3.12 presents the number of low pressure events that occurred during each hour interval of the final 24 hours of the Base simulation along with the observed pressures at the central transmission mains. The majority of low pressures occurred in conjunction with $\leq$ 5 min shut-offs of HSPs supplying the north part of the system. Twenty-five nodes (0.7% of the total system) had pressures below 20 PSI around 7 am (103 hours) in the Base model that did not correspond to HSP shut-off. These

nodes were spread throughout system and did not appear to be caused by any particular distribution system feature. Transient low pressures are a 'natural' occurrence in distribution system and typical in hydraulic modeling because of approximations and computational instabilities. As such, low pressures observed here were not considered serious defects of the logic-controlled model.

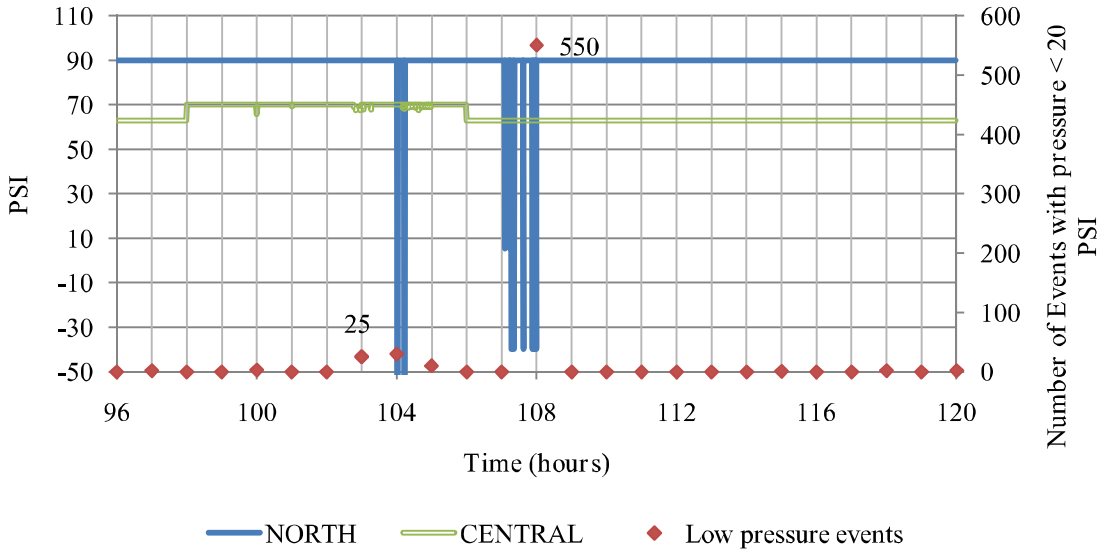

Figure 3.12: Central pressures and number of pressure events below 20 PSI during the last 24 hours of the Base simulation.

3.4.4 System Characterization

By examining the difference between the CDFs of the Base and No Tank Aging/No Dead End Aging (NTA/NDEA) scenarios, the quantitative effects of tanks or pipes leading to dead ends on the age of delivered water (based on August 22, 2007 operations) were determined. A summary of age results for these scenarios are presented in Table 3.13. No differences between the Base and NTA-All scenarios were noted below the ~90% of demand delivered point and that tanks contributed to increasing the maximum age of delivered water by approximately 50 hours. The majority of this

increase was due to the Lanier Mountain tanks, which accounted for 44 of the 50 hour increase in maximum delivered water age.

Table 3.13: Water age at specified points on the cumulative distribution function curves of the Base and system characterization simulations. Cells shaded green highlight where age was reduced.

Scenario	Age (hours) at % of demand delivered		
	90%	95%	100%
Base	53.3	87.8	219.6
NDEA	52.6	87.8	217.4
NTA-All	49.7	72	169.2
NTA-GS	52.6	87.8	219.6
NTA-MB	52.6	87.8	219.6
NTA-NRCS	52.6	85.6	218.9
NTA-BGN	53.3	87.8	219.6
NTA-RQ	52.6	80.6	219.6
NTA-LNMTN	51.1	74.8	175.7
NTA-GRAY	52.6	87.8	218.9

Figure 3.13 presents the top tail of the CDF curves of the Base, NTA-All and NTA-LNMTN scenarios. Comparison of the NTA-All and Base scenario CDF curves indicated 12% of the delivered water with the highest age had lower age in the NTA-All scenario. The percentage of demand provided by tanks on August 22, 2007 was 10.2%, which was close to the 12% of the demand shown to have water age affected by tanks. This result had two implications. First, it suggested the size and layout of the pipe network accounted for 88% of the age of delivered water. Second, by improving the management tanks, the quality of the oldest 12% water received by the customers consuming the water with the highest age could be improved. This proportion differed

from the system volume contained in storage tanks and the pipe network where tanks accounted for 33% and pipes 67% of the system volume.

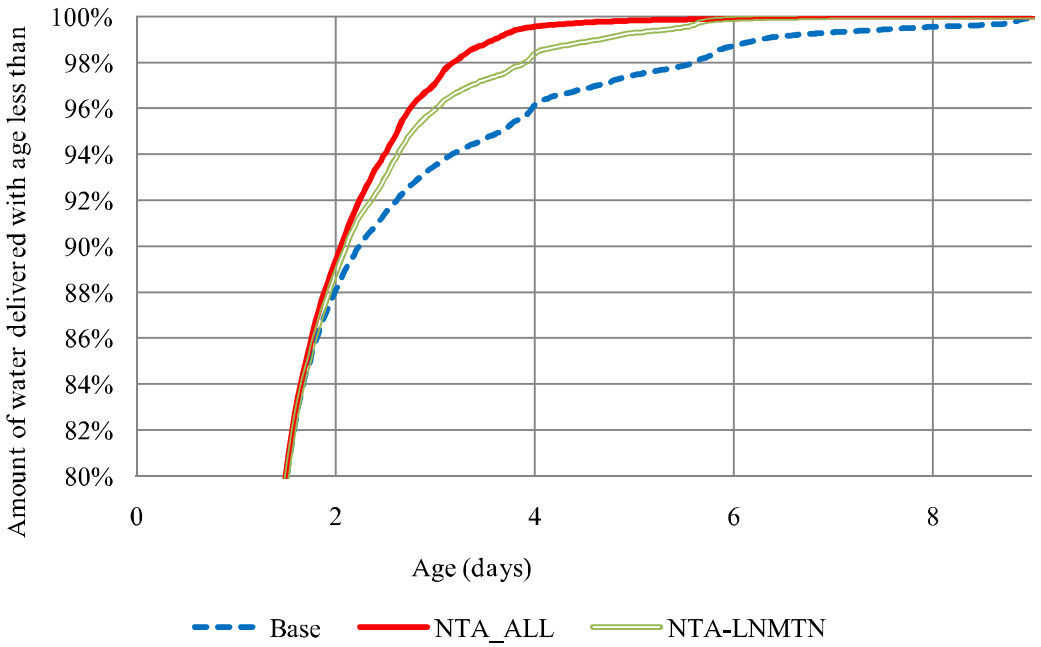

Figure 3.13: Cumulative distribution function curves for Base, NTA-All, and NTA-LNMTN simulations.

A map of the difference in average water age of the last 24 hours of simulation between the Base and NTA-All scenarios is presented in Figure 3.14, and indicates where the tanks had the highest impact on water age in the Base scenario. The three circled areas were affected the most by tanks, with the greatest effect noted in the southern portion of the network. The Lanier Mountain tanks were responsible for increasing the age in the southern section of the network, while the Rock Quarry tank affected the northeastern region and the Norcross, Medlock Bridge and Goshen Springs tank the circled region in the west. These areas corresponded to the areas with the highest ages in the system in the Base scenario (Figure 3.11, page 169). Further investigation showed that even nodes that were under the highest influence of tanks only owed a maximum of

~50% of their average water age to water from tanks. This suggested in the area south of the Lanier Mountain tanks, which received old water due to distribution as well as the influence of storage, the elevated water age was due more to distribution than to storage.

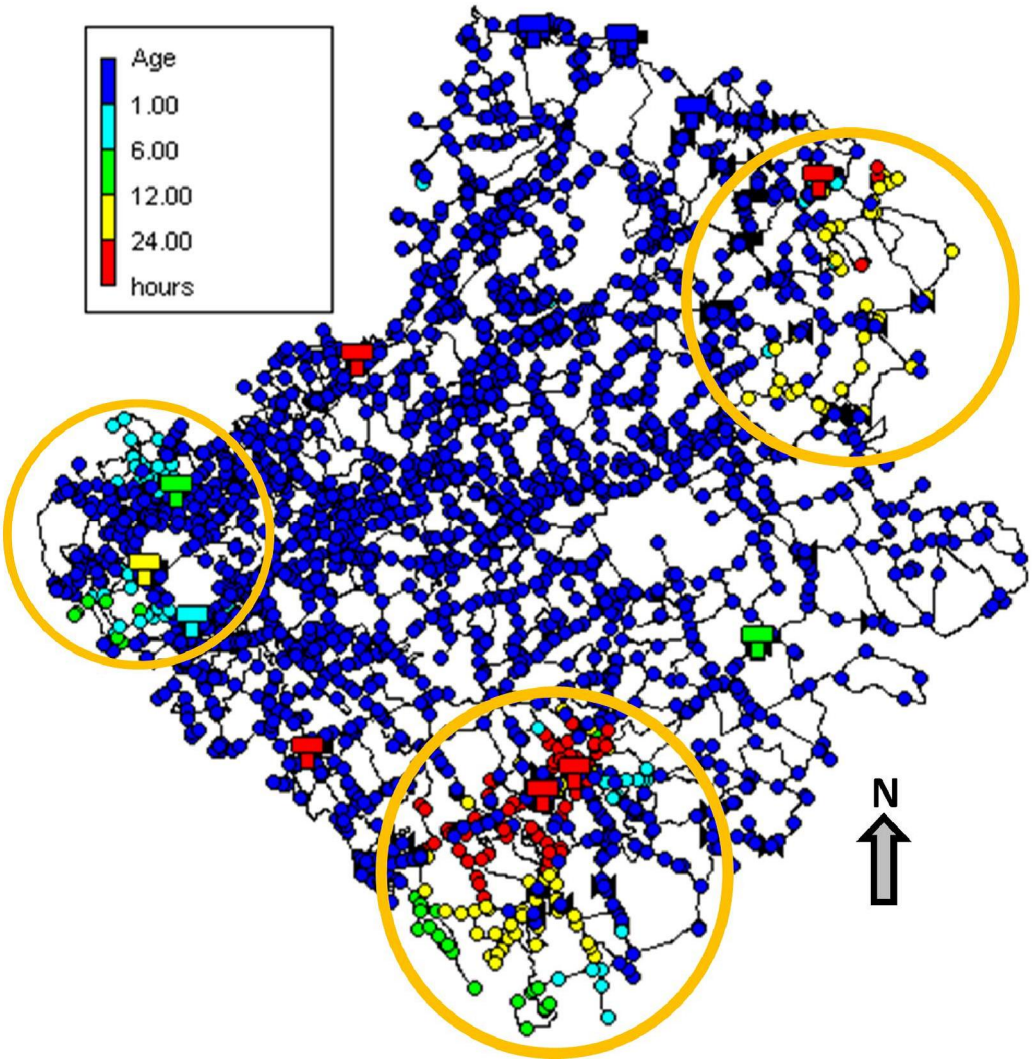

Figure 3.14: Difference in age between Base scenario and NTA-All.

The Lanier Mountain tanks did not provide a large amount of the system demand on the modeled day (0.8%). As consequence, these tanks increased water age in the south-central part of the DWDS by 6 to 24 hours. Part of the negative effect of the Lanier Mountain tanks on water age may have been due to its influence on the Nob Hill

tank. The Nob Hill tank is small, but some of the water leaving the Lanier Mountain tanks was subjected to a second period of storage in it, further increasing water age due to storage in this sector. The Rock Quarry tank did not change the maximum age however approximately 8% of the delivered water was affected by storage in this tank.

Results of the NDEA scenario indicated dead end nodes did not significantly affect the CDF curve and reduced the maximum age of delivered water by only 2.2 hours. This suggested dead end nodes had a less important impact on the age than did the tanks. Demand at dead ends constituted 31% of the total daily volume; however, many of these nodes had very high base demand and were only dead ends due to model skeletonization (Gianella, 2010). The effect of dead end nodes was noted mainly in the southern tip of the distribution system, the same area affected by the Lanier Mountain tanks and the region with the highest water age in general. The effect of increased aging in low-demand dead end nodes increased average water ages near the Lanier Mountain tank by only 30 minutes to 1 hour.

Overall, system characterization results indicated that under operations of the base simulated day, the physical layout of the distribution system had the biggest effect on the age of delivered water, followed by system tanks. System storage plays a much larger role in increasing the age of delivered water than the effect of dead end nodes. This could have been because the majority of dead ends were due to model skeletonization and therefore had high demand. Of the tanks, the Lanier Mountain location had the highest impact on delivered water age, which coincided with the area where ages were noted to be the highest in the Base scenario.

3.4.5 Operational Scenarios

Scenario simulations were run to accomplish two goals: 1) determine which operational scenarios the utility might implement to improve the quality of delivered water and 2) address the hypothesis that reducing tank turnover time improves the age of delivered water. A summary of the effect of all scenarios on water age is presented first, followed by an examination of the results of scenarios found to be most effective at reducing the age of delivered water. Scenarios are discussed based on their effect on water age and system hydraulics. Results of the examination of the relationship between tank turnover times and the age of delivered water are then presented.

All metrics used in the following sections are based on the final 24 hours of a 5 day simulation, except in the Blow-Off scenario in which the first 24 hours of the simulation were examined. Metrics used were based on the CDF curve, node statistics, and tank turnover times. Scenarios were compared primarily by their effect on the top tail (the portion above the 50% point) of the CDF curves with an emphasis on the maximum age of delivered water. Analysis focused on the top portion of the curve as it represented the delivered water with the highest age and little to no change in water age was observed below the median. Average water age, DBP, and free chlorine concentrations were used to compare spatial effects of operational scenarios. Average tank turnover times were calculated based on the water quality definition.

Table 3.14 presents the water ages observed at selected points on the CDF curves of the Base and operational scenarios. Cells shaded red contain observations with a higher age than the Base scenario while those shaded green highlight observations with an age lower than the Base scenario. The alternative operational scenarios delivered water ages that were generally no more than 2 hours different from the Base CDF below the 90% point, implying that operational scenarios examined only changed the age of ~ 10% of consumed water.

Table 3.14: Summary of water age at specified points of the cumulative distribution function curves for the Base and operational scenarios (hours).

Scenario	0%	5%	10%	25%	50%	75%	90%	95%	100%
Base	10.8	16.6	18.7	20.9	25.9	33.1	53.3	87.8	219.6
1GRAY-C	11.5	17.3	19.4	22.3	27.4	33.8	52.6	80.6	184.3
PRV-2	10.8	17.3	18.7	21.6	26.6	34.6	63.4	91.4	207.4
30R-BIG	9.4	15.8	18.0	20.9	25.9	33.1	49.7	69.8	211.7
30R-ALL	10.8	17.3	18.7	21.6	26.6	33.1	46.1	65.5	213.1
PRV-1	9.4	15.8	17.3	20.2	25.2	31.7	45.4	77.8	213.8
1LMN-C	10.1	16.6	18.0	20.9	25.9	33.1	52.6	85.0	217.4
FT-RQ	10.8	17.3	18.7	22.3	27.4	34.6	55.4	82.8	218.9
MB&GS-C	9.4	15.8	18.0	20.2	25.2	31.7	49.7	77.0	218.9
FT-LMN	10.8	16.6	18.0	20.9	25.9	33.1	52.6	89.3	251.3
FT-GRAY	10.1	15.8	18.0	20.2	25.9	33.1	53.3	90.0	311.0

Eight of the operational scenarios examined reduced the maximum age of delivered water and two caused an increase. The 1GRAY-C scenario decreased the maximum water age by more than 24 hours. PRV-2 showed the next best decrease in maximum age (12 hours), but it also increased the water age of 70% of the water delivered. The scenarios where the largest tanks were forced to fill and drain (FT-RQ, FT-LMN, and FT-GRAY) did not appear to improve the delivered water age. The FT-

RQ scenario resulted in a maximum water age reduction of less than 1 hour while the FT-LMN and FT-GRAY scenarios led to increases in the maximum age of delivered water.

By subtracting the points of the CDF curve that represent the water age where 5% of the water is delivered from the age where 95% of the water is delivered, the age range of 90% of the delivered water was determined. This metric focused on the 'center' of the CDF curve rather than the top tail and indicated the variability of the age of delivered water. Table 3.15 shows the 90% range of delivered water age for each scenario. In seven scenarios this value was reduced as compared to the Base scenario, suggesting a lower and more consistent delivered water age.

Table 3.15: Water age variability for each scenario (measured by the 90% range of delivered water age)

Scenario	95% -5%
Base	71.2
30R-ALL	48.2
30R-BIG	54
MB&GS-C	61.2
PRV-1	62
1GRAY-C	63.3
FT-RQ	65.5
1LMN-C	68.4
FT-LMN	72.7
PRV-2	74.1
FT-GRAY	74.2

Five of the scenarios examined reduced the variability in delivered water age by more than 8 hours. These were:

- 1 Grayson tank closed
- Medlock Bridge and Goshen Springs tanks closed

- Volume of large tanks reduced by 30%
- Volume of all tanks reduced by 30%
- Changing central pressures once per day (PRV-1)

Results of each of these scenarios, which were considered the best operational strategies of those examined, are critically presented in the following sections.

3.4.5.1 Tank Closures – 1 Grayson and Medlock Bridge/Goshen Springs

Tank closure scenarios were run with the intention that, by reducing the volume of stored water at the Grayson, Lanier Mountain, or Medlock Bridge/Goshen Springs locations, the tanks that were left open would be used more and their turnover times reduced. Of these three scenarios, closure of one Grayson tank (1GRAY-C) and closure of both the Medlock Bridge/Goshen Springs tanks (MB&GS-C) showed the most promise to reduce the maximum water age and the age variability of delivered water. Closure of one of the Grayson tanks reduced the total system storage by 10 MG (16%), while closure of the Medlock Bridge/Goshen Springs tanks reduced system storage by 4 MG (6%).

One Grayson Tank Closed

The 1GRAY-C scenario increased the median age by 1.5 hours but reduced the maximum age of delivered water by 35 hours. Figure 3.15 shows the CDF of the Base and 1GRAY-C scenarios. This figure illustrates the top portion of the CDF curve was consistently shifted to the left by closing one of the Grayson tanks. This shift reduced the age of 8% of the water with the highest age by 3 hours or more as compared to the Base scenario.

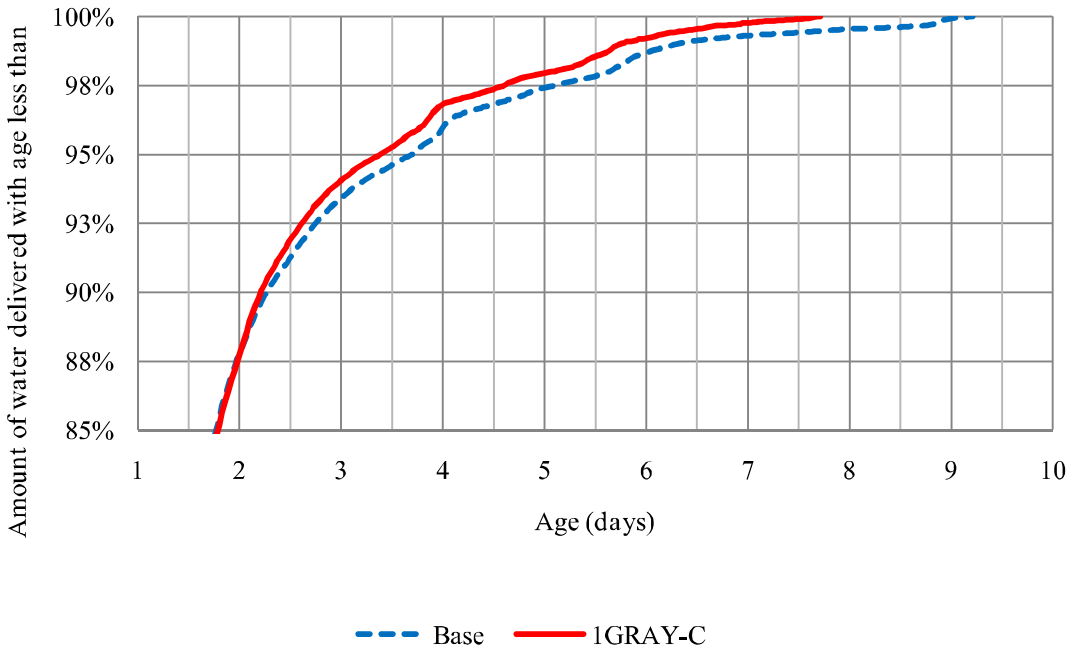

Figure 3.15: Cumulative distribution function of 1GRAY-C and Base scenarios.

The main advantage of the 1GRAY-C scenario was the turnover time of the other Grayson tank that was left open improved. A comparison of turnover times observed in the Base and 1GRAY-C scenarios is presented in Table 3.16 and shows the turnover time of Grayson tank 2 was reduced by 1.2 days by closing Grayson tank 1. Grayson tank 2 had a much higher level variation in the 1GRAY-C scenario than was noted in any other operational scenario, leading to the reduction in turnover time. Closing one Grayson tank did not appear to affect the turnover times of the smaller system tanks (Medlock Bridge, Goshen Springs, Norcross), but did lead to increases in the turnover times and reduced use of the Lanier Mountain tanks

Table 3.16: Turnover times of 1GRAY-C and Base scenario.

Tank	Base (days)	1GRAY-C (days)
Bogan	1.0	1.0
Goshen Springs	2.7	2.5
Grayson 1	3.5	CLOSED
Grayson 2	3.8	2.6
Lanier Mountain 1	24.5	31.4
Lanier Mountain 2	18.4	19.6
Lanier Mountain 3	27.6	33.3
Medlock Bridge	3.8	3.6
Nob Hill	2.8	2.7
Norcross	5.7	5.7
Rock Quarry	8.5	8.6

Table 3.17 presents the average water ages in the tanks during the last 24 hours of simulation under the Base and 1GRAY-C scenarios. These results, along with those presented in Table 3.16, suggested the turnover time of the Lanier Mountain tanks may have been increased by the 1GRAY-C scenario, but the average age in these tanks were not changed significantly. Conversely, the turnover time of the Nob Hill tank was not changed appreciably but the average age of water in the tank was reduced by almost a day by the 1 GRAY-C scenario.

Table 3.17: Average water age in tanks in Base and 1GRAY-C scenarios.

Tank	Base Average Age (days)	1 Grayson Closed Average Age (days)	% Difference
Bogan	1	1.01	1
Goshen Springs	2.2	2.11	-4
Grayson1	5.1	CLOSED	CLOSED
Grayson2	2.9	2.06	-29
Lanier Mountain 1	14.4	14.5	0
Lanier Mountain 2	11.1	11	-1
Lanier Mountain 3	14.7	14.8	1
Medlock Bridge	2.7	2.67	-1
Nob Hill	6.5	5.07	-22
Norcross	4.2	4.09	-3
Rock Quarry	5.3	5.09	-4

The main drawback of the 1GRAY-C scenario was the reduced use of the Lanier Mountain tanks. Reduction in use of the Lanier Mountain tanks led to an improvement of average water age in the southern portion of the system, as shown in Figure 3.16. The nodes in this area received less water that had been subjected to storage in the Lanier Mountain tanks, decreasing the average water age.

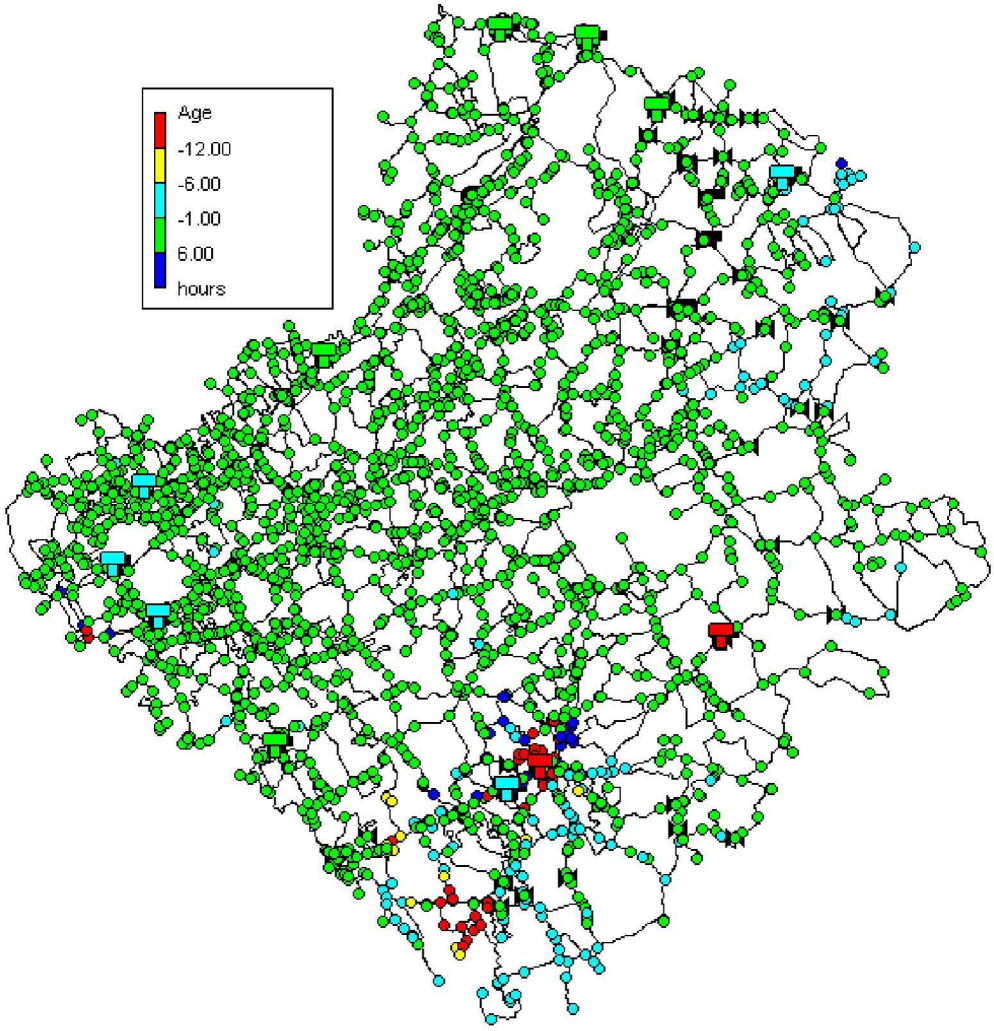

Figure 3.16: Change in average water age caused by the 1GRAY-C scenario.

Medlock Bridge and Goshen Springs Tanks Closed

Closure of the Medlock Bridge and Goshen Springs (MB&GS-C) tanks was planned by the utility. Simulation of this scenario showed the maximum age of delivered water was only reduced by 1 hour by not using these tanks, while the median age of delivered water was improved by 10 hours. Figure 3.17 presents the CDF of the age of delivered water in this scenario and illustrates how the curve of MB&GS-C was shifted to the left of the Base, indicating a system-wide reduction in delivered water age.

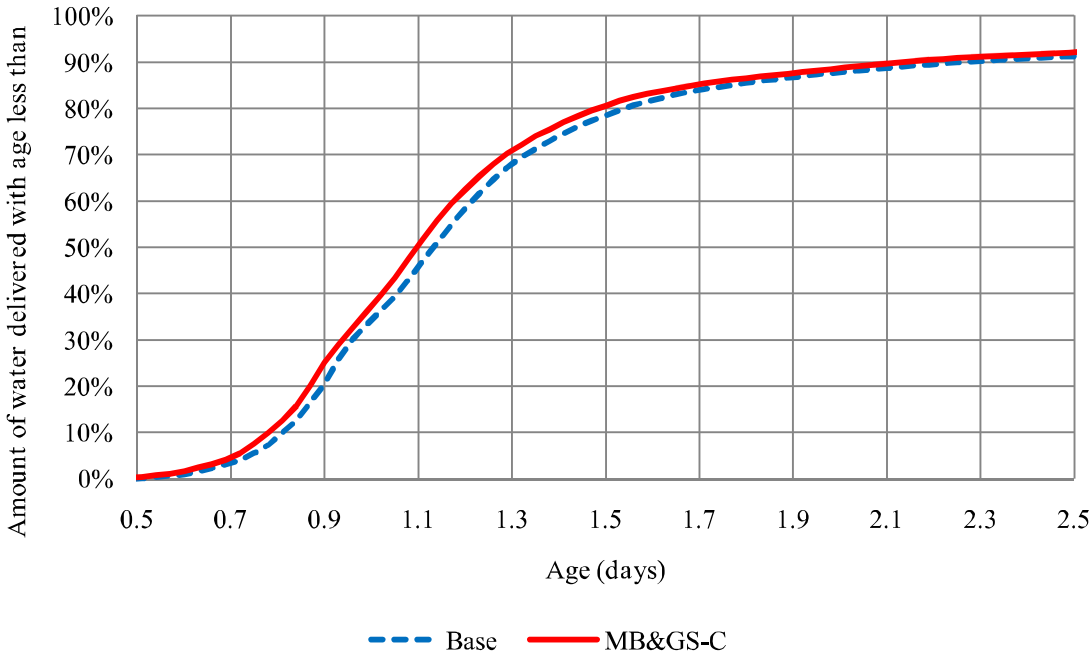

Figure 3.17: Cumulative distribution function curve of Base and MB&GS-C scenarios.

The benefits of the MB&GS-C scenario were the increased operational flexibility of the Norcross tank and the reduction in water age at nodes near the Medlock Bridge (MB) and Goshen Springs (GS) tanks. Since less water was supplied by the MB and GS tanks, the Norcross tank was used more, leading to a 6% greater level variation in this tank under the MB&GS-C scenario than observed in the Base. Table 3.18 presents the average water age in the tanks under the Base and 1MB&GS-C scenarios and shows the average age in the Norcross tank was reduced by 36% by closing the MB and GS tanks.

Table 3.18: Average water age in tanks in Base and MB&GS-C scenarios.

Tank	Base Average Age (days)	Medlock Bridge and Goshen Springs Closed Average Age (days)	% Difference
Bogan	1.0	1.0	0
Goshen Springs	2.2	CLOSED	CLOSED
Grayson1	5.1	5.7	12
Grayson2	2.9	2.9	0
Lanier Mountain 1	14.4	14.7	2
Lanier Mountain 2	11.1	11.7	5
Lanier Mountain 3	14.7	14.9	1
Medlock Bridge	2.7	CLOSED	CLOSED
Nob Hill	6.5	5.7	-12
Norcross	4.2	2.7	-36
Rock Quarry	5.3	5.4	2

Closure of the MB and GS tanks, reduced the average water age near these tanks since the demand was supplied by water that had not been subjected to storage. Figure 3.18 presents a map of where and how average water ages were affected by this scenario. Since the MB and GS tanks were closed, logic-based controls altered the operations of other system tanks, causing both increases and reductions in average water age throughout the system as compared to the Base scenario. One notable effect was the 12% increase in average water age in the Grayson 1 tank (shown in Table 3.18) under this scenario. Instantaneous low/negative system pressures were observed between 10-11am and 4-5pm on the 5th day of simulation; however, these events may be hydraulic artifacts and are not likely to be a concern for the Gwinnett County utility.

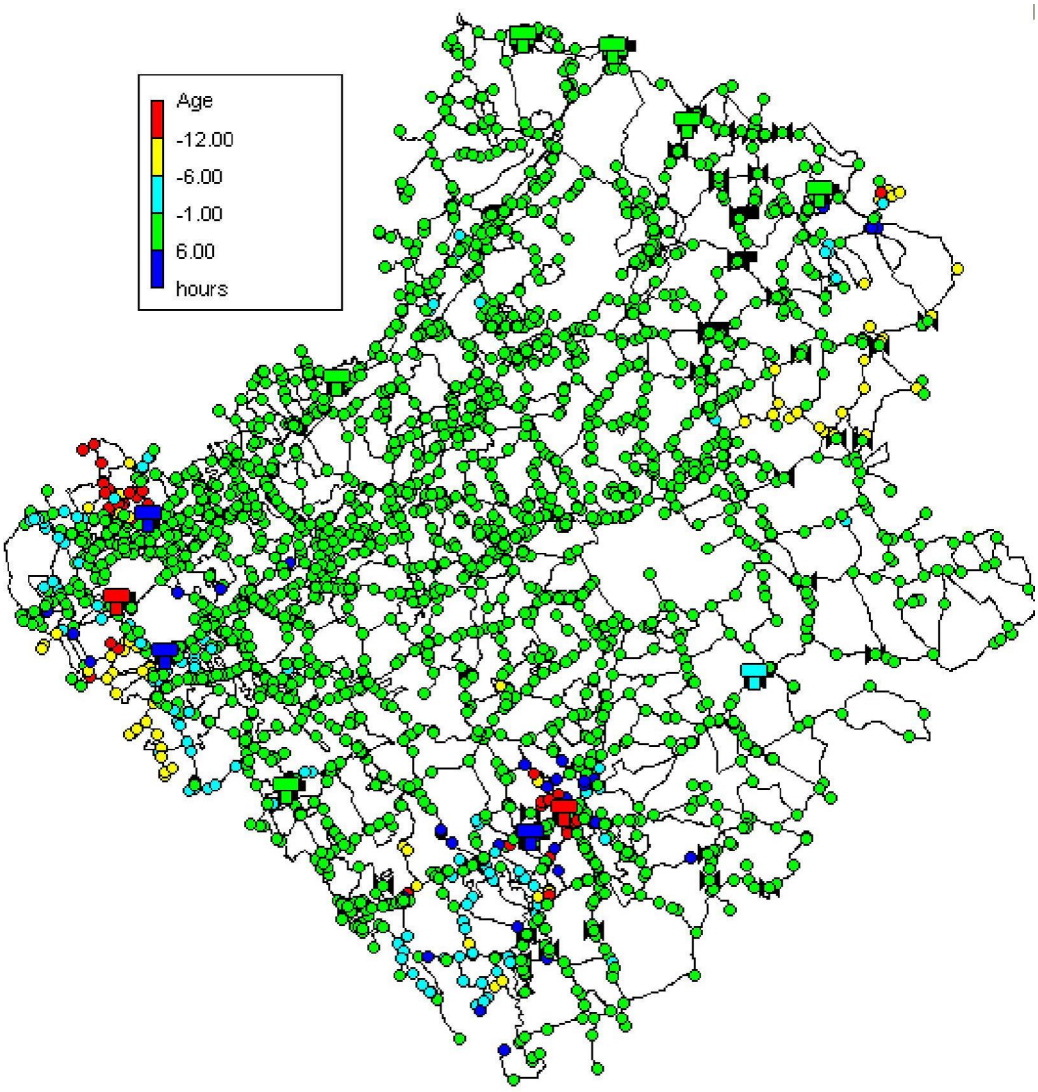

Figure 3.18: Change in average age caused by the MB&GS-C scenario.

3.4.5.2 Decrease in Tank Volumes –30%-LRG and 30%-All

The scenario where the volumes of all the system tanks were reduced (30%-All) showed the highest potential for reducing the 90% age range of delivered water, while volume reduction of only the largest system tanks decreased (30%-LRG) the maximum age of delivered water by 7 to 8 hours. Preliminary analysis of 10, 20, and 30% volume reductions for both scenarios indicated water age was improved in proportion to volume reduction and led to further testing using 30% volume reduction. Figure 3.19 presents the

CDF curves for the 30%-All and 30%-LRG scenarios compared to that of the Base. The results of the two scenarios were similar in their ability to reduce water age although their affect on the amount of available system storage was quite different. In the scenario where the volume of only the large tanks was reduced total system storage was reduced by 21% while it was decreased by 30% when all tank volumes were reduced.

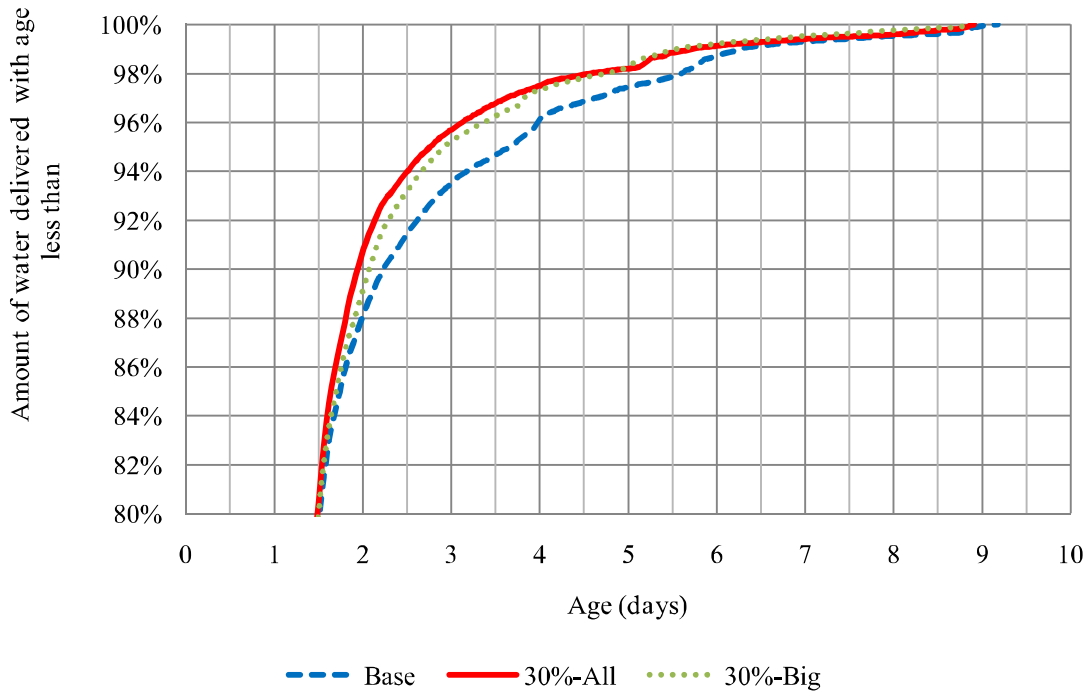

Figure 3.19: Cumulative distribution function curves for scenarios where volume of all and big tanks was reduced by 30%.

Thirty Percent Volume Reduction of Large Tanks

The 30%-LRG scenario resulted in a maximum delivered water age that was 8 hours less than observed in the Base scenario. By reducing the volume of the largest tanks, the age of 11% of delivered water with the highest age was reduced by 3 hours or more, as shown in Figure 3.19. This scenario reduced the average age near Lanier Mountain and Rock Quarry by decreased use of these tanks.

Turnover times observed in the 30%-All and 30%-LRG tank volume reduction scenarios are presented in Table 3.19. A benefit of the 30%-LRG scenario was its ability to reduce the turnover times in the majority of system tanks. The mechanisms of the turnover reductions were different between the large (Lanier Mountain) and small (Medlock, Norcross, and Goshen) tanks. The turnover times of the smaller tanks were reduced because of increased use, while reductions at larger tanks (Lanier Mountain) were due to decreased initial water levels. Turnover calculations are dependent on the flow of water into and the volume of water in the tank. If the flow of water into a tank over a 24-hour period increases, the turnover time will decrease. Likewise, if the volume of water in a tank is decreased the turnover time will decrease. Therefore, reductions in turnover time observed in the tank volume reduction scenarios were due primarily to the changes made to the initial volume of the tanks

Table 3.19: Average tank turnover times observed in the Base, 30%-All and 30%-LRG scenarios.

Tank	Base (days)	All Tanks 30% (days)	Large Tanks 30% (days)
Bogan	1.0	1.0	1.0
Goshen Springs	2.7	1.4	2.5
Grayson 1	3.5	0.5	3.5
Grayson 2	3.8	0.6	5.5
Lanier Mountain 1	24.5	15.0	17.3
Lanier Mountain 2	18.4	11.6	10.5
Lanier Mountain 3	27.6	15.6	18.4
Medlock Bridge	3.8	1.9	3.7
Nob Hill	2.8	2.8	2.8
Norcross	5.7	0.5	5.3
Rock Quarry	8.5	46.5	45.5

Table 3.20 shows the average water age during the final 24 hours of the Base and 30% LRG simulations. These results illustrate the average water ages in the tanks where turnover time was reduced in the 30%-LRG scenario were also decreased; however, the reduction in average water age in each of these tanks was no greater than 17%.

Table 3.20: Average water age in tanks in Base and 30%-LRG scenarios.

Tank	Base Average Age (days)	30% -Large Average Age (days)	% Difference
Bogan	1.0	1.0	0
Goshen Springs	2.2	2.1	-8
Grayson1	5.1	6.4	25
Grayson2	2.9	3.7	26
Lanier Mountain 1	14.4	12.9	-11
Lanier Mountain 2	11.1	9.2	-17
Lanier Mountain 3	14.7	13.1	-11
Medlock Bridge	2.7	2.7	0
Nob Hill	6.5	5.4	-17
Norcross	4.2	4.0	-4
Rock Quarry	5.3	8.2	56

The drawbacks of the 30%-LRG scenario were the increased turnover times noted for the Grayson and Rock Quarry tanks and the reduction in use of storage as the mechanism of reducing water age. The Grayson tanks did not drain as often in the 30%-LRG scenario as noted in the Base scenario, leading to longer retention times. Results in Table 3.20 show the increased turnover time in the Grayson tanks led to a ~25% increase in average water age in those tanks. The increased turnover times observed for the Rock Quarry tanks were due to severely reduced level fluctuation, which was an artifact of flow-based logical controls for this tank (see APPENDIX J). Figure 3.20 presents a map of the differences in average age between the Base and 30%-LRG scenario. Figure 3.20 shows that reductions in average water age due to the 30%-LRG scenario occurred in the areas around the Rock Quarry and Lanier Mountain tanks because these tanks supplied less demand.

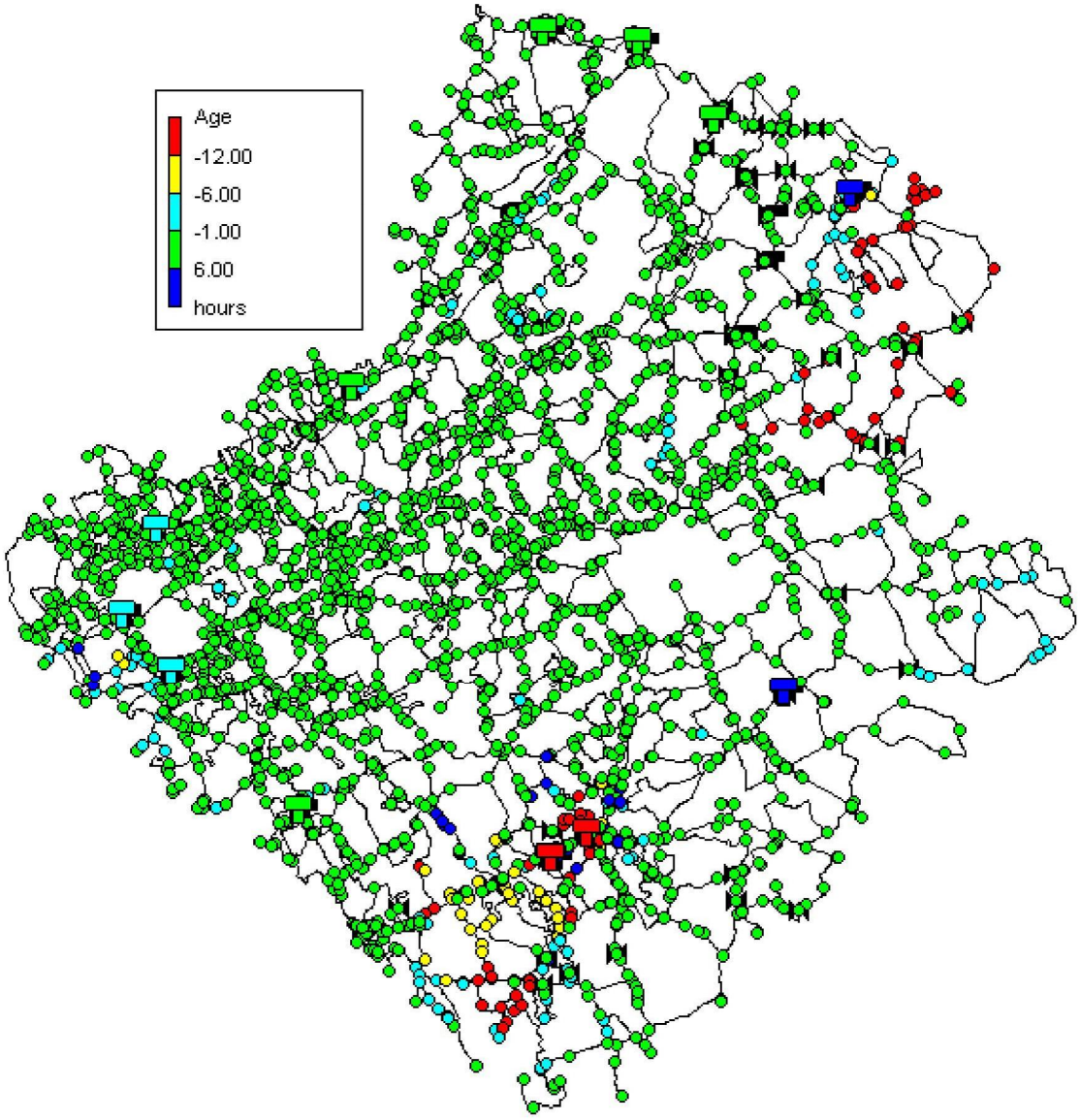

Figure 3.20: Change in average age caused by the 30%-LRG scenario.

30% Volume Reduction of All Tanks

Reducing the volumes of all tanks by 30% decreased the maximum age of delivered water by 7 hours and reduced the age of the 15% of delivered water with highest age by 3 hours or more, as illustrated in Figure 3.19. This scenario had the highest reduction in 90% range, reducing the age variability of delivered water age by 24

hours. As shown in Table 3.15, the 90% range of delivered water age of the Base scenario was 3 days, while in the 30%-All scenario it was reduced to 2 days.

Advantages of the 30%-All scenario were the reductions in turnover times and average water ages at nodes near system tanks. Tank turnover times were 'automatically' decreased by reducing the total volumes and initial levels of system tanks. However, increased water level fluctuations in the Goshen Springs and Medlock Bridge tanks under this scenario led to true reductions in turnover times for these tanks. Conversely, the reduced turnover times at the Lanier Mountain tanks appeared to be due to initial and top level reductions rather than increase level fluctuations caused by operational changes. Table 3.21 shows the average water age during the final 24 hours of the Base and 30%-All simulations. This table illustrates that regardless of the mechanism of turnover time reduction, the average age in the majority of tanks was reduced by the 30%-All scenario.

Table 3.21: Average water age in tanks in Base and 30%-All scenarios.

Tank	Base Average Age (days)	30% -All Average Age (days)	% Difference
Bogan	1.0	1.0	0
Goshen Springs	2.2	1.6	-27
Grayson1	5.1	8.4	65
Grayson2	2.9	1.4	-50
Lanier Mountain 1	14.4	12.6	-13
Lanier Mountain 2	11.1	9.2	-17
Lanier Mountain 3	14.7	13.0	-11
Medlock Bridge	2.7	2.0	-28
Nob Hill	6.5	6.2	-5
Norcross	4.2	2.0	-52
Rock Quarry	5.3	8.1	54

Disadvantages of the 30%-All scenario were the excessive draining or filling of tanks and the observation of low system pressures. Over the course of the 120-hour simulation, the 30%-All scenario caused the Grayson and Norcross tanks to drain almost completely. Excessive draining led to the observation of very low turnover times in these tanks (~ 12 hours). Pressure analysis revealed low pressure events occurred around noon, suggesting operations were not able to maintain system pressure set points under this scenario. This could have been because of tanks that had drained completely.

Overall, the 30%-All scenario reduced storage more that the 30%-LRG, 1GRAY-C, and MB&GS-C scenarios but did not appear to have a much larger reduction on maximum water age. Reduction of the volume of all tanks did appear to have a greater capacity to reduce the distribution of water age in the network, based on the 90% range of delivered water ages and CDF curve. A drawback of the tank volume reduction scenarios was that a large part of the system water age reduction was not achieved by using the

tanks more due to the reduced operational volume increasing tank turnover, but instead by avoiding the use of storage tanks. Still, results indicated volume reduction of tanks could improve the age of delivered water and average age in the storage tanks without compromising a large amount of available system storage.

3.4.5.3 Changing Central Distribution Pressures - PRV-1

The goal of testing the effects of changes in the pressure supplied by the high service pumps following the treatment plant was to enhance operational flexibility by increasing reliance on storage tanks to provide demand. Of the many possible central pressure management strategies, two scenarios of were examined. Scenario PRV-1 tested the effect of increasing the central pressures at night and decreasing them during the day. PRV-2 examined the effect of changing central pressures twice over the course of 24 hours, decreasing central pressures when demand was high and increasing them when demand was low. Pressure results showed that the alternative central pressures could be maintained in both scenarios (see APPENDIX M). Figure 3.21 presents the top 75% of the CDF curves of the Base, PRV-1 and PRV-2 scenarios. Although PRV-2 reduced the maximum water age by 6 hours more than the PRV-1 scenario, PRV-1 reduced the age of a much greater amount of delivered water. Another important improvement made by the PRV-1 scenario not achieved by PRV-2 was the reduction in the 90% range of the delivered water ages.

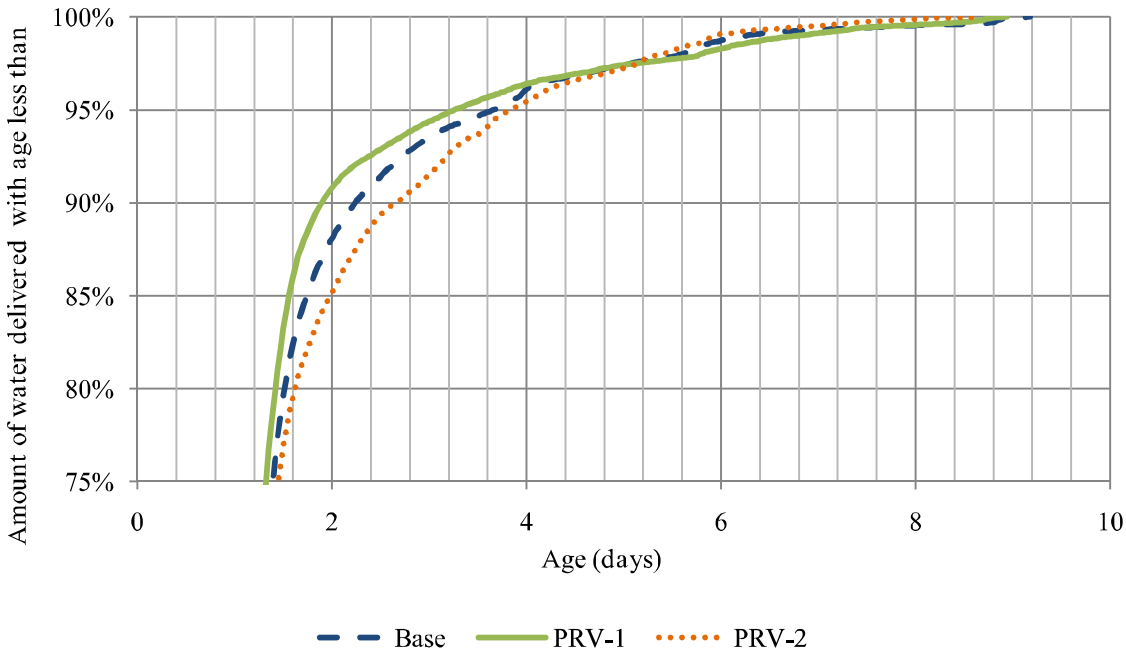

Figure 3.21: Cumulative distribution function curves of the PRV-1, PRV-2 and Base scenarios.

PRV-1

The PRV-1 scenario reduced the maximum water age by nearly 6 hours and the 90% age range of delivered water by 10 hours. Although it resulted in a relatively small reduction in maximum water age, the PRV-1 scenario reduced the age of 18% of delivered water with the highest age by 3 hours or more. This was the largest of all the operational scenarios tested, suggesting this operational approach had the highest capacity to reduce water age throughout the system.

The main benefit of the PRV-1 scenario was its ability to improve operational flexibility of the tanks without leading to negative pressures. Table 3.22 presents the average water age in the tanks during the last 24 hours of the Base and PRV-1 scenarios. These results show the improved operational flexibility of the smaller tanks lead to lower average water ages in the smaller system tanks (Bogan, Goshen Springs, Medlock

Bridge, and Norcross) without leading to high average water ages in the larger system tanks.

Table 3.22: Average water age in tanks in Base and PRV-1 scenarios.

Tank	Base Average Age (days)	PRV-1 Average Age (days)	% Difference
Bogan	1.0	0.9	-10
Goshen Springs	2.2	1.3	-41
Grayson1	5.1	5.6	10
Grayson2	2.9	2.6	-10
Lanier Mountain 1	14.4	14.6	1
Lanier Mountain 2	11.1	11.5	3
Lanier Mountain 3	14.7	14.8	0
Medlock Bridge	2.7	1.2	-56
Nob Hill	6.5	7.7	19
Norcross	4.2	1.3	-69
Rock Quarry	5.3	7.1	34

Figure 3.22 presents the map of differences in average water age observed in the Base and PRV-1 scenarios. This map shows that average water age was reduced around the Medlock Bridge/Goshen Springs/Norcross and the Rock Quarry tanks using the PRV-1 scenario. The Medlock Bridge, Goshen Springs, and Norcross tanks had lower turnover times, lower average water ages, and higher water level variations under this scenario as compared to the Base scenario. These results indicated the PRV-1 scenario and operations used on the base day could be implemented to reduce the water age near these tanks.

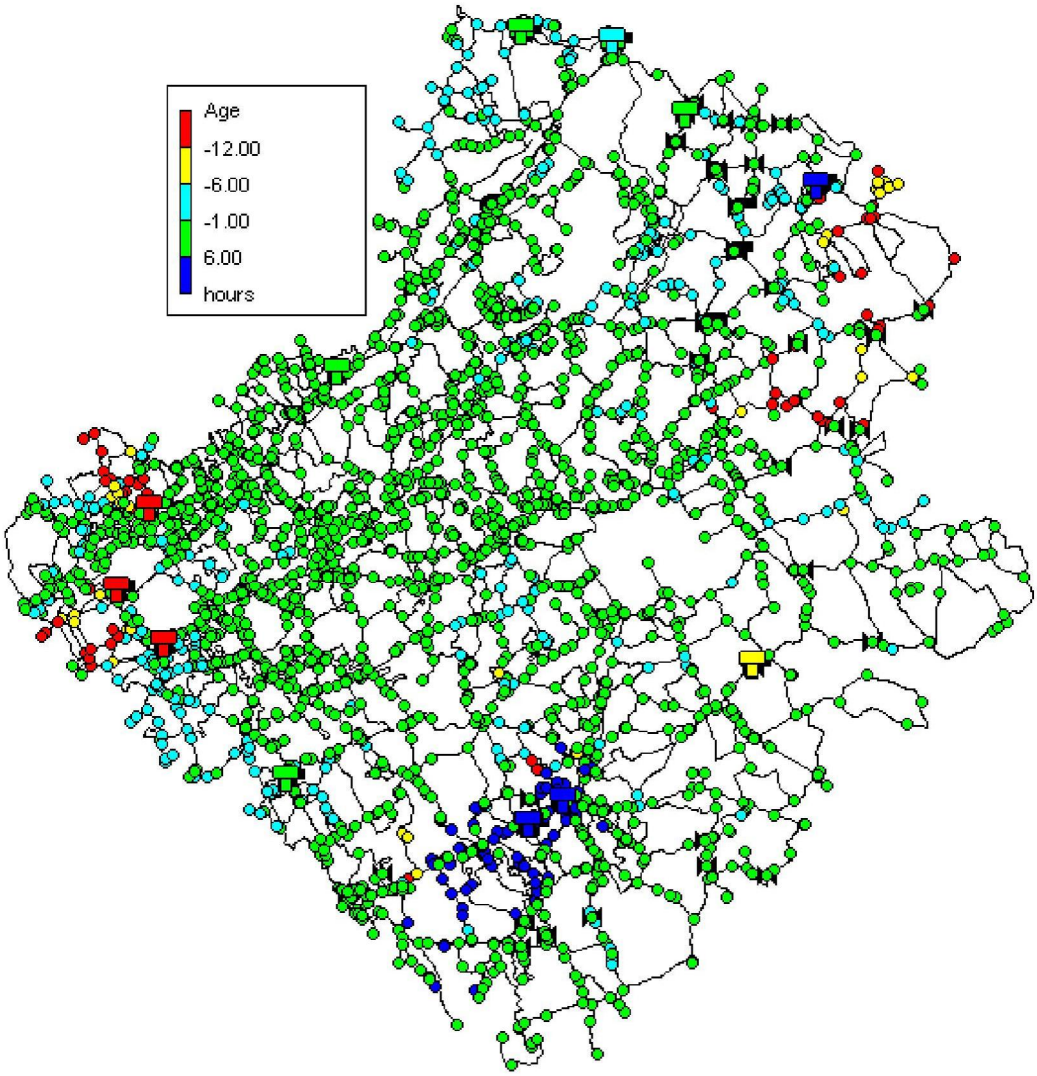

Figure 3.22: Effect of PRV-1 on average water age as compared to the Base scenario.

Increased operational flexibility also appeared to be a drawback of this scenario, since logical controls led tanks to drain completely to or approach their minimum level because they were attempting to maintain system pressures as instructed by logical controls. The higher average water age observed around the Lanier Mountain tanks was attributed to increased draining and decreased filling of these tanks. As noted in other scenarios, flow-based control of the Rock Quarry tank prevented it from draining, leading

to an 8 day increase in tank turnover time under this scenario and reduced average water ages surrounding this tank, as shown in Figure 3.22.

Operational Scenario Summary

Eight of the 10 alternative scenarios examined reduced the variability of age of delivered water (based on the 95-5% range) in the GCWDS. A summary of the five scenarios determined to have the highest reduction on maximum or system-wide water age are presented in Table 3.23 along with the observed benefits and drawbacks of their application. This table illustrates that some scenarios affected the age of more delivered water, while others had greater age reduction impacts on smaller volumes of water. No individual scenario was shown to be the best by each metric examined.

Table 3.23: Summary of the five best alternative operational scenarios.

Operational Scenario[+]	Amount of Demand With Reduced Age	Reduction of Maximum Water Age (hours)	Reduction in Storage Volume	PROS	CONS
1GRAY-C	8%	35.3	16%	Allowed for higher level variation and reduction in turnover time of the open Grayson tank.	Increased turnover time of Lanier Mountain tanks. Reduced water age around Lanier Mountain by reliance on tanks to provide demand.
MB&GS-C	11%	1.0	6%	Allowed for higher level variation of the Norcross tank.	Low system pressures between 10-11am and 4-5 pm.
30%-LRG	11%	7.8	21%	Reduced turnover time in smaller tanks.	Reduced water age around Lanier Mountain and Rock Quarry by decreased use of tanks.
30%-All	15%	6.5	30%	Reduced turnover times for all tanks. Led to higher level variation in Goshen, Medlock, and Norcross tanks.	Caused an unsustainable amount of draining of Norcross and Grayson tanks. Resulted in more filling and less draining of the Lanier Mountain tanks.
PRV-1	18%	5.8	---	Provided operational flexibility to drain tanks without leading to negative pressures.	Led to tanks draining completely or approaching their minimum level.

[+] See Table 3.5 on page 152 for scenario descriptions.

3.4.5.4 Combination of Best Operational Scenarios

A scenario that combined three of the five best scenarios presented in Table 3.23 was examined. This combined scenario incorporated the Medlock Bridge and Goshen Springs tanks closures (MB&GS-C), reduction in operational volume of the three largest tanks (30%-LRG), and adjustment of the central distribution pressures as the PRV-1 scenario. In addition, the Base and Combined scenarios were adjusted to avoid the sloshing (i.e. re-storage of water) observed at the Grayson tanks by combining the two 10MG tanks into one 20 MG total volume tank (the new Base scenario is referred to as the 'adjusted Base'). The combined scenario reduced the maximum delivered water age by 28 hours and decreased the age of 19% of delivered water by more than 3 hours as compared to the adjusted Base scenario. This was an improvement of 21 hours and 1% over the individual scenarios, respectively. However, the 90% age range of delivered water was only decreased by five hours, whereas the five best individual scenarios listed in Table 3.23 reduced the 95-5% range of delivered water age by 8 hours or more.

Table 3.24: Water age at specified points on the cumulative distribution function curve for the adjusted Base and Combined scenarios.

Point on CDF curve	Adjusted Base (hours)	Combined (hours)	Difference (hours)
5%	18.0	17.3	0.7
50%	27.4	26.6	0.7
90%	53.2	48.2	5.0
95%	82.1	76.3	5.8
100%	193.0	164.9	28.1
95%-5%	64.1	59.0	5.0

The benefits of the Combined scenario were the lack of significant negative pressure events, and the reduction of average water ages near the Medlock Bridge/Goshen Springs tanks and the Rock Quarry tank. The main drawback of this scenario was the increased average water ages observed near the Lanier Mountain tanks. These results were similar to the benefits and drawbacks noted in the individual scenarios incorporated into the combined scenario. A few pressure observations below 20 PSI were noted in the Combined scenario; however, these events were similar in number and temporal distribution to those noted for the adjusted Base scenario.

Table 3.25 shows the average water ages in the tanks during the last 24 hours of the adjusted Base and Combined scenarios. These results demonstrate the Norcross and Lanier Mountain tanks had the highest reduction in average age. However, in the case of the Norcross tank, the observed reduction in age was achieved by complete draining of the tanks during portions of the simulation. This occurred because the PRV-1 and Medlock Bridge and Goshen Springs tank closure scenarios individually led to a high capability to drain this tank. By combining these scenarios, the Norcross tank is relied on to supply a large amount of demand in the western tip of the system, leading to an unsustainable amount of draining.

Figure 3.23 presents the reduction in average water ages throughout the system by the Combined scenario. The average water age reductions by the Combined scenario were only slightly different from those of the PRV-1 scenario presented in Figure 3.22 (page 199). The most notable differences were in the areas near the Goshen Springs and Lanier Mountain tanks where the average age was decreased in the Combined scenario but not in the PRV-1 scenario. Since the Goshen Springs and Medlock Bridge tanks were

closed in the combined scenario, the area of decreased average age near the Goshen Springs tanks resulted from demand in that area being supplied by water that had not been stored. Where the average water age was reduced in the area south of the Lanier Mountain tanks by the Combined scenario (as compared to the PRV-1 scenario), the reduction appeared to be a consequence of the reduction of the operational volume of the large tanks, since the same area experienced reduced average age in the 30%-LRG scenario (shown in Figure 3.20, page 193).

Table 3.25: Average water age in tanks in the adjusted Base and Combined scenarios.

Tank	Adjusted Base Average Age (days)	Combined Average Age (days)	% Difference
Bogan	1.0	1.0	0
Grayson	3.1	3.5	12
Nob Hill	5.0	6.4	28
Lanier Mountain 1	14.5	12.0	-17
Lanier Mountain 2	11.0	8.6	-22
Lanier Mountain 3	14.8	12.1	-18
Norcross	4.0	0.8	-80
Rock Quarry	5.1	6.2	22

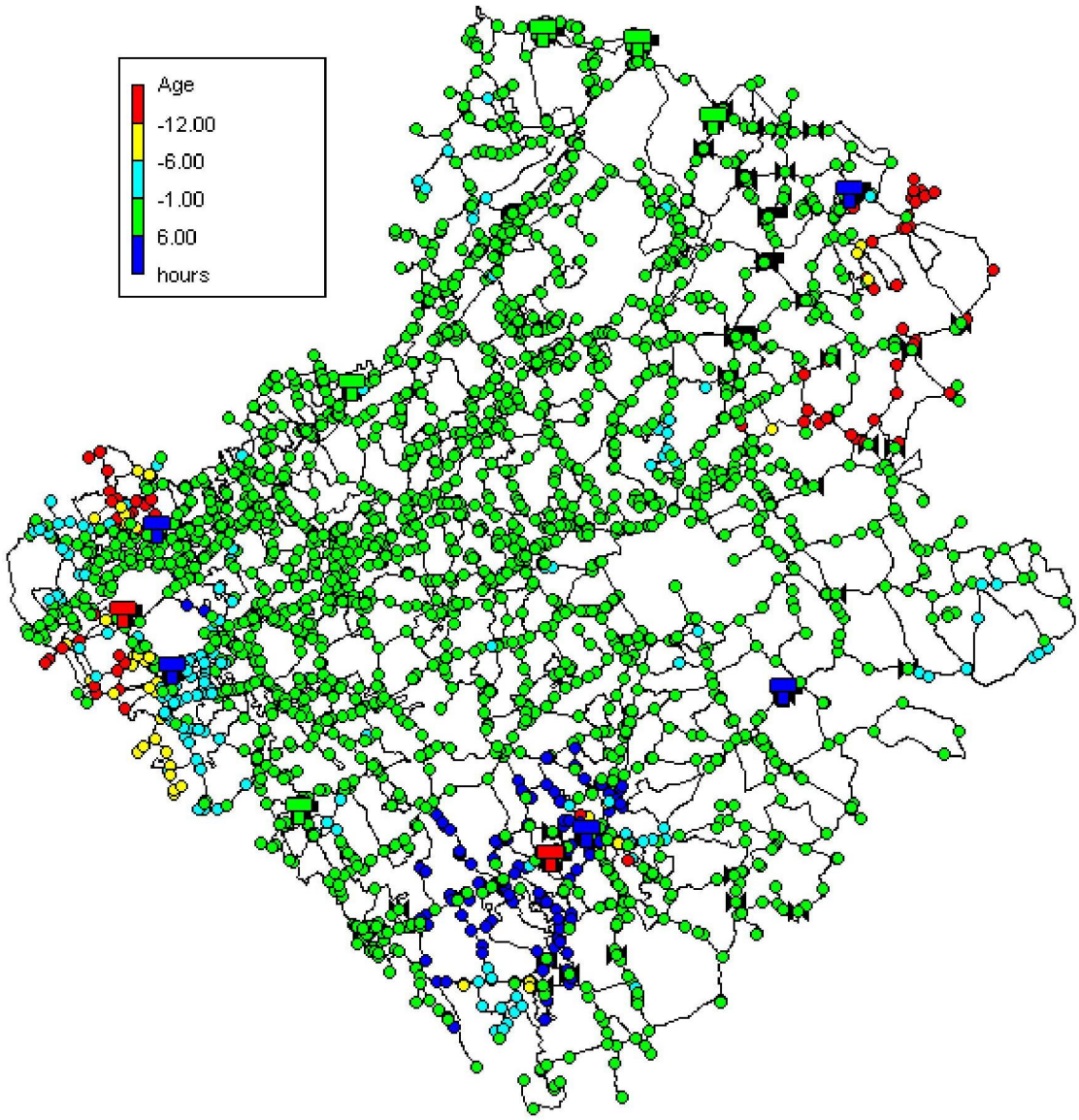

Figure 3.23: Effect of Combined scenario on average water age as compared to the adjusted Base scenario.

3.4.5.5 Implementation of a Blow-off

Blow-offs are commonly employed as temporary measures to reduce high water age in specific areas of distribution systems. A blow-off (BO) was simulated in the GCWDS by applying a period of augmented demand (100 GPM) at node 726 from 12 am to 3 pm. Node 726 was a low demand dead-end node located in the southern area of the

network near the Lanier Mountain tanks (base demand = 3.32 GPM). To avoid providing the increased demand by water from the Lanier Mountain tanks, controls were implemented to prevent them from draining during the blow-off period. Figure 3.24 presents the water age observed at node 726 in the Base and BO scenarios with the blow-off period marked with dashed lines. This graph shows the water age at node 726 decreased in the first ~30 minutes of the blow-off, but then resulted in a water age of 1.5 days more than observed in the Base scenario. This suggested the 3 hour period of high demand may not have been sufficient to pull fresher water into this part of the system.

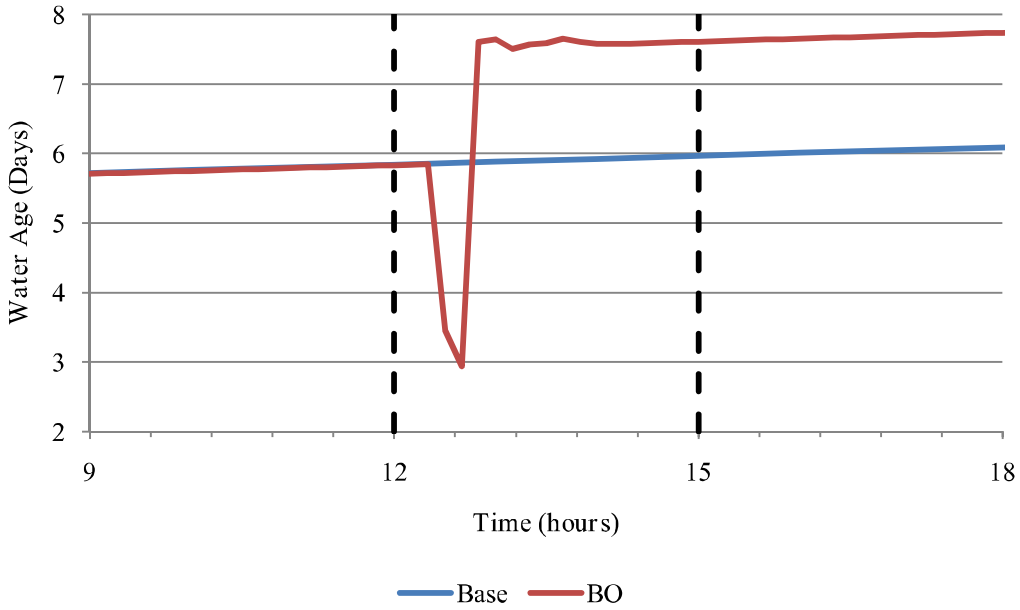

Figure 3.24: Water age at node 726 observed in the Base and BO scenarios.

Blow-offs are considered an effective way to reduce water age, but their impact is spatially and temporally limited. The BO scenario reduced the maximum delivered water age by 10 hours. However, this was most likely due to changes in operations to accommodate the blow-off rather than the removal of high age water. Since the Lanier Mountain tanks were not allowed to drain during the blow-off, nodes around these tanks

received less stored water than they did in the Base scenario. Overall, this scenario demonstrated that blow-offs must be carefully planned and managed to ensure they improve rather than negatively impact water quality. The benefits of blow-offs in removing sediment from pipes were not evaluated in this research.

3.4.6 Relationship between Tank Turnover Times and Delivered Water Age

The hypothesis that decreasing tank turnover times significantly improves water age in the distribution system was addressed using the results of the operational scenario simulations. Although all the operational scenarios examined aimed to decrease tank turnover time, three sets of tank-management scenarios were tested specifically to improve filling and draining. The first examined the effect of reducing the operational volume of all the tanks in the system and the second applied volume reduction to only the largest tanks in the network (Lanier Mountain, Grayson, and Rock Quarry). The third set of simulations forced tank filling and draining of the largest system tanks. Examination of the three sets of scenarios that used changed tank management to improve turnover time is followed by a summary of data from all scenarios.

Volume Reduction Scenarios

In developing scenarios where the maximum water levels of the tanks were reduced, there were instances where the model-specified initial tank water level was higher than the maximum water level allowed by the reduced volume scenario. When this occurred, the initial tank water level was reduced. The initial level of each tank was reduced except for the Grayson tanks in the 30%-LRG scenario. Since the total volume of tanks was initially lower in these scenarios, these changes in the initial conditions led to a ‘forced’ reduction in tank turnover time for the affected tanks.

In the 30%-LRG scenario, turnover times (shown in Table 3.19, page 191) were reduced for all tanks except Grayson. Since the initial conditions of the smaller tanks were not changed, this result suggested a true decrease in the turnover times of small tanks due to operations. However, in the scenarios where the volumes of all tanks were reduced, the decrease in turnover times observed could be attributed to the changes in initial conditions for all tanks. The tanks where turnover increased in the 30%-All scenarios were affected by a decrease in inflow. For example, the observed decrease in the turnover times of the Lanier Mountain tanks may have been due only to the reduction in initial volume, not operational changes, while the increase in the Rock Quarry turnover suggested that flow into this tank was drastically decreased.

Table 3.26 presents the water age results at specified points on the CDF curve for the tank volume reduction scenarios. This table shows the water age results for the volume reductions of only the largest tanks were similar to the corresponding volume reduction of all tanks. Whether or not the age of delivered water was decreased by these scenarios depended on the metric used to evaluate water age reduction. According to the maximum delivered water age, water quality was not greatly improved by either of the volume reduction scenarios. However, considering the age of 95% of the water delivered as the indicator, the water age was improved by at 24 hours in the all-tank volumes reduced scenarios. Although the median water age was not changed, the age of water in the highest percentile of delivered water was improved.

Table 3.26: Cumulative distribution function-based system water age results for tank volume reduction scenarios.

Point on CDF curve	Base (days)	All reduced by 30% (days)	Big reduced by 30% (day)s
50% - Median Age	1.1	1.1	1.1
95%	3.7	2.7	2.9
100% Maximum Age	9.2	8.9	8.8

Although 30%-All and 30%-LRG led to different effects on the maximum delivered water age, both scenarios led to reductions in the tank turnover times (excluding the Rock Quarry tank). This suggested the maximum water ages predicted in these scenarios were not affected by the tank turnover times. In general, tank volume reduction scenarios did not appear to reduce the age of delivered water due to increased tank turnover. Hydraulic results suggested that the age of delivered water was reduced in these scenarios because of avoidance of storage and reduced dependence on water from tanks to supply demand.

Forced Tank Turnover Scenarios

Forced filling and draining of the largest tanks in the distribution system reduced their turnover times and led to turnover time reductions in other tanks. Table 3.27 presents the turnover times observed when specific tanks were forced to fill and drain and Table 3.28 displays water age results at specified points on the CDF curve for the forced turnover scenarios. Results showed when Grayson tanks were forced to fill and drain the turnover time of the Lanier Mountain tanks were reduced more than those of the Grayson tanks and vice versa. Very short turnover times noted for the Grayson tanks in the FT-LMN scenario were due to excessive draining of these tanks over the 120 hour

simulation. The hydraulics leading to these results are examined in detail in APPENDIX N.

Table 3.27: Tank turnover times observed in forced turnover of tank scenarios. Values in bold represent tanks that were forced to fill and drain.

Tank	Base (days)	FT-GRAY (days)	FT-LMN (days)	FT-RQ (days)
Bogan	1.0	1.0	1.0	1.0
Goshen Springs	2.7	2.3	2.3	2.3
Grayson 1	3.5	2.7	0.3	1.5
Grayson 2	3.8	3.0	0.4	1.6
Nob Hill	2.8	2.8	2.9	3.4
Lanier Mountain 1	24.5	14.6	10.4	25.6
Lanier Mountain 2	18.4	9.5	8.8	18.2
Lanier Mountain 3	27.6	17.3	11.8	26.4
Medlock Bridge	3.8	2.8	2.6	3.4
Norcross	5.7	3.3	3.3	3.4
Rock Quarry	8.5	10.6	11.2	6.8

Table 3.28: Cumulative distribution function-based system water age results for forced tank turnover scenarios.

Point on CDF curve	Base (days)	FT-GRAY (days)	FT-LMN (days)	FT-RQ (days)
50% - Median WA	1.1	1.1	1.1	1.1
95%	3.7	3.8	3.7	3.5
100% Maximum WA	9.2	13.0	10.5	9.1

Despite the decrease in turnover time noted for the scenarios where tanks were forced to fill and drain, the maximum age of delivered water was increased. The FT-GRAY scenario led to a reduced turnover time but increased the maximum delivered water age by 2 hours and the age at 95% delivered by 4 days. Approximately 8% of demanded water had a higher water age in the FT-GRAY than in the Base scenario. The

FT-LMN scenario also reduced turnover times of the majority of system tanks and resulted in a maximum delivered water age that was 1.3 days greater than observed in the Base scenario. By comparison, the FT-RQ scenario did not significantly reduce tank turnover times but led to a five hour age reduction at 95% of supplied demand and a one hour decrease in maximum water age.

Results from these scenarios suggested reducing the turnover time of the largest tanks by forcing them to fill and drain did not improve system water quality. In scenarios where tanks were not being turned over very quickly, they were providing less water to supply system demand. By forcing the tanks to fill and drain, it appeared more demand was supplied by older water from the tanks rather than water that had not been subjected to storage, leading to higher water ages in these scenarios.

All Scenarios

When data collected from all the operational scenarios were considered, results confirmed that the turnover time was related to the average age of water in the tank. Figure 3.25 presents a scatter plot of the average age of water in a tank versus its turnover time. A moderately-strong relationship between the two was noted with an R^2 value of 0.63. However, the turnover time of the tanks did not appear to have as strong a correlation with the age of delivered water. Table 3.29 presents the quantitative relationship (R^2 values) between the turnover times and the water age observed at the specified point of the CDF for each tank. The largest tanks (Grayson and Lanier Mountain) had turnover times that were the most related to delivered water age, however the R^2 values for these tanks were quite low, with a maximum of 0.39. These results indicated large tanks had a bigger effect on system water age than the smaller tanks and

that improved turnover of any one particular tank did not directly equate to reduced water age at demand nodes.

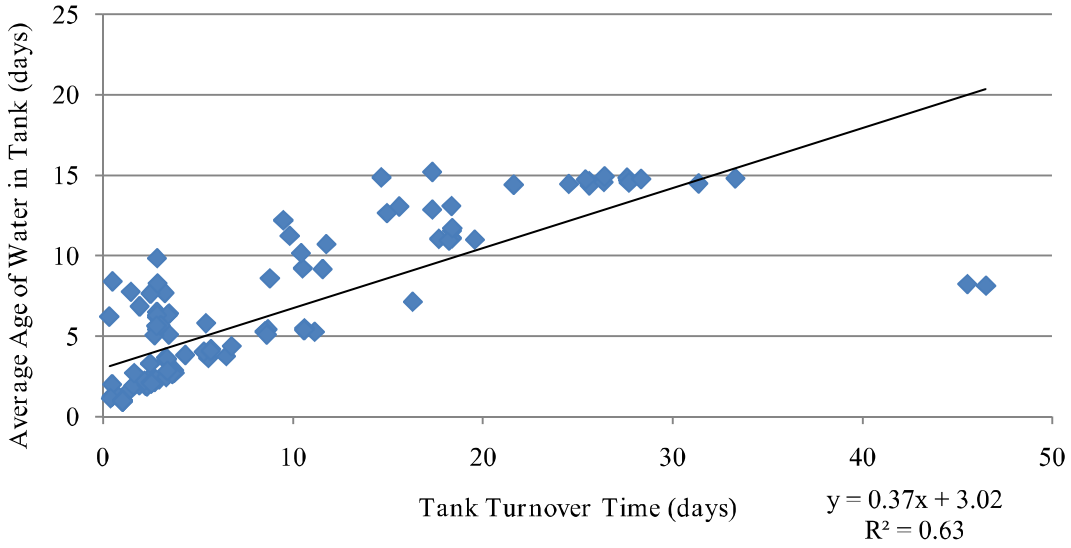

Figure 3.25: Modeled average tank water age vs. hydraulic turnover time for all tanks and scenarios.

Table 3.29: R^2 values between turnover time of each tank and age of delivered water at specified points on the cumulative distribution function curve.

Tank	0%	5%	10%	25%	50%	75%	90%	95%	100%	95% -5%
Bogan	0.01	0.04	0.03	0.03	0.03	0.11	0.26	0.01	0.07	0.01
Goshen Springs	0.19	0.14	0.03	0.14	0.19	0.28	0.03	0.03	0.00	0.02
Grayson 1	0.28	0.14	0.39	0.27	0.28	0.05	0.00	0.00	0.17	0.00
Grayson 2	0.07	0.04	0.00	0.01	0.01	0.03	0.24	0.02	0.03	0.03
Nob Hill	0.05	0.02	0.12	0.00	0.00	0.03	0.16	0.03	0.00	0.03
Lanier 1	0.01	0.00	0.03	0.00	0.01	0.00	0.00	0.02	0.01	0.02
Lanier 2	0.03	0.07	0.14	0.09	0.04	0.00	0.03	0.00	0.33	0.00
Lanier 3	0.03	0.06	0.16	0.10	0.06	0.02	0.07	0.02	0.34	0.01
Medlock Bridge	0.19	0.14	0.03	0.14	0.19	0.28	0.03	0.03	0.00	0.02
Norcross	0.17	0.03	0.29	0.13	0.16	0.30	0.30	0.14	0.01	0.13
Rock Quarry	0.07	0.01	0.01	0.00	0.00	0.03	0.28	0.70	0.02	0.69

Examination of the results of all operational scenarios indicated that decreased tank turnover time did not always reduce the age of delivered water. This conclusion seemed contrary to common thinking, which dictates that tank turnover improves water quality. However, the findings of this study and common thinking can be integrated to fully understand the impact of tank operations on consumed water quality.

While reduced tank turnover time improved the age of water in the tanks, this improvement was not passed on to the network in the form of reduced age at demand nodes. This may have been due to the limited effect of tanks on the overall system water age suggested by the NTA scenario results. Conversely, the age of delivered water may have been augmented by increased reliance on tanks to supply demand although less water was being put into the tanks (thus less mixing of stored water with fresh water was occurring). Increased turnover improved water quality in the tank but decreased the quality of the water in the distribution system since more demand is being supplied by water that has been stored in tanks rather than water directly from the treatment plant.

3.4.7 Water Quality Results for Scenarios at IDSE Sampling Locations

The average TTHM, HAA5, and Cl^- concentrations at IDSE sampling locations caused by operational scenarios tested are presented in APPENDIX O. Since the kinetic equations used to calculate water quality parameters relied solely on time, the places in the network where the age was the lowest were generally found to have the highest Cl^- concentration and lowest DBP concentrations. Twelve sampling points were selected by the Gwinnett County utility based on their IDSE study. These twelve points corresponded to eleven points in the skeletonized model used in this study since sampling locations #5 and #6 corresponded to the same skeletonized model node. Sampling point

#4 was identified as the Medlock Bridge storage tank. Large changes in average DBP and Cl^- concentrations were observed at this location. These changes were due to greater differences in water age in tanks as compared to the ones observed at the sampled network nodes. Tanks were modeled as completely mixed as opposed to pipes, in which plug flow (e.g., no mixing) occurred; therefore, greater amounts of water were accounted for in the average age, and DBP and Cl^- concentrations of tanks than in the average age, and DBP and Cl^- concentrations of pipes.

Results of the NTA simulations indicated which tanks had an effect on IDSE sampling points. NTA-All results suggested that under the Base scenario tanks contributed very little to DBP concentrations at IDSE sampling points. Individual tank NTA results showed the Lanier Mountain tanks had a small effect on location 8 and the Grayson tanks effected concentrations at locations 8, 10, and 12. Of the scenarios considered, 1LMN-C and PRV-1 led to decreases in DBP concentrations at 8 and 10 of the 11 sampling points, respectively. Average percent differences in DBP and Cl^- concentrations at sampling locations for these scenarios are presented in Table 3.30 and Table 3.31 . The MB&GS-C scenario led to increased DBPs and decreased Cl^- at all sampling locations, as shown in Table 3.32. With the exception of the Medlock Bridge location (location 4), all operational scenarios decreased DBP concentrations by a maximum of 4.4% at the IDSE sampling points, while Cl^- was increased by a maximum of 0.9% over the Base scenario. Disinfection byproduct formation kinetics are complicated and interpretation of the DBP results is affected by the validity of the kinetics used in the model. Model kinetics limited the TTHMs to a maximum that was lower than observed in field tests of the DWDS. However, it should also be kept in mind

the water quality model used was simplified and did not account for important factors such as pipe wall interactions.

Table 3.30: Percent difference between the average DBP and chlorine results of the one Lanier Mountain tank closed (1LMN-C) and Base scenarios at IDSE sampling points.

IDSE Sampling Location	Average TTHM difference	Average HAA5 difference	Average Cl^- difference
1	0.5%	0.4%	-0.1%
2	-1.1%	-0.9%	0.1%
3	-0.5%	-0.1%	0.0%
4	-8.0%	-9.9%	2.5%
5&6	-0.8%	-0.9%	0.2%
7	-0.5%	-0.4%	0.0%
8	-1.0%	-2.1%	0.9%
9	-0.1%	-0.1%	0.0%
10	-2.8%	-1.4%	0.0%
11	-4.3%	-4.4%	0.1%
12	1.4%	3.4%	-0.4%

Table 3.31: Percent difference between the average DBP and chlorine the results of the PRV-1 and Base scenarios at IDSE sampling points.

IDSE Sampling Location	Average TTHM difference	Average HAA5 difference	Average Cl^- difference
1	0.4%	0.3%	-0.1%
2	0.1%	0.1%	0.0%
3	-0.2%	-0.1%	0.0%
4	-49.4%	-56.8%	14.4%
5&6	-0.2%	-0.3%	0.1%
7	-0.2%	0.0%	0.0%
8	1.4%	1.9%	-0.7%
9	-0.4%	-0.4%	0.0%
10	-0.4%	-0.1%	0.0%
11	-1.4%	-1.2%	0.0%
12	-0.3%	-0.1%	0.0%

Table 3.32: Percent difference between the average DBP and chlorine results of the Medlock Bridge and Goshen Springs tanks closed (MB&GS-C) and Base scenarios at IDSE sampling points.

IDSE Sampling Location	Average TTHM difference	Average HAA5 difference	Average Cl^- difference
1	0.6%	0.5%	-0.1%
2	1.2%	1.5%	-0.2%
3	0.7%	1.3%	-0.1%
4	CLOSED		
5&6	1.1%	1.3%	-0.3%
7	1.1%	1.8%	-0.1%
8	0.9%	1.5%	-0.7%
9	0.1%	0.1%	0.0%
10	8.5%	11.2%	-0.7%
11	4.6%	5.6%	-0.2%
12	6.7%	9.3%	-0.9%

3.4.8 Cost Analyses

Approximate cost analyses showed the majority of operational scenarios did not significantly affect the daily expenditure due to pumping. It is important to note that constant pump efficiencies were used for many locations rather than curves that related efficiency to delivered head. The use of average efficiencies adversely affected the accuracy of calculated costs. In addition, the approximate method used to represent VSPs (e.g., by a pump that was always on followed by a pressure reducing valve set to deliver the desired pump output pressure or head, which is discussed in APPENDIX L) had the drawback of misrepresenting the energy use of the pumps.

As presented in Table 3.33, the alternative management scenarios did not have large affects on the daily operational cost. The exceptions were the FT-GRAY and PRV-1 scenarios. The FT-GRAY scenario augmented the daily cost by roughly $1,630 to a total of $15,175 per day. The PRV-1 scenario increased the operational cost to $64,811,

or 5-fold that of the Base. Inspection of energy use data showed the higher daily costs were due to increased use of low efficiency pumps (41%) with moderately high energy costs (9.8 cents/kWh) at the Lanier Mountain tanks.

Table 3.33: Maximum reduction of the age of delivered water and approximate daily cost of pumping.

Operational Scenario	Reduction of Maximum Delivered Age (hours)	Approximate Daily Cost (USD)
1GRAY-C	-35.28	$13,686
PRV-2	-12.24	$13,347
30%-LRG	-7.92	$13,202
30%-All	-6.48	$13,071
PRV-1	-5.76	$64,811
1LMN- C	-2.16	$13,321
FT-RQ	-0.72	$13,514
MB&GS- C	-0.72	$13,123
Base	0	$13,545
FT-LMN	31.68	$13,740
FT-GRAY	91.44	$15,175

3.5 Discussion

Hydraulic models mimic drinking water distribution systems, making them a useful tool to make predictions and inexpensively assess responses to operational changes. In this study, novel methods for system characterization and analysis were developed using EPANET and its MSX extension. These methods facilitated an investigation into which physical network features were responsible for high water age observed in the system. The developed methods were then applied to a logic-controlled hydraulic model that replicated the actions of system operators to evaluate the ability of

11 different operational scenarios to reduce the water age and improve water quality in the Gwinnett County water distribution system.

Simulation and Model Characterization Methods

This study produced several novel ways to simulate and analyze water quality using EPANET and its MSX extension. The EPANET-MSX system was used to perform water age analyses and characterize the effect of specific system features on water quality in the network. A new definition of tank turnover time was used to account for the variability of age that occurs in storage tanks. The empirical cumulative distribution function (CDF) of the age of delivered water provided a graphical method to visualize system age. Methods developed to compare the CDF between scenarios were found to be easier to relate and more meaningful than standard statistical methods for comparing distributions when applied to water quality data.

Multi-species water quality model. Using EPANET MSX for water quality and system characterization had clear benefits and drawbacks. The main disadvantage was the inability to obtain data for both hydraulic and water quality parameters using the same simulation; therefore at least two simulations were required for each scenario tested. However, because the MSX system saves hydraulics at user-specified time steps and the EPANET2 toolkit uses event-driven time-step regardless of the user-specified time-step, the results of the two simulations could be different. The EPANET GUI may be useful to visualize flows, pressures and ages on a map of the system, but it does not have the capabilities to model anything beyond hydraulics and one water quality constituent.

The benefits of the MSX system outweigh the drawbacks. As shown in the present study, the multi-species water quality modeling can be used to identify the

physical features of the network responsible for high water age through simulations where water does not age/react in tanks and/or dead end nodes. The results obtained from the scenarios where water did not age or react in system tanks or at dead ends (NDEA and NTA scenarios) were similar to analysis using the trace function available in EPANET2. However, the trace function in EPANET2 only allows for determining the percentage of water originating from a specified node and gives no indication to the effect on quality. With the multi-species model, there is the additional capability of quantifying the effect DWDS assets (i.e., tanks) may have on age or on the concentration of a chemical in the distribution system. Simulation results provide meaningful information to determine where to focus actions to improve distribution system operations. In addition, by running age, DBP, and Cl^- simulations concurrently, the connection between water age, quality, and hydraulics can be investigated.

Turnover time. The redefinition of the turnover time using a dilution-based approach provided both a qualitative and quantitative improvement over the classic, purely hydraulic definition. Qualitatively, thinking of turnover as dilution rather than as volume replacement, is a way to better link this metric to water quality characteristics. This provides operators, managers, and researchers with a more consistent quantitative measure of how water quality is being affected within the tank. Quantitatively, the water quality definition of tank turnover is more conservative than the hydraulic definition and requires greater operational effort to ensure that tanks are being turned over completely. A criticism of the dilution definition used herein was that it was simplified to represent tanks that were considered completely mixed, which is generally uncommon among storage tanks. However, the completely-mixed assumption widely employed among

DWDS modelers and still represents a more realistic turnover time than that predicted by the hydraulic definition alone.

Water age distribution. Use of the cumulative distribution function allowed for a snapshot view of the effect an alternative operational scenario had on the delivered water age distribution in the DWDS. The CDFs showed quickly and clearly that the median age of delivered water was not greatly affected by the operational changes and was easily employed to determine what percent of the highest age water could be reduced under the scenario examined. Numerical comparison was accomplished by comparing values derived from the upper tail of the CDF curve.

The metrics used to compare scenarios, including the data for the CDF, were taken from the fifth day of the five day simulation (except in the case of the BO scenario). This approach was taken to allow for a new steady state operation to be achieved under the new scenario simulation. However, results suggested using the turnover time on the 5^{th} day was not necessarily a good metric. Since some scenarios caused tanks to drain excessively by the fifth day of simulation, the turnover observed was very low. However, this was because little or no water was left in the tank, not because the tank was being operated in a more optimal manner.

Logical Controls

The logical controls developed for this system were an improvement over time driven controls as they were more reactive to system changes. Controls were developed based on pressures and had a time component to ensure tanks did not drain at improper times. Pressures observed in the model, especially those used to control tank and pump operation, generally repeated over a 24-hour period and did not seem to change

significantly due to the operational changes made by alternative scenarios. System pressures are related to the demands directly by the Bernoulli conservation of energy equation. Subsequently, by controlling the system based on pressure, operators are responding to system demands. Through creating controls that represented only 24-hours of demand, the model appeared to suffer from representing only one day of decision-making and not the general heuristics used.

Problems were encountered by duplicating tank heads on the base modeled day to develop logic-based controls. In some cases, controls did not mimic what an operator would actually do in favor of creating a control that led to the correct head pattern for a tank. This led to problems particularly for controls based on flow and time (for filling tanks during the night). Analyses of the Rock Quarry tank results highlighted that pressure based controls were more responsive than flow based. Controls based on flow in pipes that that did not vary when operations were changed functioned like time-based controls and operations did not change when alternative scenarios were simulated. Similarly, nightly tank filling was done with time-based controls and did not always allow tanks to fill to the level that may have been achieved by the operators. A better option for tank filling would have been to require tanks to fill back to a specific level, regardless of the time required. These issues may have led to the common problem noted in many of the scenario simulations where the tanks were used less in when they might have been expected to be used more.

Base Scenario and System Characterization

Simulation of the Base scenario for 23 days (18 days to reach steady states age + 5 days) indicated the areas with highest water age were those located the furthest from

the treatment plant. This agreed with the results of previous studies (Kim et al., 2006), and was logical, as the water that had further to travel would likely have the longest retention time in the system. System characterization scenarios showed that the areas that were affected by storage tanks also supplied the areas furthest from the treatment plant. This indicated that in addition to having high water retention time due to distance from the treatment plant, these the zones were also areas receiving water from tanks.

System Pressure

Low and negative transient pressures are common in distribution systems. "A variety of water distribution system operations may result in pressure fluctuations that can lead to the occurrence of relatively brief (transient) low or negative pressures" (Gullick et al., 2004). The occurrence of negative pressures is especially of concern due to the possibility of backsiphonage that could draw contaminants into the distribution system. The models used in this study exhibited short periods of low and negative pressure, however, these may not necessarily be interpreted as 'true' pressure surge events. Hydraulic models used for pressure surge analysis are more intricate and make different assumptions about the compressibility of water and pipe flexibility (Laptos, 2009). The negative and low pressures noted here were determined to be due in large part to a computational artifact in the software because of the way the high service pumps were run. To a lesser extent, the observed low pressure events may have reflected changes in pump operation and demands and suggest model controls are unable to maintain these at certain times. Simulation results showed operational scenarios that were the most successful at reducing water age experienced some negative pressure

events. Many of these could be explained by low pressures occurring at the central transmission mains where several model-platform instigated shut-offs were observed.

Scenario Simulations

Simulation of 11 different alternative operational scenarios suggested which strategies were most effective in reducing the age of delivered water and should be further investigated. The Base scenario system characterization investigation suggested tanks negatively affected the age of only 12% of delivered water, indicating that network layout was responsible for 88% of aging.

PRV

Scenarios PRV-1 and PRV-2 where central pressures were varied introduced operational buffer with regard to system pressure allowing for easier filling and draining of tanks. By increasing pressure system tanks could be filled faster, which may reduce water age. Since it resulted in higher water ages the PRV-2 scenario may have been too extreme a solution.

Volume Reduction

The differences in water age were not very different between the reduction of only the big tanks and the reduction of all tanks, suggesting the reduction of volume in all system tanks was not necessary to achieve a reduction in water age. This might have been expected since the tanks did not supply much of the system demand (10% on the modeled day) and the large tanks supplied the majority of that (6%). By reducing the operational water levels in a tank, turnover times are reduced, as shown in the volume reduction scenarios by ‘automatic’ reductions in turnover time when the initial tank level

was reduced. This indicated water quality could be improved and tank turnovers reduced with a reduction of only 8 MG of system storage.

Tank Closures

Tank closures resulted in bigger decreases in storage volume (in the case of the Grayson tanks) but also allowed for more operational flexibility of the tanks that remained open. Reductions in delivered water age observed after 5 days of operations in these scenarios appeared to be due mainly to the decreased use of water from tanks to supply demand. This was observed not only in the areas of the closed tanks, but also near the tanks whose operations were not changed (e.g., Lanier Mountain tanks supplied less demand when one Grayson tanks was closed). This result highlights an inadequacy of relying on the logical controls used herein since operators may not use the same heuristics as those represented if a system change as large as a 10 MG tank closure is made.

Forced Filling and Draining

While forced filling and draining of the large tanks was expected to improve water age, these scenarios led to higher water ages in the distribution system. The observed level variations in these tanks were lower under the forced turnover scenarios than in the Base condition; however, whereas in the Base scenario the tank filled and drained once in a day, in the forced filling and draining scenarios tanks filled and drained 2 to 5 times a day. Age of delivered water was most likely augmented by increased use of the tanks to supply demand although even though the age of the water leaving the tanks was lower. The results suggested forced turnover did not improve the maximum observed water age. Under the specific tank controls applied in this study, these

scenarios did not improve the age of delivered water and led to significant increases in the maximum age of delivered water.

Combination of Best Scenarios

When 3 of the 5 best operational approaches were combined into one operational scenario, the average water ages throughout the system and the amount of delivered water with reduced age were very similar to those observed in the individual scenarios. However, the main benefit of the Combined scenario was that the maximum delivered water age was reduced by nearly 1 day more than noted in individual scenarios. Otherwise this scenario had the same hydraulic benefits and drawbacks of the scenarios from which it was created. The benefits included the reductions in average water age near the Medlock Bridge/Goshen Springs and Rock Quarry tanks, reductions in average water age in the Lanier Mountain tanks, while the drawbacks remained the unsustainable amount of draining occurring from the Norcross tank and the increased average water ages near the Lanier Mountain Tanks.

Water Quality

Water quality modeling is more complicated than hydraulic modeling due to its reliance on complex reactions of formation and decay of DBPs and chlorine that occur in the network. The approach to DBP and Cl^- modeling used in this study was simplified since reaction constants were based on time only and not influenced by available chlorine or NOM substrate and only bulk water reaction equations were used (wall reactions were ignored). Moreover, the maximum achievable DBP concentrations used were lower than the USEPA's maximum contaminant limits. Routine monitoring and tracer test data available from the Gwinnett County system were not observed to pass the 80 μg/l and 60

μg/l MCLs for TTHMs and HAAs, respectively; however, maximum values of 75.2 μg/l and 41.9 μg/l have been observed. In comparison, the TTHM kinetics of Kim and coworkers allowed for maximum TTHM and HAA5 concentrations of 58.5 μg/l and 49.3, respectively (2006). Water quality results presented here were limited by the quality of information available for modeling and have been addressed by presenting percentage differences between the Base and scenario results for changes in DBP and Cl^- concentrations. Overall, the operational scenarios considered did not significantly reduce the DBP concentrations at the majority of IDSE sampling nodes.

3.6 Summary

In this study EPANET-MSX was successfully adapted for modeling water age and to quantitatively determine where individual tanks and pipes affected age under the Base scenario. The cumulative distribution function was used to comprehensively examine water age and the age of delivered water was considered at multiple points on the curve to quantitatively compare scenario results. However, metrics calculated based on the 5th day of changed operations may not have been representative of the water age reductions achieved by a scenario due to excessive draining of tanks and their unrealistic reduced volume on the final day of simulation.

Logical controls developed using a 24-hour repeating demand period led to system pressures that had a 24-hour periodicity which made some control points behave as if they were time-based. This demonstrated that in order to create a system model that functions in the same way operators would control it, a modeler should strive to create a model that represents a general condition, not a particular 24-hour period. In the Gwinnett County system, the majority of scenarios did not have drastic effects on system

pressure so the timing of tank filling and draining tanks was unchanged for several tanks across simulations.

The Base simulation showed Areas on the edges of the Gwinnett network and furthest from the Lanier Filter Plant tended to have the highest water age. These results were in agreement with previous water age modeling efforts of the GCWDS. Aging of water in the Gwinnett County system under the base modeled day was due predominantly to the pipe layout and demand while storage of water in tanks affected the age of only 12% of delivered water. This water was delivered at the edges of the network and appeared to come mainly from the Lanier Mountain tanks. In the Base model 90% of demand was supplied by water with an age less than or equal to 2.2 days and five percent of the demand was supplied with water with an age greater than 3.7 days. Transient pressures below 20 PSI occurred sporadically in the Base scenario and were often due to local flow instabilities caused the approach used to model variable speed pumps.

Alternative Operational Scenarios

Of the eleven scenarios examined, five reduced the variability of the delivered water age by 8 hours or more: Closing one of the Grayson tanks, closing the Medlock Bridge and Goshen Springs tanks, increasing the central pressures at night and decreasing them during the day, reducing the volume of all tanks by 30%, and reducing the volume of only large tanks by 30%.

Closure of one of the Grayson tanks was the only scenario that reduced the maximum water age by more than 24 hours. Closing one Grayson tank led to a reduction in the age of 8% the delivered water by more than 3 hours and decreased the total system storage by 16%. However, this was accomplished through the reduced use of the Lanier

Mountain tanks. Closure of the Medlock Bridge/Goshen Springs tanks reduced system storage by 4 MG (7%). Maximum water age was reduced by only 1 hour by removal of these tanks, but the system-wide water age was improved. Low system pressures were observed between 10-11am and 4-5pm on the 5th day of simulation of this scenario.

The scenarios where the volumes of tanks were reduced showed the highest potential for reducing the 90% range of the age of delivered water. When the volumes of the three largest system tanks were reduced, total system storage was reduced by 21% and the maximum delivered water age was decreased by 7 hours. When all tank volumes were decreased by 30%, the maximum delivered water age was reduced by 8 hours.

Changing central pressures appeared to provide more operational flexibility of some system tanks and led to a reduction in maximum water age. Although the twice-daily adjustments made to the central pressures in the PRV-2 reduced the maximum water age by 6 hours more than the PRV-1 scenario, PRV-1 reduced the age of a greater amount of the delivered water. PRV-1 affected the water age of the most consumed water of all the operational scenarios and reduced the age of 18% the delivered water by more than 3 hours.

The Combined scenario that included the Medlock Bridge and Goshen Springs tanks closures, reduction in operational volume of the three largest tanks, and daily adjustment of the central distribution pressures scenario had the main benefit of reducing the maximum delivered water age by nearly one day more than noted in individual scenarios. Otherwise this scenario had the same hydraulic benefits and drawbacks of the scenarios from which it was created

In general, simulations indicated that reducing the turnover time of the largest tanks by forcing them to fill and drain did not improve system water quality. When tanks were not being turned over very quickly, they were providing less water to supply system demand. By forcing the tanks to fill and drain, more demand was supplied by older water from the tanks rather than water that had not been subjected to storage, leading to higher system water ages. Operational scenario results highlighted an alternative way to achieve improved water quality in the region of a tank –to avoid storage.

The relationship between the average age of water in a tank versus its turnover time had an R^2 value of 0.63. However, the turnover time of the tanks did not appear to have as strong a correlation with the age of water in the system. Large tanks had a bigger effect on delivered water age than the smaller tanks.

Water quality modeling indicated that the operational scenarios examined did not result in significant DBP reductions in the distribution system. With the exception of the Medlock Bridge location, system characterization results suggested tanks contributed very little to DBP concentrations at IDSE sampling points under the Base scenario. Although this could be the result of the kinetic parameters used in the model not adequately reflecting the actual DBP formation reactions occurring in the distribution system. Operational scenarios decreased DBP concentrations by a maximum of 4.4% at the IDSE sampling points, while free Cl was increased by a maximum of 0.9% over the Base scenario. In addition, alternative management scenarios did not have large affects on the daily operational cost. The two exceptions where the operational cost was increased to may have been caused by the approximations used in the pump efficiency input data.

3.7 Conclusions

This research led to several important findings: First, by applying the system characterization simulations where water in the tanks did not age, a utility can measure the effect that storage tanks have on the quality of delivered water. In the case of Gwinnett county it was determined that the tanks only affected the age of 12% of delivered water on the Base day. This suggested the pipe layout and system demand have greater effects on water age than tank operation in this system. Second, through analyzing data using the cumulative distribution function, it was observed that it is very difficult to change the median age of delivered water in the Gwinnett system; however, focusing the analysis on the top tail of the CDF curve allowed for the determination of operational scenarios that could reduce the age of water delivered to customers receiving water with the longest retention times. The maximum delivered water age on the Base day was 9.1 days, but by changing operation of the distribution system the maximum delivered age was determined to be as low as 7.6 days and as high as 13.0 days. Finally, the percentage of water that had been stored then delivered to Gwinnett county customers was small (10.8%), but was predominantly received by model nodes furthest from the treatment plant. The water ages at these nodes were lower in alternative scenarios where they received a less water from storage tanks, which indicated changing the hydraulic regime in these areas could lead to reductions in the age of consumed water.

3.8 Perspectives and Suggestions for Future Research

The major benefit of this work to the DWDS research community is the multi-species water quality modeling approach using EPANET MSX software. Currently, no studies that have used the MSX toolkit to model water age have appeared in peer-

reviewed journals, yet the ability to model water age along with DBPs and free chlorine concentration is important for determining the interaction between these variables in distribution systems. The MSX system also allows researchers to determine the source of again in the system. By conducting a few simple simulations at the outset of a project, a modeler can determine the major cause of water quality deterioration and the amount of improvement that may be achieved by fixing it. In this way, efforts could be focused on the most effective courses of action for distributed water quality optimization.

The scenario testing conducted this work was deductive and determined possible ways to approach changing operations to reduce delivered water age. Future work should focus on optimizing these scenarios (closure of 1 Grayson tank, PRV-1, volume reduction of large tanks) for maximum water age and DBP reduction and to ensure the hydraulic needs of the system are met. In this study one possible combination of the most successful scenarios was examined. Several other combinations are possible and results from simulations of other combinations of the five best scenarios identified could also provide interesting insight into the DWDS and guide future operational strategies.

Results were based on the response of the logic-controlled model developed for this system. While they were an improvement over time-based controls, the logic-based model had shortcomings that may have affected the observed results. Further development of logical controls may improve the utility of the hydraulic model to forecast system water quality and the operations that could be used to optimize them. By creating more robust filling rules and relying on controls that reproduce a set of general guidelines rather than the specific operations noted over a certain time period, the usefulness of this model for further studies could be improved.

As the GCWDS is very large, it could be divided into zones and simulated on a zone-by-zone basis. Since the problem zones of the DWDS have been established, models of the extreme south, west, and east portions of the network could be the focus of further research. This approach would allow for a more detailed hydraulic analysis and may provide solid data for the utility to use in determining ways to ameliorate the water quality in problem areas of the network. In addition, it would be beneficial to collect detailed data on the disinfection byproduct kinetics in the GCWDS to improve the validity of future water quality modeling studies.

Of the system tanks examined, the Bogan tank showed interesting results since it was operated in a flow-though manner. System characterization scenarios showed the Bogan tank did not have any effect on the delivered water age and its turnover time remained the same (1 day) in nearly each operational scenario tested. This indicated operating other tanks in a flow through manner may also improve water age, especially in the areas near the Lanier Mountain tanks. Flow-through operation has the benefit of added tank mixing to avoid stagnation while providing demand and emergency storage. Since the Lanier Mountain tanks are ground storage tanks, flow-through operation may be feasible although significant tank retrofitting would be required. Because there are three large tanks at this location, further consideration would need to be given to exactly how optimal flow-through operation might be achieved. Further investigation into this topic could prove interesting

While this study focused on operational changes, results suggested the physical layout of the system caused the majority of water aging in the Gwinnett County system. Since pipe layout was found to be a significant cause of water aging, physical changes

such as valving or pipe looping should be explored for the greatest reduction in delivered water age. The hydraulic model developed herein could be used to simulate possible physical changes and assess their ability to improve delivered water age. Studies using evolutionary algorithms have found that closing a few pipes in a network with excess carrying capacity produced an overall reduction of water age in the test network (Prasad and Walters, 2006). This approach could prove to be challenging to apply, given the size of the Gwinnett system, but may deliver the greatest improvement in delivered water quality.

REFERENCES

Amburgey, J. E. (2002). Improving Filtration for Removal of Cryptosporidium Oocysts and Particles from Drinking Water. Civil and Environmental Engineering. Atlanta, GA, Georgia Institute of Technology: 326.

American Public Health Association, American Water Works Association and Water Pollution Control Federation (1998). Standard Methods for the Examination of Water and Wastewater, 20th edition. Washington, DC, American Public Health Association.

American Type Culture Collection. Manassas, VA

American Water Works Association and American Water Works Association Research Foundation (1992). Water Industry Database: Utility Profiles. Denver, CO, AWWA.

Amirtharajah, A. and K. M. Mills (1982). "Rapid-Mix Design for Mechanisms of Alum Coagulation." Journal of the American Water Works Association 74(4): 210-216.

Arniella, E. F. (2007). Demand Allocation for the Gwinnett County, GA, Hydraulic and Water Quality Model Setup. World Environmental and Water Resources Congress, Tampa, FL, ASCE.

Arrowood, M. J. and K. Donaldson (1996). "Improved Purification Methods for Calf-Derived Cryptosporidium Parvum Oocysts Using Discontinuous Sucrose and Cesium Chloride Gradients." Journal Eukaryotic Microbiology 43(5): 89S.

Assavasilavasukul, P., B. L. Lau, G. W. Harrington, R. M. Hoffman and M. A. Borchardt (2008). "Effect of Pathogen Concentrations on Removal of Cryptosporidium and Giardia by Conventional Drinking Water Treatment." Water Research 42(10-11): 2678-2690.

AWWA (2005). Computer Modeling of Water Distribution Systems. AWWA Manual M32. Denver, CO, American Water Works Association: 159.

Bielmeier, S. R., D. S. Best, D. L. Guidici and M. G. Narotsky (2001). "Pregnancy Loss in the Rate Caused by Bromidichloromethane." Toxicological Sciences 59(2): 309-315.

Booth, F. (1950). "The Cataphoresis of Spherical, Solid Non-Conducting Particles in a Symmetrical Electrolyte." Proceedings of the Royal Society of London. Series A. Mathematical and Physical Sciences 203: 514-533.

Boulos, P. F., M. Moore, P. Hsiung and D. Thomas (2001). Optimal Pump Operation of Water Distribution Systems Using Genetic Algorithms. AWWA Distribution System Symposium, Denver, CO, American Water Works Association.

Brandt, M. J. (2007). Managing Distribution Retention Time to Improve Water Quality-Phase Ii: Guidance Manual. Denver, CO, AWWARF.

Brown, R. A. and D. A. Cornwell (2007). "Using Spore Removal to Monitor Plant Performance for Cryptosporidium Removal." Journal of the American Water Works Association 99(3): 95-109.

Brush, C. F., M. F. Walter, L. J. Anguish and W. C. Ghiorse (1998). "Influence of Pretreatment and Experimental Conditions on Electrophoretic Mobility and Hydrophobicity of Cryptosporidium Parvum Oocysts." Applied and Environmental Microbiology 64(11): 4439-4445.

Bull, R. J. and R. C. Kopfler (1991). Health Effects of Disinfectants and Disinfection by-Products. Denver, CO, AWWARF.

Bundy, J. (2001). Disinfection by-Product Analysis and Modeling in the Gwinnett County, Georgia, Water Distribution System. Civil and Environmental Engineering. Atlanta, GA, Georgia Institute of Technology: 176.

Bunn, S. (2006). Pump Scheduling Optimization in Four US Cities: Case Studies. 8th Annual Water Distribution Systems Analysis Symposium, Cincinnati, OH ASCE.

Burlingame, G. and G. Brock (1985). "Water-Quality Deterioration in Treated-Water Storage Tanks." Journal of the American Water Works Association 77(4): 60.

Centers for Disease Control and Prevention DPDx. (2008). "Cryptosporidiosis." Retrieved January 16, 2009, from http://www.dpd.cdc.gov/dpdx/HTML/Cryptosporidiosis.htm.

Chadderton, R. A., G. L. Christensen and P. Henry-Unrath (1992). Implementation and Optimization of Distribution Flushing Programs. Denver, CO, AWWARF: 88.

Chadderton, R. A., G. L. Christensen and P. Henry-Unrath (1993). "Planning a Distribution System Flushing Program." Journal of the American Water Works Association 85(7): 89-94.

Cheung, P. B. (2006). Computational Tools for Water Quality Modeling in Hydraulic Networks Calibration Model. Bordeaux, Hydraulic and Civil Engineering Research Unit, CEMAGREF: 24.

Clark, R. M., W. M. Grayman, R. M. Males and A. F. Hess (1993). "Modeling Contaminant Propigation in Drinking Water Distribution Systems." Journal of Environmental Engineering-ASCE 119(2): 349-364.

Cleasby, J. L. and G. S. Logsdon (1999). Granular Bed and Precoat Filtration. Water Quality and Treatment. R. D. Letterman. New York, McGraw-Hill, Inc.: 8.1-8.98.

Committee on Public Water Supply Distribution Systems, National Research Council (2006). Drinking Water Distribution Systems: Assessing and Reducing Risks. Washington, DC, National Academy of Sciences.

Cromeans, T. L., X. Lu, D. D. Erdman, C. D. Humphrey and V. R. Hill (2008). "Development of Plaque Assays for Adenoviruses 40 and 41." Journal of Virological Methods 151(1): 140-145.

Cromeans, T., H. A. Fields and M. D. Sobsey (1989). "Replication Kinetics and Cytopathic Effect of Hepatitis a Virus." Journal of General Virology 70: 2051-2062.

Dai, X. J. and R. M. Holzalski (2003). "Evaluation of Microspheres as Surrogates for Cryptosporidium Parvum Oocysts in Filtration Experiments." Environmental Science & Technology 37(5): 1037-1042.

Delgado, A. V., F. Gonzalez-Caballero, R. J. Hunter, L. K. Koopal and J. Lyklema (2007). "Measurement and Interpretation of Electrokinetic Phenomena." Journal of Colloid and Interface Science 309(2): 194-224.

Deshiikan, S. R. and K. D. Papadopoulos (1998). "Modified Booth Equation for the Calculation of Zeta Potential." Colloid and Polymer Science 276(2): 117-124.

Dugan, N. R. and D. J. Williams (2004). "Removal of Cryptosporidium by In-Line Filtration: Effects of Coagulant Type, Filter Loading Rate and Temperature." Journal of Water Supply Research and Technology-AQUA 53(1): 1-15.

Dugan, N. R., K. R. Fox, J. H. Owens, and R. J. Miltner (2001). "Controlling Cryptosporidium Oocysts Using Conventional Treatment." Journal of the American Water Works Association 93(12): 64-76.

Edwards, J. and J. Maher (2008). "Water Quality Considerations for Distribution System Storage Facilities." Journal of the American Water Works Association 100(7): 60-65.

Edzwald, J. K. and J. E. Tobiason (1999). "Enhanced Coagulation: US Requirements and a Braoder View." Water Science and Technology 40(9): 63-70.

Edzwald, J. K. and M. B. Kelley (1998). "Control of Cryptosporidium: from Reservoirs to Clarifiers to Filters." Water Science and Technology 37(2): 1-8.

Edzwald, J. K., J. E. Tobiason, L. M. Parento, M. B. Kelley, G. S. Kaminski, H. J. Dunn and P. B. Galant (2000). "Giardia and Cryptosporidium Removals by Clarification and Filtration under Challenge Conditions." Journal of the American Water Works Association 92(12): 70-84.

Einolf, C. W. and E. L. Carstensen (1967). "Bacterial Conductivity in the Determination of Surface Charge by Microelectrophoresis." Biochimica et Biophysica Acta 148: 506-516.

Emelko, M. B. (2003). "Removal of Viable and Inactivated Cryptosporidium by Dual- and Tri-Media Filtration." Water Research 37(12): 2998-3008.

Emelko, M. B., P. M. Huck and B. M. Coffey (2005). "A Review of Cryptosporidium Removal by Granular Media Filtration." Journal of the American Water Works Association 97(12): 101-115.

Federation of Canadian Municipalities (2003). Water Quality in Distribution Systems: A Best Practice by the National Guide to Sustainable Municipal Infrastructure. Retrieved June 2, 2010, from http://gmf.fcm.ca/files/Infraguide/Potable_Water/Monitor_water_quality_distr_syst_727k.pdf

Gauthier, V., M. C. Besner, B. Barbeau, R. Millette and M. Prevost (2000). "Storage Tank Management to Improve Drinking Water Quality:Case Study." Journal of Water Resources Planning and Management-ASCE 126(4): 221-228.

Gianella, E. (2010). Personal Communication. A. Polaczyk. Atlanta, GA.

Grayman, W. M. (2006). A Quarter of a Century of Water Quality Modeling in Distribution Systems. Water Distribution Systems Analysis Symposium, Cincinnati, OH, WDSA.

Grayman, W. M. and R. M. Clark (1993). "Using Computer Models to Determine the Effect of Storage on Water Quality." Journal of the American Water Works Association 85(7): 67-77.

Grayman, W. M., R. A. Deininger, A. Green, B. F. Boulos, R. W. Bowcock and C. C. Godwin (1996). "Water Quality and Mixing Models for Tanks and Reservoirs." Journal of the American Water Works Association 88(7): 60-73.

Gullick, R. W., M. Lechevallier, R. C. Svindland and M. Friedman (2004). "Occurrence of Transient Low and Negative Pressures in Distribution Systems." Journal of the American Water Works Association 96(11): 52-66.

Haas, C. N., K. French, G. R. Finch and R. K. Guest (2001). Data Review on the Physical/Chemical Removal of Cryptosporidium. Denver, AWWARF: 96.

Hanson, A., G. Kirmeyer, P. Gilmore, S. Banack and C. Huston (2007). "What to Do with Unavoidable Dead Ends." OPFLOW 33(2): 20-23.

Harrington, G. W., I. Xagoraraki, P. Assavasilavasukul and J. H. Standridge (2003). "Effect of Filtration Conditions on Removal of Emerging Waterborne Pathogens." Journal of the American Water Works Association 95(12): 95-104.

Harrington, G., P. Assavasilavasukul, B. Lau, R. Hoffman and M. Borchardt (2007). Effect of Pathogen Removal Concentration on Pathogen Removal in Conventional Surface Water Treatment. Water Quality Technology Conference, Charlotte, NC, AWWA.

Hendricks, D. (2006). Water Treatment Unit Processes: Physical and Chemical. Boca Raton, CRC: 1266.

Hendricks, D. W., W. F. Clunie, G. D. Sturbaum, D. A. Klein, T. L. Champlin, P. Kugrens, J. Hirsch, B. McCourt, G. R. Nordby, M. D. Sobsey, D. J. Hunt and M. J. Allen (2005). "Filtration Removals of Microorganisms and Particles." Journal of Environmental Engineering-ASCE 131(12): 1621-1632.

Henry, D. C. (1931). "The Cataphoresis of Suspended Particles. Part I: The Equation of Cataphoresis." Proceedings of the Royal Society of London. Series A, Containing Papers of a Mathematical and Physical Character 133(821): 106-129.

Hong, Y. and D. G. Brown (2008). "Electrostatic Behavior of the Charge-Regulated Bacterial Cell Surface." Langmuir 24(9): 5003-5009.

Huck, P. M., B. M. Coffey, M. B. Emelko, D. D. Maurizio, R. M. Slawson, W. B. Anderson and J. Van Den Oever (2002). "Effects of Filter Operation on Cryptosporidium Removal." Journal of the American Water Works Association 94(6): 97-111.

Huque, M. F. (1988). "Experiences with Meta-Analysis in NDA Submissions." Proceedings of the Biopharmaceutical Section of the American Statistical Association 2: 28-33.

Johnson, P. N. and A. Amirtharajah (1983). "Ferric-Chloride and Alum as Single and Dual Coagulants." Journal of the American Water Works Association 75(5): 232-239.

Keck, C. M. (2006). Cyclosporine Nanosuspensions: Optimised Size Characterisation & Oral Formulations. Biology, Chemistry, and Pharmacy. Berlin, Free University of Berlin.

Kennedy, M. S., S. Moegling, S. Sarikelle and K. Suravallop (1993). "Assessing the Effects of Storage Tank Design on Water Quality." Journal of the American Water Works Association 85(7): 78-88.

Kight, J. (2008). Personal Communication. A. Polaczyk. Buford, GA.

Kim, J. , Y. Park and J. E. Amburgey (2006). Lanier Filter Plant Treatment Process and Distribution System Study.

Kirmeyer, G. J., M. Friedman, J. Clement, A. Sandvig, P. F. Noran, K. D. Martel, D. Smith, M. Lechevallier, C. Volk and E. Antoun (2000). Guidance Manual for

Maintaining Distribution System Water Quality. Project #357. AWWA. Denver, CO.

Lawler, D. F.&M. M. Benjamin 2003. Granular Media Filtration. Water Quality Engineering: Physical and Chemical Treatment Processes, McGraw-Hill: 896.

Laptos, K. (2009). Personal Communication. A. Polaczyk. Charlotte, NC.

LeChevallier, M. W. and K. K. Au (2004). Water Treatment and Pathogen Control: Process Efficiency in Achieving Safe Drinking Water. London, Published on behalf of the World Health Organization by IWA Publishing.

LeChevallier, M. W., W. D. Norton and R. G. Lee (1991). "Giardia and Cryptosporidium spp. in Filtered Drinking Water Supplies." Applied and Environmental Microbiology 57(9): 2617-2621.

Letterman, R. D., A. Amirtharajah and C. R. O'Melia (1999). Coagulation and Flocculation. Water Quality and Treatment. R. D. Letterman. New York, McGraw-Hill, Inc.: 6.2-6.66.

Lide, D. R., Ed. (2004). CRC Handbook of Chemistry and Physics, 84th Edition. Boca Raton, CRC Press: 2616.

Lopez-Garcia, J. J., C. Grosse and J. Horno (2007). "A New Generalization of the Standard Electrokinetic Model." Journal of Physical Chemistry B 111(30): 8985-8992.

Lopez-Garcia, J. J., C. Grosse and J. Horno (2009). "On the use of the Stern-Layer and the Charged-Layer Formalisms for the Interpretation of Dielectric and Electrokinetic Properties of Colloidal Suspensions." Journal of Colloid and Interface Science 329(2): 384-389.

Lyklema, J. and M. Minor (1998). "On Surface Conduction and Its Role in Electrokinetics." Colloids and Surfaces A-Physicochemical and Engineering Aspects 140(1): 33-41.

Lytle, D. A., C. H. Johnson and E. W. Rice (2002). "A Systematic Comparison of the Electrokinetic Properties of Environmentally Important Microorganisms in Water." Colloids and Surfaces B-Biointerfaces 24(2): 91-101.

Malvern Instruments Ltd. (2007). Zetasizer Nano User Manual. MAN0317 Issue 3.0. Malvern, UK.

Malvern Instruments Ltd. (2008). Simplifying the Measurement of Zeta Potential Using M3-PALS. Worcestershire, Malvern Instruments Ltd.

Malvern Instruments Ltd. (2010). The Accuracy and Precision Expected from Dynamic Light Scattering Measurements. Worcestershire, Malvern Instruments Ltd.

Mangelsdorf, C. S. and L. R. White (1990). "Effects of Stern-Layer Conductance on Electrokinetic Transport Properties of Colloidal Particles." Journal of the Chemical Society, Faraday Transactions 86(16): 2859-2870.

Mangelsdorf, C. S. and L. R. White (1998). "The Dynamic Double Layer Part 1: Theory of a Mobile Stern Layer." Journal of the Chemical Society, Faraday Transactions 94(16): 2441-2452.

Martell, K. D., G. J. Kirmeyer, B. M. Murphy, P. F. Noran, L. Kirby, T. W. Lund, J. L. Anderson, R. Medhurst and M. Caprara (2002). "Preventing Water Quality Deterioration in Finished Water Storage Facilities." Journal of the American Water Works Association 94(4): 139-148.

Mazounie, P., F. Bernazeau and P. Alla (2000). "Removal of Cryptosporidium by High Rate Contact Filtration: The Performance of the Prospect Water Filtration Plant During the Sydney Water Crisis." Water Science and Technology 41(7): 93-101.

Moncho, A., F. Martinez-Lopez and R. Hidalgo-Alvarez (2001). "Comparative Study of Theories of Conversion of Electrophoretic Mobility into Zeta-Potential." Colloids and Surfaces a-Physicochemical and Engineering Aspects 192(1-3): 215-226.

Montgomery, D. C. and E. A. Peck (1982). Introduction to Linear Regression Analysis. New York, John Wiley & Sons: 504.

Mosley, L.M., K.A. Hunter, and W.A. Ducker (2003). "Forces between Colloid Particles in Natural Waters." Environmental Science and Technology 37(15): 3303-3308.

Murphy, L. J., G. C. Dandy and A. R. Simpson (1994). Optimum Design and Operation of Pumped Water Distribution Systems. International Conference on Hydraulics in Civil Engineering, University of Queensland-Brisbane.

Nieminski, E. C. and J. E. Ongerth (1995). "Removing Giardia and Cryptosporidium by Conventional Treatment and Direct Filtration." Journal of the American Water Works Association 87(9): 96-106.

Nitivattananon, V., E. C. Sadowski and R. G. Quimpo (1996). "Optimization of Water Supply System Operation." Journal of Water Supply Research and Technology-AQUA 122(5): 374-384.

O'Brien, R. W. and L. R. White (1978). "Electrophoretic Mobility of a Spherical Colloidal Particle." Journal of the Chemical Society-Faraday Transactions II 74 1607-1626.

O'Brien, R. W. and R. J. Hunter (1981). "The Electrophoretic Mobility of Large Colloidal Particles." Canadian Journal of Chemistry 59: 1878-1887.

Ohshima, H. (1994). "A Simple Expression for Henry's Function for the Retardation Effect in Electrophoresis of Spherical Colloidal Particles." Journal of Colloid and Interface Science 168(1): 269-271.

Ohshima, H. (2000a). "Electrophoretic Mobility of Soft Particles in Concentrated Suspensions." Journal of Colloid and Interface Science 225(1): 233-242.

Ohshima, H. (2000b). "On the General Expression for the Electrophoretic Mobility of a Soft Particle." Journal of Colloid and Interface Science 228(1): 190-193.

Ohshima, H. (2001). "Electrokinetic Phenomena in a Concentrated Suspension of Soft Particles." Colloids and Surfaces a-Physicochemical and Engineering Aspects 195(1-3): 129-134.

Ohshima, H. (2006). "Electrophoresis of Soft Particles: Analytic Approximations." Electrophoresis 27(3): 526-533.

O'Melia, C. R. and W. Stumm (1967). "Theory of Water Filtration." Journal of the American Water Works Association 59(11): 1393.

Ongerth, J. E. and J. P. Pecoraro (1995). "Removing Cryptosporidium Using Multimedia Filters." Journal of the American Water Works Association 87(12): 83-89.

Patania, N. L., J. G. Jacangelo, L. Cummings, A. Wilczak, K. Riley and J. Oppenheimer (1995). Optimization of Filtration for Cyst Removal. Project # 703. Denver, CO, American Water Works Research Foundation.

Pennington, R. and T. Jakubowski (2007). "Stop Leaks, Save Money: A Comprehensive Leak-Detection Study Resulted in Fast Revenue Recovery for Gwinnett County, GA." OPFLOW 33(5)16-17.

Prasad, T. D. and G. A. Walters (2006). "Minimizing Residence Time by Rerouting Flows to Improve Water Quality in Distribution Networks." Engineering Optimization 38(8): 923-939.

Prasanthi, H., S. Vigneswaran, and H.B. Dharmappa (1997). “Effect of Particle Concentration on the Entire Cycle of Filtration. Water Science and Technology 35(8) 91-102.

Qian, S. S., M. Donnelly, D. C. Schmelling, M. Messner, K. G. Linden and C. Cotton (2004). "Ultraviolet Light Inactivation of Protozoa in Drinking Water: A Bayesian Meta-Analysis." Water Research 38(2): 317-326.

Ranucci, L., H. M. Muller, G. Larosa, I. Reckmann, M. A. Gomez-Morales, F. Spano, E. Pozio and A. Crisanti (1993). "Characterization and Immunolocalization of a Cryptosporidium Protein Containing Repeated Amino Acid Motifs." Infection and Immunity 61(6): 2367-2356.

Rawlings, J. O., S. G. Pantula and D. A. Dickey (1998). Applied Regression Analysis: A Research Tool. New York, New York, Springer-Verlag.

Rossman, L. A. (2000). EPANET 2 Users Manual. Cincinnati, OH, U.S. Environmental Protection Agency, National Risk Management Research Laboratory,Office of Research and Development: 200.

Sennett, P. and J. P. Oliver (1965). "Colloidal Dispersions, Electrokinetic Effects, and the Concept of Zeta Potential." Journal of Industrial and Engineering Chemistry 57(8): 33-49.

Shang, F., J. G. Uber and L. A. Rossman (2008a). Epanet Multi-Species Extension User's Manual. Cincinnati, OH, US Environmental Protection Agency: 115.

Shang, F., J. G. Uber and L. A. Rossman (2008b). "Modeling Reaction and Transport of Multiple Species in Water Distribution Systems." Environmental Science & Technology 42(3): 808-814.

Shi, W., B. A. D. Stocker and J. Adler (1996). "Effect of the Surface Composition of Motile Escherichia Coli and Motile Salmonella Species on the Direction of Galvanotaxis." Journal of Bacteriology 178(4): 1113-1119.

Singer, P. C. (1994). "Control of Disinfection By-Products in Drinking Water." Journal of Environmental Engineering-ASCE 120(4): 727-744.

Speight, V. and F. A. DiGiano (2003). Water Quality Models for Anlaysis of Small System Operation: Case Study of Carthage, NC. World Water and Environmental Resource Congress, Philadelphia, PA.

States, S., R. Tomko, M. Scheuring and L. Casson (2002). "Enhanced Coagulation and Removal of Cryptosporidium." Journal of the American Water Works Association 94(11): 67-77.

Stumm, W. and J. J. Morgan (1996). Aquatic Chemistry. Third Edition. New York, New York, Wiley Interscience.

Swertfeger, J., D. H. Metz, J. Demarco, A. Braghetta and J. G. Jacangelo (1999). "Effect of Filter Media on Cyst and Oocyst Removal." Journal of the American Water Works Association 91(9): 90-100.

The Mathworks MATLAB. Natick, MA.

The SAS Institiute Inc. (2007). The REG. Procedure Model Statement. Cary, NC.

Toader, V. (2009). Pump Efficiencies and Energy Tariffs. A. Polaczyk. Charlotte.

U.S. Army Center for Health Promotion and Preventative Medicine (1997). Maintaining High Drinking Water Quality in Finished Water Storage Tanks and Reservoirs:

USACHPPM Information Paper No. IP 31-019. Aberdeen Proving Ground, MD, U.S. ARMY.

USEPA (1998). National Primary Drinking Water Regulations: Disinfectants and Disinfection by-Products; Final Rule. Federal Register. 63: 69389-69476.

USEPA (2002a). Effects of Water Age on Distribution System Water Quality. Office of Water. Retrieved June 2, 2010, from http://www.epa.gov/ogwdw/disinfection/tcr/pdfs/whitepaper_tcr_waterdistribution.pdf

USEPA (2002b). Finished Water Storage Facilities. Office of Water. Retrieved June 2, 2010, from http://www.epa.gov/ogwdw/disinfection/tcr/pdfs/whitepaper_tcr_storage.pdf

USEPA (2005). Occurrence and Exposure Assessment for the Final Long Term 2 Enhanced Surface Water Treatment Rule. Office of Water. EPA 815-R-06-002 (4606-M).

USEPA. (2006). "Stage 2 Disinfectants and Disinfection Byproduct Rule (Stage 2 DBP Rule)." Retrieved September 15, 2007, from http://www.epa.gov/safewater/disinfection/stage2/index.html.

USEPA. (2007a). The Long Term 2 Enhanced Surface Water Treatment Rule (LT2 Rule) State Implementation Guidance. EPA 816-R-07-006

USEPA. (2007b). "Drinking Water Contaminants." Retrieved October 15, 2007, from http://www.epa.gov/safewater/contaminants/index.html.

USEPA (2007c). Simultaneous Compliance Guidance Manual for the Long Term 2 and Stage 2 DBP Rules. Washington, US EPA: 462.

USEPA. (2007d). "Stage 2 Disinfectants and Disinfection Byproduct Rule (Stage 2 DBP Rule): Initial Distribution System Evaluation Guidance Manual." Retrieved September 15, 2007, from (http://www.epa.gov/safewater/disinfection/stage2/compliance_idse.html.

Van Benschoten, J.E. and J.K. Edzwald. (1990) "Chemical Aspects of Coagulation Using Aluminum Salts – I. Hydrolytic reactions of Alum and Polyaluminum Chloride." Water Research 24(12): 1519-1526.

Van Benschoten, J.E., J.K. Edzwald, and M.A. Rahman. (1992) "Effects of Temperature and pH on Residual Aluminum for Alum and Polyaluminum Coagulants." Water Supply 10(4):49-54.

Van Der Wal, A., M. Minor, W. Norde, A. J. B. Zehnder and J. Lyklema (1997). "Electrokinetic Potential of Bacterial Cells." Langmuir 13(2): 165-171.

Van Loosdrecht, M. C. M., J. Lyklema, W. Norde, G. Schraa and A. J. B. Zehnder (1987). "Electrophoretic Mobility and Hydrophobicity as a Measure to Predict the Initial Steps of Bacterial Adhesion." Applied and Environmental Microbiology 53(8): 1898-1901.

Waller, K., S. H. Swan, G. Delorenze and B. Hopkins (1998). "Trihalomethanes in Drinking Water and Spontaneous Abortion." Epidemiology 9(2): 134-140.

Walski, T. M. (2007). Personal Communication. A. Polaczyk.

Walski, T. M., D. V. Chase, D. A. Savic, W. Grayman, S. Beckwith and E. Koelle (2003). Advanced Water Distribution Modeling and Management. Waterbury, CT, Bentley Institute Press.

Water Supply Committee of the Great Lakes--Upper Mississippi River Board of State and Provincial Public Health and Environmental Managers (2007). Recommended Standards for Water Works: Policies for the Review and Approval of Plans and Specifications for Public Water Supplies. Albany, Health Research, Inc. Retrieved June 2, 2010, from http://10statesstandards.com/waterstandards.html

Williams, D. J. and N. R. Dugan (2003). Removal of Crytposporidium by in-Line Filtration as a Function of Oocyst Age and Preservation Method. Water Quality Technology Conference, Philadelphia, PA, AWWA.

Wilson, W. W., M.M. Wade, S. C. Holman and F. R. Champlin (2001). "Status of Methods for Assessing Bacterial Cell Surface Charge Properties Based on Zeta Potential Measurements." Journal of Microbiological Methods 43(3): 153-164.

Xagoraraki, I., G. W. Harrington, P. Assavasilavasukul and J. H. Standridge (2004). "Removal of Emerging Waterborne Pathogens and Pathogen Indicators by Pilot-Scale Conventional Treatment." Journal of the American Water Works Association 96(5): 102-113.

Yao, K. M., M. T. Habibian and C. R. O'Melia (1971). "Water and Wastewater Filtration: Concepts and Applications." Environmental Science and Technology 5(11): 1105.

Yates, R. S. (1997). Optimizing Direct Filtration Processes for Cryptosporidium Removal. Water Quality Technology Conference, Denver.

Yunus, Z., V. Mason, C. E. Verduzco-Luque and G. H. Markx (2002). "A Simple Method for the Measurement of Bacterial Particle Conductivities." Journal of Microbiological Methods 51(3): 401-406.

Zukoski, C. F. and D. A. Saville (1986). "The Interpretation of Electrokinetic Measurements Using a Dynamic Model of the Stern Layer." Journal of Colloid and Interface Science 114(1): 32-44.

APPENDIX A: FIRST ORDER DERIVATIVES OF ZETA POTENTIAL EQUATIONS

Helmholtz-Smoluchowski: $$\frac{\partial \zeta}{\partial u_e} = \frac{\eta}{\varepsilon_{rs}\varepsilon_0}$$

Henry: $$\frac{\partial \zeta}{\partial u_e} = \frac{3\eta}{2\varepsilon_{rs}\varepsilon_0 f(\kappa\alpha)}$$

Hückel-Onsager: $$\frac{\partial \zeta}{\partial u_e} = \frac{3\eta}{2\varepsilon_{rs}\varepsilon_0}$$

O'Brien and Hunter:

$$\frac{\partial \zeta}{\partial u_e} = \frac{kT}{e} * \left(7520 \Big/ \left(\frac{3}{2} - \frac{\left[3 + 6\ln 2\left(-e^x\right)\right] * \left(2 + b\exp\left(\frac{x}{2}\right)\right) - \left[\frac{1}{2} b\exp\left(\frac{x}{2}\right)\right] * \left(3x + 6\ln 2 * \left(1 - \exp(x)\right)\right)}{\left(2 + b\exp\left(\frac{x}{2}\right)\right)^2} \right) \right)$$

where:

$$b = \frac{\kappa\alpha}{1.552} \quad \text{and} \quad x = \frac{e\zeta}{kT}$$

Modified Booth:

$$\frac{\partial \zeta}{\partial u_e} = 7520 * \left(25.7 * \left(\frac{1}{f_1} - \left[\frac{\left(\left(3C_3 * \frac{E^2}{f_1^3} \right) + 4C_4 * \frac{E^3}{f_1^4} \right) * \left(f_1 + 3C_3 \left(\frac{E}{f_1} \right)^2 + 4C_4 \left(\frac{E}{f_1} \right)^3 \right) - \left(6C_3 * \left(\frac{E}{f_1^2} \right) + 12C_4 * \left(\frac{E^2}{f_1^3} \right) \right) * \left(C_3 \left(\frac{E}{f_1} \right)^3 + \right)}{\left(f_1 + 3C_3 \left(\frac{E}{f_1} \right)^2 + 4C_4 \left(\frac{E}{f_1} \right)^3 \right)^2} \right] \right) \right)$$

where

$$C_3 = z^2 f_3^*(\kappa\alpha) + 38.6z \left[\frac{1}{\Lambda_+^0} + \frac{1}{\Lambda_-^0} \right] Z_3^*(\kappa\alpha) \qquad C_4 = 38.6z^2 \left[\frac{1}{\Lambda_+^0} - \frac{1}{\Lambda_-^0} \right] Z_4^*(\kappa\alpha)$$

$E = 7520u_e$ where u_e is expressed in cm^2/Vs

f_1 is the Henry function and f_3^*, Z_3^*, and Z_4^* are the Booth relaxation functions for a given $\kappa\alpha$

APPENDIX B: RELATIONSHIP BETWEEN OOCYST SPIKE CONCENTRATION AND LOG REMOVAL

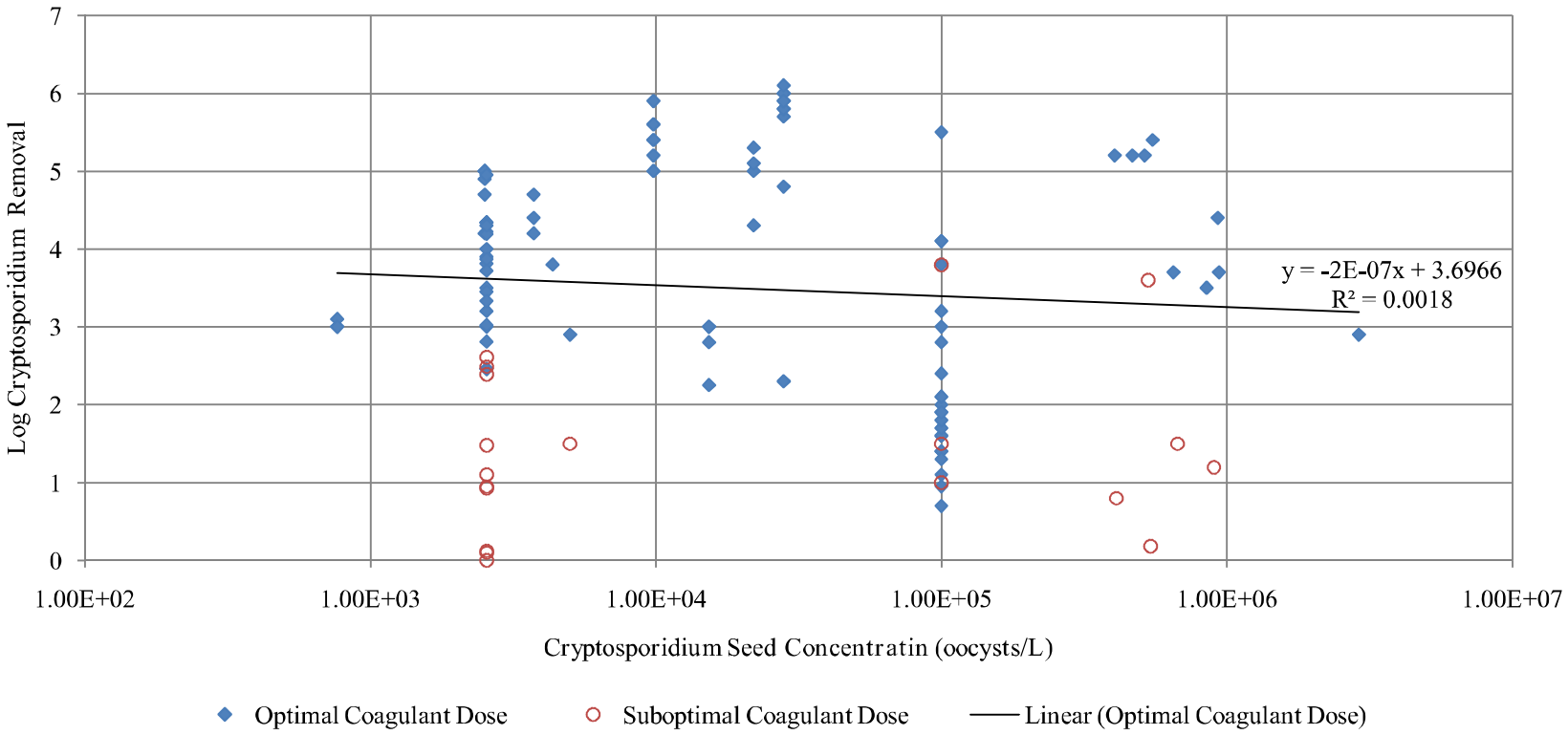

APPENDIX C: META-ANALYSIS DATABASE

Treatment Train: C = conventional, D = direct, I = inline
Portion of Filter Run: SS=steady state, (E)BT= (Early) breakthrough
Method:

1. Vacuum filtration/ IFA
2. Cytometry
3. IFA- Std. Methods. Sect. 9711A
4. 1622 CEC
5. Vacuum filtration, removal from membrane, centrifugation, then IFA
6. 1623 - IDEXX Genera Filter-Max and FM. Typically achieved 25% recovery
7. ICR - yarn wound filters

Obs #	Source	Treatment Train	Log Removal	Alum (mg/L)	FeCl (mg/L)	PACl (mg/L)	Total Metal Ion (mg/L)	Polymer (mg/L)	Coag. pH	Temp. (°C)	pOH	Infl. Turb (NTU)	Effl. Turb (NTU)	Filtration rate (m/h)	Raw TOC (mg/L)	Depth 1 (cm)	Depth 2 (cm)	Effective size 1 (mm)	Effective size 2 (mm)	Portion of filter run	Optimal Coag. dose?	Method
80	Amburgey, 2002	D	1.8		0.7	1.35	0.1	1.35	7	11	7.5	2.3	0.05	7.3	2	122	30	1.4	0.55	SS	Y	1
81	Amburgey, 2002	D	1.9		0.7	1.35	0.1	1.35	7	11	7.5	2.3	0.05	7.3	2	122	30	1.4	0.55	SS	Y	1
82	Amburgey, 2002	D	1.9		0.7	1.35	0.1	1.35	7	11	7.5	2.3	0.05	7.3	2	122	30	1.4	0.55	SS	Y	1
83	Amburgey, 2002	D	1.6		0.6	1.25	0.1	1.25	6.7	24	7.3	1.8	0.1	7.3	2	122	30	1.4	0.55	SS	Y	1
84	Amburgey, 2002	D	1.6		0.6	1.25	0.1	1.25	6.7	24	7.3	1.8	0.1	7.3	2	122	30	1.4	0.55	SS	Y	1
85	Amburgey, 2002	D	1.7		0.6	1.25	0.1	1.25	6.7	24	7.3	1.8	0.1	7.3	2	122	30	1.4	0.55	SS	Y	1
401	Amburgey, 2002	D	1.5		0.46	1	0.1	1	7.3	25	6.7	1.6	0.18	12.2	2	122	30	1.4	0.55	SS	N	1
17	Dugan & Williams, 2004	I	3.2	20			1.8	0	7.4	20	6.8	0.22	0.082	10	2.2	51	25	1	0.44	SS	Y	2
18	Dugan & Williams, 2004	I	2.8	20			1.8	0	7.9	4.5	6.8	0.22	0.11	5	1.9	51	25	1	0.44	SS	Y	2
68	Dugan & Williams, 2004	I	4.1		10		2.1	0	7.6	4.5	7.1	0.26	0.24	5	2.3	51	25	1	0.44	SS	Y	2
70	Dugan & Williams, 2004	I	4.1		10		2.1	0	7.9	20	6.3	0.2	0.071	5	2.1	51	25	1	0.44	SS	Y	2
502	Dugan & Williams, 2004	I	1.1	20			1.8	0		4.5		0.28	0.38	10		51	25	1	0.44	EBT	Y	2

Obs #	Source	Treatment Train	Log Removal	Alum (mg/L)	FeCl (mg/L)	PACl (mg/L)	Total Metal Ion (mg/L)	Polymer (mg/L)	Coag. pH	Temp. (°C)	pOH	Infl. Turb (NTU)	Effl. Turb (NTU)	Filtration rate (m/h)	Raw TOC (mg/L)	Depth 1 (cm)	Depth 2 (cm)	Effective size 1 (mm)	Effective size 2 (mm)	Portion of filter run	Optimal Coag. dose?	Method
503	Dugan & Williams, 2004	1	1.4		10		2.1	0		4.5		0.26	0.48	10	1.5	51	25	1	0.44	EBT	Y	2
505	Dugan & Williams, 2004	1	0.95	20			1.8	0		20		0.22	0.15	10	2.2	51	25	1	0.44	BT	Y	2
507	Dugan & Williams, 2004	1	1.9	20			1.8	0		4.5		0.22	0.37	5	1.9	51	25	1	0.44	BT	Y	2
1	Dugan et al, 2001	C	3.7	60			5.4	0		20		23		5		51	25	1	0.44	SS	Y	5
2	Dugan et al, 2001	C	3.5	50			4.5	0		20		103		5		51	25	1	0.44	SS	Y	5
10	Dugan et al, 2001	C	2.9	30			2.7	0		20		88		5		51	25	1	0.44	SS	Y	5
35	Dugan et al, 2001	C	4.4	10			0.9	0		20		19		5		51	25	1	0.44	SS	Y	5
67	Dugan et al, 2001	C	3.7		15		3.1	0		20		28		5		51	25	1	0.44	SS	Y	5
402	Dugan et al, 2001	C	0.18	1			0.1	0		20		2.3		5		51	25	1	0.44	SS	N	5
403	Dugan et al, 2001	C	0.8	5			0.5	0		20		3.1		5		51	25	1	0.44	SS	N	5
404	Dugan et al, 2001	C	1.5	5			0.5	0		20		23		5		51	25	1	0.44	SS	N	5
405	Dugan et al, 2001	C	3.6		4		0.8	0		20		6.1		5		51	25	1	0.44	SS	N	5
406	Dugan et al, 2001	C	1.2	10			0.9	0		20		63		5		51	25	1	0.44	SS	N	5
22	Edzwald & Kelley, 1998	C	4.9	20			1.8	0	6.5	5	8.2	1.9	0.05	7.3	2.8					SS	Y	7
23	Edzwald & Kelley, 1998	C	4.2	20			1.8	0	6.5	5	8.2	1.9	0.05	14.6	2.8					SS	Y	7
58	Edzwald & Kelley, 1998	C	5		17.5		3.6	0	6	5	8.7	1.9	0.05	7.3	2.8					SS	Y	7
59	Edzwald & Kelley, 1998	C	5		17.5		3.6	0	6	5	8.7	1.9	0.05	14.6	2.8					SS	Y	7
71	Edzwald & Kelley, 1998	1	4.7		6	2.4	1.2	2.4	6.5				0.1	7.3						SS	Y	7
40	Emelko, 2003	1	5.2	5			0.5	0	6.9			3.5	0.05	7.5		70	30	1	0.5	SS	Y	1
41	Emelko, 2003	1	5.2	5			0.5	0	6.9			3.5	0.05	7.5		70	30	1	0.5	SS	Y	1
42	Emelko, 2003	1	5.4	5			0.5	0	6.9			3.5	0.06	7.5		65	35	1	0.4	SS	Y	1
43	Emelko, 2003	1	5.2	5			0.5	0	6.9			3.5	0.08	7.5		65	35	1	0.4	SS	Y	1
44	Emelko, 2003	1	4	5			0.5	0	6.9			3.5	0.1	10		70	30	1	0.5	SS	Y	1
104	Harrington et al, 2003	C	2	80			7.2	0	7.35	16	7.0	3.7	0.18	12.3		46	31	1	0.5	SS	Y	2
105	Harrington et al, 2003	C	2.1	70			6.3	0	5.7	12	8.8	8.6	0.1	9.8		46	31	1	0.5	SS	Y	2

Obs #	Source	Treatment Train	Log Removal	Alum (mg/L)	FeCl (mg/L)	PACl (mg/L)	Total Metal Ion (mg/L)	Polymer (mg/L)	Coag. pH	Temp. (°C)	pOH	Inf. Turb (NTU)	Eff. Turb (NTU)	Filtration rate (m/h)	Raw TOC (mg/L)	Depth 1 (cm)	Depth 2 (cm)	Effective size 1 (mm)	Effective size 2 (mm)	Portion of filter run	Optimal Coag. dose?	Method
106	Harrington et al, 2003	C	1.7	70			6.3	0	7	12	7.5	8.6	0.11	9.8		76		1		SS	Y	2
107	Harrington et al, 2003	C	1.8	70			6.3	0	7	12	7.5	8.6	0.1	9.8		38	39	1	0.4	SS	Y	2
108	Harrington et al, 2003	C	1.4	50			4.5	0	7.46	14	6.9		0.16	9.8		46	31	1	0.5	SS	Y	2
501	Harrington et al, 2003	C	0.7	50			4.5	0	7.46	14	6.9		1.7	9.8		46	31	1	0.5	EBT	Y	2
506	Harrington et al, 2003	C	1.3	50			4.5	0	7.46	14	6.9		0.2	9.8		46	31	1	0.5	BT	Y	2
204	Hendricks et al., 2005	I	0	0			0.0	0		7.21984		3.35		12.2		0	0	0	0	SS	Y	3
206	Hendricks et al., 2005	I	0.124367	0			0.0	0		7.15433		4.12		12.2		0	0	0	0	SS	Y	3
211	Hendricks et al., 2005	I	2.81	26			2.3	0	6.4674	8.04371	8.1	3.5	0.07	12.2		940	0	0.9	0	SS	Y	3
218	Hendricks et al., 2005	I	1.1	0			0.0	0	6.8558	8.92381	7.7	3.24	3.02	12.2		330	330	0.9	0.5	SS	Y	3
219	Hendricks et al., 2005	I	0.95	0			0.0	0	6.839	8.78388	7.7	3.21	2.97	12.2		940	0	0.9	0	SS	Y	3
221	Hendricks et al., 2005	I	0.1	0			0.0	0	6.961	9.52966	7.6	3.35	3.16	12.2		0	0	0	0	SS	Y	3
223	Hendricks et al., 2005	I	3.5	26			2.3	0	6.2832	9.35856	8.3	3.27	0.08	12.2		330	330	0.9	0.5	SS	Y	3
230	Hendricks et al., 2005	I	3.2	26			2.3	0	6.4421	9.04957	8.1	1.16	0.06	12.2		940	0	0.9	0	SS	Y	3
235	Hendricks et al., 2005	I	3.81	26			2.3	0	6.4455	7.29622	8.2	1.07	0.07	12.2		940	0	0.9	0	SS	Y	3
237	Hendricks et al., 2005	I	3.72	26			2.3	0	6.6558	6.33723	8.0	1	0.07	12.2		940	0	0.9	0	SS	Y	3
238	Hendricks et al., 2005	I	3.45	26			2.3	0	6.7108	6.24298	8.0	1.25	0.06	12.2		940	0	0.9	0	SS	Y	3
242	Hendricks et al., 2005	I	1.48	13			1.2	0		4.19145		1.175	0.48	12.2		940	0	0.9	0	SS	N	3
243	Hendricks et al., 2005	I	2.39	13			1.2	0	6.0542	4.20171	8.7	1.142	0.47	12.2		940	0	0.9	0	SS	N	3
244	Hendricks et al., 2005	I	2.49	13			1.2	0	6.0048	2.8293	8.8	1.279	0.49	12.2		330	330	0.9	0.5	SS	N	3
247	Hendricks et al., 2005	I	2.61	13			1.2	0	5.6341	2.463	9.2	1.27	0.82	12.2		940	0	0.9	0	SS	N	3
248	Hendricks et al., 2005	C	0.93	0			0.0	0	8.3394	2.47553	6.5	1.59	1.52	12.2		940	0	0.9	0	SS	Y	3
251	Hendricks et al., 2005	C	4.22	26			2.3	0	5.7723	2.52679	9.0	1.29	0.1	12.2		940	0	0.9	0	SS	Y	3

Obs #	Source	Treatment Train	Log Removal	Alum (mg/L)	FeCl (mg/L)	PACl (mg/L)	Total Metal Ion (mg/L)	Polymer (mg/L)	Coag. pH	Temp. (°C)	pOH	Infl. Turb (NTU)	Eff. Turb (NTU)	Filtration rate (m/h)	Raw TOC (mg/L)	Depth 1 (cm)	Depth 2 (cm)	Effective size 1 (mm)	Effective size 2 (mm)	Portion of filter run	Optimal Coag. dose?	Method
252	Hendricks et al., 2005	C	4.34	26			2.3	0	5.8664	2.17947	9.0	1.29	0.09	12.2		940	0	0.9	0	SS	Y	3
256	Hendricks et al., 2005	C	4.34	26			2.3	0	6.0186	2.60055	8.8	1.49	0.15	12.2		940	0	0.9	0	SS	Y	3
258	Hendricks et al., 2005	I	3.9	26			2.3	0	5.5081	3.49249	9.3	1.52	0.08	12.2		940	0	0.9	0	SS	Y	3
260	Hendricks et al., 2005	C	4.95	26			2.3	0	5.5575	3.91868	9.2	1.42	0.09	12.2		940	0	0.9	0	SS	Y	3
262	Hendricks et al., 2005	C	4.19	26			2.3	0	6.1636	5.85956	8.5	1.78	0.08	12.2		940	0	0.9	0	SS	Y	3
264	Hendricks et al., 2005	I	4	26			2.3	0	6.1623	6.51526	8.5	2.293	0.06	12.2		940	0	0.9	0	SS	Y	3
265	Hendricks et al., 2005	I	2.46	26			2.3	0	5.9987	6.66776	8.7	2.712	0.08	12.2		940	0	0.9	0	SS	Y	3
266	Hendricks et al., 2005	I	4.3	26			2.3	0	5.9646	6.60887	8.7	2.543	0.05	12.2		940	0	0.9	0	SS	Y	3
267	Hendricks et al., 2005	I	3	26			2.3	0	5.9761	6.66422	8.7		0.06	12.2		940	0	0.9	0	SS	Y	3
269	Hendricks et al., 2005	I	3.33	26			2.3	0	5.9717	6.74344	8.7	2.72	0.07	12.2		940	0	0.9	0	SS	Y	3
270	Hendricks et al., 2005	I	2.46	26			2.3	0	6.08	6.44484	8.6	2.465	0.07	12.2		940	0	0.9	0	SS	Y	3
271	Hendricks et al., 2005	I	3.02	26			2.3	0	6.03	7.40179	8.6	2.363	0.06	12.2		940	0	0.9	0	SS	Y	3
272	Hendricks et al., 2005	I	3.87	26			2.3	0	5.8393	7.87854	8.8	2.63	0.07	12.2		940	0	0.9	0	SS	Y	3
6	Huck et al, 2002	C	5.5	38			3.4	0	6	13	8.4	1.9	0.03	6.4	5	46	28	1.1	0.52	SS	Y	3
39	Huck et al, 2002	D	3	5		1.5	0.5	1.5	7.9	19	6.3	1.4	0.05	9.8	2.8	51	20	1.1	0.47	SS	Y	3
407	Huck et al, 2002	D	1	2.5		0.75	0.2	0.75		19		1.4	0.16	9.8	2.8	51	20	1.1	0.47	SS	N	3
408	Huck et al, 2002	C	3.8	19			1.7	0		13		1.9	0.2	6.4	5	46	28	1.1	0.52	SS	N	3
504	Huck et al, 2002	C	1.4	38			3.4	0	6	13	8.4	1.9	0.56	6.4	5	46	28	1.1	0.52	EBT	Y	3
508	Huck et al, 2002	C	2.1	38			3.4	0	6	13	8.4	1.9	0.17	6.4	5	46	28	1.1	0.52	BT	Y	3
509	Huck et al, 2002	D	2.4	5		1.5	0.5	1.5	7.9	19	6.3	1.4	0.05	9.8	2.8	51	20	1.1	0.47	BT	Y	3
75	Mazounie et al, 2000	I	3.8		2	0.75	0.4	0.75		19		0.63	0.06	8		210	0	1.8	0	SS	Y	4
33	Nieminski & Ongerth, 1995	C	3	12		1.3	1.1	1.3				23	0.15	14	2.3	51	61			SS	Y	5
38	Nieminski & Ongerth, 1995	D	3	6		3	0.5	3				4	0.15	14	2.3	51	61			SS	Y	5
90	Nieminski &	C	2.25			0.5	2.2	0.5				28	0.15	11.7	1.8					SS	Y	5

Obs #	Source	Treatment Train	Log Removal	Alum (mg/L)	FeCl (mg/L)	PACl (mg/L)	Total Metal Ion (mg/L)	Polymer (mg/L)	Coag. pH	Temp. (°C)	pOH	Inft. Turb (NTU)	Eff. Turb (NTU)	Filtration rate (m/h)	Raw TOC (mg/L)	Depth 1 (cm)	Depth 2 (cm)	Effective size 1 (mm)	Effective size 2 (mm)	Portion of filter run	Optimal Coag. dose?	Method
	Ongerth, 1995																					
91	Nieminski & Ongerth, 1995	D	2.8			0.5	2.2	0.5				2.5	0.15	11.7	1.8					SS	Y	5
34	Ongerth & Pecoraro, 1995	D	2.9	10			0.9	0	6.5	19	7.7	0.39	0.07	12.2		46	37	1.1	0.35	SS	Y	5
409	Ongerth & Pecoraro, 1995	D	1.5	5			0.5	0	6.5	14	7.9	0.56	0.36	12.2		46	37	1.1	0.35	SS	N	5
7	Patania et al, 1995	C	4.2	33		2.3	3.0	2.3		21		4.4	0.13	14.7	3.9	109	13	1.3	0.5	SS	Y	1
8	Patania et al, 1995	C	4.7	33		2.3	3.0	2.3		21		4.4	0.08	7.3	3.9	109	13	1.3	0.5	SS	Y	1
9	Patania et al, 1995	C	4.4	33		2.3	3.0	2.3		21		4.4	0.1	14.7	3.9	109	0	1.3	0	SS	Y	1
13	Patania et al, 1995	C	5	22.1		0.49	2.0	0.49	7.6	20	6.6	12.7	0.04	4.9		37	0	0.5	0	SS	Y	1
36	Patania et al, 1995	C	5.3	7.5		0.41	0.7	0.41	7.8	17	6.5	1.1	0.05	4.9		37	0	0.5	0	SS	Y	1
37	Patania et al, 1995	C	4.3	7.1		0.39	0.6	0.39	7.7	21	6.4	0.9	0.03	6.1		37	0	0.5	0	SS	Y	1
46	Patania et al, 1995	1	3	3		2.1	0.3	2.1	6.35	7	8.3	1.2	0.07	12.2	1.7	203	25	1.25	0.6	SS	Y	1
47	Patania et al, 1995	1	3.1	3		2.1	0.3	2.1	6.35	16	8.0	1.2	0.09	19.6	1.7	203	25	1.25	0.6	SS	Y	1
48	Patania et al, 1995	1	3	3		2.1	0.3	2.1	6.35	16	8.0	1.2	0.09	19.6	1.7	203	25	1	0.5	SS	Y	1
50	Patania et al, 1995	C	5.1		19.9		4.1	0	7.4	22	6.7	9.9	0.05	4.9		37	0	0.5	0	SS	Y	1
60	Patania et al, 1995	C	5.6		15	1	3.1	1	7.1	14	7.3	2.4	0.04	14.7		152	25	1.1	0.5	SS	Y	1
61	Patania et al, 1995	C	5.9		15	1	3.1	1	7.1	14	7.3	2.4	0.04	14.7		152	25	1.1	0.5	SS	Y	1
62	Patania et al, 1995	C	5.4		15		3.1	0	6.7	18	7.5	2.2	0.05	14.7	1.8	102	25	1	0.5	SS	Y	1
63	Patania et al, 1995	C	5		15		3.1	0	6.7	15	7.7	2.2	0.05	14.7	1.8	152	25	1.1	0.5	SS	Y	1
64	Patania et al, 1995	C	5.2		15		3.1	0	6.7	18	7.5	2.2	0.05	14.7	1.8	152	25	1.1	0.5	SS	Y	1
65	Patania et al, 1995	C	5.4		15	1	3.1	1	7.1	14	7.3	2.4	0.04	14.7		102	25	1	0.5	SS	Y	1
27	States et al, 2002	C	2.3	17			1.5	0	5	5	9.7		0.062	2.4		46	30	1.1	0.57	SS	Y	6
28	States et al, 2002	C	5.7	17			1.5	0	6.5	13	7.9		0.053	2.4		46	30	1.1	0.57	SS	Y	6
30	States et al, 2002	C	6	17			1.5	0	5	3	9.8		0.05	2.4		46	30	1.1	0.57	SS	Y	6
51	States et al, 2002	C	6		18		3.7	0	5	22	9.1		0.053	2.4		46	30	1.1	0.57	SS	Y	6
52	States et al, 2002	C	5.8		18		3.7	0	6.5	21	7.6		0.077	2.4		46	30	1.1	0.57	SS	Y	6
53	States et al, 2002	C	4.8		18		3.7	0	8.2	22	5.9		0.102	2.4		46	30	1.1	0.57	SS	Y	6
57	States et al, 2002	C	6.1		18		3.7	0	8	17	6.3		0.059	2.4		46	30	1.1	0.57	SS	Y	6

Obs #	Source	Treatment Train	Log Removal	Alum (mg/L)	FeCl (mg/L)	PACl (mg/L)	Total Metal Ion (mg/L)	Polymer (mg/L)	Coag. pH	Temp. (°C)	pOH	Infl. Turb (NTU)	Eff. Turb (NTU)	Filtration rate (m/h)	Raw TOC (mg/L)	Depth 1 (cm)	Depth 2 (cm)	Effective size 1 (mm)	Effective size 2 (mm)	Portion of filter run	Optimal Coag. dose?	Method
87	States et al, 2002	C	5.8			27.5	8.5	0	6.5	14	7.9		0.057	2.4		46	30	1.1	0.57	SS	Y	6
88	States et al, 2002	C	5.9			27.5	8.5	0	5	17	9.3		0.047	2.4		46	30	1.1	0.57	SS	Y	6
89	States et al, 2002	C	5.9			27.5	8.5	0	8	17	6.3		0.11	2.4		46	30	1.1	0.57	SS	Y	6
20	Williams & Dugan, 2003	I	3.8	20			1.8	0				0.25	0.07	5	2	51	25	1	0.4	SS	Y	1
45	Yates et al, 1997	D	3.7	5		1	0.5	1	8			0.5	0.06	14.7		51	20	1	0.6	SS	Y	1
73	Yates et al, 1997	D	4.5		3	1	0.6	1	8			0.5	0.06	14.7		51	20	1	0.6	SS	Y	1

APPENDIX D: RESULTS OF ALTERNATIVE VARIABLE SELECTION PROCEDURES FOR DATA SUBSETS

Alternative variable selection procedures for regression model formulations described in this appendix provide a comparison to the "best" variable subsets presented in the text.

Full Data Set with Treatment Train Variable

Backwards elimination and stepwise selection procedures resulted in the same linear model. This model included the polymer dose, portion of filter run, coagulant optimality, and treatment train variables in addition to an intercept term. In comparison, the forward selection procedure produced a model similar to that of the backward and stepwise methods with the included parameters of effluent turbidity and filtration rate. The adjusted R^2 value of the stepwise and backward selection models was 0.68, while that of the forward selection model was 0.69. The backward selection model was selected for further analysis since the addition of the effluent turbidity and filtration rate parameters did not significantly improve the model R^2 value.

In order to investigate this data set further, stepwise selection procedures were run on the subset of the data collected only during steady state filter operation and when optimal coagulant dose was used. Repeated stepwise selection produced a model derived from 82 of the 87 observations available, and contained effective size and treatment train variables in addition to an intercept term. This model had an adjusted R^2 value of 0.37 and a RMSE of 1.05.

Metal Ion > 0.4 mg/L (Conventional Treatment)

In comparison to the backward elimination procedure that produced the best model for the MI> 0.4 mg/L subset, repeated stepwise and forward selection procedures resulted in models with lower R^2 values. Repeated stepwise selection resulted in a model that contained effluent turbidity, portion of filter run and the intercept, used 89 observations, and had an adjusted R^2 value of 0.36 and an RMSE of 1.16. The final forward selection procedure produced a model that used 65 observations, had an R^2 value of 0.37, an RMSE of 1.16 and included the variables of polymer dose, pOH, effluent turbidity, portion of filter run, coagulant dose optimality, filtration rate, and intercept.

Metal Ion < 0.4 mg/L (Direct/Inline Treatment)

Repeated forward selection applied to the MI < 0.4 mg/L data set resulted in a model with 8 regressors: MI dose, pOH, media depth 1 and 2, effluent turbidity, influent turbidity, and coagulant dose optimality. While this model had an adjusted R^2 of 0.99, and RMSE of 0.064, the number of regressors in the model was excessive considering the number of observations in the data set (n=14). In comparison, when the repeated stepwise elimination procedure was run on this data set, the model produced was very similar to that of the repeated backwards procedure except that MI dose appeared in the model in place of polymer dose. The R^2 value for the polymer, media depth 1 and 2, and coagulant dose optimality model was 0.99 with an RMSE of 0.09.

APPENDIX E : ANOVA TABLES FOR STEPWISE REGRESSION MODELS BEST MODELS

Table E.1: Full data set with treatment train variable.

Source	DF	Sum of Squares	Mean Square	F	p
Model	4	170.10	42.53	36.92	<0.0001
Error	110	126.71	1.15		
Corrected Total	114	296.81			

Table E.2: Full data set without treatment train variable.

Source	DF	Sum of Squares	Mean Square	F	p
Model	5	75.51	15.10	8.31	<0.0001
Error	87	158.10	1.82		
Corrected Total	92	233.61			

Table E.3: Metal ion concentration > 0.4 mg/L.

Source	DF	Sum of Squares	Mean Square	F	p
Model	4	92.83	23.21	19.28	<0.0001
Error	92	110.72	1.20		
Corrected Total	96	203.55			

Table E.4: Metal ion concentration < 0.4 mg/L.

Source	DF	Sum of Squares	Mean Square	F	p
Model	4	14.96	3.74	36.85	<0.0001
Error	13	1.32	0.10		
Corrected Total	17	16.28			

APPENDIX F : FULL DATA SET WITHOUT TREATMENT TRAIN VARIABLE

For the full data set without a treatment train variable included, stepwise and backward elimination techniques produced the same model. This model included less variables than the forward selection model but had a similar R^2 value. The first round of stepwise selection resulted in a model containing effective size of media 1 and effective size of media 2, effluent turbidity, portion of filter run, and filtration rate variables in addition to an intercept term. This model had an R^2 value of 0.51 and used 60 of the 115 available observations. The second round of stepwise selection used 93 observations and resulted in the inclusion of all the variables in the selection set. However, with the increased number of observations included the adjusted R^2 value was reduced to 0.28. Parameter estimates for this model are presented in Table F.1. Figure F.1 presents a scatter plot of predicted versus actual removal model values shows the model does not appear to contain enough terms to account for the variability in the data.

Table F.1: Parameter estimates for full data set without treatment train variable obtained using repeated stepwise selection. Adjusted R^2 - 0.28, RMSE = 1.35, n =93

Variable	Parameter Estimate	Standard Error	t value	p
Effective Size 1	-1.61	0.79	-2.04	0.04
Effective Size 2	0.23	0.71	0.32	0.75
Effluent turbidity	-1.15	0.33	-3.53	0.00
Coagulant Dose Optimality	-0.87	0.53	-1.64	0.11
Filtration Rate	-0.06	0.04	-1.74	0.09
Intercept	6.02	0.81	7.42	<.0001

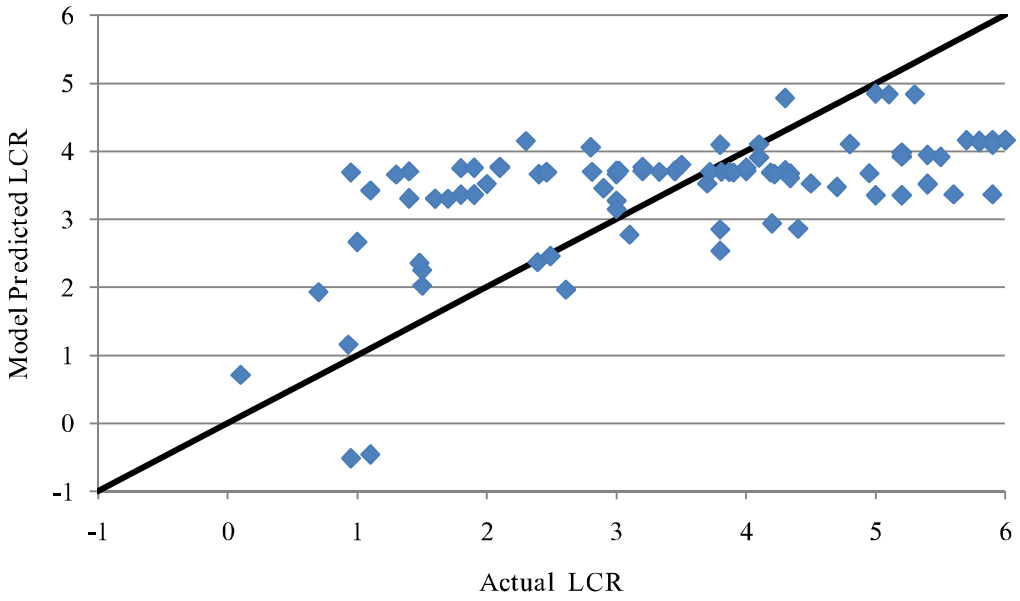

Figure F.1: Predicted vs. actual Log Cryptosporidium removal for full data set without treatment train variable model

APPENDIX G: EXCLUSION OF POLYALUMINUM CHLORIDE

The exact polyaluminum chloride formulations used by the two groups of researchers that employed it as a coagulant were not known. The PACl formula was assumed to be $Al_2Cl(OH)_5$ in order to represent a polyaluminum chloride with basicity of 83% (Van Benschoten et al., 1992). This led to a calculation that 31% of the PACl added was aluminum ion. Study authors were contacted but information regarding the percentage of aluminum ion contained in the PACl dose was unavailable. A survey of 15 commercially available PACl products indicated their aluminum content ranged from 5 to 16%. Since the assumed aluminum content was much higher, an analysis of the dataset was carried out with the five observations where PACl was used as a coagulant were removed.

The removal of PACl data affected the full and MI > 0.4 mg/L data sets. Correlation analysis using Spearman's Rho indicated correlations between continuous variables did not change significantly for either data set when the PACl data was removed. Figure G.1 is a re-creation of Figure 2.9 (page 99), which shows the relationship between Log Cryptosporidium removal and metal ion concentration, without PACl data. Figure G.1 shows correlations between removal and MI are reduced when PACl data is not included: the full data set with PACl R^2 was 0.13, but without PACl was 0.10 and the MI > 0.4 mg/L data set was R^2 0.01 with PACl and 0.001 without.

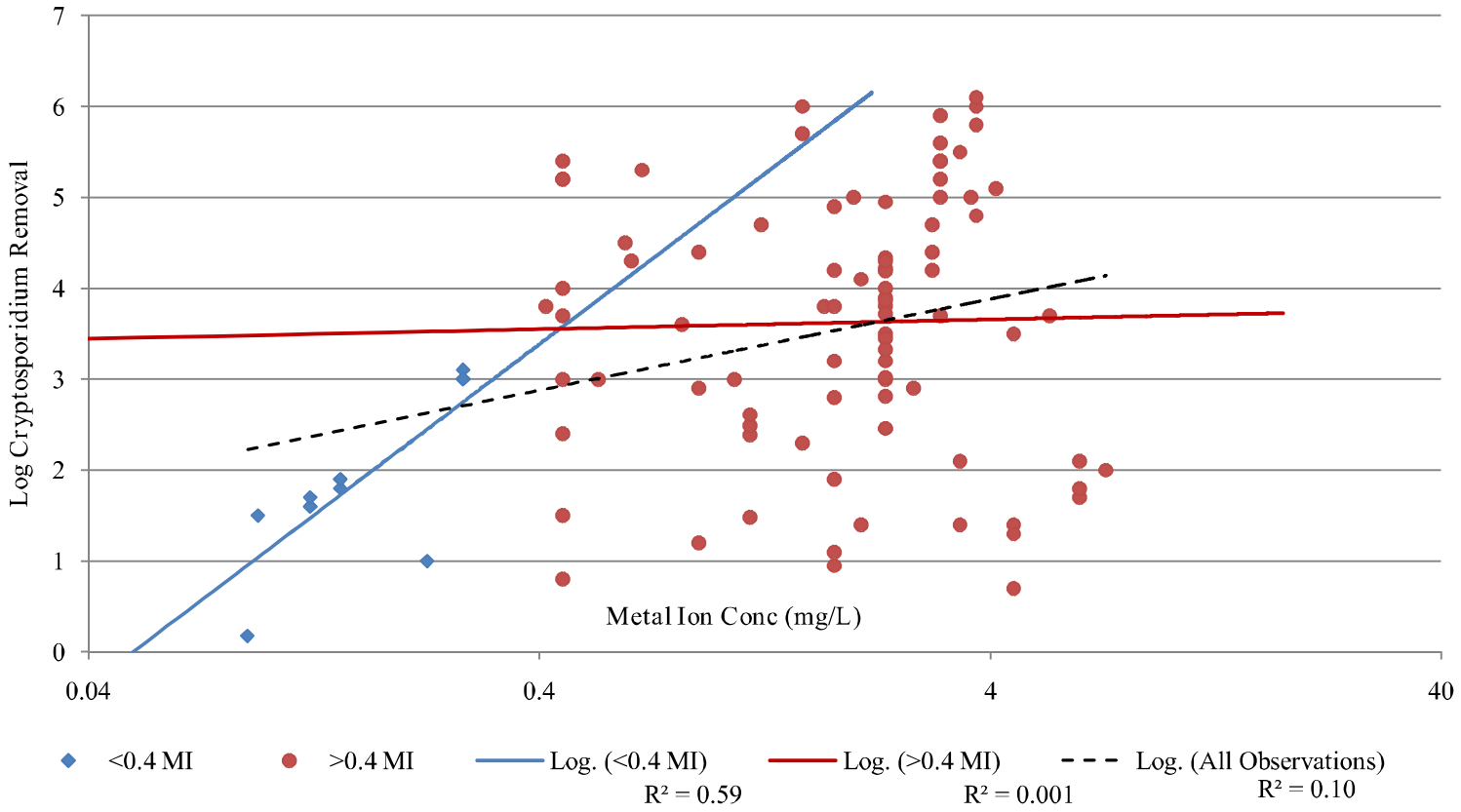

Figure G.1: Metal ion as a potential predictor of Log Cryptosporidium removal with PACl data removed.

Stepwise variable selection techniques applied to the dataset without PACl observations showed small, but potentially significant differences from the results of the data set that included PACl. The most important difference occurred in the metal ion greater than 0.4 mg/L data subset. The best model for this subset when PACl was included was obtained using the backwards variable selection procedure. This model included the portion of filter run, coagulant dose optimality, and filtrate rate variables (plus the intercept) and had an adjusted R^2 value of 0.43. The backwards variable selection procedure performed using the dataset without PACl resulted in a model with the same adjusted R^2 value (0.43) but included the metal ion variable in place of the filtrate rate variable. These results are presented in detail in Table G.1. In comparison, The R^2 value between MI and effluent turbidity was 0.36 for both the with and without PACl MI > 0.4 data sets

Table G.1: Metal ion greater than 0.4 mg/L stepwise model results with and without PACl observations included. Adjusted $R^2 = 0.43$ for both models.

WITH PACl (n=92)					WITHOUT PACl (n=97)				
Variable	Parameter Estimate	Standard Error	t value	p	Variable	Parameter Estimate	Standard Error	t value	p
Portion of Filter Run 1	-2.48	0.51	-4.89	<.0001	Portion of Filter Run 1	-2.37	0.50	-4.76	<.0001
Portion of Filter Run 2	-2.99	0.56	-5.32	<.0001	Portion of Filter Run 2	-2.86	0.55	-5.16	<.0001
Coagulant Dose Optimality	-2.03	0.37	-5.50	<.0001	Coagulant Dose Optimality	-2.21	0.38	-5.80	<.0001
Filtration Rate	-0.08	0.03	-2.81	0.006	Metal Ion Concentration	-0.17	0.08	-2.06	0.042
Intercept	4.86	0.29	16.61	<.0001	Intercept	4.50	0.24	19.00	<.0001

APPENDIX H: LOGIC-BASED CONTROLS FOR AUGUST 22, 2007 (BASE MODEL)

RULE 1
IF LINK 4 STATUS IS OPEN
THEN LINK 4491 STATUS IS CLOSED

RULE 4
IF SYSTEM CLOCKTIME <= 21.59
AND SYSTEM CLOCKTIME >= 3:59
AND NODE 318 PRESSURE <= 80
THEN LINK 3442 STATUS IS OPEN
AND LINK 8033 STATUS IS CLOSED

RULE 5
IF SYSTEM CLOCKTIME <= 21.59
AND SYSTEM CLOCKTIME >= 3:59
AND NODE 318 PRESSURE > 75
AND NODE 318 PRESSURE < 80
THEN LINK 3442 STATUS IS CLOSED
AND LINK 8033 STATUS IS CLOSED

RULE 6
IF SYSTEM CLOCKTIME <= 21.59
AND SYSTEM CLOCKTIME >= 3:59
AND NODE 318 PRESSURE >= 85
THEN LINK 3442 STATUS IS CLOSED
AND LINK 8033 STATUS IS OPEN

RULE 10
IF SYSTEM CLOCKTIME <= 22.59
AND SYSTEM CLOCKTIME >= 4:59
AND NODE 1202 PRESSURE <= 90
THEN PUMP 3443 STATUS IS OPEN
AND LINK 7792 STATUS IS CLOSED

RULE 11
IF SYSTEM CLOCKTIME <= 22.59
AND SYSTEM CLOCKTIME >= 4:59
AND NODE 1202 PRESSURE > 90
THEN PUMP 3443 STATUS IS CLOSED
AND LINK 7792 STATUS IS CLOSED

RULE 12
IF SYSTEM CLOCKTIME >= 21.59
AND SYSTEM CLOCKTIME <= 1:59
THEN PUMP 3441 STATUS IS CLOSED
AND LINK 8674 STATUS IS OPEN

RULE 13
IF SYSTEM CLOCKTIME <= 21.59
AND SYSTEM CLOCKTIME >= 4:59
AND NODE 8814 PRESSURE <= 90
THEN PUMP 3441 STATUS IS OPEN
AND LINK 8674 STATUS IS CLOSED

RULE 14
IF SYSTEM CLOCKTIME <= 21.59
AND SYSTEM CLOCKTIME >= 4:59
AND NODE 8814 PRESSURE > 90
THEN PUMP 3441 STATUS IS CLOSED
AND LINK 8674 STATUS IS CLOSED

RULE 22
IF TANK 3424 HEAD ABOVE 1296.5
THEN LINK 4491 STATUS IS CLOSED
AND LINK 4 STATUS IS OPEN
AND PUMP 3454 STATUS IS CLOSED

RULE 23
IF TANK 3424 HEAD BELOW 1291.0
THEN LINK 4491 STATUS IS OPEN
AND LINK 4 STATUS IS CLOSED
AND PUMP 3454 STATUS IS OPEN

RULE 24
IF SYSTEM CLOCKTIME <= 19
AND SYSTEM CLOCKTIME >= 0
AND LINK 7309 FLOW <= 15000
THEN LINK 8682 STATUS IS OPEN
AND LINK 3486 STATUS IS CLOSED
AND LINK 3484 STATUS IS CLOSED
AND LINK 3482 STATUS IS CLOSED
AND PUMP 3480 STATUS IS CLOSED

RULE 25
IF SYSTEM CLOCKTIME <= 19
AND SYSTEM CLOCKTIME >= 0
AND LINK 7309 FLOW > 15000
THEN PUMP 3484 STATUS IS OPEN
AND PUMP 3486 STATUS IS OPEN
AND PUMP 3480 STATUS IS OPEN
AND LINK 3482 STATUS IS OPEN
AND LINK 8682 STATUS IS CLOSED

RULE 26
IF LINK 3486 STATUS IS OPEN
AND LINK 3484 STATUS IS OPEN
AND LINK 3480 STATUS IS OPEN
AND LINK 3482 STATUS IS OPEN
THEN LINK 7460 STATUS IS OPEN
ELSE LINK 7460 STATUS IS CLOSED

RULE 27
IF NODE 2427 PRESSURE > 30
THEN LINK 3444 STATUS IS CLOSED
AND LINK 7855 STATUS IS OPEN
AND LINK 7852 STATUS IS OPEN

RULE 28
IF NODE 2427 PRESSURE <= 30
THEN LINK 3444 STATUS IS OPEN
AND LINK 7855 STATUS IS CLOSED
AND LINK 7852 STATUS IS CLOSED

RULE 29
IF LINK 7820 STATUS IS OPEN
THEN LINK 8051 STATUS IS OPEN
AND LINK 8054 STATUS IS OPEN
AND LINK 8057 STATUS IS OPEN

RULE 30
IF SYSTEM CLOCKTIME < 23
AND SYSTEM CLOCKTIME > 0:59
AND NODE 2427 PRESSURE < 35
THEN LINK 3453 STATUS IS OPEN
ELSE LINK 3453 STATUS IS CLOSED

RULE 31
IF LINK 3453 STATUS IS OPEN
THEN LINK 7820 STATUS IS CLOSED
AND LINK 8051 STATUS IS OPEN
AND LINK 8054 STATUS IS OPEN
AND LINK 8057 STATUS IS OPEN

RULE 32
IF LINK 3453 STATUS IS CLOSED
AND LINK 7820 STATUS IS CLOSED
THEN LINK 8051 STATUS IS CLOSED
AND LINK 8054 STATUS IS CLOSED
AND LINK 8057 STATUS IS CLOSED

LINK 3549 70.0000 AT CLOCKTIME 2
LINK 3549 63.0000 AT CLOCKTIME 10
LINK 7792 OPEN AT CLOCKTIME 23
LINK 7792 CLOSED AT CLOCKTIME 3
LINK 8033 OPEN AT CLOCKTIME 22
LINK 8033 CLOSED AT CLOCKTIME 24
LINK 3441 CLOSED AT CLOCKTIME 22
LINK 3442 CLOSED AT CLOCKTIME 22
LINK 3443 CLOSED AT CLOCKTIME 23
LINK 8674 OPEN AT CLOCKTIME 22
LINK 8674 CLOSED AT CLOCKTIME 2:30
LINK 3486 OPEN AT CLOCKTIME 19
LINK 3486 CLOSED AT CLOCKTIME 21
LINK 3484 OPEN AT CLOCKTIME 19
LINK 3484 CLOSED AT CLOCKTIME 21
LINK 7460 OPEN AT CLOCKTIME 19
LINK 7460 CLOSED AT CLOCKTIME 21
LINK 7820 OPEN AT CLOCKTIME 23
LINK 7820 CLOSED AT CLOCKTIME 1
LINK 8682 CLOSED AT CLOCKTIME 19

VALVE 3494 41748.0 AT CLOCKTIME 1
VALVE 3494 41730.1 AT CLOCKTIME 2
VALVE 3494 41659.5 AT CLOCKTIME 3
VALVE 3494 41560.8 AT CLOCKTIME 4
VALVE 3494 41575.4 AT CLOCKTIME 5
VALVE 3494 41505.5 AT CLOCKTIME 6
VALVE 3494 41466.2 AT CLOCKTIME 7
VALVE 3494 40426.3 AT CLOCKTIME 8
VALVE 3494 38383.5 AT CLOCKTIME 9
VALVE 3494 37829.0 AT CLOCKTIME 10
VALVE 3494 34861.9 AT CLOCKTIME 11
VALVE 3494 34918.9AT CLOCKTIME 12
VALVE 3494 34994.6 AT CLOCKTIME 13
VALVE 3494 35010.5 AT CLOCKTIME 14
VALVE 3494 35002.7 AT CLOCKTIME 15
VALVE 3494 35044.4 AT CLOCKTIME 16
VALVE 3494 35150.9 AT CLOCKTIME 17
VALVE 3494 35204.2 AT CLOCKTIME 18
VALVE 3494 34851.1 AT CLOCKTIME 19
VALVE 3494 34653.0 AT CLOCKTIME 20
VALVE 3494 34719.1 AT CLOCKTIME 21
VALVE 3494 34736.4 AT CLOCKTIME 22
VALVE 3494 34810.4 AT CLOCKTIME 23

VALVE 8551 41748.0 AT CLOCKTIME 1
VALVE 8551 41730.1 AT CLOCKTIME 2
VALVE 8551 41659.5 AT CLOCKTIME 3
VALVE 8551 41560.8 AT CLOCKTIME 4
VALVE 8551 41575.4 AT CLOCKTIME 5
VALVE 8551 41505.5 AT CLOCKTIME 6
VALVE 8551 41466.2 AT CLOCKTIME 7
VALVE 8551 40426.3 AT CLOCKTIME 8
VALVE 8551 38383.5 AT CLOCKTIME 9
VALVE 8551 37829.0 AT CLOCKTIME 10
VALVE 8551 34861.9 AT CLOCKTIME 11
VALVE 8551 34918.9 AT CLOCKTIME 12
VALVE 8551 34994.6 AT CLOCKTIME 13
VALVE 8551 35010.5 AT CLOCKTIME 14
VALVE 8551 35002.7 AT CLOCKTIME 15
VALVE 8551 35044.4 AT CLOCKTIME 16
VALVE 8551 35150.9 AT CLOCKTIME 17
VALVE 8551 35204.2 AT CLOCKTIME 18
VALVE 8551 34851.1AT CLOCKTIME 19
VALVE 8551 34653.0 AT CLOCKTIME 20
VALVE 8551 34719.0 AT CLOCKTIME 21
VALVE 8551 34736.4 AT CLOCKTIME 22
VALVE 8551 34810.4 AT CLOCKTIME 23

APPENDIX I : GRAPHS OF TANK WATER LEVELS AND KEY NODE PRESSURES FOR SCADA, TIME-CONTROLLED AND LOGIC-CONTROLLED MODELS

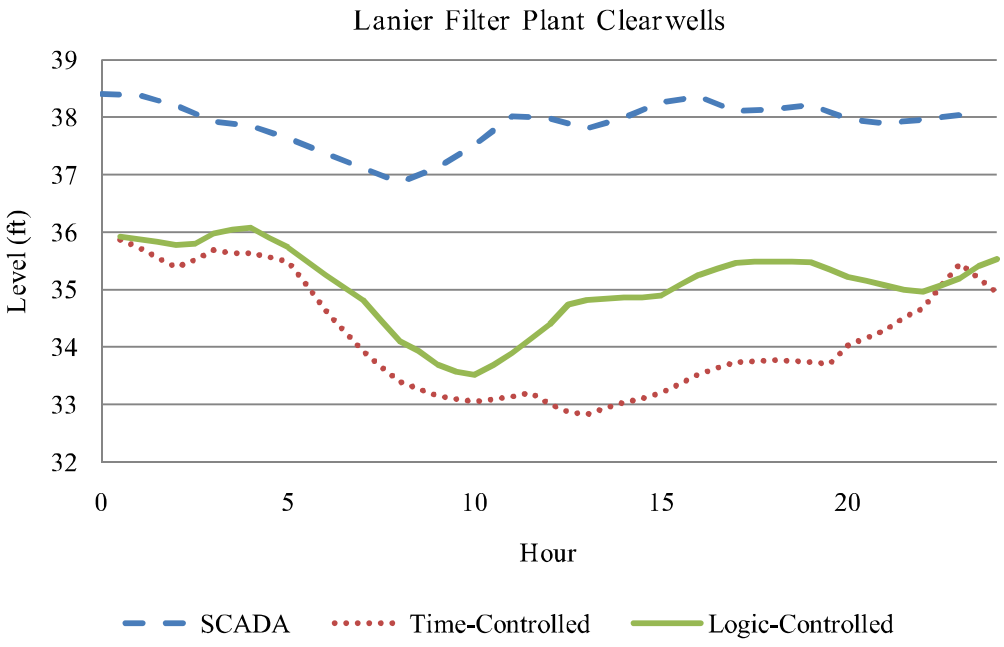

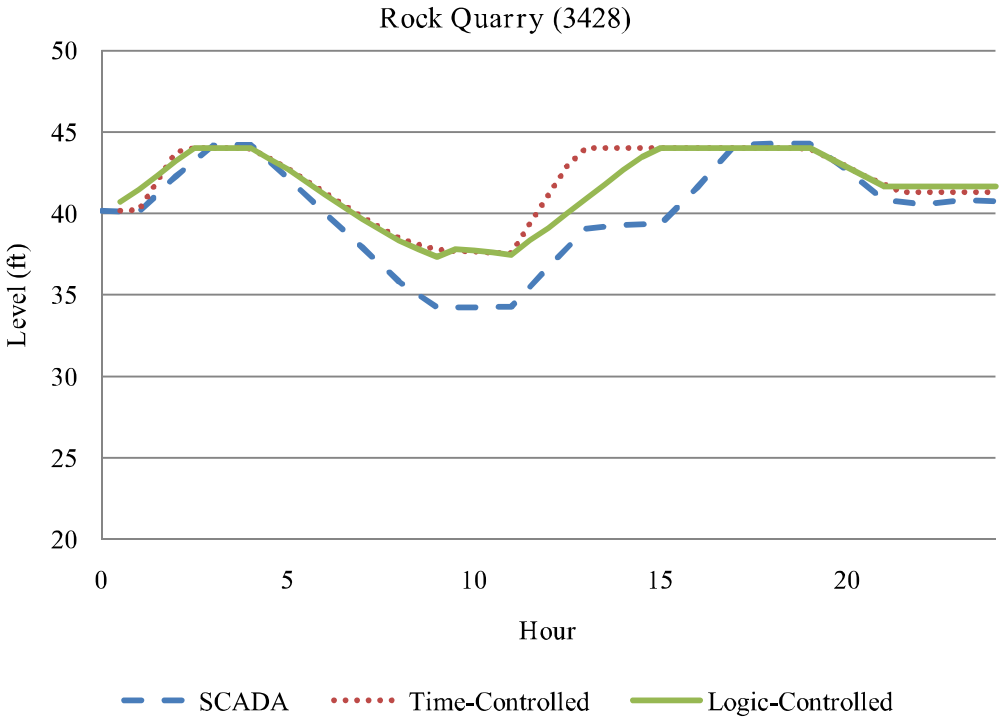

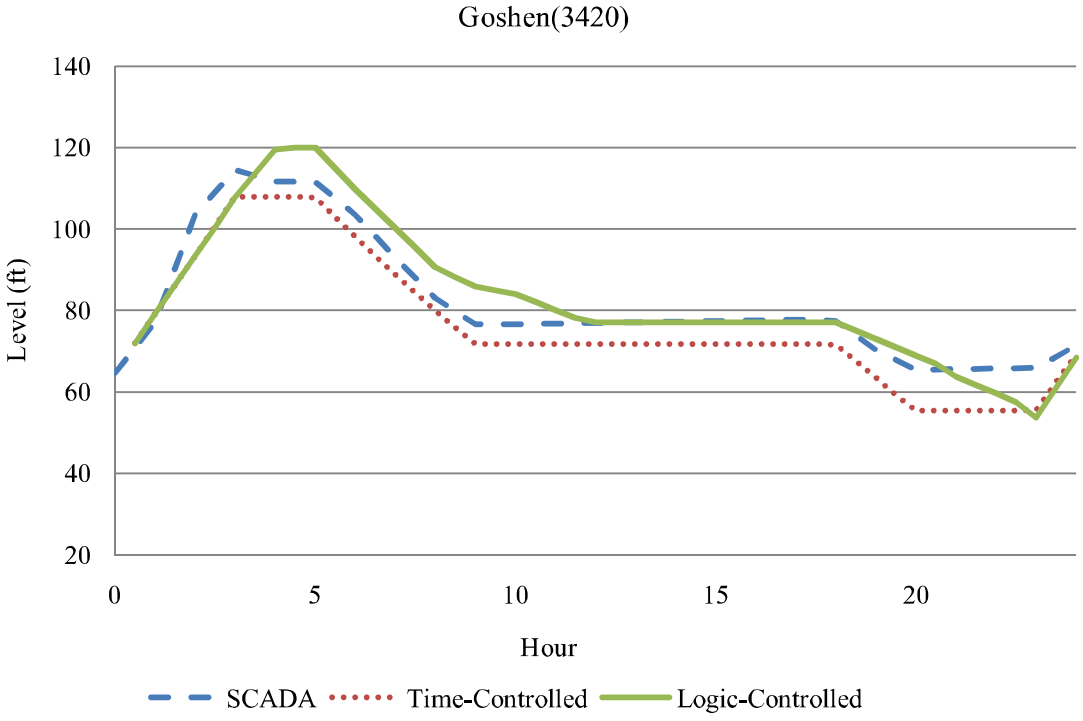
Goshen(3420)
140
120
100
80
60
40
20
Level (ft)
0
5
10
15
20
Hour
SCADA
Time-Controlled
Logic-Controlled

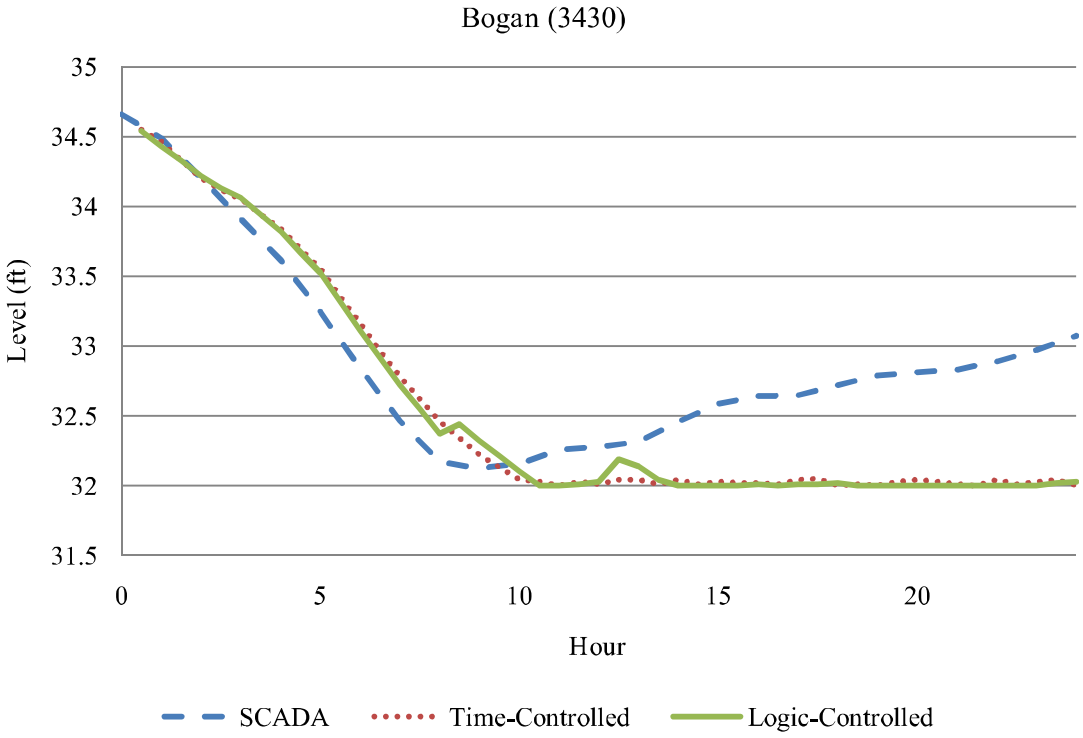
Bogan (3430)
35
34.5
34
33.5
33
32.5
32
31.5
Level (ft)
0
5
10
15
20
Hour
SCADA
Time-Controlled
Logic-Controlled

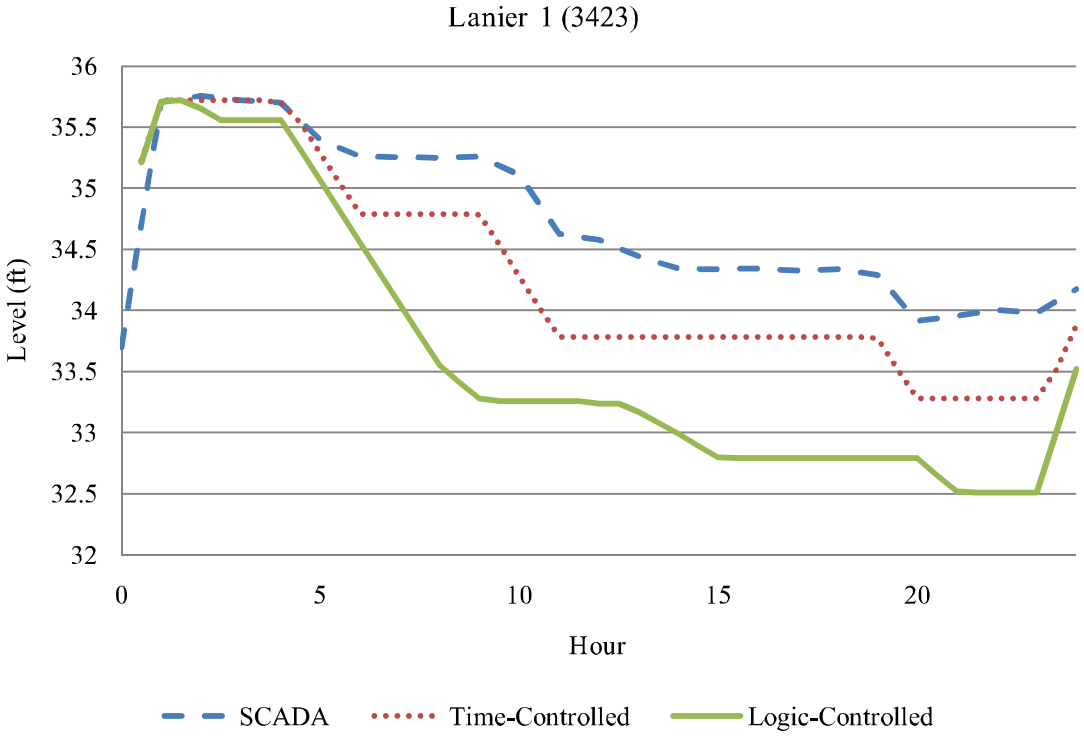
Lanier 1 (3423)
Level (ft)
36
35.5
35
34.5
34
33.5
33
32.5
32
0
5
10
15
20
Hour
SCADA
Time-Controlled
Logic-Controlled

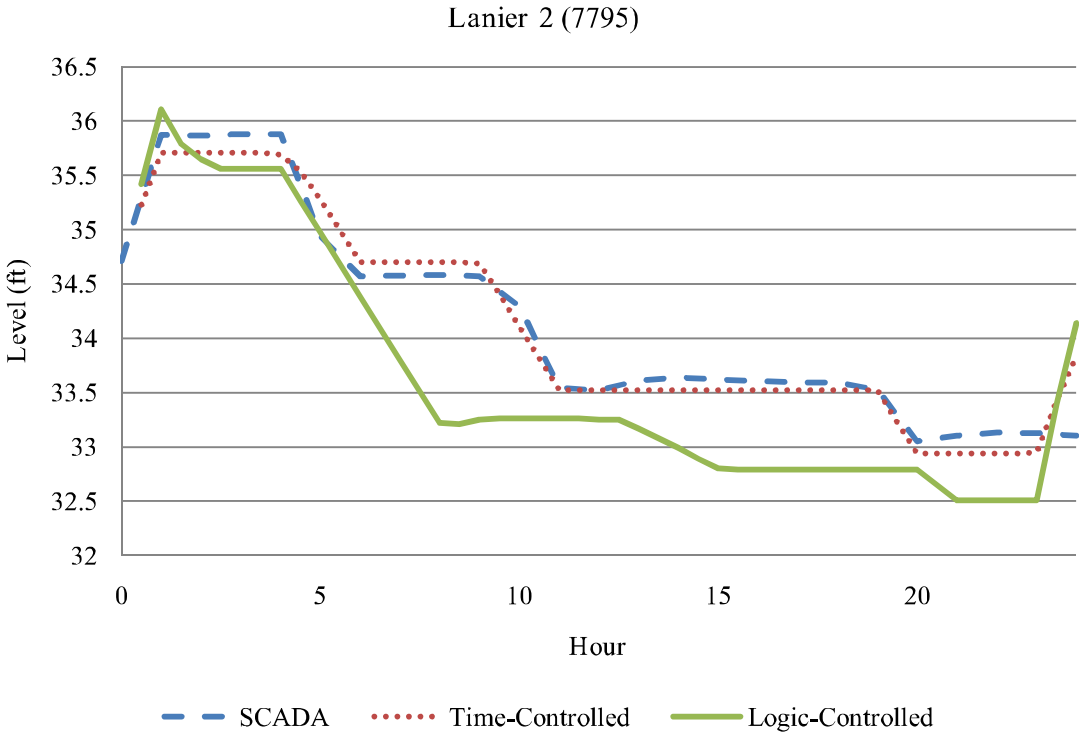
Lanier 2 (7795)
Level (ft)
36.5
36
35.5
35
34.5
34
33.5
33
32.5
32
0
5
10
15
20
Hour
SCADA
Time-Controlled
Logic-Controlled

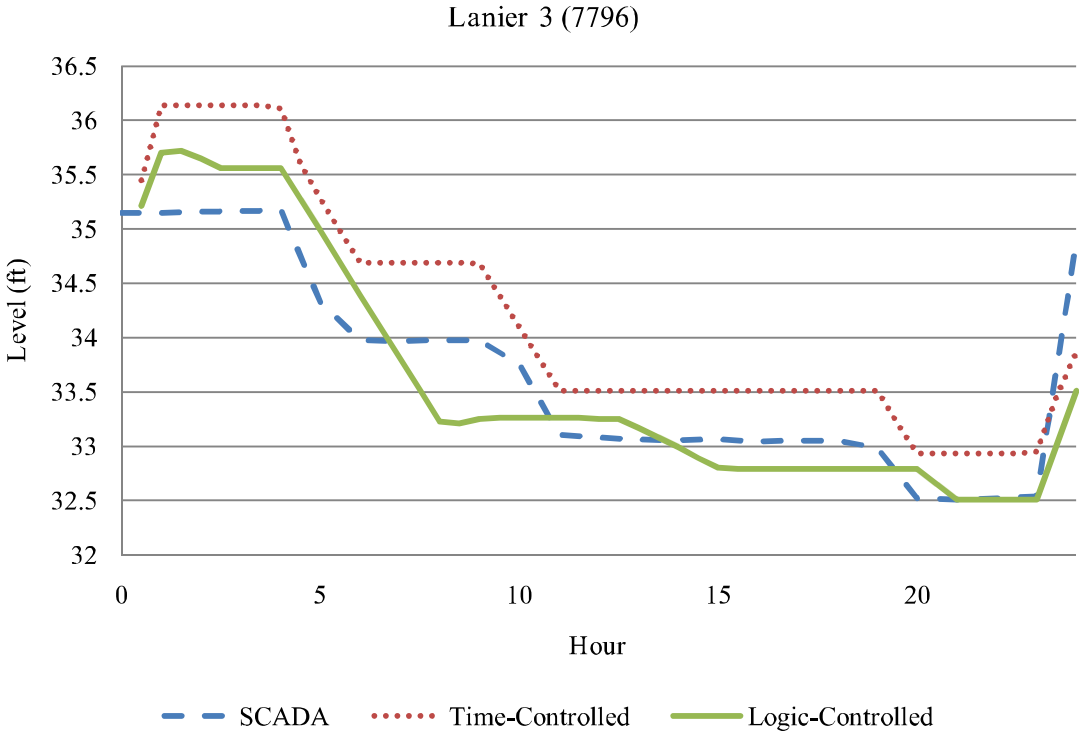
Lanier 3 (7796)
36.5
36
35.5
35
34.5
34
33.5
33
32.5
32
Level (ft)
0
5
10
15
20
Hour
SCADA
Time-Controlled
Logic-Controlled

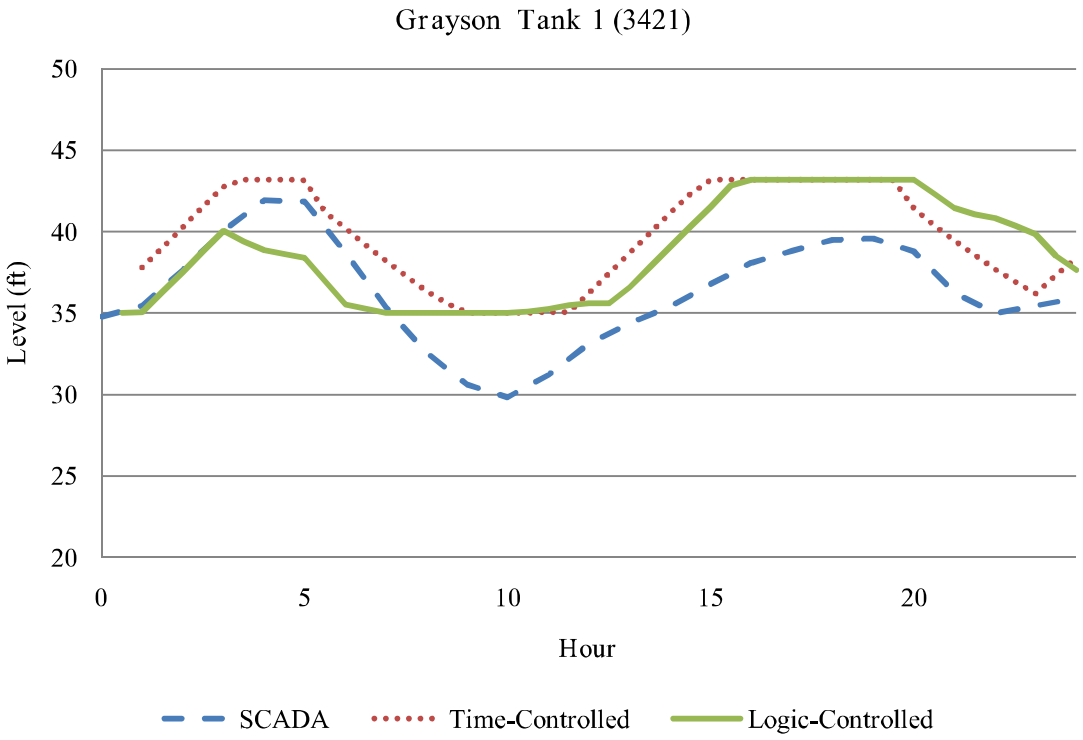
Grayson Tank 1 (3421)
50
45
40
35
30
25
20
Level (ft)
0
5
10
15
20
Hour
SCADA
Time-Controlled
Logic-Controlled

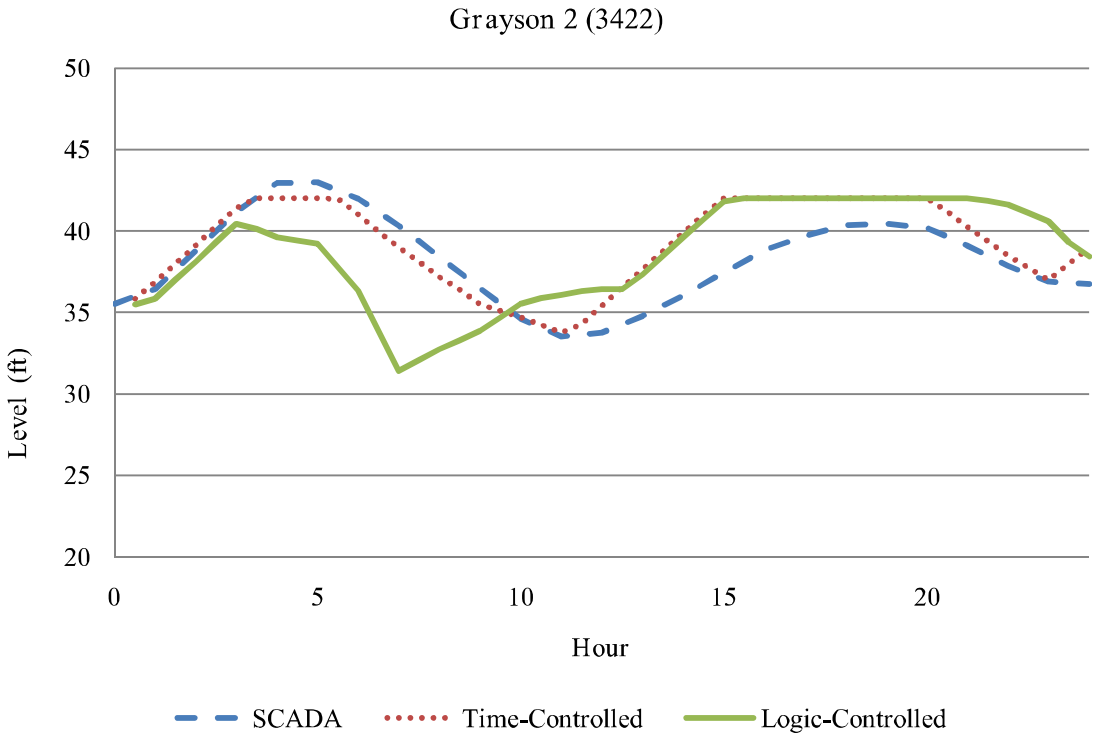
Grayson 2 (3422)
50
45
40
35
30
25
20
Level (ft)
0
5
10
15
20
Hour
SCADA
Time-Controlled
Logic-Controlled

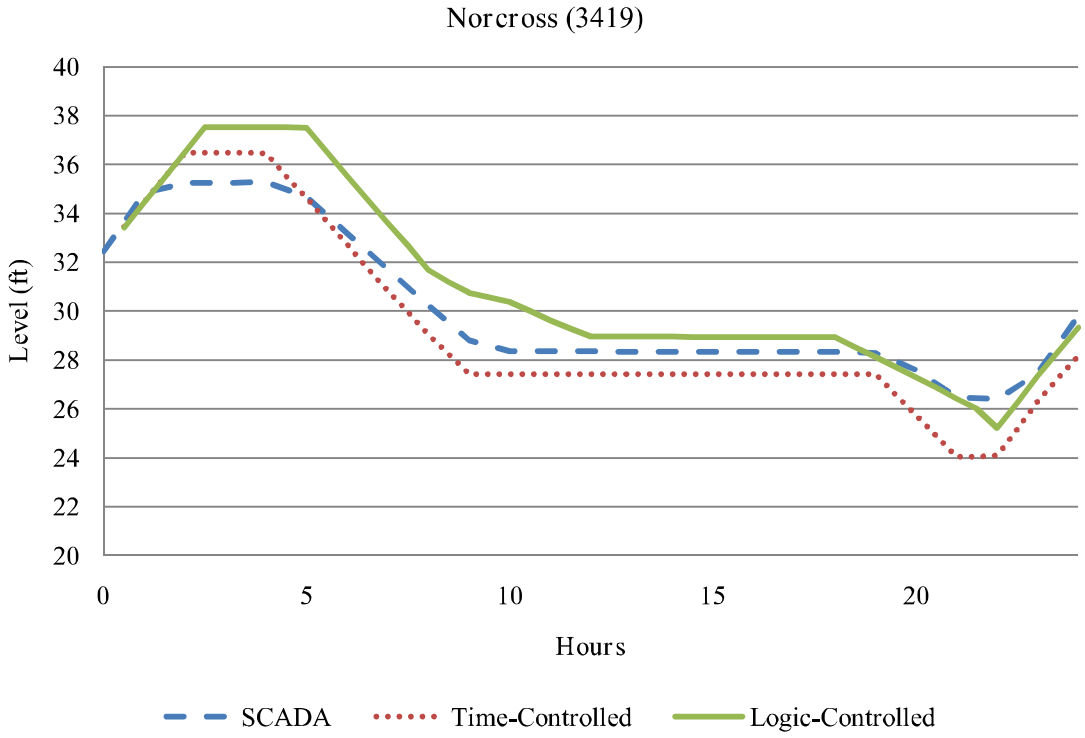
Norcross (3419)
40
38
36
34
32
30
28
26
24
22
20
Level (ft)
0
5
10
15
20
Hours
SCADA
Time-Controlled
Logic-Controlled

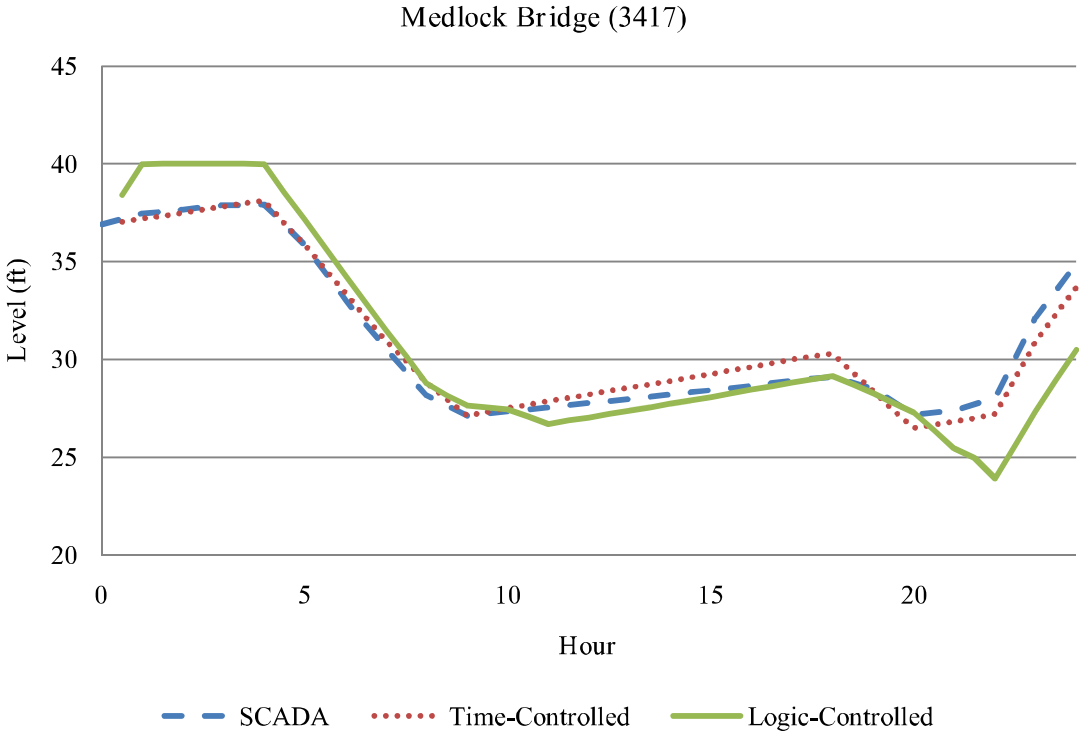
Medlock Bridge (3417)
45
40
35
30
25
20
Level (ft)
0
5
10
15
20
Hour
SCADA
Time-Controlled
Logic-Controlled

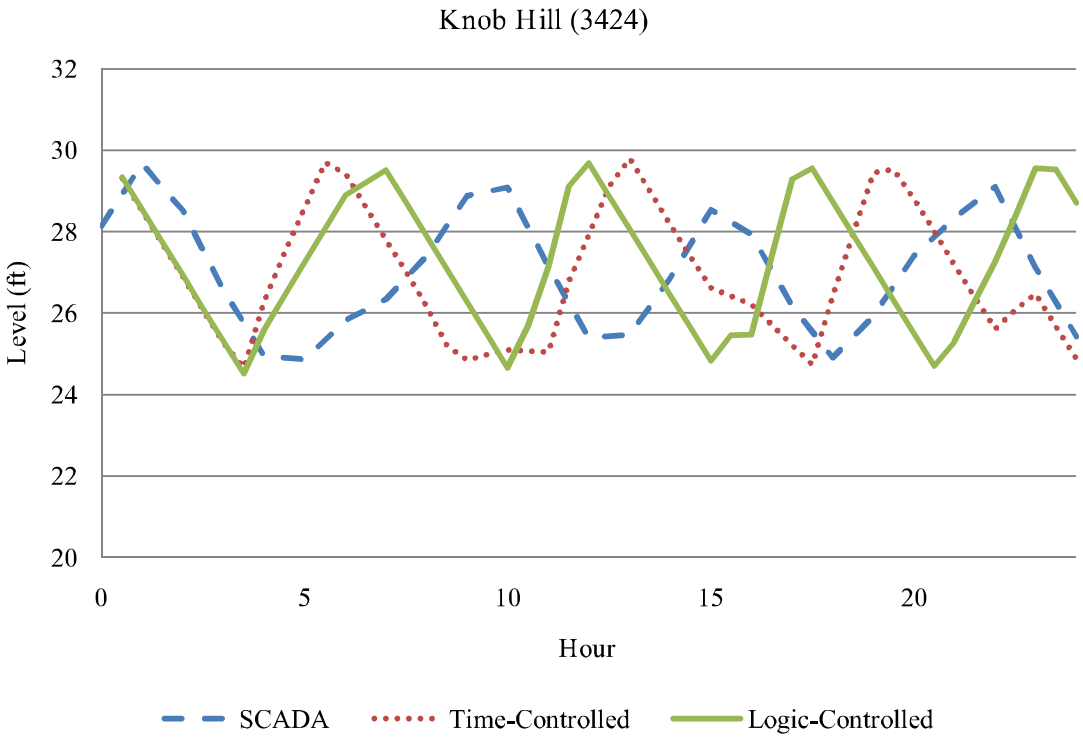
Knob Hill (3424)
32
30
28
26
24
22
20
Level (ft)
0
5
10
15
20
Hour
SCADA
Time-Controlled
Logic-Controlled

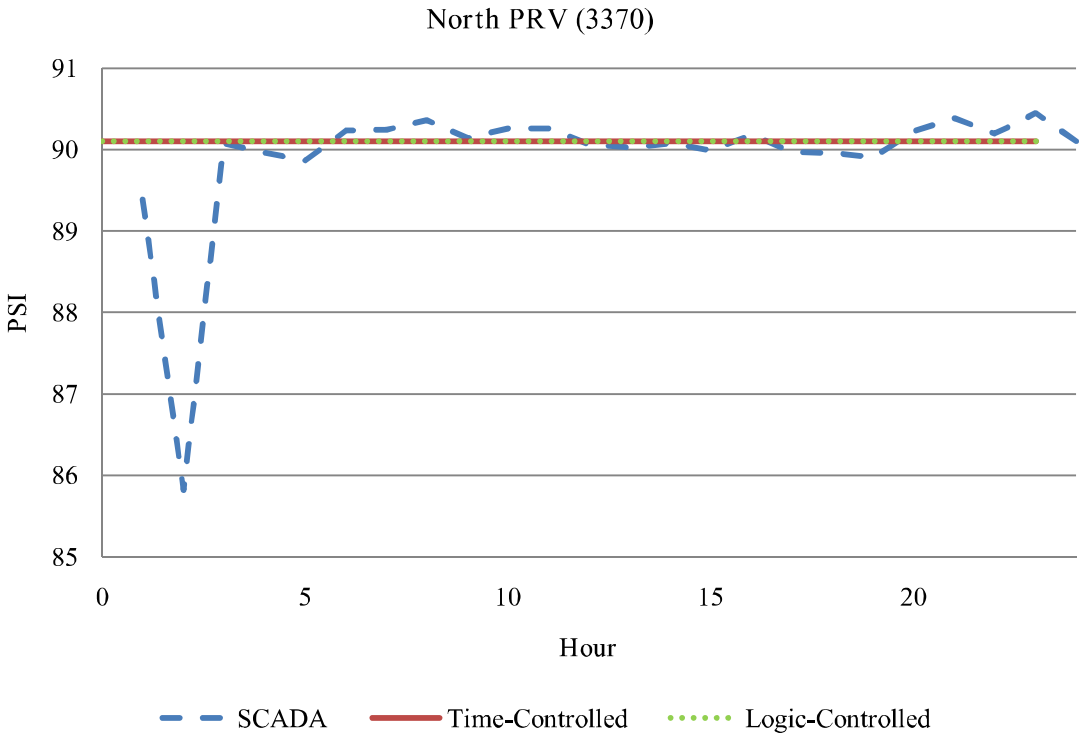
North PRV (3370)
91
90
89
88
87
86
85
PSI
0
5
10
15
20
Hour
SCADA
Time-Controlled
Logic-Controlled

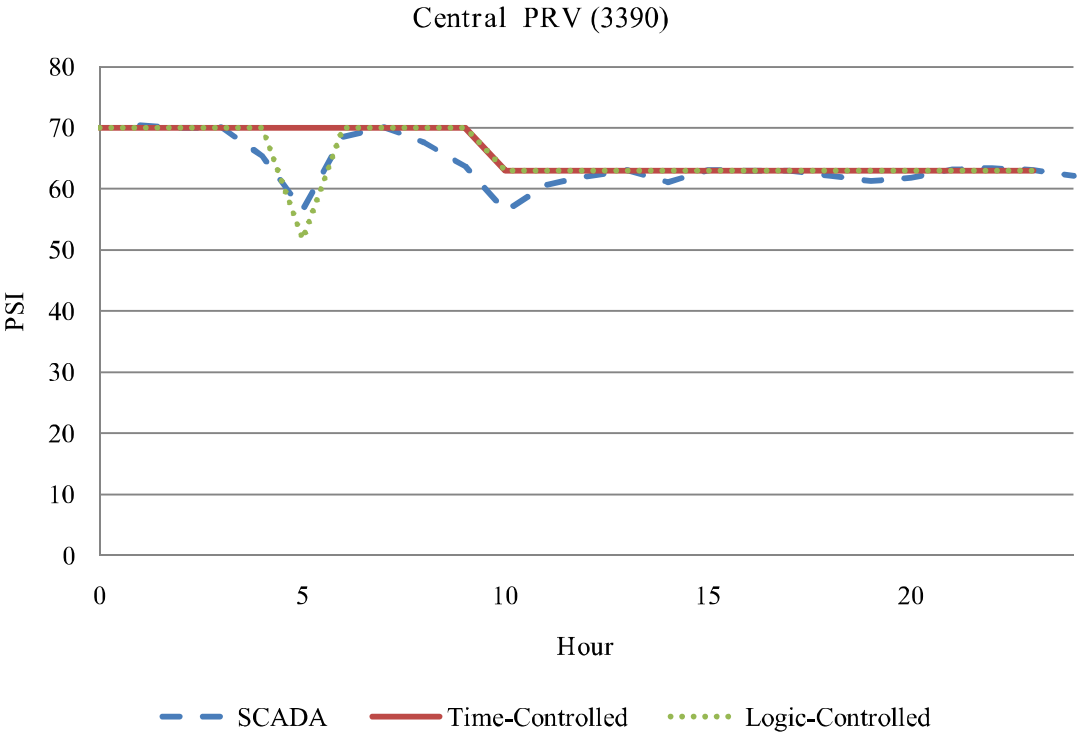
Central PRV (3390)
80
70
60
50
40
30
20
10
0
PSI
0
5
10
15
20
Hour
SCADA
Time-Controlled
Logic-Controlled

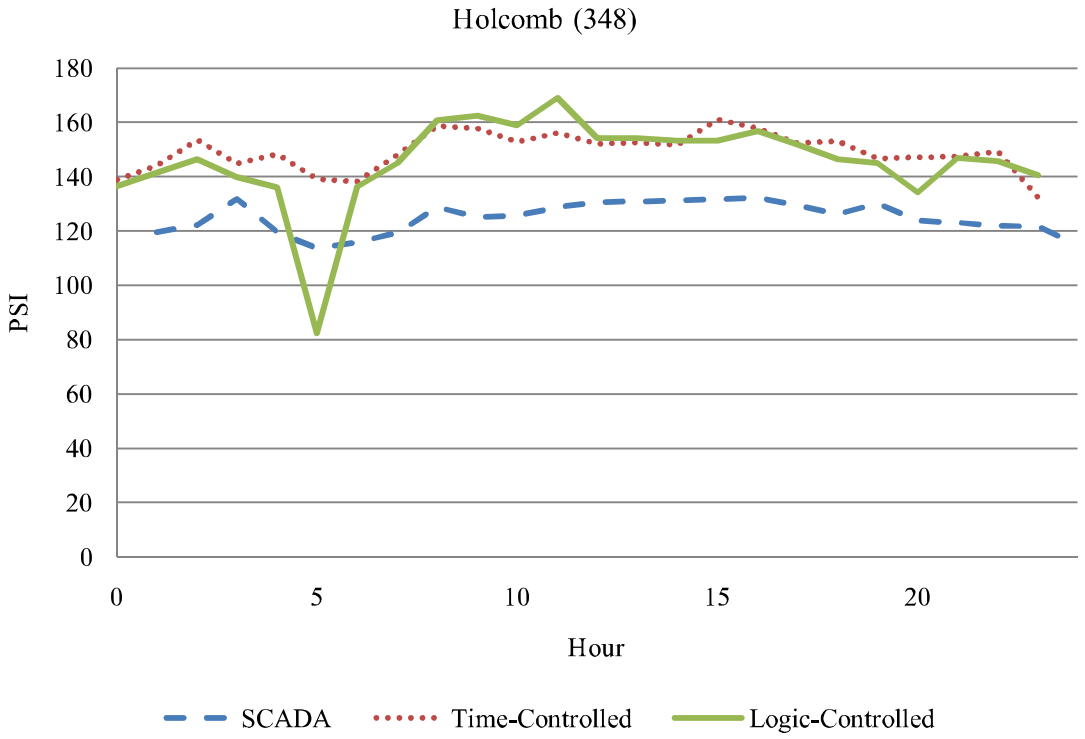
Holcomb (348)
180
160
140
120
100
80
60
40
20
0
PSI
0
5
10
15
20
Hour
SCADA
Time-Controlled
Logic-Controlled

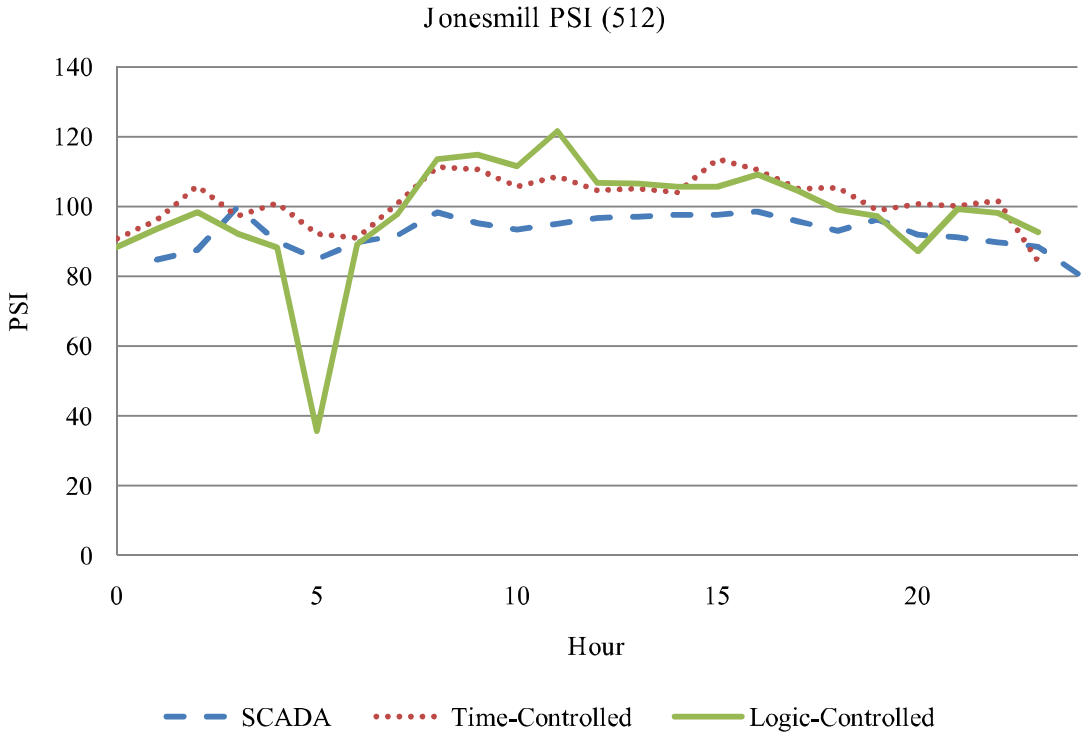
Jonesmill PSI (512)
140
120
100
80
60
40
20
0
PSI
0
5
10
15
20
Hour
SCADA
Time-Controlled
Logic-Controlled

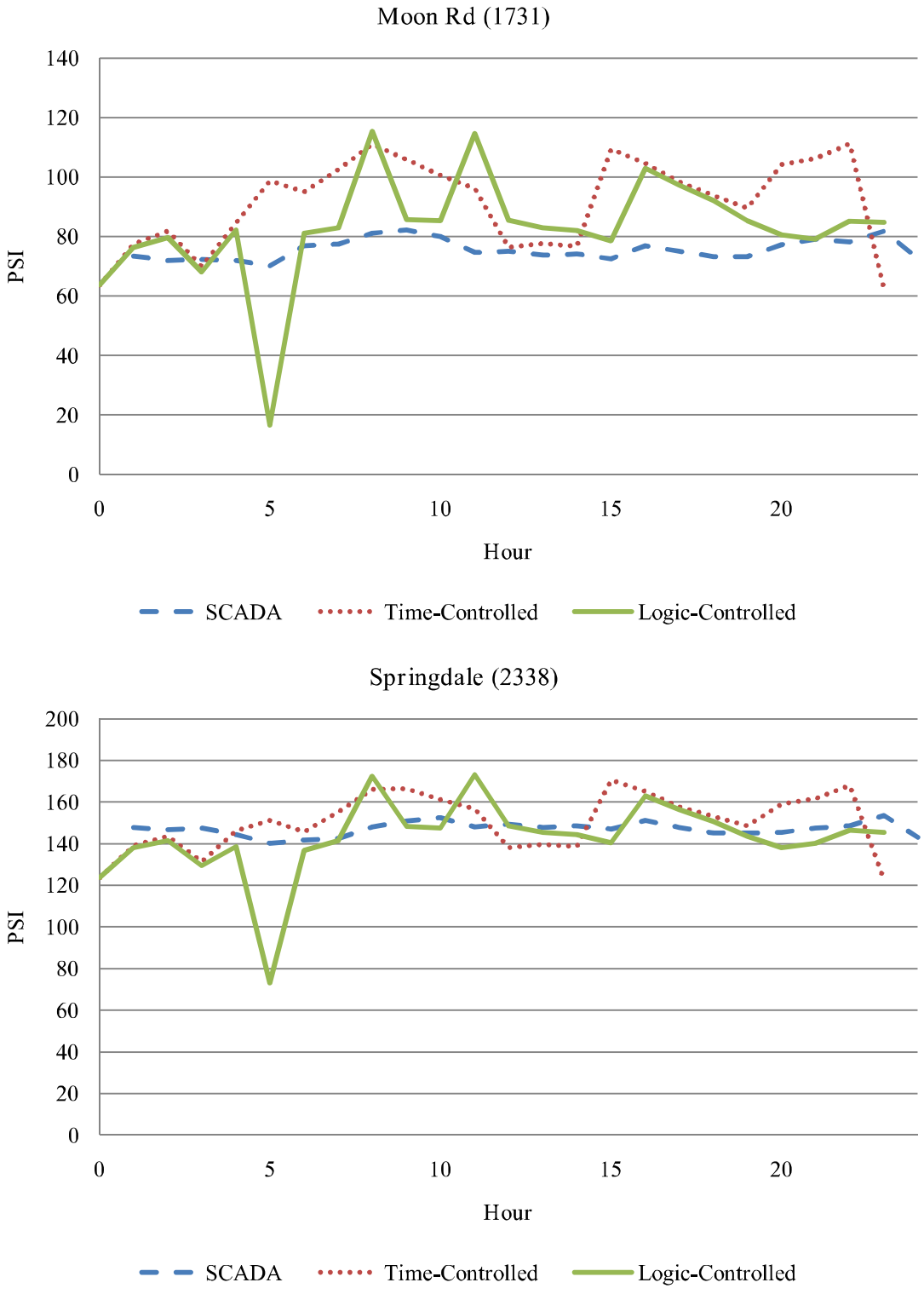
Moon Rd (1731)
PSI
140
120
100
80
60
40
20
0
0
5
10
15
20
Hour
SCADA
Time-Controlled
Logic-Controlled
Springdale (2338)
PSI
200
180
160
140
120
100
80
60
40
20
0
0
5
10
15
20
Hour
SCADA
Time-Controlled
Logic-Controlled

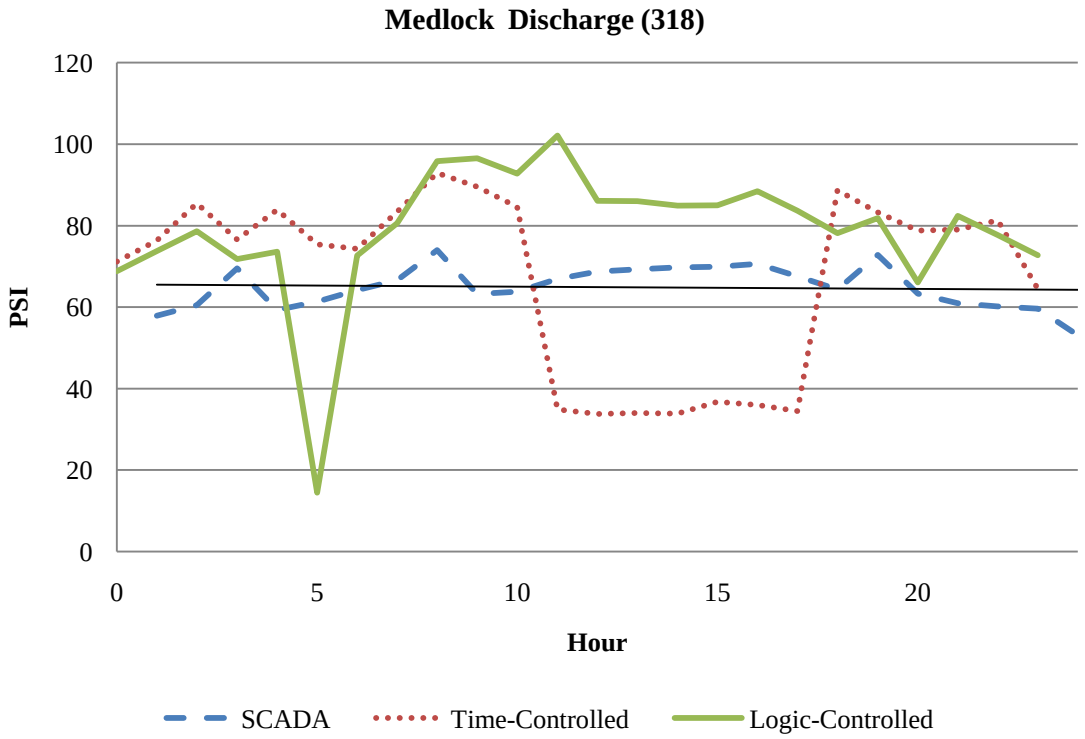
Medlock Discharge (318)
120
100
80
60
40
20
0
PSI
0
5
10
15
20
Hour
SCADA
Time-Controlled
Logic-Controlled

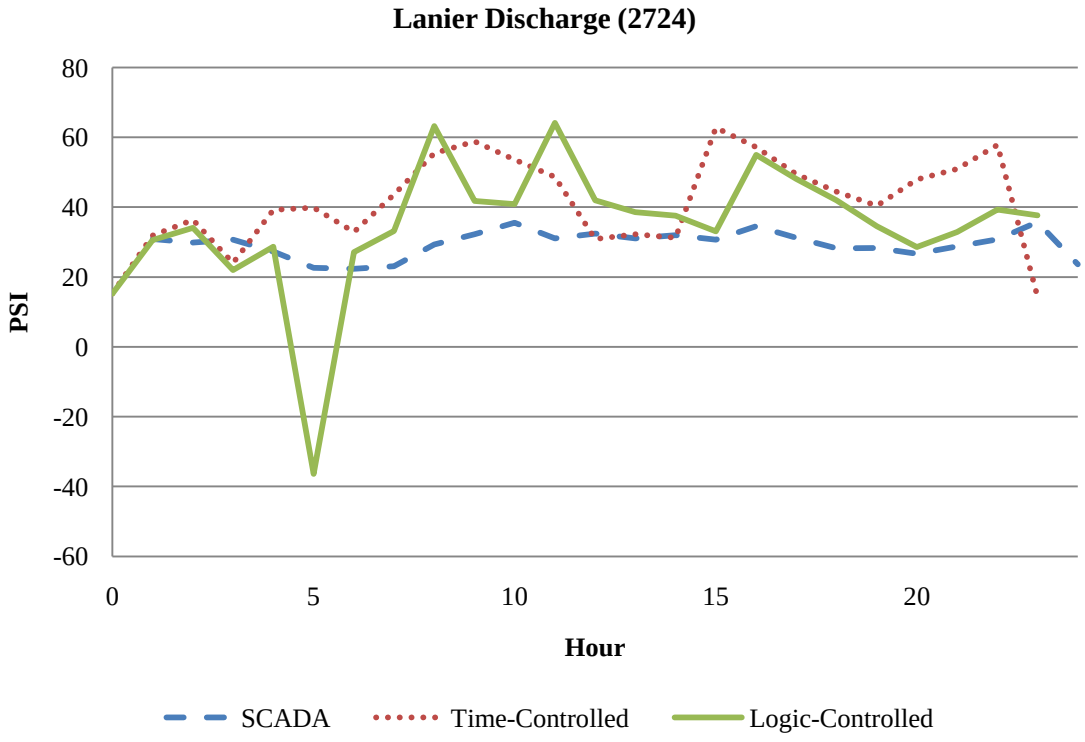
Lanier Discharge (2724)
80
60
40
20
0
-20
-40
-60
PSI
0
5
10
15
20
Hour
SCADA
Time-Controlled
Logic-Controlled

APPENDIX J : DETAILED ANALYSIS OF ROCK QUARRY TANK RESPONSE TO OPERATIONAL SCENARIOS

The Rock Quarry tank turnover time increased markedly in the volume reduction scenarios. The 30%-All and 30%-LRG increased turnover time a staggering 30 days more than was observed in the Base scenario. Figure J.1 presents the level for this tank over the last 24 hours of the Base and 30% volume reduction scenarios. This figure suggested the lower turnover time observed in the 30% volume reduction scenarios were a result of reduced water level variation. The Rock Quarry top water level was limited by the specified top tank height but was not able to drain below a certain point despite no restrictions placed on the minimum water level.

The lack of draining of the Rock Quarry appeared to be due to the logic rules controlling it. The operation of this tank was based on system clock time and flow in the North transmission main (logic-based controls number 24-26 in APPENDIX F). This control was found to best match the tank head observed on the modeled day, although less draining of this tank was also observed in the Base scenario than noted in SCADA data from the modeled day (as shown in APPENDIX I). Basing control of the tank on flow that had predictable fluctuations throughout the day and would not be expected to deviate from the base flow pattern caused the pumps and valves to function as if controlled by time. This type of control led to less draining and filling of the tank and to higher tank turnover times when the volume of the tank was reduced. Results for the Rock Quarry tank that were contrary to those of other tanks therefore came from a limitation in the control of this tank and not necessarily by the operational scenario under consideration. This point highlights the important role played by the logical controls and

their benefit over time-based controls for comparing operational scenarios, as well as the need for logical controls based on sufficiently sensitive parameters.

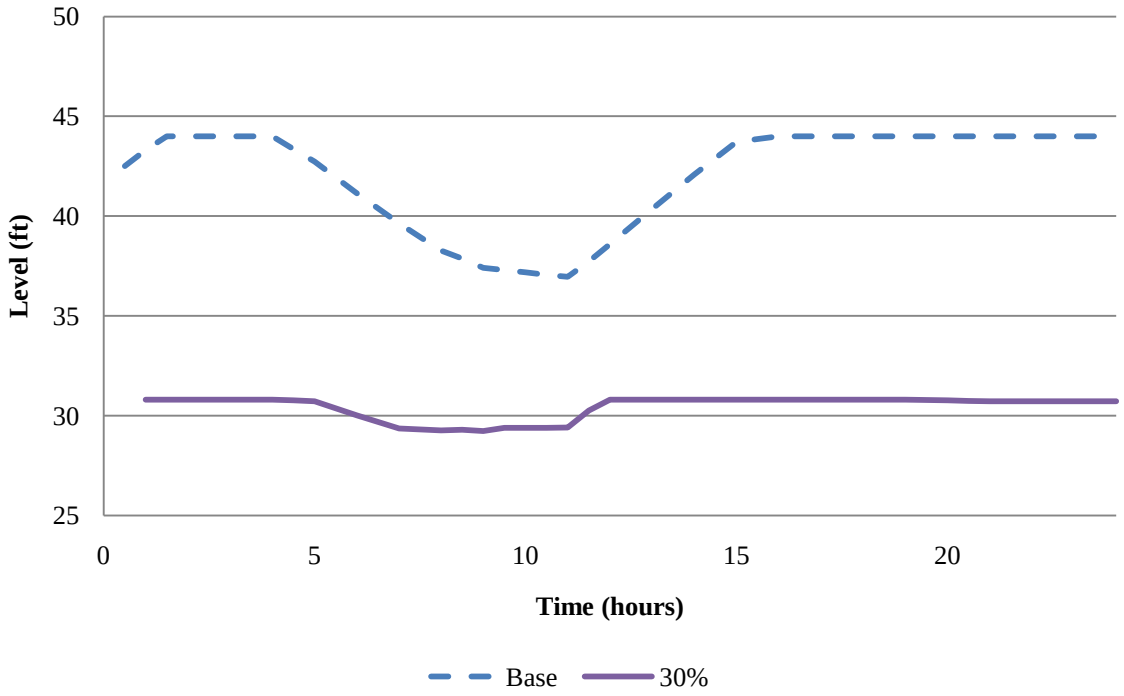

Figure J.1: Water level of Rock Quarry tank in the Base and 30% volume reduction scenarios.

APPENDIX K: EFFECTS OF TANK MIXING ASSUMPTIONS

Three simulations to determine the effect of tank mixing assumptions were run on the Gwinnett County DWDS. In these simulations the Shoal Creek and Lanier Filter Plant clearwells were treated as completely mixed and the system storage tanks specified to be either Completely Mixed (like the Base scenario), FIFO (first-in, first-out), or LIFO (last-in, first-out). All three simulations used the EPANET-MSX system to calculate age and used the same initial quality data included in the operational scenario simulations. Due to problems encountered with running alternative tank mixing schemes with EPANET-MSX (discussed below), simulations were run for 24 hours (therefore the data presented in this appendix are from this 24 period).

Figure K.1 presents the cumulative distribution functions for the three tank mixing comparison scenarios. This figure confirms the idea that tanks with a LIFO regime, would lead to a reduction in the age of delivered water while FIFO may lead to higher ages of delivered water. In the LIFO simulation the CDF curve was shifted to the right, indicating a reduction in age of delivered water, while the opposite occurred in the FIFO simulation. Results from the Completely Mixed simulation indicated a maximum delivered water age of 8.3 days, while the same parameter was 7.3 days in the LIFO simulation. However, the FIFO simulation suggested the maximum water age was greater than 30 days. It is important to note that the LFIO and FIFO results are the extremes of two assumptions regarding tank mixing, completely plug-flow or completely short-circuited. In real-world distribution systems, it would be unlikely that all the tanks would be treated as LIFO or FIFO, rather the assumed mixing regimes would most likely depend on the tank geometry and operation.

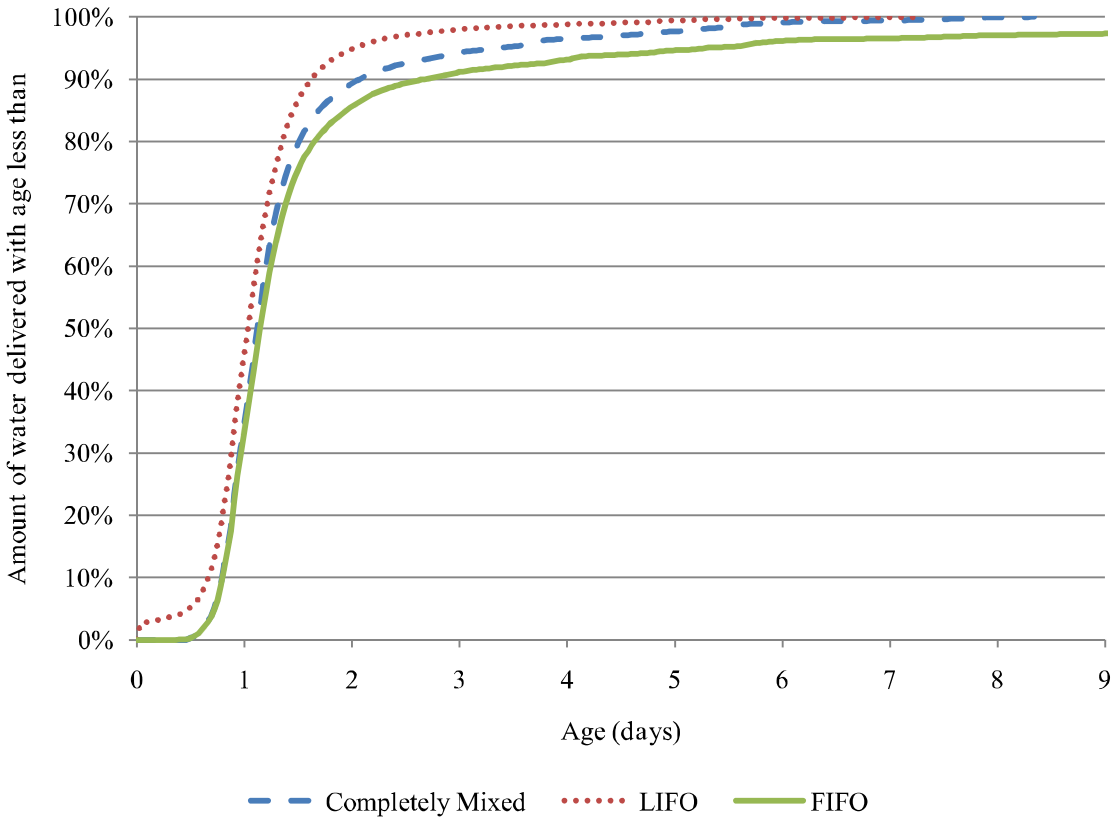

Figure K.1: Cumulative distribution function curves of Mixed, First-In-First-Out, and Last-In-First-Out tank mixing scenarios after 24 hours of simulation.

Problems were encountered when collecting data for the tanks when using the EPANET-MSX system and Programmer's Toolkit and FIFO or LIFO tank mixing regimes. Data was collected for water age at tanks using the ENGETQUAL function. This function worked fine in the completely mixed scenario since all parcels of water in the tank had the same water quality. However, under the FIFO and LIFO mixing regimes, each parcel of water is considered separate from the others, causing problems when retrieving the age of water in the tank. It appears the only way to retrieve reliable data for tank water quality when mixing regimes other than completely mixed are used is

to run the simulation using the EPANET-GUI and specifying Average under the Times>Statistic options.

APPENDIX L : VARIABLE SPEED PUMPS (VSPS)

EPANET does not yet have the capability to simply model VSPs that are set to maintain a certain pressure setting, which is common in real-world distribution systems. In the Base model the VSPs at the main transmission mains were modeled using pumps that were always on followed by a pressure reducing valve that was set to deliver the desired pump output pressure or head. This approach has two drawbacks. First, the energy use of the pumps is misrepresented. Second, flow instabilities can occur. These instabilities may have lead to the negative pressures observed in the Base model. At the times around 8 am and shortly before noon when the pumps were momentarily off, the EPANET status report indicated these pumps "could not deliver head", a warning issued when a pump is asked to operate outside the range of its delivered head to flow curve. In this case EPANET closed the pump down, potentially leading to portions of the network becoming disconnected from a water source (Rossman, 2000).

The majority of low and negative pressures observed in the Base model were thought to be due to an unstable representation of the VSPs and a computational inconsistency in EPAnet rather than actual low pressures in the system. This suggested low pressure events observed in test scenarios may be ameliorated by adjusting how the VSPs are represented. Moreover, the observed low pressures that occur when negative pressures were noted at the North and Central transmission mains could be considered negligible.

APPENDIX M: MAINTENANCE OF CENTRAL PRESSURES IN PRV SCENARIOS

Figures M.1 and M.2 present the pressures observed at the North and Central transmission mains throughout the 120 hour simulations of the Base, PRV-1 and PRV-2 scenarios. The results for the North central pressure show several instances of low pressure occurred for each scenario, particularly in PRV-1, while fewer occurred at the Central location. These transient low pressures were due to instantaneous closing of the high service sumps supplying the North transmission main because of the approximate representation of the VSPs (see APPENDIX L) and a computational inconsistency in EPANET rather than actual negative pressures in the system. It was unclear why this occurred more at the North location than the Central HSPs and why it happened more in the PRV-1 scenario than PRV-2. Overall it did not appear that these central pressures were unattainable and could not be maintained over the simulation run. Rather it may have suggested that the hydraulic model was unstable due to the 1 minute hydraulic timestep used.

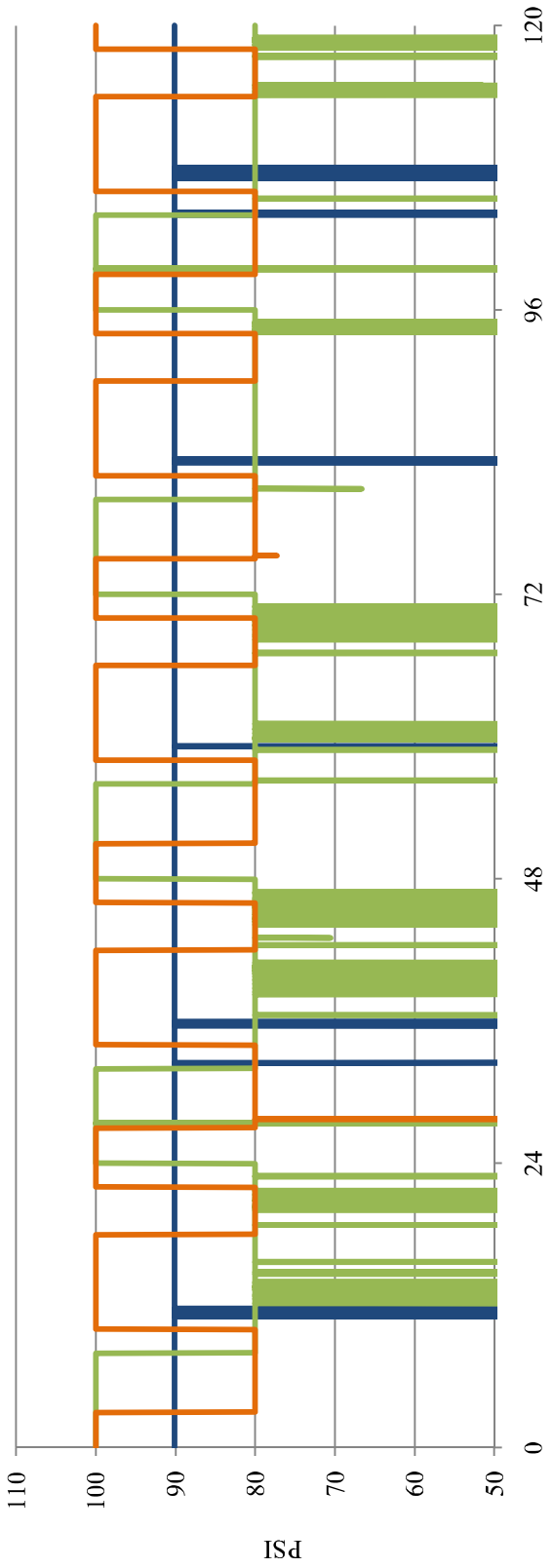

Figure M.1: Observed pressures for North transmission main.

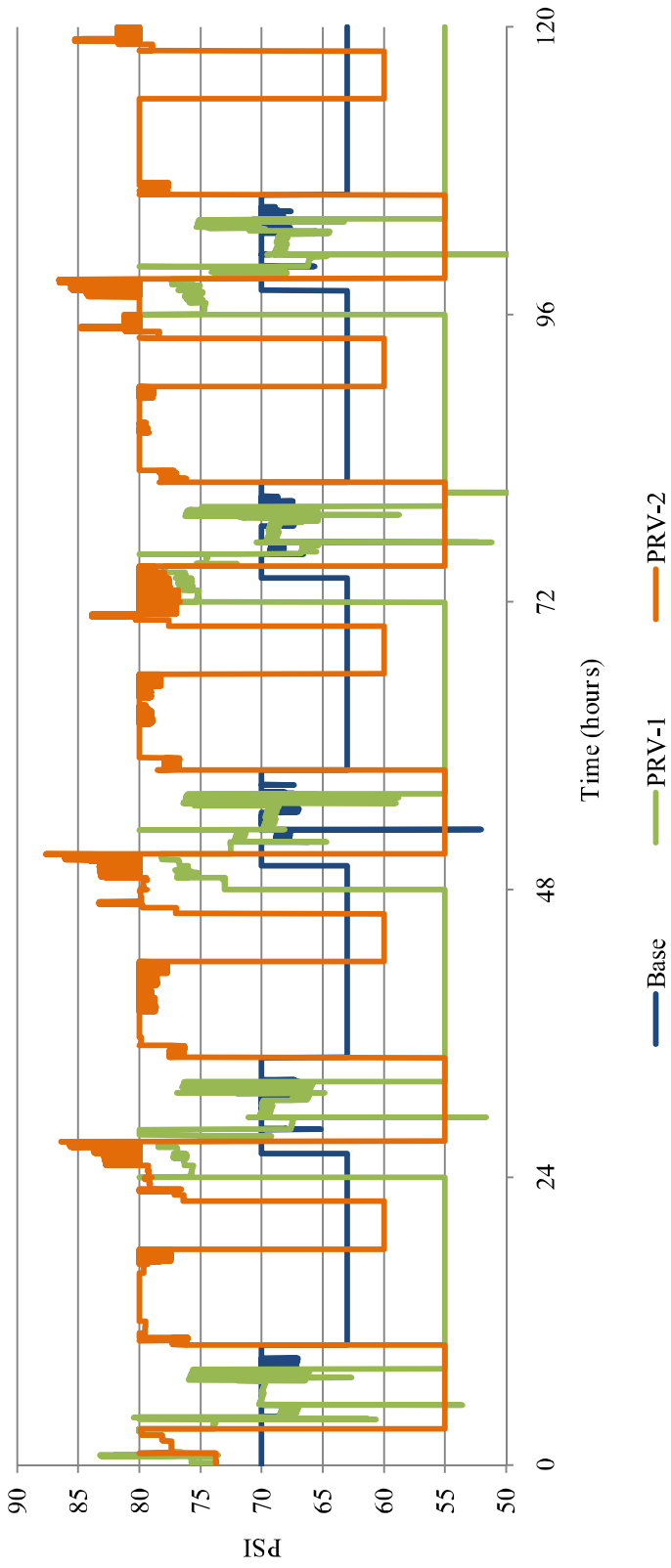

Figure M.2: Observed pressures for Central transmission main.

APPENDIX N: FT-GRAY AND FT-LMN HYDRAULICS

When the Grayson tanks were controlled based on time, the turnover time of the Lanier Mountain tanks were substantially reduced and the reduction in turnover time was more striking for these tanks than for the Grayson tanks. Turnover times for the Grayson tanks were reduced by approximately one day when these tanks were forced to fill and drain, while the reductions in turnover time noted for the Lanier Mountain tanks in this scenario were 8 to 10 days. Examination of the water level in the Lanier Mountain tanks over the 5 day simulation indicated the same filling and draining pattern occurred throughout the FT-GRAY scenario, but more water left the tank during draining. Therefore, the increased turnover time came from a consistent reduction of water in the Lanier Mountain tanks over the course of the scenario, as presented in Figure N.1. This result was likely due to the controls of the Grayson tank which kept the overall level in the Grayson tanks higher than observed in the Base scenario (shown in Figure N.2). Since demand was not being supplied by the Grayson tanks, greater draining of the Lanier Mountain tanks occurred. A similar situation occurred when the Lanier Mountain tanks were forced to fill and drain. The Grayson tanks appeared to drain excessively during this scenario, presumably to make up for the demand not supplied by the Lanier Mountain tanks, as presented in Figure N.3 and Figure N.4.

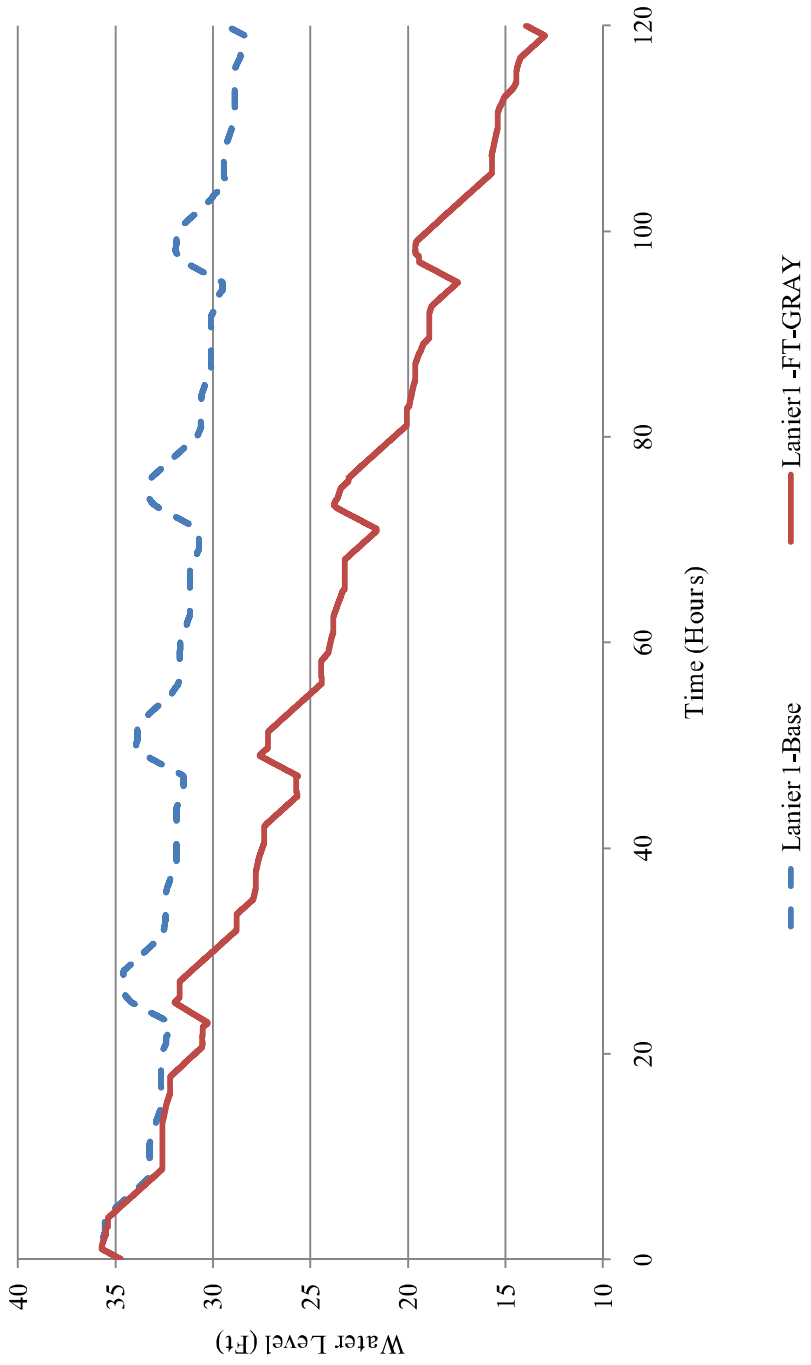

Figure N.1: Representative Lanier Mountain tank head in Base and FT-GRAY scenarios.

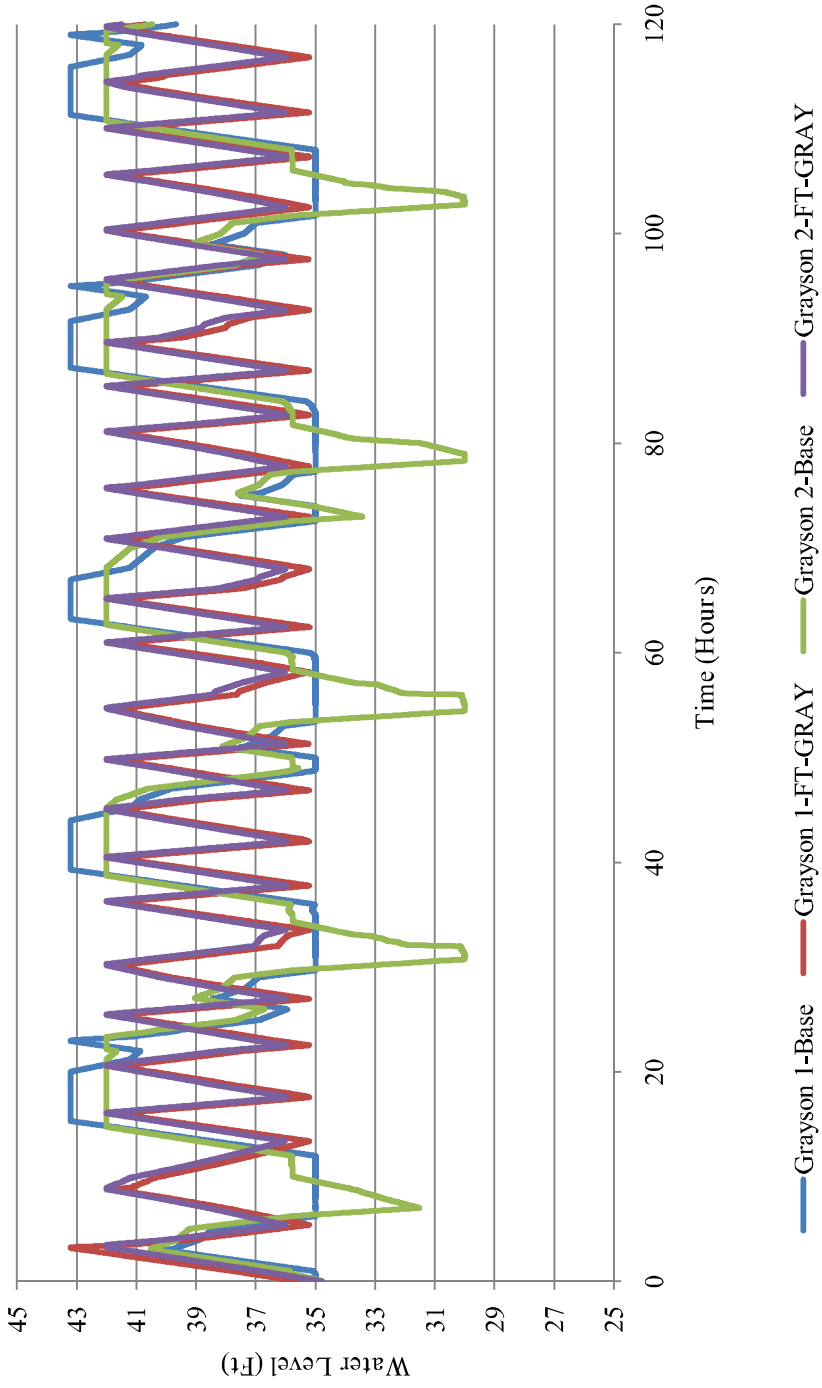

Figure N.2: Grayson tank heads in Base and FT-GRAY scenarios.

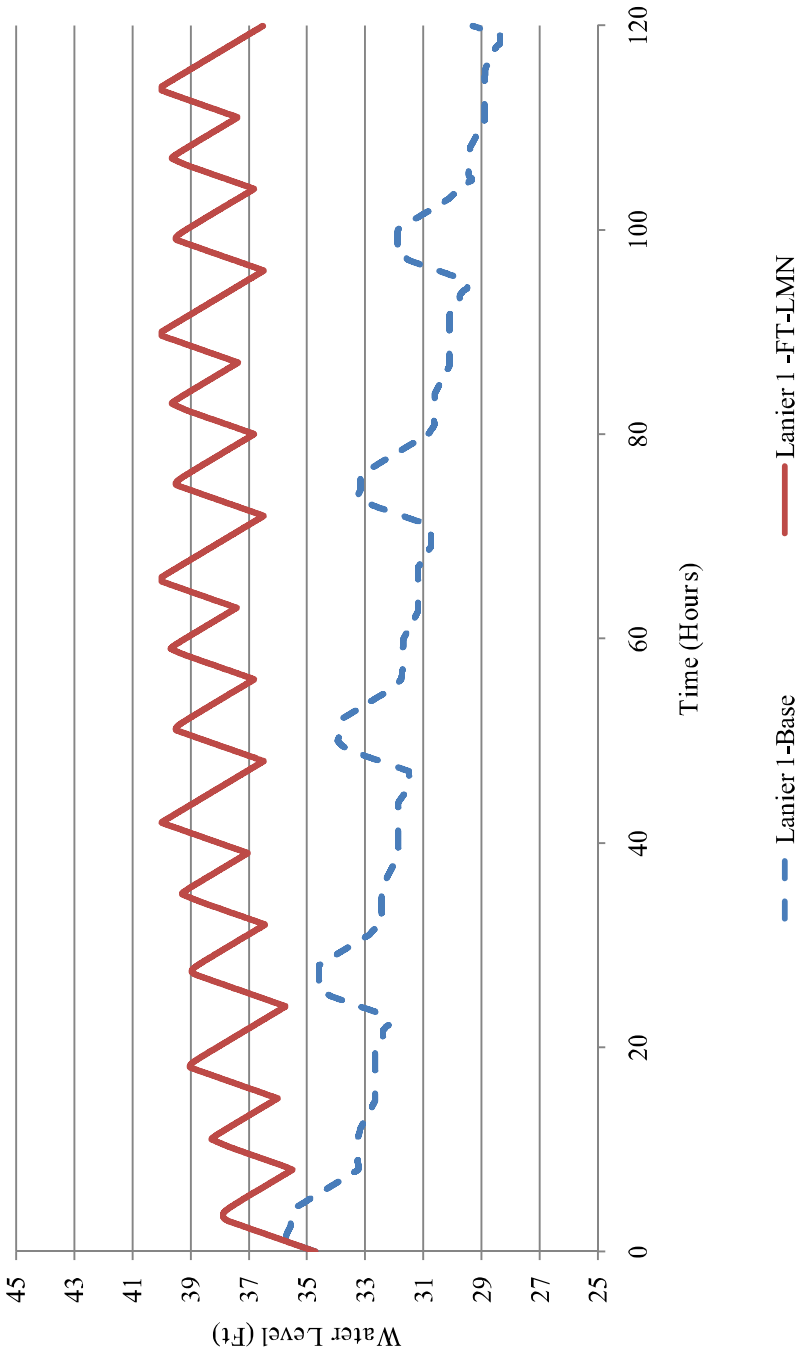

Figure N.3: Representative Lanier Mountain Tank head for Base and FT-LMN scenarios.

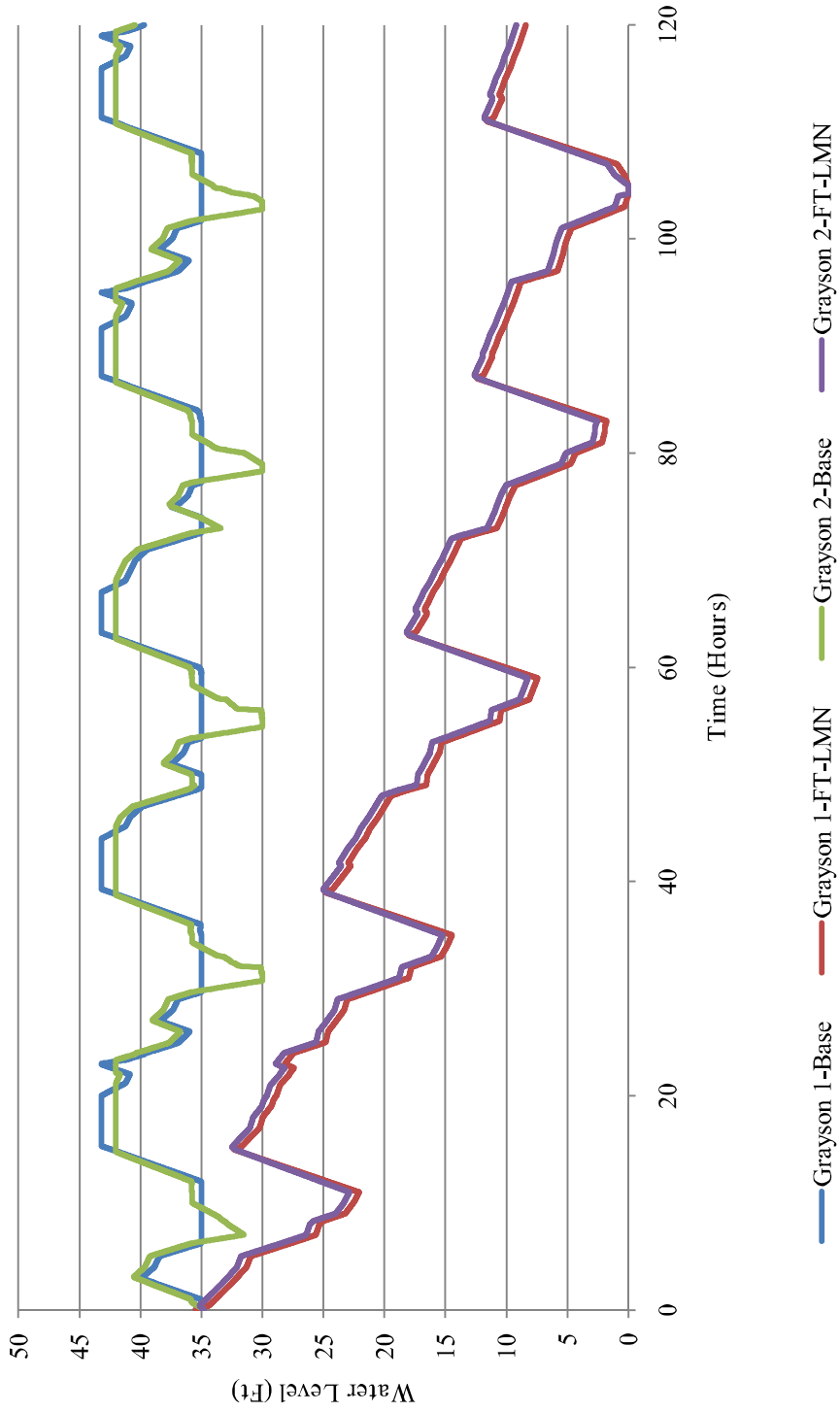

Figure N.4: Grayson tank heads in Base and FT-LMN scenarios.

APPENDIX O: IDSE SAMPLING POINT DATA

The following tables present the average Age, TTHM, HAA5, and free residual chlorine concentrations observed in the Base and operational scenarios at each IDSE sampling location over the last 24 hours of simulation.

Sampling Location 1 – Node 3348

	BASE	PRV-1	PRV-2	1LMN-C	1GRAY-C	MB&GS-C	30%-All	30%-LRG	FT-GRAY	FT-RQ
Average AGE (days)	1.90	1.88	1.85	1.90	1.91	1.90	1.92	1.81	1.88	1.89
SD AGE (days)	0.36	0.28	0.21	0.25	0.28	0.28	0.30	0.16	0.31	0.25
Max AGE (days)	3.90	2.92	2.62	2.96	3.73	3.56	4.61	2.93	3.50	3.21
Min AGE (days)	1.61	1.53	1.52	1.60	1.68	1.64	1.63	1.55	1.65	1.67
Average TTHM (µg/L)	21.53	21.62	20.99	21.64	21.37	21.66	21.72	20.94	21.68	21.47
SD TTHM (µg/L)	3.14	2.78	2.45	2.43	2.28	2.69	2.80	1.64	3.08	2.50
Max TTHM (µg/L)	37.38	31.91	29.47	31.14	34.93	34.22	33.18	28.26	36.41	33.60
Min TTHM (µg/L)	18.28	17.65	16.99	18.29	18.88	18.73	18.45	17.99	19.12	18.87
Average HAA (µg/L)	9.11	9.13	8.81	9.15	9.04	9.15	9.19	8.77	9.15	9.04
SD HAA (µg/L)	1.77	1.44	1.19	1.28	1.35	1.43	1.50	0.81	1.62	1.32
Max HAA (µg/L)	18.58	14.59	13.11	14.40	17.44	16.07	15.57	12.49	17.32	15.78
Min HAA (µg/L)	7.51	7.21	6.91	7.51	7.79	7.71	7.58	7.36	7.89	7.78
Average Cl^- (mg/L)	1.72	1.72	1.73	1.72	1.73	1.72	1.72	1.73	1.72	1.73
SD Cl^- (mg/L)	0.06	0.05	0.04	0.04	0.04	0.05	0.05	0.03	0.05	0.04
Max Cl^- (mg/L)	1.77	1.78	1.79	1.77	1.76	1.77	1.77	1.78	1.76	1.77
Min Cl^- (mg/L)	1.41	1.55	1.60	1.55	1.45	1.50	1.51	1.62	1.46	1.51

Sampling Location 2 – Node 2583

	BASE	PRV-1	PRV-2	1LMN-C	1GRAY-C	MB&GS-C	30% -All	30% -LRG	FT-GRAY	FT-RQ
Average AGE (days)	1.32	1.29	1.76	1.31	1.36	1.34	1.33	1.40	1.28	1.34
SD AGE (days)	0.04	0.05	0.96	0.06	0.03	0.06	0.06	0.26	0.06	0.05
Max AGE (days)	1.42	1.44	7.79	1.65	1.48	1.75	1.77	5.23	1.40	1.67
Min AGE (days)	1.25	1.22	1.28	1.23	1.32	1.25	1.24	1.24	1.18	1.26
Average TTHM (µg/L)	14.28	14.29	17.00	14.12	14.60	14.44	14.14	15.45	14.07	14.24
SD TTHM (µg/L)	0.56	0.67	4.35	0.58	0.54	0.56	0.56	1.80	0.84	0.63
Max TTHM (µg/L)	15.86	16.35	36.45	15.84	16.36	16.73	15.97	28.85	15.85	16.25
Min TTHM (µg/L)	13.26	13.27	13.64	13.07	13.87	13.27	13.04	13.48	12.56	13.12
Average HAA (µg/L)	5.72	5.73	7.31	5.67	5.86	5.81	5.68	6.27	5.63	5.72
SD HAA (µg/L)	0.24	0.29	2.87	0.27	0.23	0.27	0.27	0.94	0.36	0.28
Max HAA (µg/L)	6.41	6.66	22.51	6.49	6.64	7.12	6.70	16.33	6.41	6.82
Min HAA (µg/L)	5.28	5.29	5.44	5.20	5.55	5.29	5.19	5.38	4.98	5.23
Average Cl^- (mg/L)	1.83	1.83	1.77	1.83	1.82	1.83	1.83	1.81	1.83	1.83
SD Cl^- (mg/L)	0.01	0.01	0.10	0.01	0.01	0.01	0.01	0.03	0.01	0.01
Max Cl^- (mg/L)	1.84	1.84	1.84	1.84	1.83	1.84	1.84	1.84	1.85	1.84
Min Cl^- (mg/L)	1.81	1.80	1.20	1.80	1.80	1.78	1.79	1.44	1.81	1.79

Sampling Location 3 – Node 350

	BASE	PRV-1	PRV-2	1LMN-C	1GRAY-C	MB&GS-C	30%-All	30%-LRG	FT-GRAY	FT-RQ
Average AGE (days)	0.94	0.91	0.96	0.94	0.98	0.95	0.96	0.92	0.92	0.97
SD AGE (days)	0.05	0.06	0.04	0.07	0.05	0.10	0.07	0.05	0.05	0.10
Max AGE (days)	1.03	1.97	1.03	1.65	1.06	2.59	1.81	1.37	1.27	2.74
Min AGE (days)	0.86	0.81	0.89	0.85	0.90	0.88	0.87	0.85	0.84	0.88
Average TTHM (µg/L)	8.51	8.49	8.52	8.47	8.61	8.57	8.49	8.66	8.50	8.53
SD TTHM (µg/L)	0.79	0.92	0.68	0.83	0.82	0.70	0.83	0.73	0.87	0.88
Max TTHM (µg/L)	9.95	11.36	9.86	10.70	10.07	12.53	11.29	10.37	10.21	13.79
Min TTHM (µg/L)	7.18	6.90	7.26	7.06	7.26	7.55	7.14	7.41	7.13	7.09
Average HAA (µg/L)	3.30	3.30	3.31	3.30	3.34	3.34	3.31	3.36	3.30	3.33
SD HAA (µg/L)	0.32	0.38	0.28	0.35	0.33	0.33	0.36	0.30	0.35	0.39
Max HAA (µg/L)	3.89	5.58	3.85	4.95	3.94	6.69	5.17	4.38	4.21	7.33
Min HAA (µg/L)	2.76	2.65	2.80	2.71	2.79	2.91	2.75	2.86	2.74	2.73
Average Cl^- (mg/L)	1.90	1.90	1.90	1.90	1.90	1.90	1.90	1.90	1.90	1.90
SD Cl^- (mg/L)	0.01	0.01	0.01	0.01	0.01	0.01	0.01	0.01	0.01	0.01
Max Cl^- (mg/L)	1.92	1.92	1.92	1.92	1.92	1.91	1.92	1.92	1.92	1.92
Min Cl^- (mg/L)	1.88	1.81	1.89	1.84	1.88	1.76	1.83	1.86	1.87	1.74

Sampling Location 4 – Node 3417

	BASE	PRV-1	PRV-2	1LMN-C	1GRAY-C	MB&GS-C	30% -All	30% -LRG	FT-GRAY	FT-RQ
Average AGE (days)	2.73	1.24	2.17	2.47	2.67	7.08	1.97	2.66	2.29	2.61
SD AGE (days)	0.18	0.25	0.17	0.17	0.17	0.29	0.18	0.18	0.18	0.20
Max AGE (days)	3.06	1.74	2.49	2.80	2.99	7.58	2.32	2.98	2.63	2.99
Min AGE (days)	2.40	0.91	1.86	2.15	2.36	6.58	1.64	2.33	1.99	2.26
Average TTHM (µg/L)	26.71	13.50	22.42	24.57	26.25	50.77	20.37	26.24	23.63	25.58
SD TTHM (µg/L)	1.89	3.57	2.02	1.95	1.78	0.73	2.31	1.85	1.99	2.18
Max TTHM (µg/L)	29.95	19.91	26.02	28.11	29.41	51.95	24.55	29.48	27.29	29.44
Min TTHM (µg/L)	23.18	8.86	18.66	21.05	22.85	49.44	16.29	22.71	20.12	21.79
Average HAA (µg/L)	12.62	5.45	10.06	11.37	12.33	29.59	8.95	12.34	10.75	11.93
SD HAA (µg/L)	0.96	1.55	0.97	0.95	0.90	0.81	1.07	0.93	0.97	1.09
Max HAA (µg/L)	14.31	8.32	11.81	13.14	13.96	30.97	10.94	14.01	12.57	13.91
Min HAA (µg/L)	10.85	3.45	8.28	9.66	10.64	28.15	7.07	10.59	9.06	10.07
Average Cl^- (mg/L)	1.60	1.84	1.69	1.65	1.61	1.02	1.72	1.61	1.67	1.63
SD Cl^- (mg/L)	0.03	0.05	0.03	0.03	0.03	0.03	0.03	0.03	0.03	0.03
Max Cl^- (mg/L)	1.66	1.90	1.75	1.70	1.67	1.08	1.78	1.67	1.72	1.69
Min Cl^- (mg/L)	1.55	1.75	1.63	1.59	1.56	0.97	1.66	1.56	1.61	1.56

Sampling Location 5&6 – Node 1253

	BASE	PRV-1	PRV-2	1LMN-C	1GRAY-C	MB&GS-C	30% -All	30% -LRG	FT-GRAY	FT-RQ
Average AGE (days)	2.14	2.12	2.14	2.12	2.17	2.17	2.15	2.11	2.12	2.14
SD AGE (days)	0.17	0.11	0.09	0.12	0.13	0.12	0.13	0.09	0.14	0.11
Max AGE (days)	2.96	2.56	2.48	2.59	2.96	2.71	3.27	2.66	2.80	2.64
Min AGE (days)	1.96	1.92	1.93	1.91	2.03	2.00	1.92	1.90	1.90	1.95
Average TTHM (µg/L)	24.19	24.14	24.13	24.00	24.30	24.46	24.15	24.18	24.14	24.05
SD TTHM (µg/L)	1.44	1.07	1.02	1.06	1.01	1.09	1.23	0.84	1.30	1.07
Max TTHM (µg/L)	30.60	27.84	27.78	27.80	30.14	28.87	28.36	27.37	30.22	28.57
Min TTHM (µg/L)	22.37	22.24	21.91	22.08	22.84	22.92	22.00	21.83	22.00	22.10
Average HAA (µg/L)	10.46	10.43	10.41	10.36	10.51	10.59	10.44	10.43	10.42	10.37
SD HAA (µg/L)	0.83	0.57	0.52	0.58	0.60	0.59	0.67	0.43	0.70	0.58
Max HAA (µg/L)	14.33	12.38	12.28	12.48	14.14	13.01	12.78	12.05	13.83	12.91
Min HAA (µg/L)	9.49	9.42	9.28	9.32	9.74	9.76	9.29	9.25	9.28	9.34
Average Cl^- (mg/L)	1.68	1.68	1.68	1.68	1.68	1.68	1.68	1.68	1.68	1.68
SD Cl^- (mg/L)	0.03	0.02	0.02	0.02	0.02	0.02	0.02	0.01	0.02	0.02
Max Cl^- (mg/L)	1.71	1.71	1.72	1.72	1.70	1.70	1.72	1.72	1.72	1.72
Min Cl^- (mg/L)	1.55	1.62	1.62	1.62	1.56	1.60	1.61	1.63	1.57	1.60

Sampling Location 7 – Node 1920

	BASE	PRV-1	PRV-2	1LMN-C	1GRAY-C	MB&GS-C	30% -All	30% -LRG	FT-GRAY	FT-RQ
Average AGE (days)	0.85	0.81	0.87	0.84	0.88	0.86	0.89	0.83	0.83	0.91
SD AGE (days)	0.03	0.05	0.01	0.03	0.03	0.09	0.11	0.03	0.03	0.13
Max AGE (days)	0.91	1.40	0.90	1.24	0.94	2.56	1.81	1.28	1.08	2.01
Min AGE (days)	0.81	0.77	0.85	0.80	0.85	0.80	0.82	0.80	0.79	0.84
Average TTHM (µg/L)	6.98	6.97	7.05	6.95	7.08	7.06	7.06	7.19	7.03	7.12
SD TTHM (µg/L)	0.48	0.66	0.26	0.51	0.53	0.54	0.65	0.44	0.57	0.66
Max TTHM (µg/L)	8.04	9.09	7.52	8.36	7.99	11.38	9.66	8.70	8.22	10.04
Min TTHM (µg/L)	6.31	6.06	6.66	6.26	6.39	6.15	6.31	6.56	6.31	6.34
Average HAA (µg/L)	2.69	2.69	2.71	2.68	2.73	2.74	2.76	2.77	2.71	2.79
SD HAA (µg/L)	0.19	0.28	0.10	0.21	0.21	0.27	0.34	0.18	0.23	0.36
Max HAA (µg/L)	3.12	4.13	2.90	3.65	3.09	6.27	4.74	3.84	3.42	5.10
Min HAA (µg/L)	2.42	2.32	2.56	2.40	2.45	2.36	2.42	2.52	2.42	2.43
Average Cl^- (mg/L)	1.92	1.92	1.92	1.92	1.92	1.92	1.92	1.92	1.92	1.92
SD Cl^- (mg/L)	0.01	0.01	0.00	0.01	0.01	0.01	0.01	0.01	0.01	0.01
Max Cl^- (mg/L)	1.93	1.93	1.92	1.93	1.93	1.93	1.93	1.93	1.93	1.93
Min Cl^- (mg/L)	1.91	1.86	1.91	1.88	1.91	1.77	1.84	1.88	1.89	1.82

Sampling Location 8 – Node 739

	BASE	PRV-1	PRV-2	1LMN-C	1GRAY-C	MB&GS-C	30%-All	30%-LRG	FT-GRAY	FT-RQ
Average AGE (days)	3.52	3.59	4.07	3.37	3.43	3.62	3.54	3.61	3.89	3.67
SD AGE (days)	0.34	0.37	0.69	0.31	0.36	0.38	0.32	0.45	0.52	0.41
Max AGE (days)	4.73	4.60	10.36	4.53	4.67	4.52	4.41	4.56	5.58	5.07
Min AGE (days)	3.00	2.97	3.09	2.94	2.90	2.91	2.94	2.89	3.03	3.02
Average TTHM (µg/L)	35.17	35.66	36.99	34.82	34.67	35.47	35.34	35.21	36.44	35.53
SD TTHM (µg/L)	2.16	2.01	2.08	1.97	2.22	1.98	1.96	2.23	2.83	2.04
Max TTHM (µg/L)	41.05	40.72	47.21	39.67	40.24	39.80	39.73	40.03	43.16	40.04
Min TTHM (µg/L)	31.96	32.26	33.16	32.17	31.67	31.80	31.95	31.31	32.15	32.30
Average HAA (µg/L)	16.76	17.08	18.32	16.41	16.41	17.02	16.85	16.91	17.81	17.08
SD HAA (µg/L)	1.40	1.36	1.73	1.27	1.47	1.32	1.28	1.55	1.91	1.40
Max HAA (µg/L)	21.05	20.95	30.08	20.10	20.54	20.18	19.85	20.28	23.05	20.71
Min HAA (µg/L)	14.65	14.74	15.29	14.71	14.39	14.48	14.60	14.27	14.76	14.83
Average Cl^- (mg/L)	1.47	1.46	1.42	1.49	1.49	1.46	1.47	1.47	1.44	1.46
SD Cl^- (mg/L)	0.05	0.05	0.07	0.04	0.05	0.05	0.04	0.05	0.07	0.05
Max Cl^- (mg/L)	1.55	1.54	1.53	1.55	1.56	1.55	1.55	1.56	1.54	1.54
Min Cl^- (mg/L)	1.32	1.33	0.93	1.36	1.34	1.35	1.37	1.35	1.25	1.32

Sampling Location 9 – Node 3430

	BASE	PRV-1	PRV-2	1LMN-C	1GRAY-C	MB&GS-C	30% -All	30% -LRG	FT-GRAY	FT-RQ
Average AGE (days)	0.98	0.94	1.01	0.97	1.01	0.98	0.99	0.95	0.96	1.06
SD AGE (days)	0.00	0.01	0.00	0.00	0.00	0.00	0.00	0.00	0.01	0.03
Max AGE (days)	0.98	0.95	1.02	0.98	1.01	0.98	0.99	0.96	0.97	1.14
Min AGE (days)	0.98	0.93	1.00	0.97	1.00	0.97	0.98	0.95	0.95	1.03
Average TTHM (µg/L)	8.71	8.68	8.80	8.71	8.75	8.72	8.76	8.75	8.74	8.91
SD TTHM (µg/L)	0.02	0.06	0.04	0.02	0.02	0.02	0.04	0.03	0.03	0.10
Max TTHM (µg/L)	8.75	8.78	8.85	8.74	8.77	8.76	8.82	8.80	8.79	9.08
Min TTHM (µg/L)	8.67	8.56	8.73	8.67	8.70	8.68	8.69	8.69	8.69	8.75
Average HAA (µg/L)	3.48	3.47	3.52	3.48	3.49	3.48	3.50	3.49	3.49	3.63
SD HAA (µg/L)	0.01	0.02	0.01	0.01	0.01	0.01	0.02	0.01	0.01	0.08
Max HAA (µg/L)	3.49	3.50	3.54	3.49	3.51	3.50	3.52	3.52	3.51	3.80
Min HAA (µg/L)	3.47	3.42	3.49	3.46	3.48	3.47	3.47	3.47	3.47	3.52
Average Cl^- (mg/L)	1.90	1.90	1.89	1.90	1.90	1.90	1.90	1.90	1.90	1.89
SD Cl^- (mg/L)	0.00	0.00	0.00	0.00	0.00	0.00	0.00	0.00	0.00	0.00
Max Cl^- (mg/L)	1.90	1.90	1.90	1.90	1.90	1.90	1.90	1.90	1.90	1.89
Min Cl^- (mg/L)	1.90	1.89	1.89	1.90	1.89	1.90	1.89	1.89	1.89	1.88

Sampling Location 10 – Node 1756

	BASE	PRV-1	PRV-2	1LMN-C	1GRAY-C	MB&GS-C	30%-All	30%-LRG	FT-GRAY	FT-RQ
Average AGE (days)	0.99	0.96	1.31	1.00	1.03	1.09	1.06	1.08	0.93	1.06
SD AGE (days)	0.17	0.22	0.76	0.27	0.12	0.34	0.32	0.36	0.11	0.29
Max AGE (days)	1.90	3.47	5.14	3.02	3.68	3.76	3.05	3.62	1.72	3.23
Min AGE (days)	0.90	0.88	0.91	0.89	0.97	0.90	0.90	0.88	0.87	0.91
Average TTHM (µg/L)	8.92	8.89	11.03	8.67	9.38	9.68	8.94	9.89	8.64	8.96
SD TTHM (µg/L)	1.34	1.42	5.34	1.53	1.00	2.22	1.52	2.19	1.25	1.57
Max TTHM (µg/L)	13.96	18.66	28.11	16.62	18.94	20.20	16.60	19.57	17.20	17.46
Min TTHM (µg/L)	7.72	7.96	7.76	7.67	8.38	7.84	7.70	8.05	7.64	7.66
Average HAA (µg/L)	3.53	3.52	4.74	3.47	3.67	3.92	3.62	4.01	3.38	3.60
SD HAA (µg/L)	0.72	0.82	3.08	0.93	0.51	1.28	0.99	1.30	0.60	0.95
Max HAA (µg/L)	6.69	10.68	16.54	9.26	10.98	11.58	9.27	11.16	7.57	9.81
Min HAA (µg/L)	2.98	3.07	2.99	2.96	3.24	3.02	2.97	3.11	2.94	2.95
Average Cl^- (mg/L)	1.89	1.89	1.85	1.90	1.89	1.88	1.89	1.88	1.90	1.89
SD Cl^- (mg/L)	0.02	0.03	0.10	0.03	0.02	0.04	0.04	0.04	0.02	0.03
Max Cl^- (mg/L)	1.91	1.91	1.91	1.91	1.90	1.91	1.91	1.91	1.91	1.91
Min Cl^- (mg/L)	1.78	1.63	1.43	1.68	1.62	1.60	1.68	1.62	1.77	1.66

Sampling Location 11 – Node 3250

	BASE	PRV-1	PRV-2	1LMN-C	1GRAY-C	MB&GS-C	30% -All	30% -LRG	FT-GRAY	FT-RQ
Average AGE (days)	0.77	0.73	0.80	0.75	0.82	0.80	0.82	0.77	0.74	0.84
SD AGE (days)	0.02	0.06	0.03	0.01	0.03	0.18	0.29	0.06	0.03	0.32
Max AGE (days)	0.95	1.94	0.84	0.76	0.87	3.50	5.53	2.60	1.42	4.44
Min AGE (days)	0.74	0.71	0.76	0.73	0.78	0.73	0.74	0.71	0.70	0.76
Average TTHM (µg/L)	5.69	5.62	5.83	5.45	6.06	5.96	5.77	6.11	5.55	5.71
SD TTHM (µg/L)	0.44	0.33	0.41	0.23	0.50	0.68	0.86	0.48	0.36	0.81
Max TTHM (µg/L)	8.47	8.78	6.45	5.83	6.91	12.50	16.97	10.69	7.52	14.01
Min TTHM (µg/L)	5.03	5.17	5.23	5.02	5.31	5.01	5.02	5.09	4.87	5.02
Average HAA (µg/L)	2.17	2.15	2.23	2.08	2.32	2.30	2.25	2.34	2.12	2.24
SD HAA (µg/L)	0.17	0.17	0.16	0.09	0.20	0.42	0.63	0.21	0.15	0.65
Max HAA (µg/L)	3.35	4.71	2.47	2.23	2.65	7.81	11.79	6.13	3.62	9.45
Min HAA (µg/L)	1.91	1.97	1.99	1.91	2.02	1.91	1.91	1.94	1.85	1.91
Average Cl^- (mg/L)	1.94	1.94	1.93	1.94	1.93	1.93	1.93	1.93	1.94	1.93
SD Cl^- (mg/L)	0.00	0.01	0.00	0.00	0.01	0.02	0.03	0.01	0.00	0.03
Max Cl^- (mg/L)	1.94	1.94	1.94	1.94	1.94	1.94	1.94	1.94	1.95	1.94
Min Cl^- (mg/L)	1.90	1.83	1.93	1.93	1.92	1.70	1.53	1.77	1.88	1.63

Sampling Location 12 – Node 1676

	BASE	PRV-1	PRV-2	1LMN-C	1GRAY-C	MB&GS-C	30%-All	30%-LRG	FT-GRAY	FT-RQ
Average AGE (days)	1.23	1.20	1.83	1.30	1.22	1.35	1.32	1.33	1.23	1.32
SD AGE (days)	0.12	0.14	0.73	0.20	0.07	0.27	0.26	0.29	0.16	0.20
Max AGE (days)	1.65	2.21	3.30	2.17	1.99	2.55	2.23	2.50	1.93	2.22
Min AGE (days)	1.08	1.01	1.09	1.04	1.12	1.11	1.06	1.08	1.06	1.10
Average TTHM (µg/L)	12.47	12.44	16.43	12.65	12.39	13.31	12.39	13.32	12.96	12.78
SD TTHM (µg/L)	0.90	0.82	5.07	1.14	0.58	1.54	1.09	1.68	1.58	0.96
Max TTHM (µg/L)	14.97	15.68	24.65	15.13	14.82	17.68	15.17	17.92	19.64	15.51
Min TTHM (µg/L)	10.77	10.30	10.85	10.22	11.08	11.25	10.39	11.24	10.77	10.91
Average HAA (µg/L)	5.01	5.01	7.36	5.19	4.93	5.48	5.10	5.50	5.22	5.22
SD HAA (µg/L)	0.49	0.49	2.96	0.67	0.30	0.94	0.75	1.03	0.80	0.63
Max HAA (µg/L)	6.59	7.68	12.66	7.40	6.96	8.85	7.34	8.79	8.68	7.54
Min HAA (µg/L)	4.22	4.03	4.25	3.99	4.35	4.42	4.07	4.42	4.22	4.28
Average Cl^- (mg/L)	1.85	1.85	1.77	1.84	1.85	1.83	1.84	1.83	1.84	1.84
SD Cl^- (mg/L)	0.02	0.02	0.10	0.02	0.01	0.03	0.03	0.04	0.03	0.02
Max Cl^- (mg/L)	1.87	1.88	1.87	1.88	1.87	1.87	1.88	1.87	1.87	1.87
Min Cl^- (mg/L)	1.80	1.75	1.59	1.76	1.78	1.71	1.76	1.71	1.73	1.75